INVESTIGATION OF LIQUEFACTION POTENTIAL OF SAND-TIRE GRANULATED RUBBER MIXTURE THAT USED AROUND THE BURIED PIPES WITH SHAKE TABLE TESTS

A Thesis Submitted to
the Graduate School of Engineering and Sciences of
İzmir Institute of Technology
in Partial Fulfillment of the Requirements for the Degree of

DOCTOR OF PHILOSOPHY

in Civil Engineering

by
Mustafa KARAMAN

June 2022
İZMİR

ACKNOWLEDGMENTS

First and foremost, I would like to express my sincere gratitude to my advisor, Prof. Nurhan Ecemiş Zeren, for her guidance and constant motivation throughout this study. I have learned so much from her, both as a person and a researcher. I also would like to thank the members of my dissertation committee, Prof. Alper Baba and Assist. Prof. Ender Başarı, for their support and guidance at times I lost my way and for their significant contributions to the study. I also thank the members of my defense jury, Prof. Yeliz Yükselen Aksoy and Assist. Prof. Volkan İşbuga, for generously offering their time and valuable comments. Special thanks go to my colleagues, Paulina Bakunowicz, Egemen Sönmez, Baturay Batarlar, Mustafa Vardaroğlu, Hasan Ceylan and İrem Kahraman. Another special thank goes to my colleague and close friend Assist. Prof. Hasan Emre Demirci, with who I am happy and proud to have worked together in several working groups in varying universities and laboratories since the day we met. We shared the cheerful moments and hard times throughout this journey. I would like to thank Assoc. Prof. Gürsoy Turan and Asist. Prof. Selçuk Saatçi for sharing the laboratory facilities with our working team and supporting me. I would like to thank Assoc. Prof. Engin Aktaş for encouraging me to be a better researcher in hard times when I felt not strong enough to succeed in this journey. I would like to thank Assoc. Prof. Hatice Esen Ökten for her supervision and support for the thesis part related to environmental geotechnical engineering. I would also like to thank Prof. Şebnem Elçi for supporting me to go abroad as a research fellow for a short period that I realized would be important in my career later. I would like to thank to Scientific and Technological Research Council of Turkey (TUBITAK) for the financial support of International Research Fellowship for Ph.D. Students (Grant No: TUBITAK BIDEB 2214-A 2017/2 1059B141700512) for my research fellowship in Universty of Surrey between 07/2018-12/2018. Also, I am grateful for the financial support provided by the Scientific and Technological Research Council of Turkey (TUBITAK—Project No: 215M402) to perform the large scale tests which are in the scope of the thesis.

My special thanks go to my parents and my beloved brother and elder sister for their endless support and sacrifice throughout my life. If it weren't for you, I wouldn't be where and who I am today. And for my wife, Gökçen I appreciate you for being endlessly patient and believing in me, even when I could not believe in myself.

ABSTRACT

INVESTIGATION OF LIQUEFACTION POTENTIAL OF SAND-TIRE GRANULATED RUBBER MIXTURE THAT USED AROUND THE BURIED PIPES WITH SHAKE TABLE TESTS

Liquefaction causes major deformations in infrastructures. The rapidly increasing of scrap car tires causes to find new areas to recycle them. It has been seen that granular rubbers to be an effective filling material with their density, permeability, compressibility and also damping characteristics for liquefaction remedation. Firstly, this study aims to explain the effect of rubbers mixed with sand on the liquefaction potential of the mixture during and after earthquakes. For this reason, one-dimensional shaking table experiments were carried out with granular rubbers-sand backfills in a large scale laminar box with varying rubber diameters and varying ratios of rubber. Secondly, the study aims to explain the effect of these mixtures on pipeline performance when used as filling around buried pipelines. Lastly, this study focuses on the possibility of rubber to contaminate groundwater with inorganics. For this purpose, a series of batch tests and column leaching tests were performed. Consequently, mixing rubbers with sand is effective in liquefaction remedation. They reduce the pore water pressure thanks to the high permeability, affect the consolidation characteristics with its permeability and compressibility, also reduce the earthquake loads with their damping facilities. In order to prevent the buried pipelines from uplifting during an earthquake, a limit criteria is suggested to design of the pipe diameter, burial depth and filling conditions with a predicted seismic load. Rubbers aren't hazardous for contaminating the inorganics into groundwater. If granular rubbers are used in environmentally sensitive areas, it is recommended to use them after a prewash process or soaking in water for a day.

Keywords: *Liquefaction, Shake Table, Buried Pipeline, Mitigation, Scrap Tire Rubber, Granulated Rubber.*

ÖZET

GÖMÜLÜ BORULAR ETRAFINDA KULLANILAN KUM- LASTİK GRANÜL KAUÇUK KARIŞIMININ SIVILAŞMA POTANSİYELİNİN SARSMA TABLASI DENEYLERİ İLE İNCELENMESİ

Sıvılaşma yeraltı yapılarında büyük deformasyonlara ve yıkımlara sebep olmaktadır. Dünyada hızla artan hurda araba lastiği, geri dönüştürülebileceği alan arayışlarına yol açmıştır. Lastik granül kauçuk gibi dönüştürülmüş malzemelerin, yoğunluğu, geçirimliliği ve sıkışabilirliği ile etkili bir dolgu malzemesi olduğu görülmüştür. Bu çalışma ilk olarak deprem sırasında ve sonrasında granül kauçukların kumla beraber kullanılmasının karışımın sıvılaşma potansiyeline etkisini açıklamayı amaçlamıştır. Bu sebeple, farklı yarıçaplarda hazırlanan granül kauçuklar farklı oranlarda kum ile karıştırılmış, büyük boyutlu laminer kutu içinde gevşek, suya doygun dolgu olarak yerleştirilmiş, tek eksenli sarsma tablası deneyleri yapılmıştır. İkinci olarak ise bu karışımların gömülü boru hatları etrafındaki dolgular olarak kullanılması durumunda boru hatları performansı üzerine etkisini açıklamayı hedeflemiştir. Bu çalışmanın son kısmı, granül kauçuk-kum dolgularının, yeraltı suyunu sızan inorganikler ile kirletme ihtimali üzerine odaklanmıştır. Bu amaçla karışımlarla bir dizi karışım deneyi ve kolon sızma deneyleri yapılmıştır. Sonuç olarak, granül kauçukların kumla karıştırılmasının sıvılaşma iyileştirmesinde etkili olduğu, granül kauçukların yüksek geçirimliliği sayesinde sadece oluşacak boşluk suyu basıncını azaltmakla kalmadığı, sıkışabilirliliği ile de dolgunun konsolidasyon karaterini çok etkilediği ve deprem yükünü sönümlendirdiği görülmüştür. Gömülü boruların deprem sırasında yukarı hareketini engellemek için bir boru çapı boru gömülü derinliğinin, dolgu koşullarının ve sismik yükleme koşulunun beraber değerlendirildiği dizayn için bir limit kriteri sunulmuştur. Sonuç olarak granül kauçukların doğal ortamda inorganik elementlerin yeraltı suyuna karışması açısından tehlikeli değildir. Granül kauçuklar çevresel koşullar açısından hassas alanlarda kullanılacak ise kullanmadan önce ön yıkama yapılması ya da bir gün süreyle suda bekletilmesi önerilmiştir.

Anahtar Kelimeler: *Sıvılşama, Sarsma Tablası, Gömülü Borular, İyileştirme, Hurda Lastik Talaşı, Lastik Yongalar.*

To my wife İmran Gökçen Yılmaz Karaman.

TABLE OF CONTENTS

LIST OF FIGURES

Figure **Page**

Figure **Page**

Figure **Page**

Figure **Page**

LIST OF TABLES

CHAPTER 1

INTRODUCTION

1.1. Statement of the Problem

Soil liquefaction is a difficult geotechnical phenomenon when it is considered in terms of understanding its causes, predictability of its consequences, and what needs to be done to prevent it. Determining the liquefaction potential of the soil under seismic effects is a very important and common research topic for geotechnical researchers. Beyond that, how the liquefaction mechanism effects infrastructures or superstructures during and after liquefaction constitutes a wide range of geotechnical issues. Researchers focus on many improvement methods that they think increase the liquefaction resistance of the soil (Containment and Reinforcement Mixing Techniques, Compaction Techniques, Drainage Techniques, etc.). Reinforcement and replacement techniques are divided into many sub-topics according to different purposes such as increasing the strength properties of soils, increasing the permeability, drainage, etc., and according to the wide variety of used materials.

One of the common applications to increase the liquefaction resistance of soil and also to decrease the effects of liquefaction on infrastructures is to add some granular materials into soils or to place them around the infrastructures. As known, conventional granular materials used as backfill are usually gravels or gravelly soils like gravel-sand mixtures due to their high permeabe structures. On the other hand, the stresses on buried structures caused by these backfill materials are important parameters for the design of such structures.

In recent years, researchers have focused on liquefaction treatments by using materials with a lower unit weight than gravel to both provide good drainage and reduce stresses on buried structures. The use of scrap car tires as a new filling material in geotechnical applications has become widespread. Scrap car tires attracted noticeable attention with their low unit weight, high permeability, high compressibility, and as well as with dynamic properties such as higher damping for seismic load. The increase in scrap car tires all over the world and the need for recycling them have also triggered these

studies. Scrap car tires began to be used whole, granulated or shredded, also alone or mixed with soils in backfills. It has been revealed that using scrap tire granulated rubbers by mixing with sand provides many benefits in terms of geotechnical aspects. But under seismic loads such as earthquakes, how it affects the liquefaction potential has been a matter of curiosity.

The pipelines used for conveying gases and fresh or sewage water in urban areas are usually buried at shallow depths like a maximum depth of 1.5m. When these pipelines cross loose liquefiable sand deposits under groundwater level, and liquefaction occurs due to seismic loadings, the pipelines are deformed or displaced upward due to the buoyance effects of pore water pressure. The effects of granulated rubber and sand mixture backfill on the response of a buried pipeline during or after liquefaction were not examined clearly in the literature yet.

Although the granulated rubber usage in filling material has advantages from a geotechnical point of view, another concern is whether the materials in the granulated rubber particles are a threat or not for groundwater quality from an environmental point of view. The materials that leachate from granulated rubber (GR) to groundwater also should be examined.

This thesis focused on the granulated rubber sand (GRS) mixtures using as backfill and investigated not only the effects of GR on the liquefaction potential of sand deposits but also the effects of GR on pipeline behavior during and after liquefaction. Also, the leaching effects of GR on groundwater quality were another concern of the thesis.

In this chapter, the questions that the thesis seeks to answer were described. The scope and objective of the thesis were explained. Afterward, the outline of the thesis was listed. Last, the liquefaction phenomenon and its mechanisms were briefly explained, and ground improvement methods for liquefaction remediation were briefly summarized.

1.2. Objective and Scope

In this thesis, the main aims are to determine the benefits of using recycled scrap tire granulated rubber (GR) by mixing them with sand under varying conditions. For these purposes, the studies were divided into three chapters. The granulated rubbers (GR) were grouped according to three different equivalent diameters. The equivalent diameters (in

the thesis, called “size”) of GR were 2.5-5mm, 5-10mm, and 10-15mm. These GRs were mixed with clean sand in different ratios by volume. These ratios were 10%GR/90%sand, 20%GR-%80sand, and30%GR-%70 sand in volume. Several experiments have been carried out using these GR and sand mixtures (GRS) and clean sand. In this section, the experimental studies were explained after the objectives of the studies were listed. The objectives can be classified into three main groups;

1) To determine the effects of the diameter of GR or mixing ratio of GR on the liquefaction potential of GRS backfill.
2) To determine the effects of the diameter of GR or mixing ratio of GR on pipeline behavior when GRS is used as backfill around the pipeline.
3) To investigate the leaching effects of GRS mixture on groundwater quality when the surface water leachate through the GRS mixture when the diameter of GR or mixing ratio of GR are varying.

For these purposes, several experimental studies were conducted as follows;

a) A series of shake table tests were conducted with loose saturated GRS mixtures for addressing objective #1.
b) A series of shake table tests were conducted with buried pipeline models into loose saturated GRS mixtures as backfill material for addressing objective #2.
c) Several batch tests and column leaching tests were performed for addressing objective #3.

1.3. Outline of the Thesis

Chapter 1 is an introduction chapter consisting of the statement of the problem, objectives, and scope of the thesis. Also, the liquefaction phenomenon and its mechanisms are briefly explained. Ground improvement methods for liquefaction remediation are briefly summarized in this chapter.

Chapter 2 is a literature review study section and is divided into five sub-sections. Firstly, the reasons for the widespread usage of scrap tires are explained with a brief industry and market research. Next, scrap tires' mechanical and physical properties are mentioned to figure out why scrap rubbers are advantageous for geotechnical improvements. An overview of the studies performed with granulated rubbers and sand

mixtures is presented. The literature studies about Chapter 3, Chapter 4, and Chapter 5 are given in Chapter 2 under the divided sub-titles.

The purpose of Chapter 3 is limited to the effects of recycled granulated rubber on the liquefaction potential of sand. In this chapter, the shake table tests performed with GRS mixture with varying GR and sand mixture conditions are explained in detail. The results of tests and comparative discussions are represented. As a result, it is determined that using GR in sands as a mixture backfill is a successful remediation method against liquefaction and its consequences.

Chapter 4 is related to liquefaction remedation with recycled rubber sand mixtures and its effect on buried pipelines. In this chapter, the shake table tests are performed with buried pipeline models into a GRS mixture with varying conditions. The pipe response and the effects of GR on the pipe behavior are discussed. A novel design limit is suggested which was related to backfill condition, burial depth of pipe and diameter of the pipe, and also the seismic load to prevent the pipelines against the liquefaction and also the uplift force of pore water pressure in backfill.

Chapter 5 presents a series of batch tests and column leaching tests performed with GRS backfills to figure out the change in contamination of inorganic elements in groundwater when the GRS mixture varies. The results are discussed, and the contaminant is compared with varying GR. As a result, it is figured out that GR is not toxic material for groundwater and the environment if it is used above the groundwater level. Also, it was suggested that they should be rewashed or soaked in water for 6 hours to 1 day if they are used below the groundwater level as a mixture in sand deposits.

Chapter 6 summarizes the concluding remarks of each chapter and gives suggestions for future studies.

1.4. Liquefaction Phenomenon

Liquefaction is a phenomenon in which the strength and stiffness of a soil decrease under earthquakes or rapid cyclic loads. In other and simpler terms, it is the phenomenon that saturated or partially saturated sand/silty-sand behaves like a liquid even though it is normally solid under cyclic load. “Liquefied”, as a term in soil mechanics, was first used in Hazen's (1920) publication describing the failure of the Calaveras Dam in California in 1918. The soil deformations and related structural deformations observed after many

major earthquakes, especially the 1964 Niigata, Japan earthquake, made it necessary to understand the liquefaction phenomenon, define the liquefaction mechanism, and develop the improvement methods.

Generally, soil mechanics accept soil as a continuous mass and analyze it with the principles of continuum mechanics. It divides the continuous mass into infinitesimal pieces and defines the properties of the whole mass for these pieces. However, the soil consists of grains and voids (water and air) and, in reality, does not fit this continuum concept. Sand behavior is based on principles of effective stress and dilatancy. Effective stress is defined as the difference between the total stress and pore pressure in fully saturated soil. The number of the modes to be considered is found using the expression in Eq 1.1.;

$$\sigma' = \sigma - u \tag{1.1}$$

where σ is the total stress, σ' is effective stress, and u is pore water pressure.

Dilatancy means the change in volume of granular material subjected to shear deformation. As shown in Figure 1.1.a, the loose sand grains are subjected to shear force under the drained condition. Particles move into pores and reduce the volume. In Figure 1.1.b, dense sand particles are subjected to shear force, and the particles move on each other and cause to increase in volume. A material is called dilative if its volume increases with increasing shear (positive dilatancy), and contractive if the volume decreases with increasing shear (negative dilatancy). Dilatancy is a property specific to granular materials.

As shown in Figure 1.1.a, loose dry sand subjected to an earthquake simply compacts and densifies. On the other hand, if the loose sand is completely saturated (water fills the voids between the particles), densification cannot occur until the water is displaced (water in voids is incompressible). Therefore, the first reaction of loosely saturated sand to cyclic loading is the pressure increase in the pore water. Before cyclic loading, the soil element is subjected to confining stress due to the weight of the overlying soil (Figure 1.2.a). Before any volume change, the initial response of loose saturated sand to cyclic loading is an increase in pore water pressure. When cyclic shear stresses are applied, loose sand tends to reduce its volume, but this does not happen immediately. Because initially, the loading duration is shorter than the duration passes to start water to drain. Confining stress decreases equal to the increase in pore water pressure to keep the volume constant.

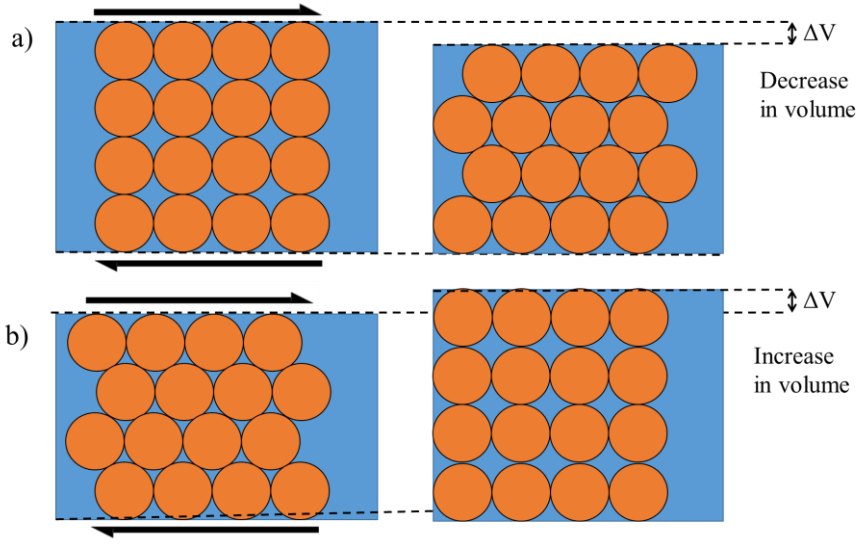

Figure 1.1. Concept of dilatancy

(a) initially loose sand, (b) initially dense sand under drained conditions

As a result, contact stresses between soil particles disappear, and soil loses its strength. If the sand deposit is loose enough, the magnitude of cyclic loading is great enough, pore water pressure increases until it becomes equal to confining pressure (Ishihara,1985). This state is called liquefaction, and there is no effective stress in this state (Figure 1.2.b). After liquefaction, soil particles begin to settle, and excess pore water pressure decreases and dissipates. Effective stress between particles increases, and the sand grains settle denser than the initial state (Figure 1.2.c). As seen in Figure 1.2, there are three stages in the process of soil liquefaction; a) before liquefaction; excess pore water pressure built up, b) during liquefaction; excess pore water pressure is equal to total confining stress, and effective stress is zero, c) dissipation of excess pore water pressure; soil grains are settling.

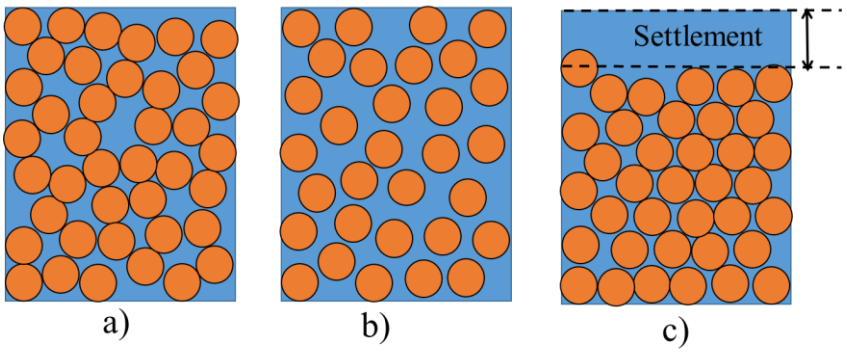

Figure 1.2. Saturated loose sand when subjected to cyclic loading;

(a) before liquefaction; (b) during liquefaction, (c) after liquefaction.

Investigating the causes and effects of soil liquefaction can be summarized in a few steps by looking for answers to the questions given below;

- Are the soils at the site liquefiable or not? (susceptibility)
- Is the ground motion of an earthquake (or design earthquake) strong enough to trigger liquefaction? (triggering)
- If liquefaction occurs, what will be the final ground deformation? (ground deformations)
- What will be the effect of the liquefaction on the seismic performance of structures? (effects on structures)
- If the liquefaction-induced deformations are not tolerable, what remediation method should be used? (mitigation)

The next two sections will describe the liquefaction susceptibility of soils and the remediation methods.

1.4.1. Liquefaction susceptibility

Soil liquefaction susceptibility depends on three main effects; soil properties, geological conditions, and ground motion characteristics. In short, the logic is that; if the site is a loose sandy deposit, the groundwater table is high, the soil is saturated, and the magnitude of the earthquake is large enough, the duration of the earthquake is long enough, liquefaction is expected. All the factors are summarized in Figure 1.3.

The geological conditions give us both to find the physical properties of the deposits and the information about groundwater and the topographic characteristics of the site. Youd and Perkins (1978) investigated the relationship between geomorphology and the liquefaction susceptibility for various regions and summarized it in a table. Table 1.1 shows the susceptibility of sedimentary deposits to liquefaction during strong seismic shaking (Youd and Perkins,1978). Generally, the younger and looser sediment is more susceptible to liquefaction than the old and dense ones. Holocene delta, river channel, flood plain, Aeolian deposits, and poorly compacted fills are most vulnerable to liquefaction.

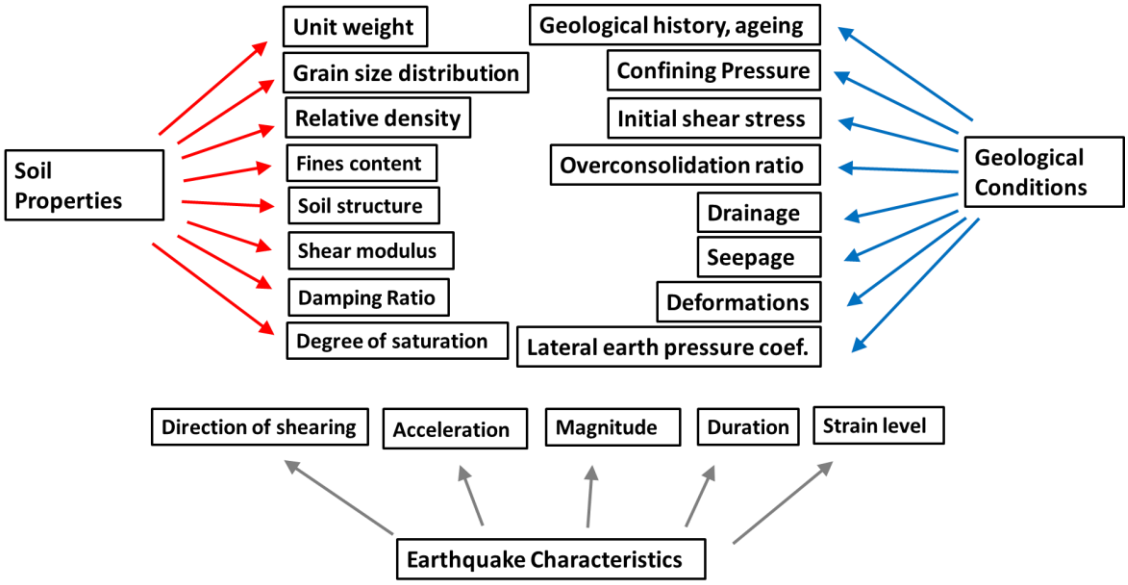

Figure 1.3.Factors affecting liquefaction susceptibility

Particle size, gradation, and shape of particles are also highly related to liquefaction susceptibility. Uniformly graded soils are more susceptible than well-graded soils to changing the volume and tend to build up pore pressure more easily. Tsuchida and (1970) has proposed zones in terms of grain size distribution expressed highly potentially liquefiable, potentially liquefiable, and not liquefiable soils (Figure 1.4). There are two charts, Figure 1.4. a can be used when the uniformity coefficient ($C_u = D_{60}/D_{10}$) is less than 3.5, also Figure 1.4. b can be used when C_u is bigger than 3.5. Although current studies show that these limits are not always correct, they still have widespread use. Certainly, the grain size distribution is not a decisive criterion alone, but it gives a significant insight into the soil liquefaction susceptibility.

Table 1.1. Susceptibility of sedimentary deposits to liquefaction

(Edited from Youd and Perkins, 1978)

Type of deposits	General distribution of cohesionless sediments	Susceptibility of cohesionless sediments to liquefaction when saturated, by age of deposits			
		<500 years	Holocene	Pleistocene	Pre-Pleistocene
Continental Deposits					
River channel	Locally variable	Very High	High	Low	Very low
Flood plain	Locally variable	High	Moderate	Low	Very low
Alluvial fan, plain	Widespread	Moderate	Low	Low	Very low
Marine terraces, plain	Widespread	-	Low	Very low	Very low
Delta and fan-delta	Widespread	High	Moderate	Low	Very low
Lacustrine and playa	Variable	High	Moderate	Low	Very low
Colluvium	Variable	High	Moderate	Low	Very low
Talus	Widespread	Low	Low	Very low	Very low
Dunes	Widespread	High	Moderate	Low	Very low
Loess	Variable	High	High	High	-
Glacial till	Variable	Low	Low	Very low	Very low
Tuff	Rare	Low	Low	Very low	Very low
Tephra	Widespread	High	High	-	-
Residual soils	Rare	Low	Low	Very low	Very low
Sebka	Locally variable	High	Moderate	Low	Very low
Coastal zone					
Delta	Widespread	Very High	High	Low	Very low
Estuarine	Locally variable	High	Moderate	Low	Very low
Beach					
High energy	Widespread	Moderate	Low	Very low	Very low
Low energy	Widespread	High	Moderate	Low	Very low
Lagoonal	Locally variable	High	Moderate	Low	Very low
Foreshore	Locally variable	High	Moderate	Low	Very low
Artificial					
Uncompacted fill	Variable	Very high	-	-	-
Compacted fill	Variable	-	-	-	-

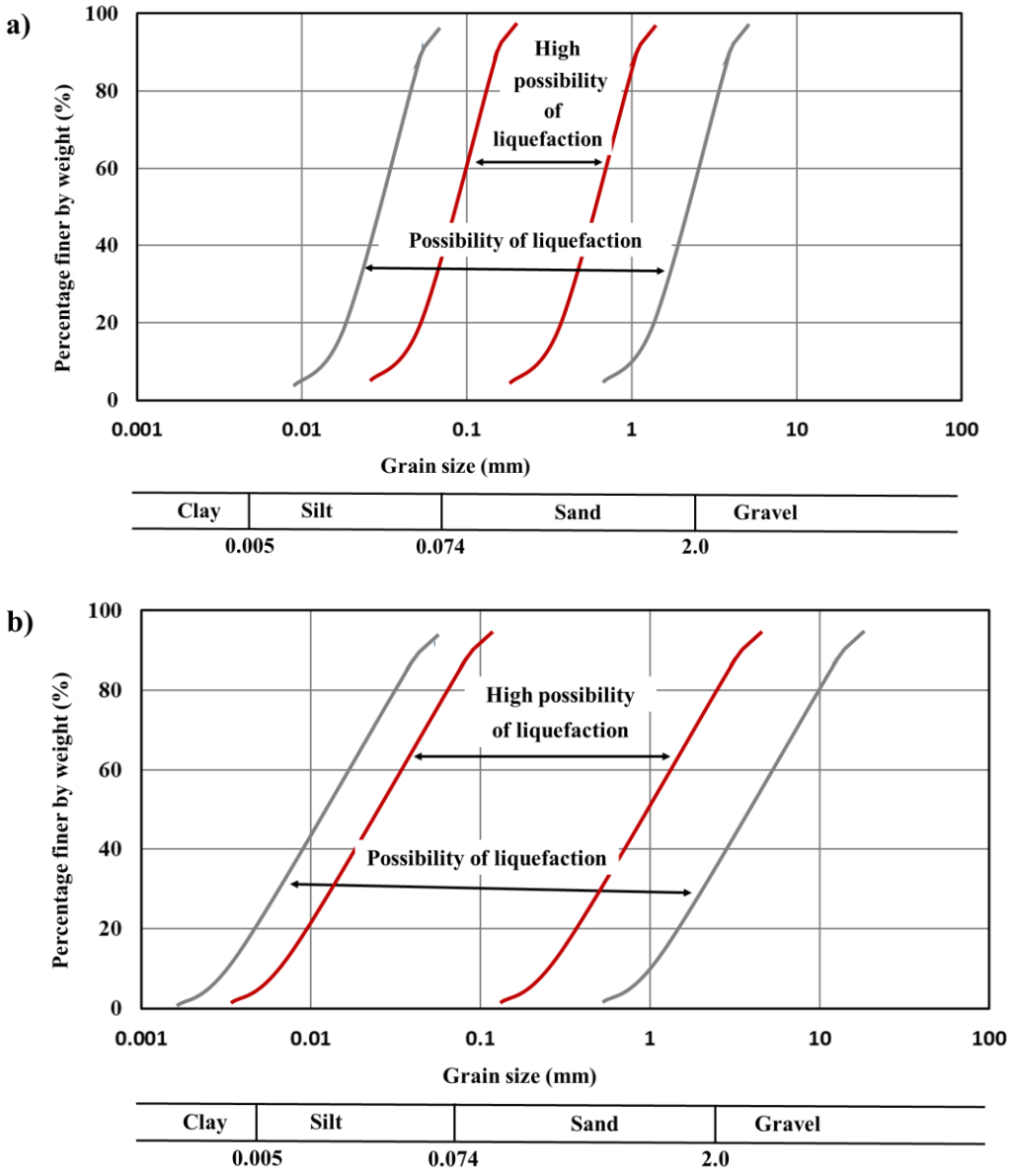

Figure 1.4. Relationship between grain size and liquefaction potential

a) soil with a low coefficient of uniformity, $C_u < 3.5$;

b) soil with a high coefficient of uniformity, $C_u > 3.5$

1.4.2. Liquefaction Remediation

Ground improvement methods for liquefaction remediation are very diverse and are based on one or more of the following principles; (a) solidification, (b) reinforcement and containment, (c) drainage, (d) increasing in-situ stress, and (e) soil replacement. Ground improvement applications for liquefaction remediation and their principles are summarized in Figure 1.5.

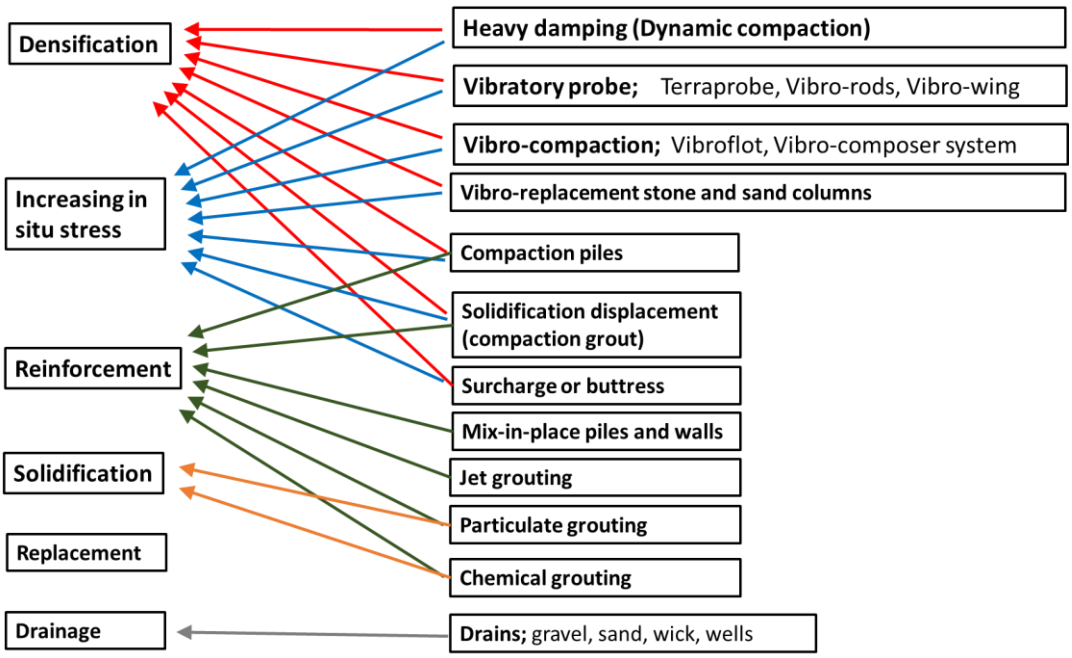

Figure 1.5. Summary of the most common liquefaction remediation methods.

Densification or compaction methods allow the voids in soil to be reduced and the density to be increased. Compaction methods increase the shear strength and liquefaction resistance of the soil. Vibratory or impact compaction methods are the most common method for loose sand layers. Dynamic compaction, rapid impact compaction, compaction, impact roller compaction, deep vibro-compaction, vibro-rod compaction, compaction piling, and stone or sand columns are the most common densification techniques.

The production of more stable soil particles is also a method of liquefaction improvement. This can be achieved by mixing additives such as cement and bentonite with the soil and filling the voids in the soil with these binders. These methods not only prevent excessive pore water pressure but also increase the shear strength of the soil thanks to the increased cohesion. The most common solidification methods are deep soil mixing, jet injection, and permeation injection techniques.

Reinforcement is made to reduce the shear deformation of the ground during an earthquake and reduce the development of excess pore water pressures. It also has tasks such as increasing the bearing capacity and preventing large deformation of structures by limiting the lateral spreading of the soil during and after an earthquake. Reinforcement is

carried out by placing diaphragm walls, sheet piles, case walls, or a grid of rigid column elements such as piles.

It is possible to prevent or reduce excess pore pressure by placing drains. These drainage methods are made using gravel, geosynthetics, or piles with a drainage function. The main purpose of these methods is to delay the development of excess pore pressure and allow water to flow from the liquefaction zone to the non-liquefaction zone.

Another parameter affecting the liquefaction resistance is the initial stress state of the soil. Increasing the lateral stresses in the soil can decrease the shear stress, thus increasing the liquefaction resistance. Stone columns, compression piles, or compression grouts are used to increase lateral stress. Preloading (temporarily loading the soil to consolidate it) is another technique to increase the lateral stress.

In addition, if the water table is lowered under the liquefiable soil layer, liquefaction is prevented because the absence of water makes it impossible to create excessive pore water pressure. The water table can be lowered under the liquefiable soil layer with any dewatering method. Because if there is no water, pore pressure does not occur (Cox and Griffiths, 2010).

The replacement method, which is defined as removing liquefiable material and replacing it with non-liquefiable material, is also an important and common liquefaction improvement method. Since the grain size distribution is a very effective parameter in the liquefaction potential of soils, it was mentioned in the previous section (Figure 1.4). Well-compacted gravel is the most common filling material. On the other hand, with the increase in the variety of materials in geotechnical applications, many artificial filling materials have been developed in recent years. Because these materials are human-made, they can be easily tested and their properties can be determined clearly. This makes the replacement method reliable (Idriss ve Boulanger, 2008).

Mixing the removed liquefiable sand with another granular filling material and replacing it again can also be considered as a combination of replacement and reinforcement methods. These materials are usually fiber, recycled concrete, recycled rubber, etc. It is pretty common to use them as backfill materials for geotechnical applications such as diaphragm walls, retaining walls, caissons, and sheet piles. Also, the usage of these materials as backfill around infrastructures (i.e., buried pipelines, galleries, utility holes, shafts, etc.) is increasing day by day all around the world.

CHAPTER 2

LITERATURE STUDY

2.1. Introduction

Several literature studies related to the use of granulated rubber and sand mixture are given in this Chapter. First, scrap tire recycling industries and market researches are given and the main motivations for using the recycling scrap car tire granulated rubbers in geotechnical applications are described in terms of economic reasons. Next, scrap tires' mechanical and physical properties are mentioned to figure out why scrap rubbers are advantageous for geotechnical improvements. An overview of the studies performed with granulated rubbers and sand mixtures is presented.

The background information of research about the use of scrap tire-granulated rubber on liquefaction improvement in sands are represented in detail as a literature survey of Chapter 3. The history of research on the usage of scrap granulated rubbers and their effect on buried structures are explained in detail for Chapter 4. The relevant history of research is given about how the granulated rubbers used in geotechnical applications effects groundwater and aquatic life environmentally for Chapter 5.

2.2. Recycling of Waste Tire

The use of car tires is rapidly increasing due to the increase in vehicle usage and highway networks worldwide. The number of waste tires produced worldwide is tremendous, with over 1 billion tons growing each year (Thomas and Gupta, 2016). The United States Tire Manufacturers Association (USTMA, 2020) reported 264 million scrap tires (about 4.5 megatons) were generated in 2019. According to USTMA (2020), the usage of generated scrap tire disposition is shown in Figure 2.1. As seen in Figure 2.1.a., The usage areas of crap tires in 2019 were 36.8% of the total as tire-derived fuel, 24.4% of the total as ground rubber; 14.3% as land disposed of; and 5.1% in civil engineering applications, and 9.7% in other industries. Also, USTMA (2020) gave some of the market trends of scrap tires, which show the increase of waste tires from 2011 to 2019 in detail (Figure 2.1. b-c). The European Tire and Rubber Manufacturers' Association (ETRMA, 2019) published data covering 32 countries and mentioned that

3.5 megatons of scrap tires were generated in 2018. As a summary of the report, 53.6% of total scrap tires were used as granulated in several industries; 34.8% of total scrap tires were used for energy recovery in cement kilns, fuels, etc.; and 2.6% of the total was used in civil engineering application while 8% of total scrap tires were unknown or stocked (ETRMA, 2019), (Figure 2.2).

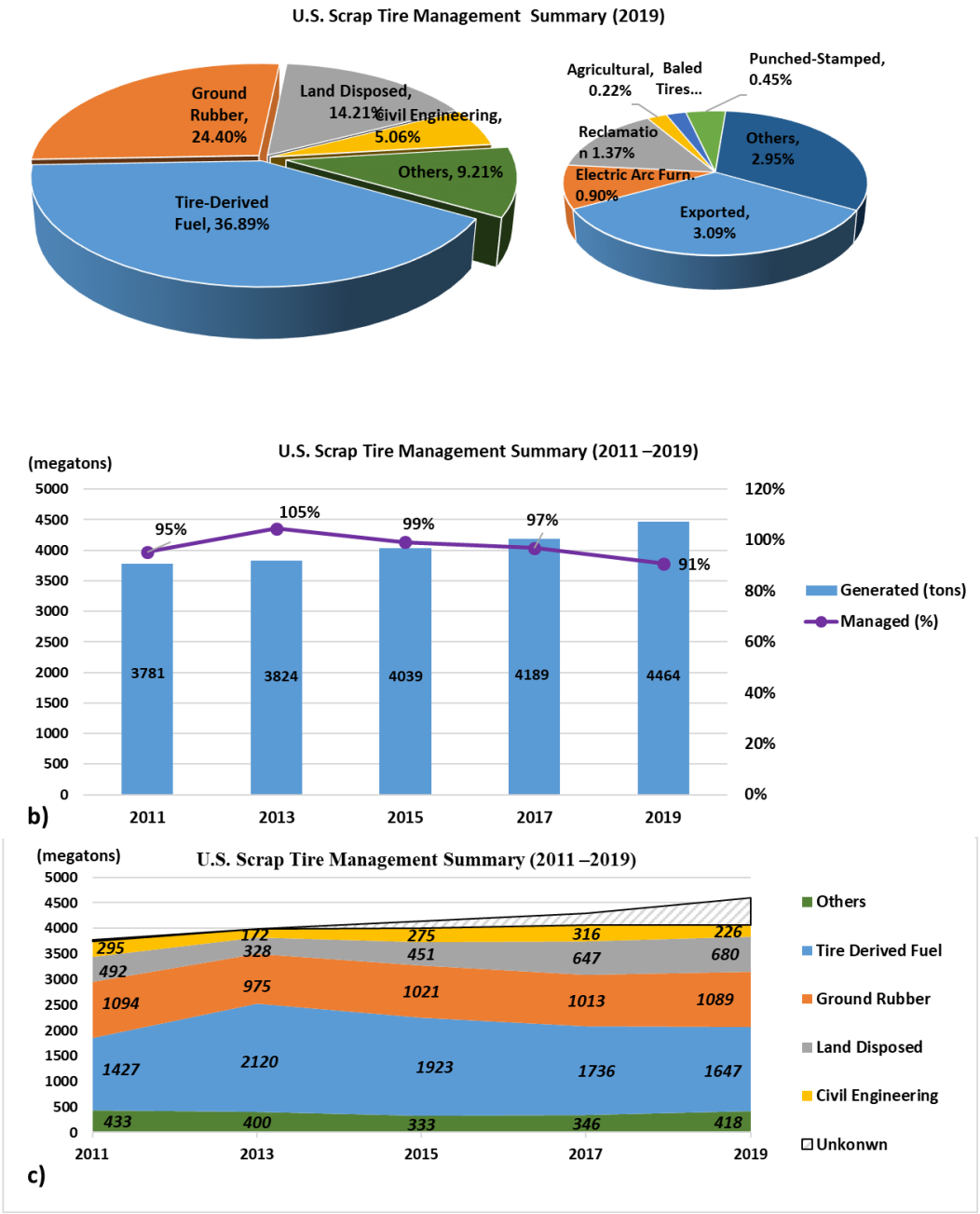

Figure 2.1. USA Scrap Tire Market,

a) 2019 waste tire management summary, b) Trends summary between 2016–2019, and c) Trends summary between 2016–2019 in detail.

As seen in Figure 2.1 and Figure 2.2, scrap tire management is a huge industry and is growing rapidly year by year all around the world. As a natural result, recycling is becoming more important with the rapid growth of scrap tires in the last decade. Figure 2.1 shows that despite all recycling applications, there is still an increment of unknown or uncontrolled stock lands and landfills in the United States of America. Similarly, Figure 2.2 shows that the recycling applications covering 32 European Union countries have been successful, but the ratio of uncontrolled or stocked scrap tires is still high.

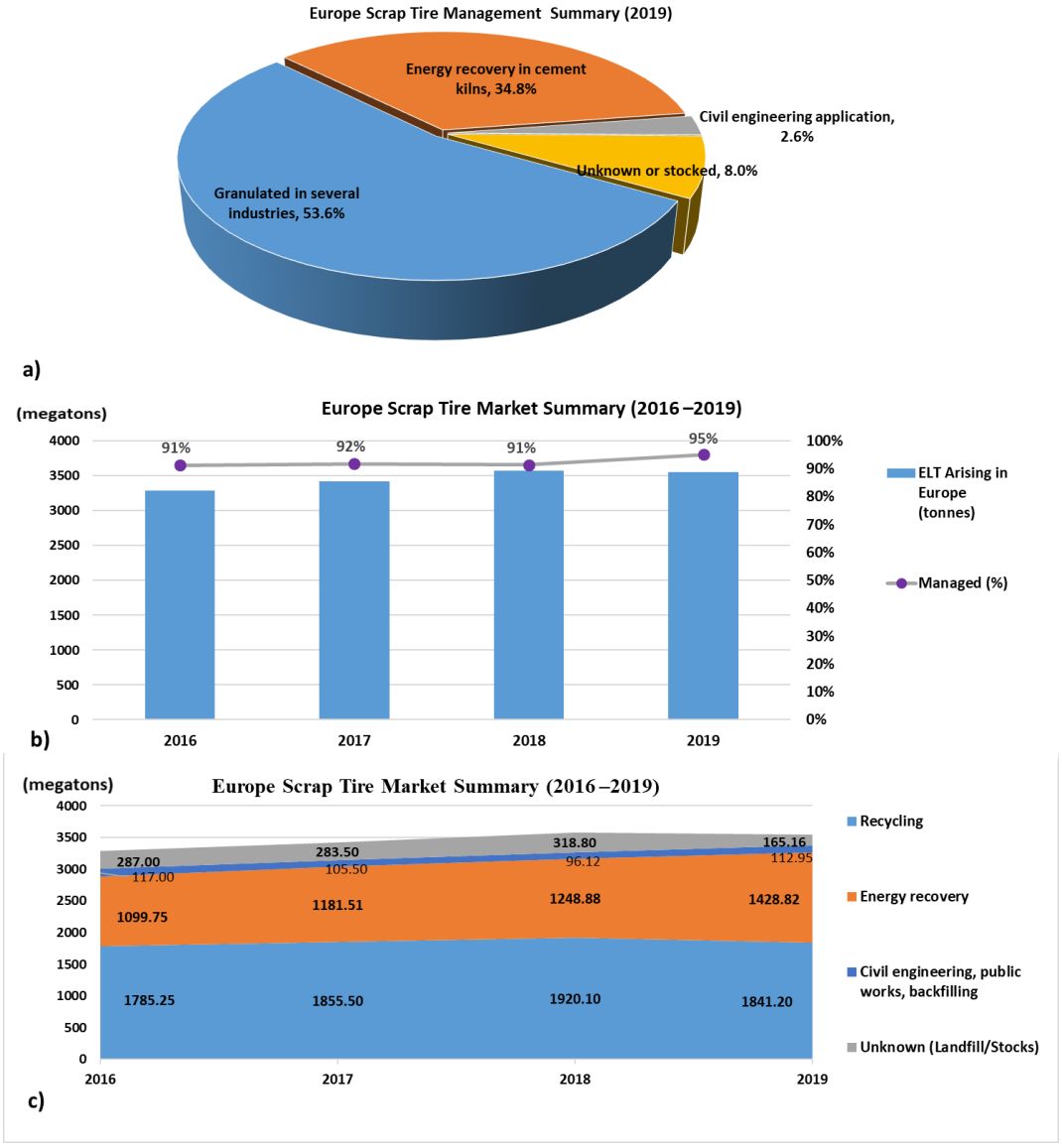

Figure 2.2. Europe Scrap Tire Market,

a) 2019 waste tire management summary, b) Trends summary between 2016–2019, and c) Trends summary between 2016–2019 in detail.

Recent reports have indicated that the recycling of waste tires was improving both in America and Europe. This improvement was achieved by governments' regulations mandating the recycling of rubber tires and by the efforts of tire manufacturers. Despite improving recycling industries and regulations, stocking and uncontrolled landfilling of rubber tires are still common in many countries. Another interesting result in the reports is that the use of recycled scrap tires in civil engineering applications is very low and has not increased significantly over the years. Figure 2.3 shows an example of a wildly landfilling of scrap tires. These wild stock areas pose many dangers and threats. It is true that scrap tires, which are very difficult to store, take up a lot of space, but this is not their most harmful effect.

In addition to effects such as environmental and visual pollution, their extremely flammable structures make them very dangerous areas for large fires. Considering that such illegal wild stockpiles are generally located in urban areas and industrial zones in developing countries, they are seen to be of great danger. For all these reasons, it is very important to use the products obtained from the recycling of scrap tires in engineering applications.

Figure 2.3. Wild landfill of scrap tires
(Source: ETRMA, 2019)

The most common and important method of recycling scrap tires is to use tires by cutting them into small pieces. ASTM D6270-22; Standard Practice for Use of Scrap Tires in Civil Engineering Applications explains the scrap tires classifications according to the shape and size of the pieces. These are commonly referred to as tire-derived aggregate, granulated rubber, shredded rubber, or powdered rubber (ASTM6270-20). There are many scrap tire rubber size classification methods in the literature (ASTM6270-20; Mitchell and Soga., 2005; Li et al., 2016; Busic et al., 2018). The most common ones are summarized in Table 2.1.

Thanks to the widespread scrap tire recycling and shredding technologies, it has attracted the attention of researchers working in civil engineering. Granulated rubber has been the subject of many studies. Granulated rubber will be referred to as "GR" in this study. GRs are considered to be very useful in geotechnical applications due to their suitable mechanical and physical properties. The following section will briefly explain the reasons for using GRs mixed with sand in geotechnical applications.

Table 2.1. Definition and size of waste tire rubber
(Modified from Liu et al., 2020).

Definition	Size	Shape	Referance
Granulated rubber	<0.425–12 mm	Irregular	
Ground rubber	<0.425–12 mm	Irregular	
Powdered rubber	<0.425 mm	Irregular	
Tire chips	12–50 mm	Basic geometrical	ASTM6270-20
Tire-derived aggregate	12–305 mm	Basic geometrical	
Tire shreds	50–305 mm	Basic geometrical	
Whole Tire	-	Unprocessed	
Cuts	>300 mm	Irregular	
Shred	~50-300 mm	Irregular	
Chips	~10-15 mm	Irregular	
Granulate	~1-10 mm	-	Mitchell and Soga (2005)
Powder	<1 mm	-	
Fine Powder	<500 µm	Finely dispresed	
Buffings	1-25 mm	Elongated	
Whole tire	-	Untreated	
chipped/ shredded/ rubber aggregate	13–76 mm	-	Busic et al. (2018)
crumb rubber	0.425–4.75 mm	-	
ground rubber	<0.425 mm	-	
fiber rubber aggregate	average length of 12.5 mm	-	
rubber chips	10–25 mm		Li et al. (2016)
ground rubber	0.5–4.75 mm		
crumb rubber	0.5–1.5 mm		

2.3. Granulated Rubber and Sand Mixtures

GR's mechanical and physical properties make it very suitable for most of the civil engineering applications. The most significant one is lightweight. Its lightweight feature reduces forces on embankments, retaining walls, bridge abutments, and slopes. This makes it suitable to replace the conventional backfill materials. GR has high hydraulic conductivity, which makes it a good drainage material. GR has been used as an embankment fill material, a retaining wall backfill material, and backfill material around buried pipelines thanks to its lightweight and high permeable characterisitcs. Also, GR's viscoelastic properties make it a good material for seismic projects with dynamic/cyclic loading. Figure 2.4 shows an example application of filling GR around the natural gas pipeline from Kiefer Landfill Sacramento County, California, USA.

The ASTM D6270-20 standard divides GR used in engineering applications into two basic types, Type A and Type B. The size of Type A material is roughly 75 to 100 mm, and the size of Type B material is roughly 150 to 300 mm. There are also two classes of filling layers associated with them; Class I and Class II. Class I is GR filling layers that are less than 1 m in height, and Class II defines GR filling layers between 1 and 3 meters in height. Generally, Type A materials are used for Class 1 fillings, and Type B materials are used for Class 2 fillings.

Figure 2.4. Example of GR filling application around the pipeline.
(Source: California Department of Resources Recycling and Recovery Report, 2016)

One of the most common applications of GR is mixing with sands to use as backfill material. Studies on GR in sand generally focus on shear properties, permeability, compression and deformation behavior, and dynamic properties of GR-sand mixture (GRS).

2.3.1. Compressibility

The coefficient of compressibility indicates the compression properties of rubber-sand mixtures. Liu et al. (2018) stated that the increase in the GR ratio in the mixture under the same vertical stress can increase the compressibility coefficient, especially when it exceeds 20%, and the increase in the compressibility coefficient is drastical.

Bosscher et al. (1997) explained that embankments made of sand and reinforced with GR perform well even under heavy traffic loads. Edil et al. (1994) indicated that elastic deformations can be eliminated in embankments by preloading sand-GR mixtures, thanks to the high compressibility of GR.

Humphrey et al. (2000) also noted that laboratory-measured GR deformation was overestimated compared to field measurements. Previous studies performed for determining the compression characteristics of GR are listed in Table 2.2.

Table 2.2. Summary of Compression tests for GR in literature
(Edited from Liu et al., 2020)

Referance	Compaction Method	Loading Method	σ_{max} (kPa)	ε_{max} (%)
Humphrey et al., 1993	Standard Compaction	Constant Deformation Rate (CDR) =13mm/min	480	43
Edil et al., 1994	Standard Compaction	-	690	37
Yoon et al., 2006	40 times with spatula	Each load level for 10 min	120	23
Moo Young et al., 2003	5 layer with 60% standard comp. energy	CDR =13mm/min	480	40
			110	~28
Rowe at al., 2005	No compaction	-	110	~35
			110	~50
			110	~50
Warith., 2006	No compaction	Applying stress to determined strains	150	48
			150	44
			252	47
Shalaby et al., 2005	No compaction		510	47
			700	47
			150	30
Wartman., 2007	Standard Compaction	CDR =13mm/min	150	43
			150	50
			190	28

2.3.2. Shear Properties

Edil and Bosscher (1994) performed a series of large-scale shear tests and derived that the sand-GR mixture had higher strength than the clean sand. Additionally, dense sand-GR mixtures have stronger shear strength than that of a lower dense mixture. Additionally, when the volume ratio of GR was 10%, a greater shear strength occurred compared with the pure sand under low or medium loads.

Tatlisoz et al. (1998) performed a large-scale shear test on sandy silt/sand-GR mixtures and obtained that the shear strength of the sand-GR increased with the increasing GR ratio when the volume ratio of GR was less than 30%.

Ghazavi and Sakhi (2000) indicated that the nonlinear phenomenon was observed in the shear strength under different GR ratios. While Zhang et al. (2018) proposed a linear relationship between the internal friction angle and GR ratio.

Gotteland et al. (2005) showed that the orientation (i.e., horizontal and vertical directions) of GR generate a significant influence on the internal friction angle of the sand-GR mixtures.

There are several studies which were performed shear tests to analyze the sand-GR mixtures' shear strength behavior under various conditions. All were concluded that the addition of GR can improve the internal friction angle (Attom., 2006; Christ and Park., 2010; Marto et al., 2013). A summary of shear strength parameters obtained from previous studies is presented in Table 2.3 (Edinçliler et al., 2010.; Liu et al., 2020).

Table 2.3. Summary of Shear Strength data for Sand-GR mixture in literature (Edited from Liu et al., 2020)

Referance	Test Method	Material	Unit Weight (kN/m^3)	Shear Strenght Parameters	
				c (kPa)	ϕ (^{o})
Humphrey et al., 1993	Large Scale Direct Shear 305x305x228mm	Tire Chips <76mm	7.0	8.6	25
			6.8	11.5	19
				7.7	25
Tatlisöz et al., 1998	Large Scale Direct Shear D=280mm H=300mm	Sand/Tire Chips =9/1	15.6	2	46
		Sand/Tire Chips=8/2	14.5	2	50
		Sand/Tire Chips=7/3	13.3	2	52
Attom et al., 2006	Large Scale Direct Shear 300x300mm	Sand/Tire Shred =9/1	14.0	2	30
			15.0	2	37
			15.5	2	41
Edil et al., 2007	Large Scale Direct Shear 300x300x300mm	2<Tire B. <40mm Sand/Tire Buffings =95/5	15.2	10.4	28.2
		Sand/Tire Buffings =9/1	14.9	10.4	28.2
		Sand/Tire Buffings =8/2	14.2	10.4	28.2
		Sand/Tire Buffings =7/3	13.6	10.4	28.2
Edinçlileret al., 2010	Large Scale Direct Shear 300x300x300mm	8mm <Tire B. <10mm Sand/Tire Buffings =9/1	5.5	7.6	28.2
		Sand/Tire Buffings =8/2	14.0	10.4	28.2
		Sand/Tire Buffings =7/3	13.5	10.4	28..2
			12.0	10.4	28.2
			10.1	10.4	28.2

2.3.3. Hydraulic Conductivity

GRS is a suitable drainage material in geotechnical drainage applications due to their high hydraulic conductivity which is attributed to their large void structure. Edil et al., (1994) studied about effects of the GR ratio in sand or vertical pressure on the permeability of mixtures. GR has high hydraulic conductivity (nearly 1 cm/s) under unconfined pressure conditions. Additionally, the overburden pressure could dramatically decrease the hydraulic conductivity because the void between particles is narrowed, and the seepage path between particles is reduced. (Edil et al. 1994).

2.3.4. Dynamic Properties

GR has high damping characteristics. Hence, GRS mixtures can provide a significant reduction in stress or displacements under the conditions of vibration or cyclic loading. This makes sand-GR mixtures an important material to be studied in earthquake engineering. There are several investigations in the literature focused on the dynamic behavior of rubber-sand mixtures, as numerical studies (Kenada et al., 2007; Pitilakis et al., 2011; and Tsang et al., 2009) and as experimental studies (Edil et al., 1994; Zornberg et al., 2004). Feng et al. (2000) analyzed the dynamic properties of sand-GR mixtures with the grain size of D_{GR}/D_{sand}=6. They figured out that the maximum shear modulus reduced significantly without clearly enhancing the damping ratio for a small strain range.

Anastasiadis et al. (2012) indicated that the initial shear modulus decreased and the damping ratio increased with the increase of the GR ratio. However, the increasing confining pressure enhanced the initial shear modulus and decreased the initial damping ratio. Senetakis et al. (2012) indicated that the confining pressure, GR content, and particle size affected the small-strain shear modulus. Similarly, Li et al. (2019) concluded that the GR particles' size had a significant influence on the shear modulus in the small strain range.

Edinçliler and Yıldız (2021) studied a comprehensive literature review and summarized the dynamic tests performed on sand and rubber mixtures, together with their results. The researches and their results, which are edited from Edinçliler and Yıldız (2021) are shown in the Table 2.4.

.

Table 2.4. Dynamic tests performed on sand-granulated rubber mixtures and results (Edited from Edinçliler and Yıldız , 2021)

Reference	Soil type	Rubber type	Rubber content	Type of Dynamic Tests	Confining Pressure (kPa)	Comments
Feng and Sutter (2000)	Ottawa sand	Granulated Rubber	0, 27, 29, 42, 45, 49, 73, 76, 100 (%) by weight	Resonant Column Test	69, 207, 345, 483	* Shear modulus and damping ratio of sand-rubber mixtures are influenced by rubber inclusion. * Damping ratio increased slightly with confinement pressure for the 100% rubber, an opposite response from soil. This may be because under increasing confining stress, the size of inter-particle contacts between particles increases significantly due to the presence of rubber.
Edincliler et al. (2004)	Sand	Tire buffing	0, 10 (%) by weight	Dynamic Triaxial Test	20, 40, 80	*Addition of 10% by weight tire buffing to sand decreased the shear modulus, while causing a major increase in damping.
Pamukcu and Akbulut (2006)	Ottawa sand and Georgia kaolinite clay	Ground tire rubber	0, 4.8, 6.9, 9.1, 11.1, 13 (%) by weight	Resonant column test	34, 103, 207	*Shear modulus of the mixture increased with the addition of rubber particles. * Similar to the damping ratio behavior, this improvement increased after about 30% rubber volume by soil mineral volume.
Anastasiadis et al. (2012a)	Dry sand Saturated sand	Granulated rubber material composed of recycled tire shreds (D_{50}: 0.40, 1.50, 2.80)	0, 5, 10, 15, 25, 35 (%) by weight	Low-amplitude, High-amplitude torsional resonant column test	25, 50, 100, 200, 400	*Small-strain shear modulus of the sand/rubber mixtures decreases and the damping ratio increases with increasing rubber content and decreasing mean confining pressure. * The specimen's geometry affects the small-strain behavior of the specimens.
Anastasiadis et al. (2012b)	Rounded fluvial sand, angular sandy gravel (D_{50}: 0.27–7.80)	Granulated rubber (D_{50}: 0.34–2.80)	0, 5, 10, 15, 25, 35 (%) by weight	Fixed free type longitudinal-torsional resonant column test	25, 50, 100, 200, 400	* Due to the deformability of rubber particles as well as to the interaction of soil rubber particles, soil-rubber mixtures exhibit higher small-strain damping ratio as the percentage of rubber increases. * Three main factors are affecting the response of soil-rubber mixtures: (a) the percentage of rubber, (b) the relative size of soil particles in comparison to the rubber particles, and (c) the grain size characteristics of the soil part of the mixtures.
Nakhaei et al. (2012)	River type granular soil	Granulated rubber	0, 8, 10, 14 (%) by weight	Large scale cyclic triaxial test	50, 100, 200, 300	* Shear modulus decreased with an increase in rubber inclusion and confining pressures. * Damping ratio decreased with an increase in rubber inclusion at 50 and 100 kPa confining pressures. However, for 200 and 300 kPa confining pressures, the results were vice versa. * Damping ratio in granular soil-granulated rubber mixtures increased as the confining pressure increased. This was the reverse for granular soil without rubber inclusion.
Senetakis et al. (2012a)	Fluvial sand, quarry sandy gravel	Granulated rubber (D_{50}: 0.34–2.80)	0, 5, 10, 15, 25, 35 (%) by weight	Torsional resonant column test	25, 50, 100, 200, 400	The small-strain shear modulus and damping ratio of the sand rubber mixtures are affected by the confining pressure, the content of rubber, the grain-size characteristics and dynamic properties of the intact soils (having 0% rubber) and the relative size of soil versus rubber particles.
Senetakis et al. (2012b)	Dry river sand, saturated river sand	Granulated rubber	0, 5, 10, 15, 25, 35, 0, 5, 10, 15 (%) by weight	High-amplitude torsional resonant column test	50, 100, 200, 400	At a specific confining pressure, sand-rubber mixtures exhibit more linear G/G_0-logγ and D_T-log γ curves as the rubber content increases.
Ehsani et al. (2015)	Firoozkooh sand	Fine, coarse granular rubber	10, 15, 30 (%) by weight	Cyclic triaxial test, resonant column test	300	* Tire inclusion significantly reduces the shear modulus and increases the damping ratio of the mixtures. * Higher damping ratio is observed in mixtures compared to pure sand. * Shear modulus of sand and both coarse and fine rubber mixtures are influenced by rubber content.
Senetakis and Anastasiadis (2015)	Dry, moist, saturated sand	Coarse, medium grained granulated rubber	0, 5, 10, 15 (%) by weight	Resonant column test	25, 50, 100, 200, 400	* Increase of rubber content in the sand-rubber mixtures decreased the small-strain shear modulus, G_0, and increased the small-strain material damping, Ds_0.
Li et al. (2016)	Dry, saturated Fujian sand	Granulated rubber (D_{50}:0.20–0.80 mm)	0, 5, 10, 20 (%) by weight	Resonant column and cyclic triaxial test	50, 100, 200	* At a lower confinement pressure, the shear modulus decreased as the rubber fraction increased. At higher confinement pressure, the shear modulus increased as the rubber fraction increased. * Sand-rubber mixtures had slightly higher damping ratios at a lower confinement pressure. Generally, for a lower rubber fraction, the damping ratio was not significantly affected by the rubber fraction and size.
Mashiri et al. (2017)	Sand (D_{50}: 0.35)	Tire chip	0, 10, 20, 30, 40 (%) by weight	Bender element test, cyclic triaxial test	23, 46, 69, 138	* Shear modulus of sand-tire chip mixtures at large strains was influenced by the proportion of tire chip in the sand-tire chip mixture.
Sanchez et al. (2018)	Leighton Buzzard sand (D_{50}: 0.85)	Shredded rubber (D_{50}: 1.30)	0, 10, 20, 30 (%) by weight	Cyclic triaxial test	100	* Shear modulus of sand-rubber mixtures decreases with adding greater rubber inclusions. * Damping ratio of mixture is influenced by the percentage of rubber, size ratio between rubber and sand particles, number of cycles and shear strain amplitude.

Cont. on next page.

Table 2.4. (Cont.) Dynamic tests performed on sand-granulated rubber mixtures and results.

Reference	Soil type	Rubber type	Rubber content	Type of Dynamic Tests	Confining Pressure (kPa)	Comments
Okur and Umu (2018)	Sand (D_{50}: 0.53)	Chipped rubber	0, 5, 10, 15 (%) by weight	Resonant column-cyclic torsional test	50, 100, 150, 200	Rubber-sand mixtures have smaller shear modulus than clean sand, but display similar behavior at lower confining pressures. * The confining stress varying between 50 and 200 kPa has almost no effect on the strain-dependent damping behavior of the mixtures with 10% and 15% rubber content.
Madhusudhan et al. (2019b, 2019c)	River sand	Tire shred	0, 10, 30, 50, 100 (%) by weight	Cyclic triaxial test	100	* The inclusion of rubber tire shreds results in a decrease of damping ratio. * The shear modulus of pure rubber is the same at all the strain levels for both dry and saturated testing conditions. In general, the damping ratio of dry sand-rubber tire shred mixtures is found to be higher than saturated mixtures at all axial strain levels.
Sarajpoor et al. (2020)	Firoozkooh D2 sand (D_{50}: 2.30)	Crumb rubber (D_{50}: 0.83, 2.33, 6.0)	0, 17, 31, 43, 100 (%) by weight	Dynamic hollow cylinder test	100, 300, 600	* As the relative density of pure sand and sand-rubber mixtures decreased, their shear modulus decreased as well. A decrease in relative density of pure sand led to an increase in damping ratio. *With increasing the confining stress level, shear modulus of pure sand sample increased and its damping ratio decreased. * Dynamic properties of the mixtures depended on their rubber content. * Shear modulus of the mixtures decreased with increasing rubber content. * When the relative density and content of the mixtures were constant, as the rubber size increased, the shear modulus increased while the damping ratio decreased.
Rios et al. (2021)	Uniform quartz sand (D_{50}: 0.35 mm)	Powdered rubber(≤0.425mm) ground rubber (≤0.425–2mm), granulated rubber (≤0.425–12 mm), tyre chip (12–50 mm), tire shred (50–305 mm)	0, 9, 33 (%) by weight	Bender element test, cyclic triaxial test	50	* The specimen with 33% rubber content displayed more elastic behaviour with less accumulation strain than lower rubber content containing specimen * The increase in shear strength with 9% rubber addition higher than of %33 rubber content. * The addition of rubber decreases the initial soils stiffness moduli Go and Eo. * The damping ratio is reduced to its minimum with the addition of rubber.
Fakharian and Ahmad (2021)	Artificially produced Firuzkuh sand F-161 (D_{50}: 0.27)	Granulated rubber (D_{50}:3.1mm)	0, 10, 15 (%) by weight	Cyclic triaxial test	100	* The addition of granulated rubber decreased shear modulus and increased damping ratio between % 0.002–0.004 shear strain. * Initial anisotropic consolidation is not an affecting parameter on dynamic properties of granulated rubber. * The decrease in shear modulus and increase in damping ratio with increasing shear strain amplitude are independent of cycle number, rubber content and consolidation ratio. *After a certain shear strain amplitude, anisotropic consolidation has an influence on dynamic properties of rubber-sand mixtures.
Ding et al. (2021)	China ISO standard sand (D_{50}: 0.52)	Granulated rubber (D_{50}:0.71)	0, 10, 20, 30, 40 (%) by weight	Cyclic triaxial test	50, 100, 150	* The shear modulus is directly proportional to confining pressure and inversely proportional to rubber content and frequency. * A direct correlation of damping ratio with rubber content and inverse correlation with confining pressure and loading frequency indicates that granulated rubber can be used as a seismic insulation and energy dissipation material.
Edinçliler and Yıldız (2021)	Silivri sand (D_{50}:0.50)	Crumb rubber (D_{50}: 2.80), buffing rubber (D_{50}: 3.20)	0, 10, 20, 30 (%) by weight	Cyclic triaxial test	40, 100, 200	* Shear modulus and damping ratio of the mixtures are strongly influenced by the percentage of the tire crumb/tire buffing inclusions and confining pressure. * Tire waste-sand mixtures at same content have lower shear modulus and higher damping ratios that those of clean sand. The increasing confining pressure has the effect of increasing the shear modulus and decreasing the damping ratio. * Under the same experimental conditions, inclusion of tire crumb displayed higher shear modulus and damping ratio that of tire buffing inclusions. * Processing type is one of the most important factors controlling dynamic behavior of the mixtures.

As a summary of Table 2.4, it can be said that, rubber inclination increases the shear modulus and also decrases the damping ratio in most of the studies. But, in some of the studies, the conditions where the opposite occurred have been observed. It is common result for all the studies that, changing in the damping ratio and shear modulus are related to granulated rubber sizes and ratios in mixture and also confining pressures and loading conditions.

2.4. Literature Study on Liquefaction Potential of Tire Granulated Rubber - Sand Mixture

In literature, there are several studies focused on the tire granulated rubber and sand mixtures engineering properties, but they are limited when the subject is granulated rubber effects on liquefaction potential when it is used with sand as backfill.

Edil and Bosscher (1994) indicated some significant engineering properties of tire chips soil mixtures. They observed that the unit weight of tire chip fillings varies between 3 to 6 kN/m^3. Granulated rubber sand mixtures' benefits were related to the tire chips size and compaction characteristics of the mixture. The specific gravity of tire chips varies between 1.13- 1.36 and depends on the metal contents. Tire chips can be used as a mixture with sand or clay, and the major parameter to design the mixture should be compressibility characteristics. When they are used with sand, they have a higher elastic modulus. On the other hand, it can be difficult to mix the tire chips with clay in the field.

Edil and Bosscher (1994) showed that the density of a rubber sand mixture can be reduced from 17.4 kN/m^3 (of pure sand) to 9.5 kN/m^3 as rubber content varies from 0-75%, this may lead to a decrease in the shear strength and potentially change the possibility of liquefaction occurrence. However, there is evidence to show that the shear strength of loose sand becomes greater than that of dense sand with an addition of more than 10% tire chips (Edil and Bosscher, 1994).

Hyodo et al. (2007) performed undrained cyclic triaxial and monotonic shear tests with sand and tire chips-sand mixture which were mixed at various ratios by volume. Based on the results, the tire chips were significantly efficient in controlling the generation of the excess pore-water pressure induced by cyclic and monotonic shearing and also the increase of tire chips content increases the efficiency.

Promputthangkoon and Hyde (2007) investigated that adding a small amount of tire chips reduces the cyclic shear strength of rubber soil mixtures. They also suggested that random mixing of tire chips and sand caused a better shear strength than pure sand when they are at their densest state. Also, densifying the mixture can reduce the void ratio to minimize liquefaction.

Hyodoet. al. (2007) suggested that tire chips are successful drainage materials to mitigate the liquefaction because excess pore water pressure does not generate inside tire chips.

Tsang (2008; 2009) said that the damping effects of rubber-sand mixtures reduce the probability of liquefaction occurrence by decreasing both the peak and root-mean-square accelerations, which have a significant influence on the liquefaction potential of the backfill soils.

Hazarica et al. (2010) performed a series of undrained cyclic shear tests and model shake tests, including a cession type retaining wall with varying ratios of tire chips in sand-tire chips mixture to evaluate the liquefaction potential of mixtures. They observed that when tire chips ratio is 50% by the total volume of sand the prevention against to liquefaction is most effective. Also, the tire chips and sand mixtures have lower relative density compared to sand. There was no liquefaction behind the wall, and the earth pressure on the wall and residual displacement of the wall were reduced.

Bahadori and Manafi (2013) observed that tire chips can control the pore water pressure of the mixture during the earthquake and increase liquefaction resistance using a series of shaking table tests. Pure sand changed its stiffness during earthquake due to a rapid increase of excess pore water, while there was no decrease in stiffness of sand tire chips mixture. The maximum shear modulus of reinforced soil increased with increasing tire chips content in mixture due to decreasing excess pore water generation. Also, mean damping ratio is increased with increment of tire chips in sand tire mixture.

Kaneko et al (2013) conducted a series of online pseudo-dynamic response tests that a one-dimensional modeling algorithm uses directly the data obtained from soil samples. Tests were conducted on models consisting of either tire chip-mixed sand or varying layers of sand and tire chips to investigate the response characteristics of tire chips and tire chip-sand mixtures to seismic loads. The test results showed that when tire chips with low stiffness were either mixed with sand or placed alone as layers, more significant damping and seismic isolation effects were observed. Tire chips also reduced the accumulation of excess pore water pressure in the layer, preventing the liquefaction. In addition, when tire chips are installed as layers under the sand, liquefaction is not generated in the upper sandy layer because the amplitudes of the seismic waves are decreased. Also when the tire chips ratio is increased in mixture, they are more effective to prevent the liquefaction.

According to the Mittal and Gill (2016) review study, the common results of studies which focused on the liquefaction potential of granulated rubber and sand mixtures are as follows; 1) tire rubbers/chips or tire granulated rubbers have high permeability and not allow the excess pore water pressure to increase and the liquefaction

to occur 2) thanks to its compresibilty facilities, tire chips decrease the seismic load and its effects.

Noorzad and Raveshi (2017) performed triaxial tests to investigate the behavior of the sand–tire chip mixtures. The results showed that the shear strength of the mixtures decreased with the increase in the number of tire chips. These results were in contrast to previous studies, which indicated that tire chips increased the shear strength of sand–tire mixtures.

Bahadori et al. (2018) performed several shake table tests comparing the effects of rubber and gravels on liquefaction resistance and also drainage of excess pore water pressure under varying drainage column diameters. They investigated that rubber drainage columns perform better than gravel drainage columns at high relative density and high input acceleration. On the other hand, gravel drainage columns are more effective than the rubber drainage column to reduce the liquefaction effects at moderate input acceleration and low relative density. After shaking, the drainage rate is higher in gravel drains than in rubber drains.

Fakharian and Ahmad (2019) conducted a series of cyclic triaxial tests on granulated rubber-sand mixtures (GRSM) with different granulated rubber percentages (by weight) and at two different shear strain amplitudes to examine the effects of a granulated rubber and the number of cycles on the shear strength, excess pore water pressure (PWP), shear modulus and damping ratio of GRSM. They found that adding the granulated rubber decreases the shear strength, the generated excess pore water pressure, and shear strength degradation rate at any strain amplitude. Increasing rubber content within 0 to 15%, at any shear strain amplitude, has decreased the shear strength and the shear strength degradation rate because of the incompressibility and isotropic nature of granulated rubber. And at any shear strain amplitude, increasing rubber content has decreased the excess pore water pressure.

Hazarica et al. (2020) performed a series of small-scale 1g model shake table tests and cyclic undrained triaxial tests with gravel and tire chips mixture layers under a residential building foundation. They investigated that when the thickness of the reinforced layer is bigger than 2m and the gravel/tire chips ratio is 1/1 by volume in mixture, the horizontal layering method reached its best performance to prevent vibration-induced and liquefaction-induced damage to residential buildings during earthquakes.

Mukherjee and Mishra (2021) performed several consolidated undrained triaxial tests by adding tire fibers to a sand-bentonite mixture and observed that adding tire fibers

reduced the excess pore water pressure. Adding 15% tire fiber increased the effective friction angle from 21^{o} to 24^{o} and the effective cohesion from 15 to 24kPa. Also, tire fiber reduced the time for 90% consolidation of mixture increasing by the coefficient of consolidation.

As seen in the literature, adding the granulated rubber into sand causes a significant change in the mechanical and dynamic behavior of the mixture. However, the influence of granulated rubber ratio and granulated rubber diameter is still not clear on liquefaction and settlement behavior of mixture backfills.

2.5. Literature Study on Liquefaction Potential of Tire Granulated Rubber - Sand Mixture Around the Buried Pipes

2.5.1. Earthquakes in history that triggered the liquefaction of soil and damaged the pipelines

Pipelines are usually named as lifelines because of their importance in human life. These are fresh water, sewage, gas, or oil distributions. Transportation tunnels for vehicles, railways, or cables are also consisting the lifelines. In history, there have been a number of earthquakes caused to failure of lifelines. The failure of pipelines usually occurred due to the strong ground motion or large displacements when the pipeline crosses the fault mechanism. Another most effective reason for pipeline failure is liquefaction. Lateral spreading, landslides, or uplift movements due to pore pressure are the main mechanisms of liquefaction acting on the pipelines.

Investigated pipeline failures during and after large earthquakes showed that pipelines have a significant role in the urban or rural areas for human life. To understand the failure mechanism and design of prevented pipelines has become a big concern for geotechnical researchers. Nair et al. (2018) investigated the pipeline performances during the earthquakes from 1906 to 2018 and highlighted the reasons for the failures. In Table 2.5, the earthquakes were listed whose damages on pipelines were induced by liquefaction directly or indirectly by modifying the review table of Nair et al. (2018).

Table 2.5. Earthquakes in history damaged the pipelines due to the liquefaction (Modified from Nair et al. 2018).

Year	Earthquake	M_w	Damage	Source
1906	San Francisco, California	7.8	Water supply pipeline damages resulted from surface faulting, severe dynamic distortion of pipeline bridges and lateral spreading of loose granular fill caused by soil liquefaction.	O'Rourke et al. (1988)
1933	Long Beach, California	6.4	Over 500 pipeline breaks reported among which greatest concentration of pipeline failures were near bays, rivers and flood control channels	O'Rourke and McCaffrey (1984)
1971	San Fernando, California	6.7	Liquefaction-induced landslides caused a butt-welded steel pipeline to fail in tension at weld at the edge of the landslide area.	O'Rourke and Liu (1999), O'Rourke and McCaffrey (1984) Ariman (1984), Manshoori (2011)
1975	Haicheng, China	7.3	Main reason for damage was liquefaction	Quan (1988), Sun (1979,1991), Liang and Sun (2000)
1976	Tangshan, China	7.8	In Tianjin City, pipelines through many alluvial valleys were heavily damaged due to liquefaction	Sun and Shien (1983), O'Rourke and Liu (1999), Sun (1979, 1991), Liang and Sun (2000), Fu-Lu (1983)
1978	Miyagi Ken-Oki, Japan	7.7	Damage was mostly restricted to small-diameter buried pipelines.	Kubo and Isoyama (1980)
1983	Nihonkai-Chubu, japan	7.8	Damages occurred at joints, and such damages were caused at liquefied sites.	Kitaura and Miyajima (1988)
1989	Loma Prieta, California	6.9	More than 123 failures to the water distribution pipelines in San Francisco were reported due to liquefaction-induced settlement or lateral spread of ground.	O'Rourke et al. (1991), O'Rourke (1996)
1995	Kobe, Japan	6.9	Around 2,000 repairs had to be done in the water distribution system due to significant ground shaking, ground distortion, and liquefaction in the artificial fills constructed near the bay.	Eidinger and Avila (1999)
1999	Chi-Chi, Taiwan	7.6	Main causes for break and ruptures of water pipelines were vibration/ground shaking (48%), caues by liquefaction (2%).	Shih et al. (2000), Wang (2000), and Shih and Chang (2006)
1999	Izmit (Kocaeli), Turkey	7.6	An 80-km long water pipeline between Golcuk and Yalova was damaged at a number of locations. Main cause of the damage was due to ground deformations associated with liquefaction and softening of alluvial sediments.	Erdik (2001) Ansal et al. (2008)
2001	Bhuj, India	7.7	Most of the observed pipeline damages were due to liquefaction	Eidinger (2001)
2004	Cheutsu, Japan	6.8	Widespread damage to sewer pipelines was reported due to uplift behavior caused by ground settlement after	Kang et al. (2013), Hamada (2014) Hasegawa et al.(2006)
2007	Peru	8	Evidence of liquefaction-induced landslides was reported. More than 100 underground water pipelines were destroyed.	Taucer et al. (2009)
2011	Christchurch,	6.3	Damage was caused predominantly by liquefaction. Differential settlement and lateral spreading disrupted both potable water pipelines and wastewater pipelines.	Cubrinovski et al. (2011) Cubrinovski et al. (2014)

To get down more to the effects of the liquefaction on pipelines, several cases as examples were explained in detail. The Northridge Earthquake, 1994 (M_w=6.7) caused the most extensive damage to a U.S. water supply system since the 1906 San Francisco

earthquake. Three major transmission systems, which provide over three-quarters of the water for the City of Los Angeles, were disrupted. LADWP and Metropolitan Water District (MWD) trunk lines were damaged at 74 locations, and the LADWP distribution pipeline system was repaired at 1013 locations. Figure 2.5 shows a fire ruptured by failed gas pipeline behind a crater in the city center of Granada Hills, which caused several nearby homes burned. (Jeon and O'Rourke, 2005).

Figure 2.5. A fire ruptured by failed gas pipeline
in the city center of Granada Hills The during Northridge Earthquake, 1994
(M_w=6.7) (Jeon and O'Rourke, 2005).

According to the report by Orense et al. (2011), several buried structures, such as gasoline tanks shown in Figure 2.6 and buried pipes, were uplifted due to the buoyant force generated by the liquefied soil during Luzon Earthquake, 1990 (M_w=7.7). A buried water pipe along Rizal Street buckled and was thrust upward. Immediately after the earthquake, much of the town was coated in dark-grey mud and water ejected from fissures in the ground.

Figure 2.6. Uplifting of gasoline tank during Luzon Earthquake, 1990 (M_w=7.7) (Orense et al., 2011)

Yamaguchin et al.(2012) reported that six manholes were uplifted, and the maximum uplift movement was 0.5 m in the Tohoku district during the Pacific Coast of Tohoku Earthquake, 2011 (M_w=9.1). While manholes of sewage lifelines were uplifting, the manholes belonging to rainfall lifelines were not uplifted. Although sewage manholes were 3 m in depth and rainfall manholes were at 1.5 m depth, the uplifting were observed at sewage manholes. The reason of that was the liquefaction occurred at the depth of around 3m and above the liquefied soil there was silty clay layer which have low liquefaction potential. Figure 2.7.a, b, and c show the sewage manholes, while Figure 2.7.d shows the rainfall manhole after the earthquake.

Figure 2.7. Uplifting manholes during Pacific Coast of Tohoku Earthquake, 2011 (M_w 9.1) a-c) sewage network manholes, d) rainfall network manhole

Kang et al. (2014a) reported that a lot of pipeline and manhole was uplifted by liquefaction. A sewage tank in San Pedro del Valle was uplifted by approximately 1.2m in the 2010 earthquake in Maule, Chile (M_w=8.8) (Figure 2.8).

Kang et al. (2014b) observed that during the Niigata-ken Chuetsu Earthquake, 2004 (M_w=6.6). Total 1453 manholes was disturbed over a total distance of 152.2 km. The total loss of sewerage facilities was valued at 20.6 billion yen. The most severely damaged areas were in Nagaoka city, Ojiya city, and the town of Kawaguchi. The sewerage systems suffered damage mainly because of disrupted sewer pipelines. Four hundred thirty-six manholes were uplifted over a distance of 62.9 km out of a total of 1258 km of sewer pipeline in the city. (Figure 2.9)

Figure 2.8. Uplifted sewage tank after the Maule-Chile Earthquake, 2010 (M_w=8.8) (Kang et al., 2014a)

Figure 2.9. Uplifted manholes and settlement of sidewalks after the Earthquake in Niigata-ken Chuetsu, 2004 (M_w=6.6) (Kang et al., 2014b)

Figure 2.10. Uplifted manhole after the Earthquake in Niigata-ken Chuetsu, 2004 (Mw=6.6) (Tobita et al., 2009)

Figure 2.11. Uplifted manholes and settled backfill after the Noto Peninsula Earthquake, Japan, 2007 (Mw=6.9) (Kang et al., 2013)

More case studies observed a similar failure scenario consisting of pipeline uplift movements induced by liquefaction in literature, such as; Tobita et al., (2009) (Figure 2.10), Kang et al. (2013) (Figure 2.11).

One of the most recent and significant research is Cubrinovski et al. (2011) report which said buried pipe networks suffered extensive liquefaction-induced damage in the 2010-2011 Christchurch Earthquakes over approximately one-third of the city area. According to Cubrinovski et al. (2011), the wastewater system of Christchurch was hit particularly hard, resulting in numerous failures and loss of service to large areas. Out of the 1766 km long wastewater pipe network, 142 km (8%) were out of service, and 542 km (31%) were with limited service nearly one month after the earthquake. Watermains and submains are located at shallow depths, usually at about 0.8m to 1.0m depth.

Cubrinovski and Taylor (2011) determined the location of repairs/faults on the watermains network (red symbols in Figure 2.12) following the 22 February 2011 earthquake and superimposed in the background of the Figure 2.12 (with red, orange and yellow colors) is the liquefaction map. They indicated the severity of liquefaction (and associated land damage) induced by this earthquake. Preliminary GIS analyses of Cubrinovski et al. (2011) using the pipe network damage data and liquefaction observation maps showed a clear relation between the damage to the pipe network and liquefaction. Approximately 58% of the damaged pipes were in areas of moderate to severe liquefaction (red area in map), 20.2% were in areas of low to moderate liquefaction (yellow area in map), 2.5% in areas where traces of liquefaction were observed (green area in map) and the remaining 19.3% in areas where no signs of liquefaction were observed (blue area in map). They highlighted that there is a clear increase in the affected length (percentage of damage) with increasing liquefaction severity.

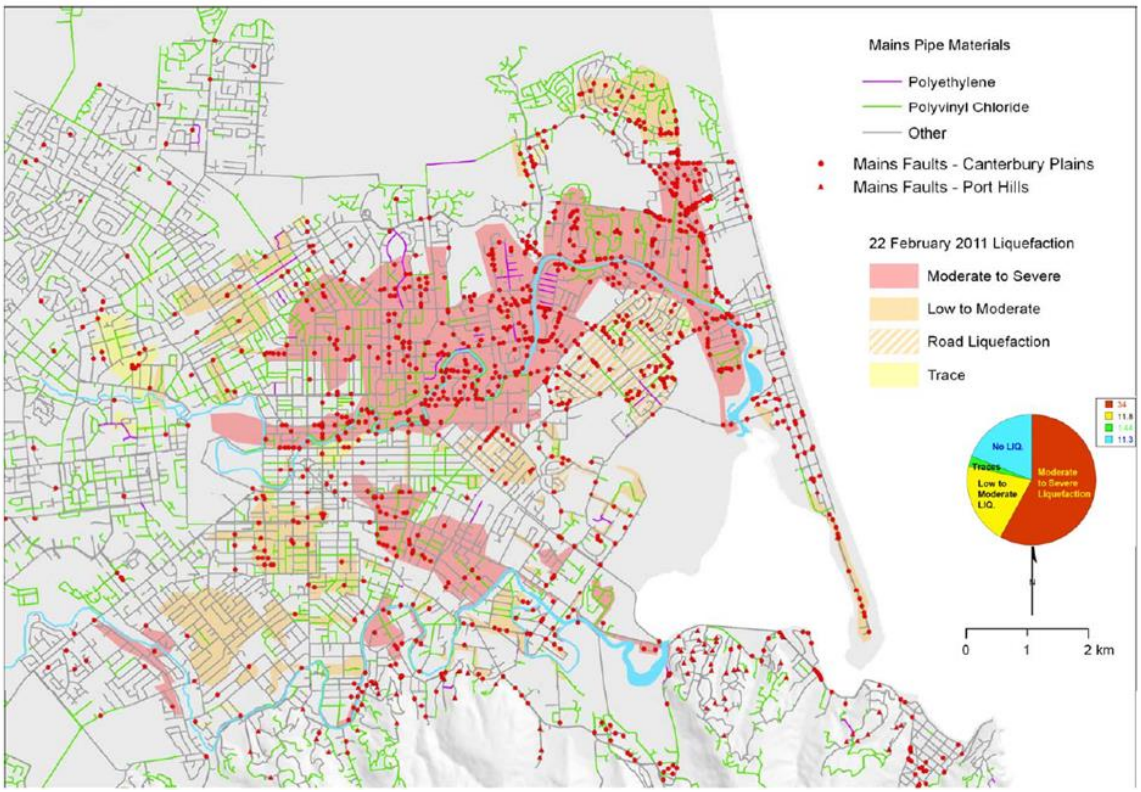

Figure 2.12. The map superimposed the liquefied areas and damaged pipeline locations (Cubrinovski et al., 2011)

2.5.2. Researches Related to the Tire Granulated Rubber-Sand Mixture Around the Buried Pipes

Several methods have been recommended in recent years to avoid the uplift of buried pipes during liquefaction (Orense 2015). Mohri et al. (1999) placed gravel above the pipe to resist flotation by increasing the dead weight. Gravels and geosynthetic materials were also applied around large-diameter buried pipes by Ling et al.(2003). The usage of these countermeasures reduced the pipe uplift by about 10%.

Uchimura et al. (2007) performed several shaking table tests on buried pipes in a tire chip–sand mixture with different tire chip contents. They realized that the sand–tire chip layer around the pipes could relieve the uplift of buried pipes and diminish the excess pore water pressure ratio.

Hazarika et al. (2010) conducted both shaking table and cyclic triaxial tests to study the effect of reinforced sand with tire chips on quay walls' liquefaction susceptibility and displacement. The results demonstrated that the excess pore water

pressure ratio decreased with the tire chips' volumetric ratio. In addition, the residual displacement of the quay wall decreased in the reinforced case.

Kaneko et al. (2013) studied the seismic isolation effects of tire chips and their effectiveness as a remedy for saturated sand liquefaction during earthquakes. They showed that a significant damping ratio and dynamic isolation effects could be detected when tire chips were mixed with sand.

Chian and Madabhushi (2014) performed both numerical model and centrifuge experiments with shallow circular structures to investigate the floatation failure at different buried depths of the structure. They also studied the influence of the magnitude of input sinusoidal earthquake shaking. They proposed a simplified mechanism and the net upward force acting on the pipe due to the liquefaction as follows;

$$F_{NET} = \left(F_B + F_{EPP}\right) - \left(F_T + F_{sp} + F_{ws}\right) \tag{2.1}$$

where; F_B is the buoyant force of the structure is governed by the Archimedes principle and equal to to the displaced volume of water multiplied by the unit weight of water (γ_w=9.81 kN/m^3) where the structure is buried, F_T is the weight of the pipe structure, F_{EPP} is the generated force by excess pore water pressure, F_{WS} is the weight of the overlying soil considering the effective surcharge of the soil acting on the structure, and F_{SP} is the shear force developed in soil. When the soil liquefaction occurs due to the earthquake, F_{sp} is reduced significantly, and the excess pore pressure generated near the invert of the structure (F_{EPP}) also contributes to the uplift force acting on the structure. When there is a positive net uplift force (F_{NET}), the structure floats as a result. Figure 2.13 shows the mechanism of forces acting on pipe during liquefaction proposed by Chian and Madabhushi (2014).

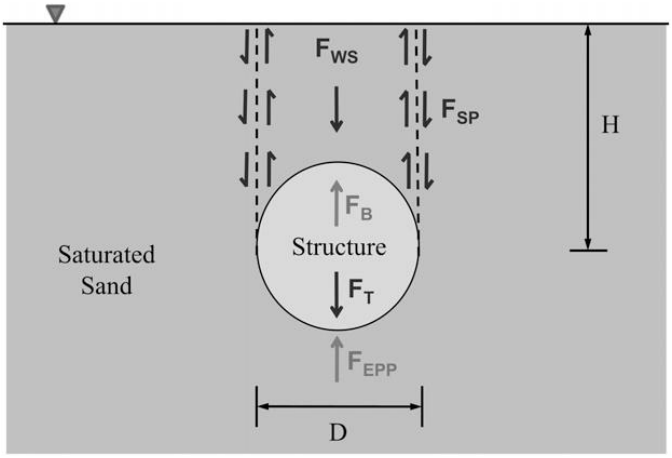

Figure 2.13. Force acting on pipe during soil liquefaction
(Chian and Madabhushi, 2014)

Chian and Madabhushi (2014) observed a higher uplift displacement of the structure for shallower buried depth, indicating the influence of overlying soil weight against floatation. They also showed that the structures commenced floatation in the presence of high excess pore pressure, but they dissipated when the earthquake shaking stopped. A stronger earthquake causes a higher rate of uplift. A constant rate of uplift of the structure was occurred after the soil liquefied, hence postulating a possible limit to shear modulus degradation of the surrounding soil caused by soil-structure interaction. This is the result of the lower excess pore-pressure generation near the structure of rigid pipelines in the liquefiable soil deposit.

Otsubo et al. (2016) conducted series of shaking model tests to investigate the performance of the recycled backfill materials to mitigate the liquefaction-induced floating of sewage pipes. One of the examined recycled materials was a mixture of tire chips and sand. They performed the shake table tests with both unliquefiable (sand with D_r=80%) and liquefiable (sand with D_r=30%) surrounding subsoils with varying thickness of granulated rubber layers. They applied shake table test with a rigid box, and to reduce the boundry effects of box, they used 1/5 scaled model with a longer horizantal witdh and smaller depths. Also to reduce the scale effects they prepeared the soil two times looser than the expected in real-life. Figure 2.14 shows schematic illustration of shaking model tests and instrumantaitons conducted by Otsubo et al. (2016).

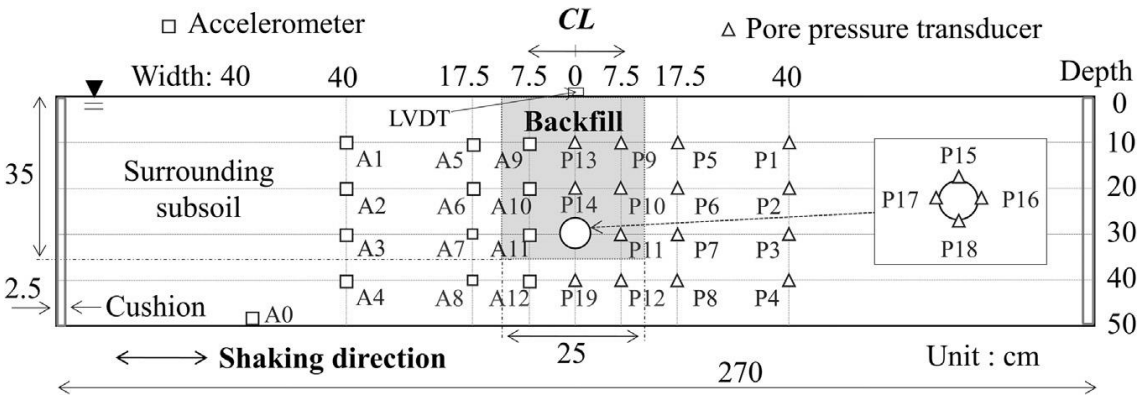

Figure 2.14. Schematic illustration of shaking model tests conducted by Otsubo et al., 2016.

They focused on the influence of the thickness of the tire chips-sand layer (H) and they filled upper part of the tire-chips-sand layer with dense sand. They founded that, despite the mitigation, the excess pore water pressure ratio was generated up to1.2 during

the shaking when H=35cm which is the question for further studies. They indicated that the excess pore water pressure ratio decreased as the thickness of the mixed layer (H) decreased. They noted that, the quick dissipation occurred thanks to the dense sand layer above the mixture layer.

Castiglia et al. (2019) performed four shaking table tests to study the effectiveness of gravel bags placed above and below the pipe to increase the stability of pipelines subjected to uplift in liquefiable soils. Also, Castiglia et al. (2020) used geogrid sheets as a remediation for the liquefaction-induced uplift of buried pipelines. They indicated that both methos effectively reduce the uplift movement of the pipe.

Izadifar (2021) evaluated the effect of using soil-rubber mixture (SRM) around the buried pipes to absorb the vibration energy, protect the pipe, and reduce pipes' deformation. According to Izadifar's (2021) results, the optimum dimension of area for using SRM around the pipe, which will reduce the pipe deformation and simultaneously makes the design economical, is a square by the dimension of three times the diameter of a circular pipe, through which the pipe is placed in the middle.

Abdullah et al. (2021) performed several California bearing ratio tests and direct shear tests to investigate the feasibility of using sand–crumb mixtures for applications such as embankment fills, backfilling for subgrades, and retaining walls, and assess the optimum crumb contents in the mixture. Mixtures of fill sand and rubber crumbs were prepared with sizes of 1–2 mm at crumb contents of 0%, 10%, 20%, and 30% by weight of dry sand. They found that the dry unit weight, CBR, dilation, and friction angle decreased as the crumb content increased, while apparent cohesion was introduced in the mixtures with the addition of crumbs, and it increased with the crumb content. Sand–crumb mixtures were effective as lightweight fill materials over soft soils. They suggested that the sand–crumb mixtures with an optimum crumb content of 20% provided the maximum reduction in lateral earth pressure when they were used as backfill materials behind retaining walls.

Li et al. (2022) presented a sensing solution for evaluating the uplift capacity of pipelines buried in sand using fiber optic strain sensing (FOSS) nerves. They investigated the upward pipe-soil interaction (PSI) through a series of scaled tests, in which the FOSS and image analysis techniques were used to capture the failure patterns.

Alzabeebee (2022) suggested a finite element model to study the efficiency of tire-derived aggregate (TDA) as a mitigation technique to reduce the additional forces applied on the pipe due to transient seismic shake. He considered a wide range of transient

seismic shakes by using earthquake records with a predominant frequency range of 0.63–2.90 Hz and a peak ground acceleration of 0.15–0.50g. Alzabeebee (2022) illustrated the effectiveness of using the TDA as a sustainable solution to reduce the shear forces and bending moments developed in the pipe wall due to the earthquake effect.

Dadkhah et al. (2022) conducted a numerical analysis to evaluate the ability of sand–tire shred mixtures to reduce peak blast pressure, which is the leading cause of damage to underground structures under surface explosion. They performed different scenarios are created by using mixture layers with different thicknesses (2, 4, and 6 m) and tire shred contents (10%, 20%, and 30%) that are subjected to various surface explosion charges (100, 500, 1000, and 5000 kg). They figured out that the thickness of the mixture layer is directly related to the dissipation of explosion energy. On the other hand, the percentage of the rubber content in the mixture is only effective in reducing peak blast pressure when the mixture layer is thick enough and successful in protecting the underground structure from surface explosion hazards.

As seen in the literature, the granulated rubber sand mixture has the benefits of decreasing earth pressure on the pipe line, decreasing the earthquake effects on pipelines in terms of reducing the seismic load, also increasing the permeability, and decreasing the excess pore water pressure, etc. However, how the granulated rubbers and sand mixtures mitigate the liquefaction and prevent or reduce the uplift movement of pipelines under the varying granulated rubbers is less known.

2.6. Literature Study on Environmental Effects of Recycled Tire Granulated Rubber on Groundwater Quality

Usage of scrap tires has become common in geotechnical and environmental engineering applications. Most of the geotechnical applications used granulated tires as retaining wall backfill, bridge abutment backfills, embankment fill, drainage or insulation layer of earth fill, and infrastructure fill (TCTC,1990; Edil and Bosscher, 1992; Edil and Bosscher, 1993; Humphrey and Katz, 2000; Humphrey and Katz, 2001; O'Shaughnessy and Garga, 2000; Aydilek et al., 2006; Edil et al., 2008; Finney et al., 2013; Hennebert et al., 2014; Selbes et al., 2015; Maeda et al., 2017). According to the physical and mechanical requirements, scrap tires can be evaluated in different sizes as whole tires, granulated or shredded (ASTM D 6270–20, 2012). As mentioned before, different

classifications in the literature divide the waste tire rubbers into the granulated rubber, the powdered rubber, the rough shreds, the tire chips, the tire-derived aggregate, etc., according to the rubber size (Li et al., 2016; Busic et al., 2018, Mitchell and Soga, 2005) (Table 2.1).

One of the most common usages of scrap tires is a granulated rubber (GR) produced by granulating tires and removing the fiberglass and steel belts. GR is a lightweight fill material with high compressibility and permeability. Several studies were conducted to understand the benefits of GR in geotechnical applications in terms of mechanical and physical properties. Alternatively, the environmental effects of leaching components of GR have become an issue that needs to be investigated. Several researchers have focused on the leaching characteristics of GR in terms of contamination of inorganics and organics into groundwater by field and laboratory leaching tests (TCTC, 1990; Edil and Bosscher, 1992; Bosscher et al., 1993; Humphrey and Katz, 2000; Humphrey and Katz, 2001; Maeda, 2017).

The batch test is the most commonly used test to identify the leaching characteristic. The rubbers, solution properties, and tools used in each test are different, and difficult to compare the results. For this reason, the batch test has been standardized with a procedure named Toxicity Characteristic Leaching Procedure (TCLP) to determine if a material is hazardous and regulate the level of contaminants in water (United States Environmental Protection Agency (USEPA) 1992). The EP-Toxicity test (Extraction Procedure Toxicity Test), which was developed before TCLP, is also used for classifying a waste material as hazardous. (RMA,1990). According to the RMA report (1990); there was no significant difference between the EP-toxicity and TCLP results. Another batch leaching test is Water Leach Test (WLT) (ASTM D 3987), typically used for non-hazardous materials to assess the leaching potential. In this test, the tire rubber is combined with 1400 ml of ASTM Type II deionized water in a 2L sealed container. This mixture is agitated continuously in a tumbler for 18 hr. The mixture is allowed to settle, and then the leachate is sampled and subjected to chemical analysis. TCTC (1990) performed leaching tests under four pH conditions and figured out that the highest level of metal leaching from GR occurred under acidic conditions.

Lerner et al. (1993) studied three GR sizes (2.54 x 2.54 cm; 5.08 x 5.08 cm; 10.16 x 10.16 cm), which were subjected to nine solutions with three pH levels of 5.4, 7, and 8.6 for contact time of 91 days.

Downs et al. (1996) prepared several mixtures with GR with a size of 7.62 cm x 7.62 cm (steel belted and fiberglass) and three types of soil (till, clay and peat) and sealed them for ten months.

Selbes et al. (2015) performed several leaching tests with three varying pH conditions and six different sizes of tires. They collected leachate samples 15 times in 28 days to determine the contamination as a function of tire chips' surface area. They used four sizes of GR (2.5 x 2.5 cm, 5 x 5 cm, 10 x 5 cm, 15 x 5 cm) and crumb rubber (between 1.41 mm - 2.38 mm), and used three leaching solutions with pH 4, 7, and 10. They focused on dissolved organic carbon (DOC), dissolved nitrogen (DN), and inorganic constituents. Selbes et al. (2015) indicated that increasing pH increased poly-aromatic hydrocarbons (POHs) while decreasing metal contamination and natural pH conditions is most suitable for GR applications. Selbes et al. (2015) also concluded that the degree of leaching increased with the decreasing tire size. The inorganic analyses showed an increase in Aluminum (Al), Barium (Ba), Iron (Fe), Zinc (Zn), Manganese (Mn), and they exceeded their respective drinking water standards while leaching of the following elements relatively negligible: Boron (B), Cadmium (Cd), Chromium (Cr), Lead (Pb), Selenium (Se), Cooper (Cu), Calcium (Ca), Magnesium (Mg), Sodium (Na), Potassium (K), Chloride (Cl), Fluoride (F), and sulfate (SO_4) (Selbes, 2015).

Liu (2018) performed a series of batch tests with two different sizes of tire chips under the different pH conditions and focused on the leaching of Zinc. Liu (2018) examined that the Zinc leaching was reduced by increasing the tire particle size and pH.

Another common laboratory test is the column leaching test (CLT) which represents the leaching characteristics more realistic than batch tests. First, Waste Management of Pennsylvania (1989) investigated tire chip leaching in CLT (20.3 cm diameter and 121.9 cm long).

Kim (1995) used steel containers (61 cm diameter and 91.4 cm long) for soil and tire chip column testing.

O'Shaughnessy and Garga (2000) performed CLTs on GR embedded in quartz sand with three leaching solutions with pH 3.5, 6.5, and 9.5. Aluminum, Iron, Zinc, and Manganese exceeded their drinking water standards (DWS) initially, and all other elements were below detection limits or background levels for tire chips embedded in clay.

Rowe et al. (2005) performed four CLTs (using an internal diameter of 287 mm and a total length of 813 mm columns) filled with two different shaped tire shreds (G and

P) and gravel for two years. Aluminum, zinc, iron, and copper leached from the Pand G-shreds when exposed to typical municipal solid waste leachate. The highest concentration of metals was found in the P-shred, and this is attributed to the greater abundance of exposed steel in these shreds.

Lee (2011) performed column leaching tests (CLTs) to evaluate the leaching characteristics of bottom ash, waste tires (WT), and mixtures of ash and WTs (65:35 by weight) under the different pH (4.0, 6.0, and 8.0) conditions. Lee (2011) compared the CLT results with drinking water standards of the US Environmental Protection Agency (US-EPA), the World Health Organization (WHO), and the Korea Ministry of Environment (KME). Lee (2011) evaluated that the initial concentration of Pb and Zn were slightly above the standards, while the initial concentrations of SO4 from ash and ash–WT were 8–10 times greater than the standards.

Downs et al. (1996) performed small-scale field tests using different sizes of tire chips and pH conditions. They concluded that Fe and Mn exceeded their secondary (aesthetic) drinking water standards when tire chips were placed below the water table. Hence, the usage of GR below the groundwater level is only suitable if the Fe and Mn leachate is tolerable (Downs et al., 1996).

Humphrey and Katz (2001) performed a five-year period of field tests with tire shreds with a maximum size of about 75 mm, and the soil types were marine clay, glacial till, and peat. The field experiment suggested that GR can be used as a water-saturated fill material without risking long-term water quality degradation.

Aydilek et al. (2006) conducted several laboratory and field studies to investigate the performance of tire chips as a drainage medium in landfills by comparison with the traditional filling material; gravel. They indicated that tire chips can be used as a landfill leachate collection layer, even though they may not be suitable if placed near drinking water sources.

There are several extensive review studies on the use of GRs in geotechnical applications, compiling both the advantages and disadvantages. According to Edil (2008); in GR applications, groundwater pollution caused by tire leaching was very limited in terms of many inorganics, although iron and manganese levels are increasing. If the rubber particles are placed under the groundwater level, these leaching are more effective and can be used with precautions. Contrary to this concern about environmental pollution, the substantial absorbent capacity of tire material makes it a potential material for

environmental protection and improvement when in contact with contaminated waters and leachate.

Mohajerani et al (2020) said that the common result of studies conducted in recent years is the leachate of metals is much more at low pH values, so waste tire scraps with steel belts are more suitable for use in soil or groundwater environments with neutral pH values. Mohajerani et al. (2020) added that the leaching results from laboratory procedures such as TCLP can be much higher or lower than the leaching results of scrap tire pieces used in natural soil environments.

Liu et al. (2020) listed the studies in which scrap tire particles were mixed with soil and revealed that the maximum leached metals when mixed with clay are Copper and Nickel, while the maximum leached metals when mixed with sand are Fe and Mn. They also emphasized that the mixing ratio and environment are quite effective.

CHAPTER 3

THE LIQUEFACTION POTENTIAL OF TIRE GRANULATED RUBBER - SAND MIXTURE: SHAKE TABLE TESTS

3.1. Introduction

As mentioned in Chapter 1, one of the main scope of the thesis is investigating the effects of GR on the liquefaction potential of sand deposits when GR mixed with sand. For this purpose, three different GR groups with varying diameters were mixed with clean sand with three mixing ratios and filled into a large-scale laminar box mounted on a one-direction shake table. After get the mixtures saturated, a total of ten shaking tests were performed. Excess pore water pressure, surface settlement of soil deposits, and seismic motion of shake table were recorded. According to the results, the liquefaction potentials of filling materials were compared, and the outcomes were discussed. As a result of the comparative study, the GR can be a suitable mitigation material against liquefaction when used with sand as a mixture. GR size and their ratio in sand mixture significantly affect the change of liquefaction potential and settlements of sands.

This chapter first presents when soil deposits were remediated with granulated rubbers, tire chips, tire-derived aggregates etc. Then, the materials and experimental setups used in experimental studies were explained in detail. The experimental matrix and the methods used to perform the experiments were explained. Lastly, the results were discussed, and the comparative outcomes were concluded.

3.2. Materials

A number of laboratory tests have been performed to identify the physical and mechanical properties of sand and GR used in experiments. Also, this section describes the experimental setup consisting of a shaking table, laminar box and instrumentations. In the next section, shake tests are explained in detail.

3.2.1. Silica Sand

The sand used in this study was sieved and classified as silica sand. The silica sand was purchased from a local supplier company in the Babaeski-Kırklareli region. Several experimental studies were carried out with the silica sand to define physical and mechanical properties, which were sieve analysis (ASTM D6913/D6913M-17), maximum and minimum void ratio (e_{max}-e_{min}) (ASTM D4253-16, ASTM D4253-00), and specific gravity test (ASTM D854-10). The properties of silica sand can be seen in Table 3.1 and the gradation curve in Figure 3.1. Also, the pictures and Scanning Electron Microscope (SEM) of silica sand were shown in Figure 3.2. As seen in Figure 3.2, silica sand particles were semi-ground shape. Silica sand was classified as Poorly Graded Clean Sand (SP) according to the Unified Soil Classification System (USCS). Table 3.1. shows the elements and their proportions in the sand particles found by X-ray fluorescence spectrometers (XRF) analysis. As seen in Table 3.1., silica sand contains a large amount of Silica (Si), Aluminum (Al), Iron (Fe), and Potassium (K) elements. The methodology of SEM and XRF analysis were explained in detail in the following sections.

Table 3.1. Properties of Silica Sand

Soil	D_{50} (mm)	D_{10} (mm)	D_{60} (mm)	C_U	C_C	G_S	e_{max}	e_{min}
Silica Sand	0.16	0.09	0.2	2.22	1.42	2.74	0.855	0.749

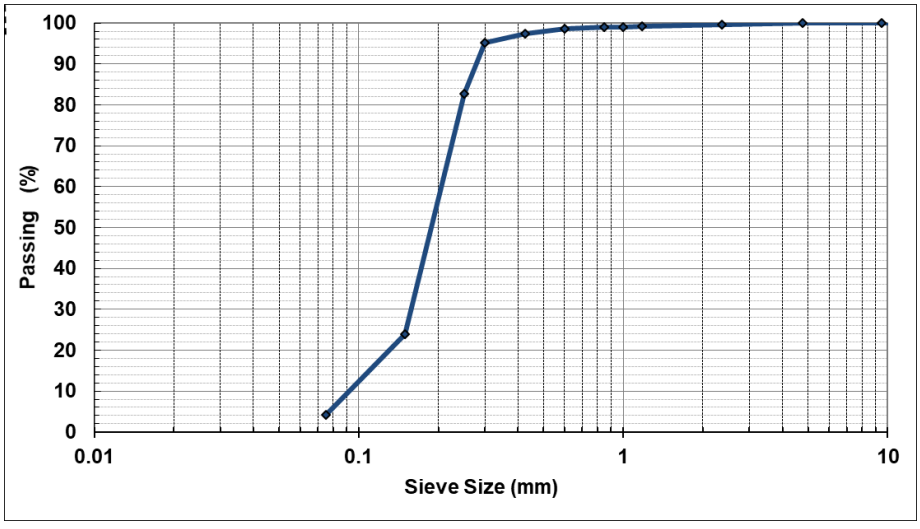

Figure 3.1. Gradation curve of silica sand

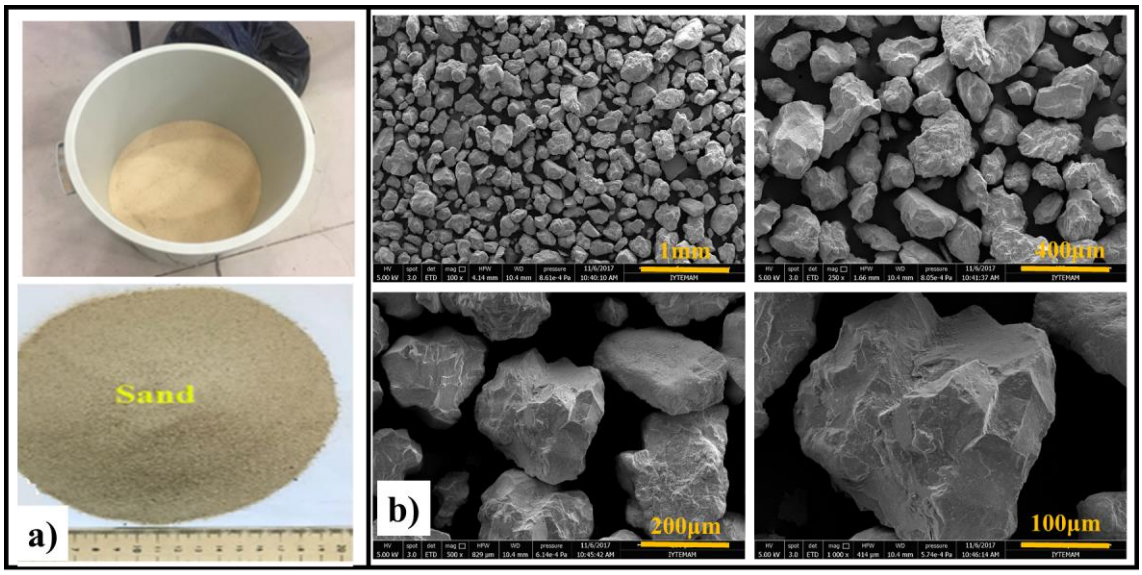

Figure 3.2. Silica sand's a) photo b) SEM pictures

Table 3.2. Elemental analysis (XRF) result of Silica Sand

Symbol	Element	Concentration (in weight)
SiO_2	Silicon	85.75%
Al_2O_3	Aluminum	9.09%
K_2O	Potassium	2.19%
Fe_2O_3	Iron	0.75%
CaO	Calcium	0.65%
P_2O_5	Phosphorus	0.50%
MgO	Magnesium	0.45%
Ba	Barium	0.38%
Na_2O	Sodium	< 0.11%
CuO	Copper	0.083%
ZrO_2	Zirconium	< 0.068%
SrO	Strontium	0.04%
MnO	Manganese	0.03%
Te	Tellurium	0.02%
SO3	Sulfur	0.01%
Cl	Chlorine	0.01%

3.2.2. Tire Granulated Rubber

The Granulated Rubber (GR) used in this study were waste tire rubber pieces purchased from a local supplier in big barrels. GR was sieved and classified into three groups according to their equivalent diameters; 2.5-5mm, 5-10mm, and 10-15mm. While

granulating, fiber and steel belts inside the waste tire were removed. The GR groups and their pictures are shown in Figure 3.3.a, while all of the GR stock in big barrels are shown in Figure 3.3.b, and the SEM picture of 2.5-5mm GR particle is shown in Figure 3.3.c. GR particles have irregular shape as seen in Figure 3.3.c.

Several experimental studies have been carried out with the GR to define physical properties, which were sieve analysis (ASTM D6913/D6913M-17) and specific gravity test (ASTM D854-10). Figure 3.4 shows the gradation curves of granulated rubbers. Checking the gradation curve of granulated rubbers (Figure 3.4) and the photos given in Figure 3.3 together, it can be said that nominating the scrap tire rubbers as "Granulated Rubber" is correct according to the ASTM D5681-20 (Table 3.).

Table 3.3. Properties of Granulated Rubbers

Granulated Rubber Size	D_{50} (mm)	D_{10} (mm)	D_{60} (mm)	D_{30} (mm)	C_U	C_C	G_S
2.5-5mm	4	3.4	4.02	3.9	1.18	1.11	1.12
5-10mm	5.8	4	6	5.6	1.50	1.31	1.19
10-15mm	10.2	10	10.4	10.1	1.04	0.98	1.28

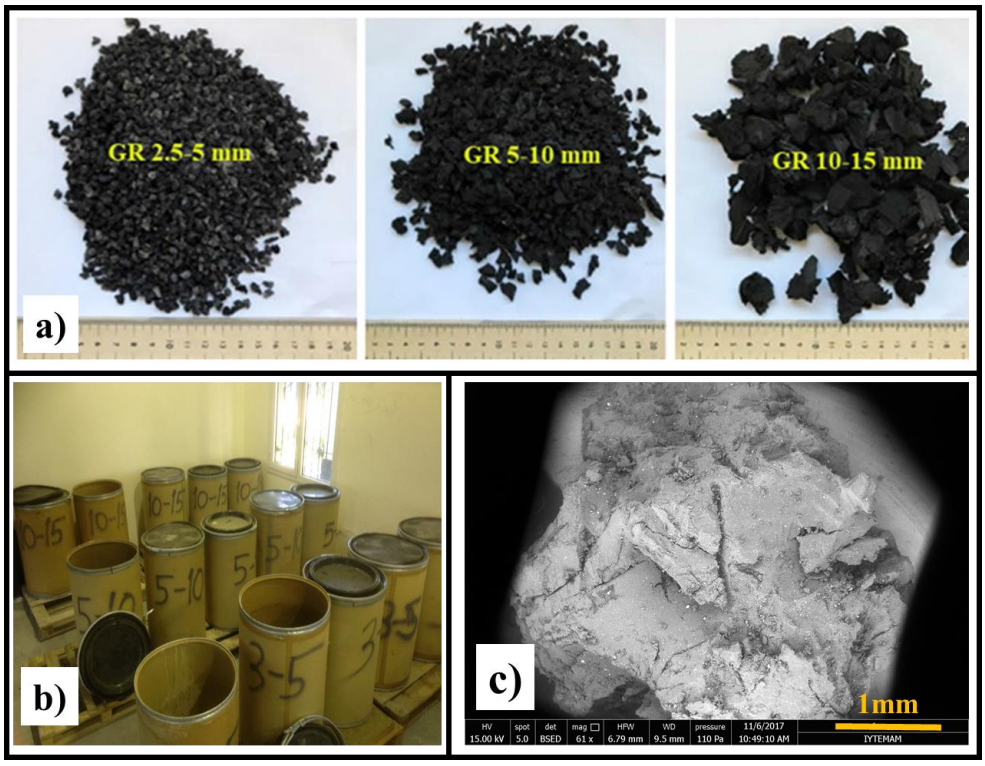

Figure 3.3. Granulated Rubber's pictures

a) groups and pictures, b) stock in big barrels, and c) SEM picture of 2.5-5mm GR particle.

Table 3.3 shows the elements and their proportions in the granulated rubber particle with a 2.5-5mm equivalent diameter found by XRF analysis. As seen in Table 3., GR contains a large amount of Zinc (Zn), Sodium (Na), Calcium (Ca), Sulfur (S04), and Magnesium (Mg) elements.

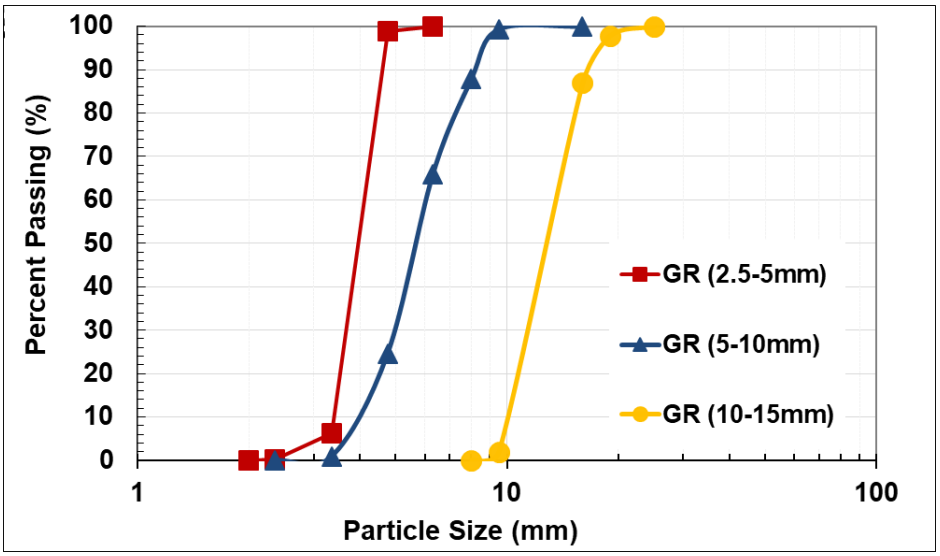

Figure 3.4. Gradation curves of Granulated Rubbers

Table 3.4. Elemental analysis (XRF) result of Granulated Rubber

Symbol	Element	Concentration (in weight)
ZnO	Zinc	27.37%
Na_2O	Sodium	25.95%
CaO	Calcium	22.26%
SO_3	Sulfur	11.12%
MgO	Magnesium	6.96%
Al_2O_3	Aluminum	3.63%
Cl	Chlorine	1.21%
WO_3	Tungsten	0.95%
CuO	Copper	0.238%
Fe_2O_3	Iron	0.113%
ZrO_2	Zirconium	< 0.068%
MnO	Manganese	0.037%
Bi	Bismuth	0.032%
Ba	Barium	0.024%
SrO	Strontium	0.020%
NiO	Nickel	0.019%
Mo	Molybdenum	0.018%
Br	Bromine	0.012%
Nb_2O_5	Niobium	0.011%
Ag	Silver	0.008%

3.3. One Dimensional Shake Table and Laminar Box

In order to understand the liquefaction resistance of sand and GRS mixtures with varying GR content, 1g shake table tests were conducted in this study. Laminar box system and CPTu system were designed for the test setup (Ecemiş, 2013). One-dimensional laminar box system is consisted of a strong floor, a 1-D shake table, a servo-motor actuator, a computer-controlled system (to give shaking to the 1-D shake table), a laminar box, and a membrane. Instrumentation and data acquisition system are described in this section in detail. The components consisting of the shake table and laminar box are explained briefly in this study; for more information about these components in detail, please see Kahraman (2013) and Ecemiş (2013).

3.3.1. Strong Floor

IZTECH - Civil Engineering Department's structural laboratory, which is well equipped for static and dynamic structural tests, has a strong floor. The strong floor has 1m thickness, and it was constructed with heavily reinforced concrete (C25) and reinforced steel (S420). The shake table was mounted on this strong floor.

3.3.2. One-Dimensional Shake Table

Dimensions of the aluminum shake table have the length of 2.04 m, the width of 0.82 m, and the thickness of 0.08 m. The load capacity of the shaking table is 16 tons, its maximum displacement is ±1m, its maximum velocity is ±1m/s, and its maximum acceleration value is 1.2g. Figure 3.9 and Figure 3.10 show the shake table and the first laminate of the laminar box mounted on the table. A servo-motor actuates the sinusoidal one-dimensional shaking of the table. A schematic representation of the shake table and actuator can be seen in Figure 3.5, and a picture of the shake table were shown in Figure 3.6. Photos of the servo-motor actuator can be seen in Figure 3.9 and Figure 3.10.a.

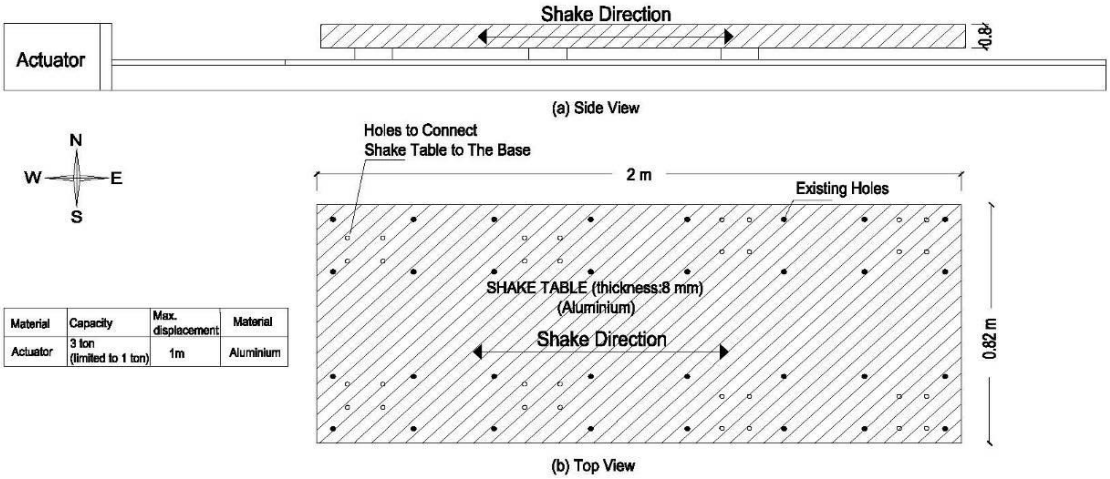

Figure 3.5. Schematic view of Shake Table

a) Side View, b) Top View (Source: Kahraman,2013)

Figure 3.6. Shake Table and first laminate mounted to shake table

3.3.3. Laminar Box

The laminar box consisted of 24 laminates, each 1.834m long and 0.62m wide. Laminates were made of I beams with a height of 0.57 and a width of 0.108m. The total height of the laminar box was 1.55m. Roller and stopper mechanisms allow them to move in one direction and stop at maximum displacement between laminates placed on top of each other (see Kahraman, 2013). The laminar box was designed by Ecemiş (2013) to simulate earthquake-induced shaking conditions in the free field in the most realistic way based on the criteria by Whitman and Lambe (1986). The maximum displacement of each laminate is 0.014m in longitudinal directions; the cumulative displacement of the laminar

box was 0.322m. Schematic illustrations of the laminar box were shown in Figure 3.7.a, while the picture of the laminar box was shown in Figure 3.8.a at the resting position. Also, the schematic illustrations of the laminar box were shown in Figure 3.7.b, while the picture of laminar box was shown in Figure 3.8.b at maximum displacement position. Figure 3.9 and Figure 3.10 show the laminar box pictures.

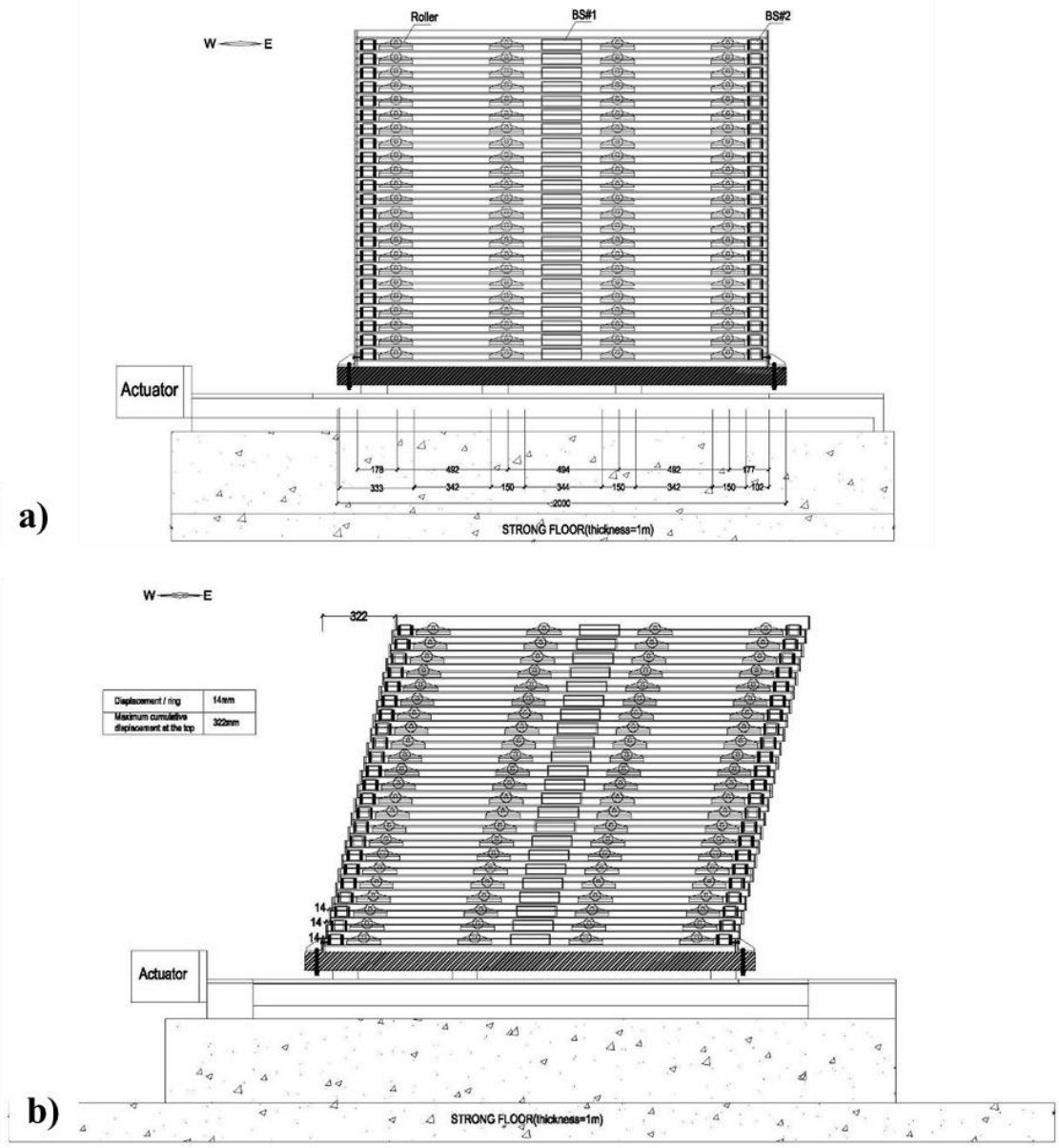

Figure 3.7. Schematic illustrations of the laminar box

a) at the resting position, and b) at maximum displacement position.

(Source: Kahraman,2013)

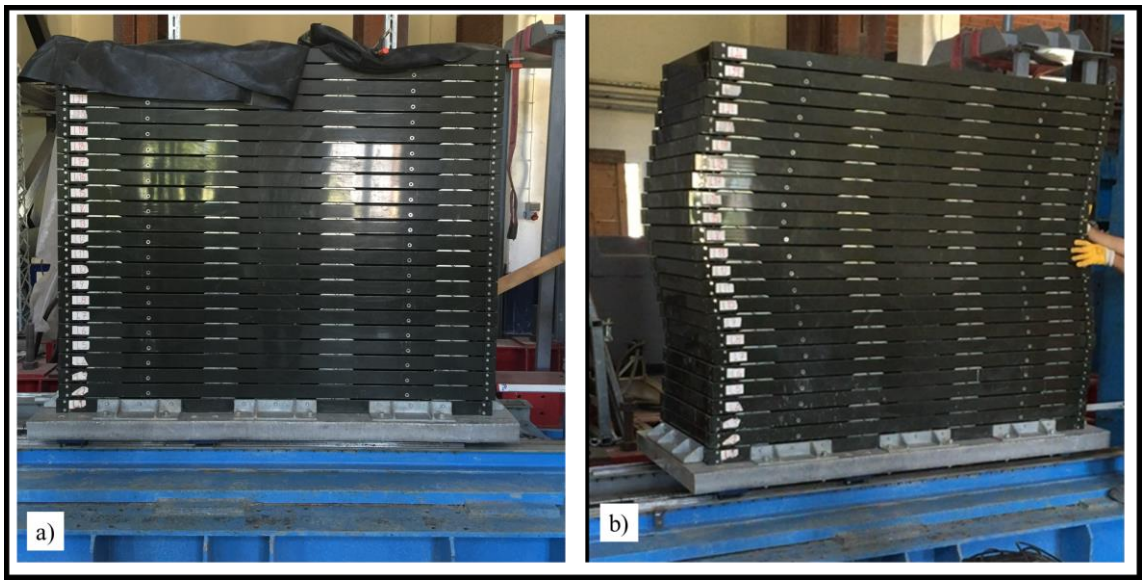

Figure 3.8. Laminar box pictures,
a) resting position, b) during its' flexible movement

3.3.4. Membrane

In this study, a 1mm thick membrane made of EPDM rubber material was used so that the shaking table simulated undrained conditions and did not prevent the free field conditions provided by the laminar box. EPDM membrane was synthetic rubber produced from ethylene and propylene materials. The dimensions of the membrane were larger than the laminar box to allow it to move freely within the laminar box. The length of the membrane was 1.8m, and the width was 0.8m. The EPDM membrane was carefully placed in the laminar box. The membrane was provided to take the same shape as the laminar box, and it was temporarily attached to the top laminate so that its form would not deform during filling the soil materials and water (Kahraman 2013, Ecemiş 2013). Figure 3.9 and Figure 3.10.b show the membrane attached to the laminar box.

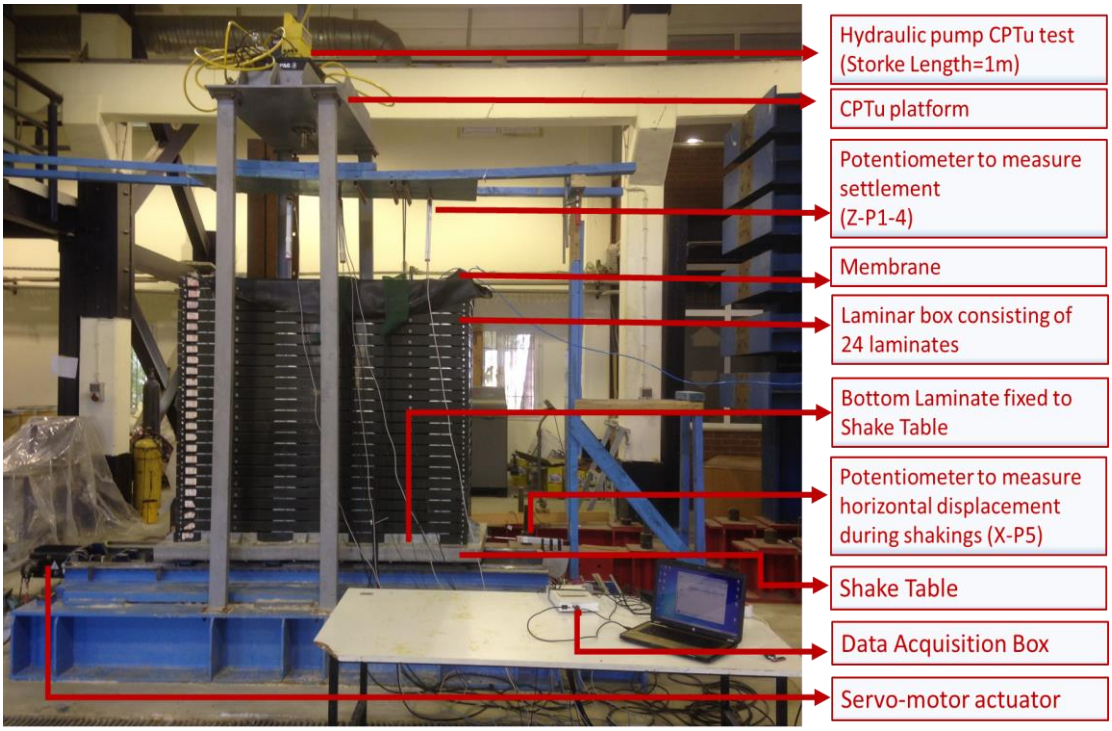

Figure 3.9. Laminar box test setup and components.

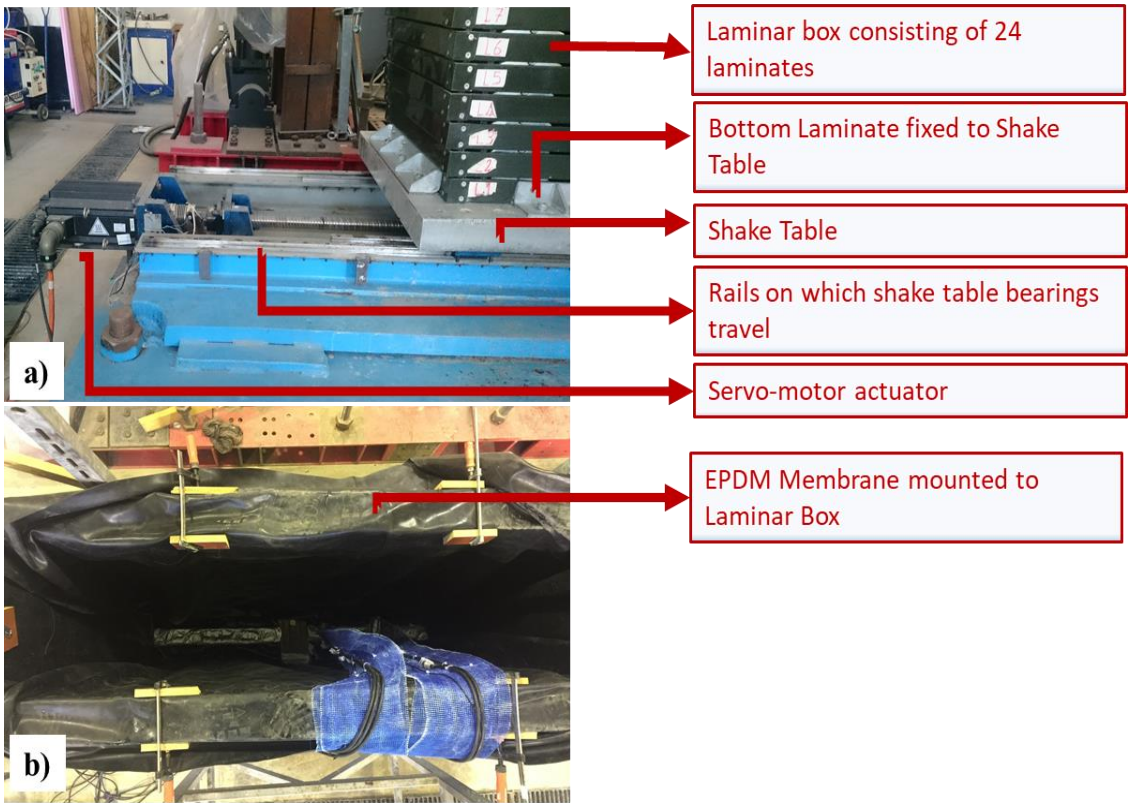

Figure 3.10. Laminar box and shake table components
a) actuator, shake table, and laminar box b) membrane

3.4. Instrumentation

Shake table tests that were conducted for this part of the experimental work required high-density sensors consisting of five pore water pressure transducers and three linear potentiometers. For Chapter 4, more instrumentations were added to this setup and explained in detail in Chapter 4.

3.4.1. Potentiometers

Three identical linear potentiometers (LPM) were used with a 300mm displacement capacity. One of the potentiometers named "X-P5" measured the horizontal displacement of the shake table tests during the shakings, while the other two potentiometers named Z-P1 and Z-P4 were placed vertically on the surface of the soil model to measure the settlement of the soil during and after shakings. Figure 3.11.a shows the linear potentiometer, which was horizontally placed to measure shake table displacement, while Figure 3.11.b shows the LPMs, which were vertically placed to measure soil settlement during and after the shaking. Figure 3.9 and Figure 3.13 show the places of the potentiometers.

The wooden plate above the laminar box setup was used to fix the LPMs placed vertically which used for measuring the level soil surface. LPM tips were intended to measure soil surface settlements, but the tips could sink into the soil that making it difficult to measure the level of the surface. For this reason, a polymer plate with a density of about ($1.5gr/cm^3$), (less than saturated soils ($1.8gr/cm^3$), and more than water ($1gr/cm^3$) was placed on the ground surface. This plate did not sink into the saturated soil before liquefaction and did not float on the water during and after liquefaction. Thus, the plate always remained on the surface of the settled soil. By mounting the tips of the vertical LPMs on this plate, soil settlement was clearly measured during and after shaking. Figure 3.11.b shows the plate on surface of soil and it was named as “settlement plate”.

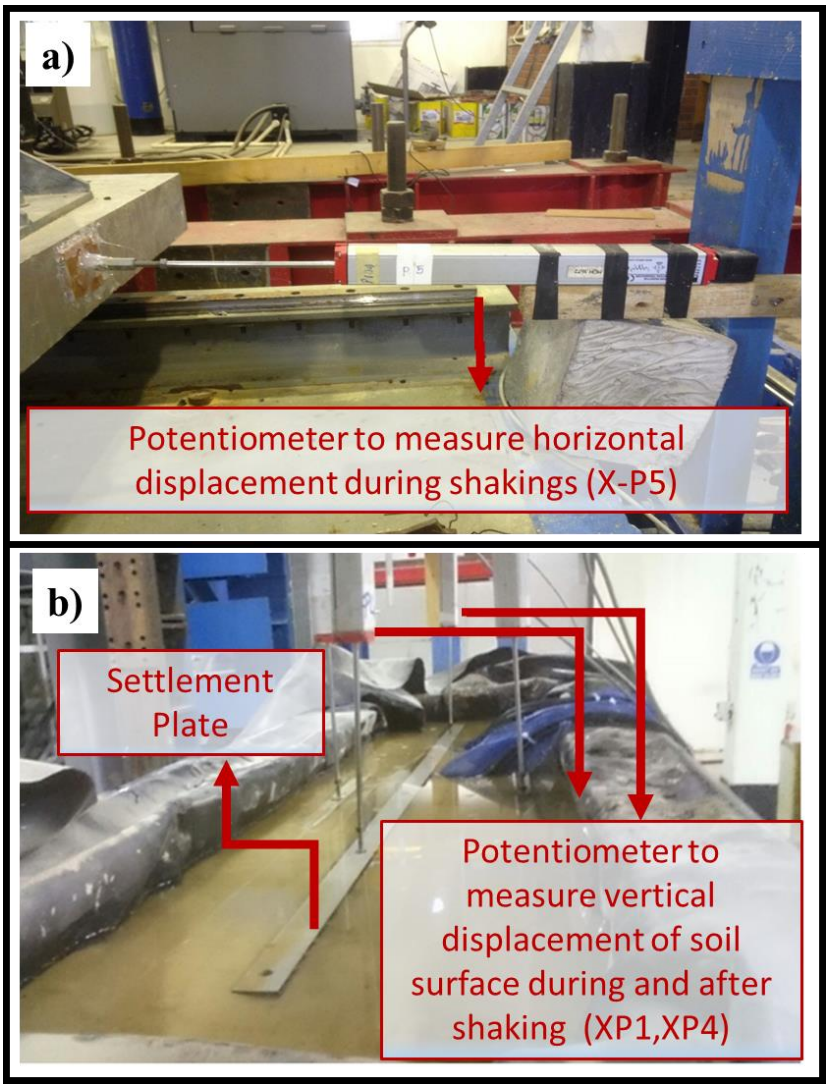

Figure 3.11. Linear Potentiometers (LPMs)

a) horizontally placed to measure shake table displacement b) vertically placed to measure the settlement of soil during and after the shaking

3.4.2. Pore Water Pressure Transducers

Excess Pore Water Pressure Transducers (EPWPT) were also placed inside the soil deposits to monitor the data of excess pore water pressure (EPWP). These data indicated soil liquefaction has occurred and recorded the initiation time of the liquefaction.

The type of the EPWPT is KPC-500, and the capacity is 500kPa. They were bought from Tokyo Sokki Kenkyujo Co. Ltd. The EPWPTs' had a cylindrical shape with 40mm diameter and 57mm length. The connection cable of the EPWPT was $0.5mm^{2,}$ and its length was 10m. EPWPT was made of strong steel materials, can resist high lateral

soil pressures, and can be buried into the soil. EPWPTs have porous filters with 30mm diameter at bottom to allow the water through inside a cell in it and can read pore water pressure values up to 500kPa with precision. These porous filters were kept waiting in water before being mounted to the EPWPTs.

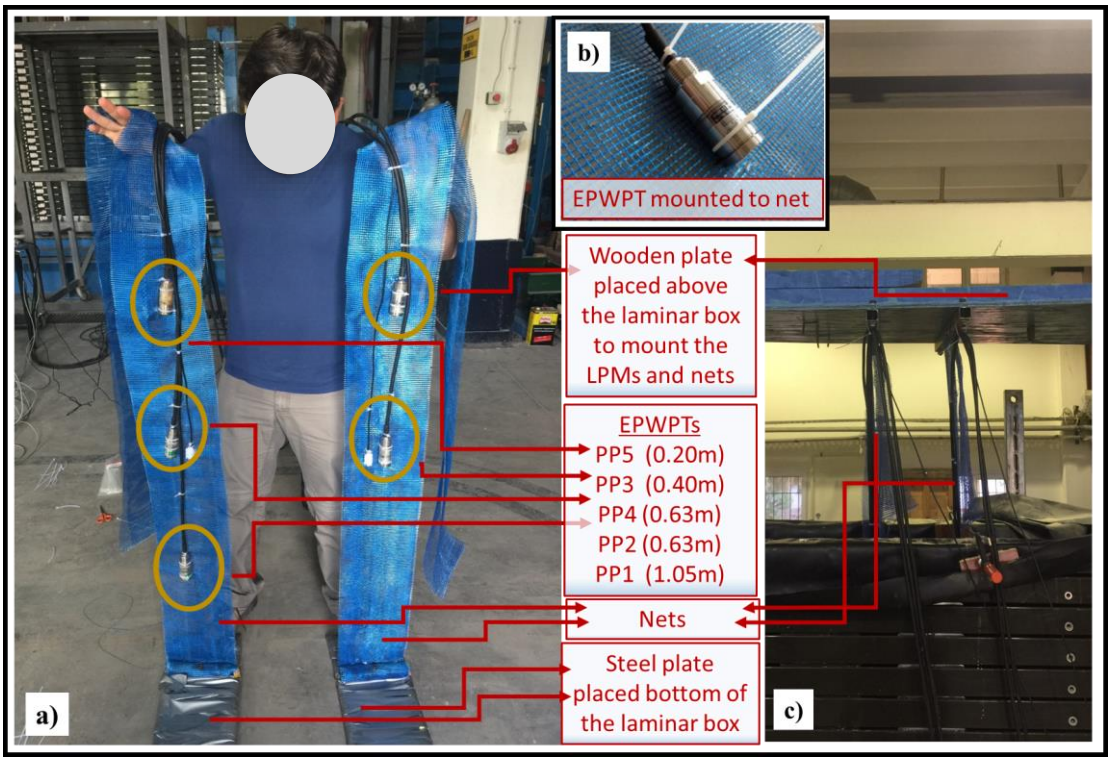

Figure 3.12. Pictures of Excess Pore Water Pressure Transducers (EPWPT) a) EPWPTs mounted to nets and steel plate at bottom, b) an EPWPT, and c) nets mounted to wooden plate above the laminar box

EPWPTs were tied on nets to place in the laminar box with different depths. Three EPWPTs were placed on a net, and two EPWPTs were placed on another net. These nets were mounted to a steel plate at the bottom of the laminar box and mounted to a wooden plate that was placed above the laminar box. Hence, nets and EPWPT were placed in two rows vertically in the soil model. Figure 3.12.a shows the nets, EPWPTs, steel plate placed at the bottom, Figure 3.12.b shows the nets mounted to wooden plate above the laminar box, and Figure 3.12.c shows a EPWPT mounted on the nets. Name of the EPWPTs were PP1, PP2, PP3, PP4, and PP5, and their depths from the surface of the filling soil in the laminar box were 1.05m, 0.63m, 0.40cm, 0.63m, and 0.20cm respectively. A schematic representation of EPWPTs' places in the test setup was shown

in Figure 3.13. After the soil filling was completed in each trial, the nets and cables of the instruments were unmounted from the wooden plate and released.

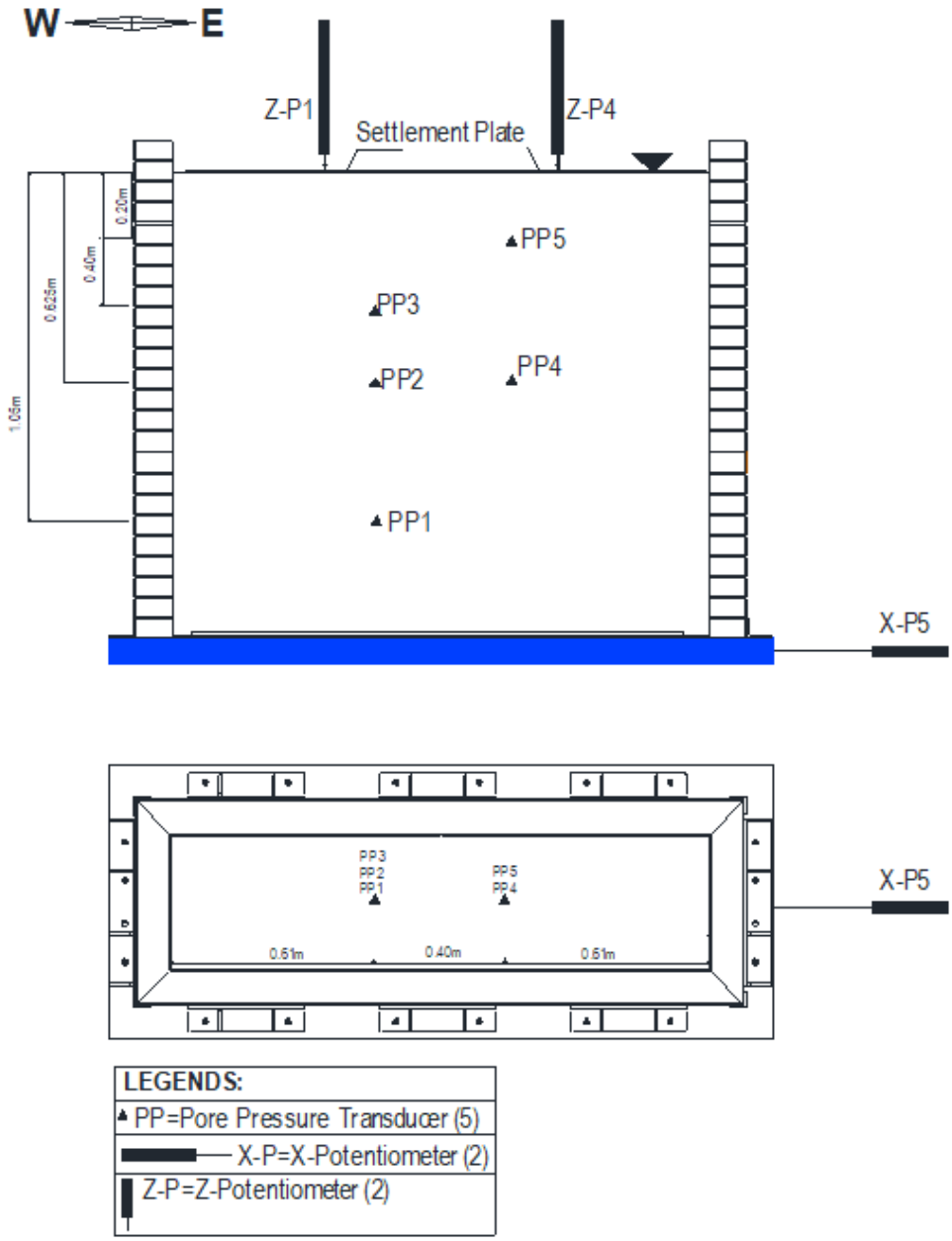

Figure 3.13. Schematic illustration of instruments of the laminar box tests.

3.4.3. Data Acquisition System and Software

LPMs and PWPTs were connected to a data acquisition box (DAQ). DAQ was used for collecting the signals from instruments and converting these signals into the proper units and engineering data which recorded during the experiments. The name of

DAQ was National Instruments' (NI) DAQPad-6259 Pinout. Figure 3.14.a shows the DAQ, Figure 3.14.b shows the DAQ with energy cable, Figure 3.14.c shows the DAQ and signal cables of all instruments, and Figure 3.14.d shows the DAQ connected to the computer. DAQ had 32 channels consisting of 16 analog and 16 digital channels. Sample rate of a single channel is 1.25MS/s, timing resolution is 50ns, timing accuracy is 50 ppm of sample rate, input coupling is DC. The input range is between ±01V and ±10V, and maximum working voltage for analog inputs is ±11V. For more information, see the manual of DAQ at www.ni.com/pdf/manuals/37521c.pdf.

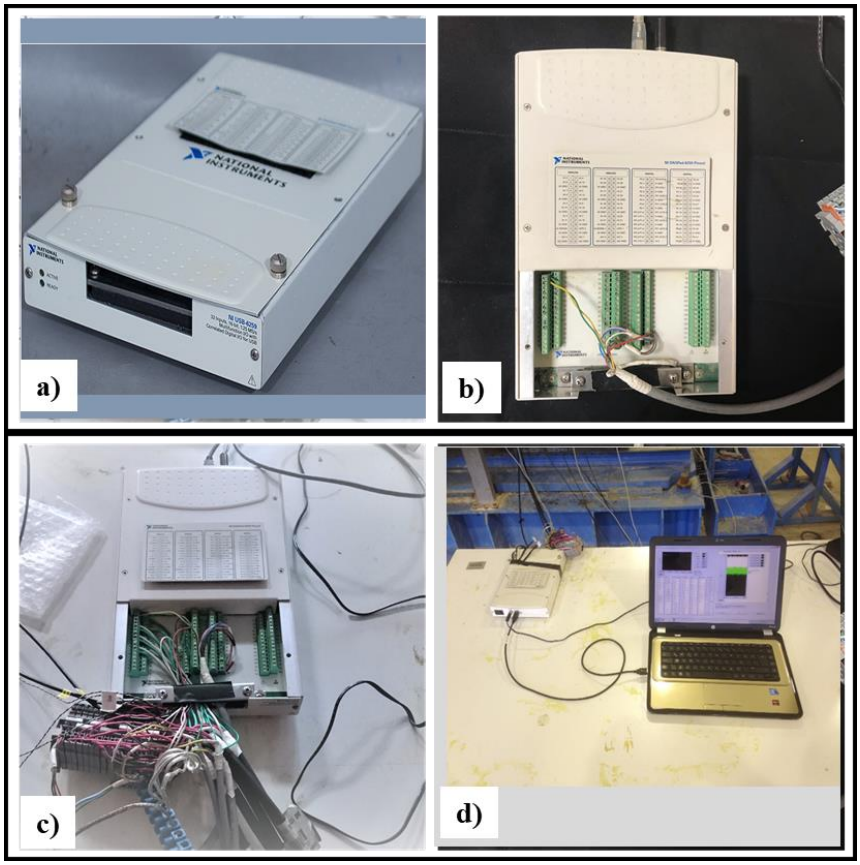

Figure 3.14. Photos of Data acquisition box (DAQ) and instruments' connections,
a) DAQ, itself, b) and c) DAQ with instruments' connection cables, d) reading the data from DAQ

All of the instruments were connected to the DAQ properly by evaluating their calibration values and features. The LabVIEW software was used to record the data of the shake table tests. LabVIEW code was written in accordance with the characteristics of the instruments, and it was ensured that all values were recorded in appropriate units. The schematic form of the LabVIEW code is shown in Figure 3.16. Preparing the code

on the schematic form is one of the features of LabVIEW. As seen in Figure 3.16, signals (as a form of voltage changes) that were collected from instruments by DAQ were defined as input by LabVIEW code in the first step. These signals were converted into engineering parameters and proper units in the second step. In the third step, a low-pass digital filter with a limit of 100Hz was applied to clear the data from noises. Also, Figure 3.16.b shows the interface of LabVIEW low-pass filtering. The user interface of LabVIEW during data recording is shown in Figure 3.15.

LabVIEW was designed to record the data with two different frequencies. Two different text files that recorded 500 data per second and 2 data per second were obtained as output for each shaking trial. As records, the data was saved as two different text files. High-frequency data (500 data per second) was used to accurately examine rapid pore water pressure or settlement changes during the shaking time (first 20 seconds). Low-frequency data (2 data per second) was used to examine the dissipation of excess pore water pressure and settlements after shaking for a long period after the shaking (4-5 minutes).

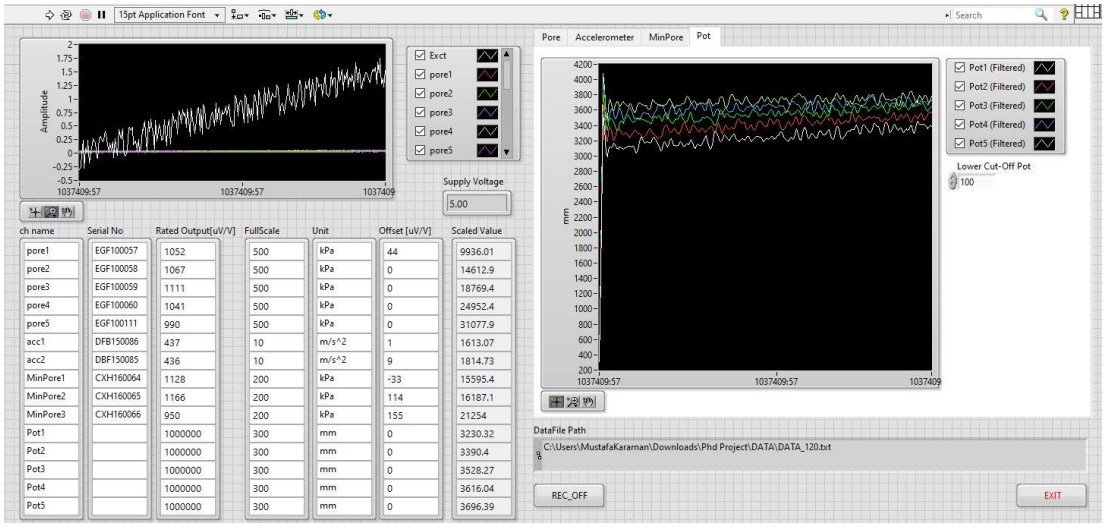

Figure 3.15. LabVIEW interface while recording data

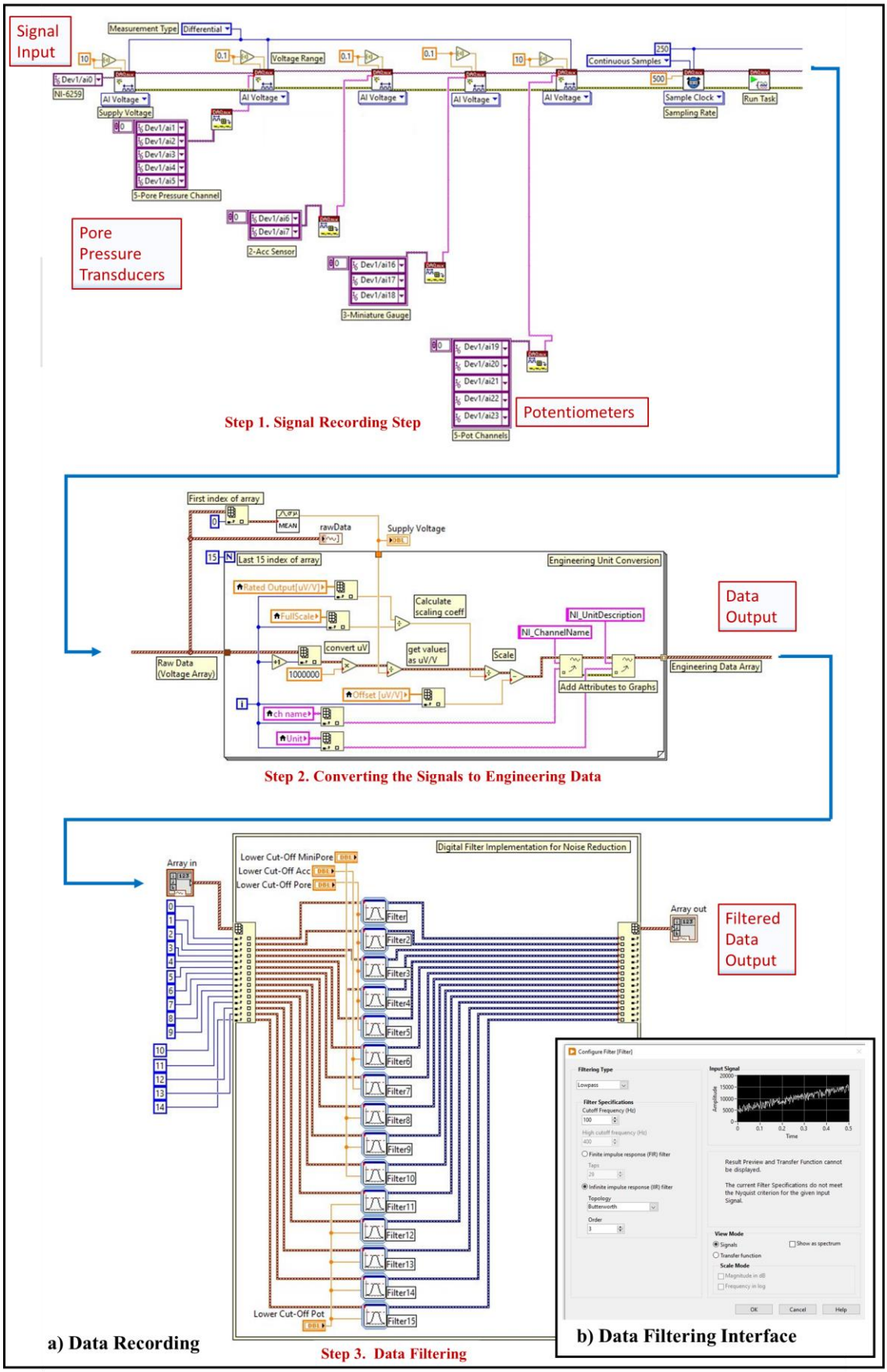

Figure 3.16. LabVIEW code for processing data

Although low pass digital filtering codes were added in the LabVIEW code and all the cables were shielded, there were a lot of noises in the recorded data for all experiments. DIAdem, a mathematical software product of National Instruments, was used to filter the noises of the data as post-operation works. All the noises in the data were cleared by applying a low pass digital filter with varying limits (0.5-50 Hz) using by DIAdem. Figure 3.17.a shows the DIAdem screen while filtering data, and Figure 3.17.b shows an example of data consist of the original and filtered data.

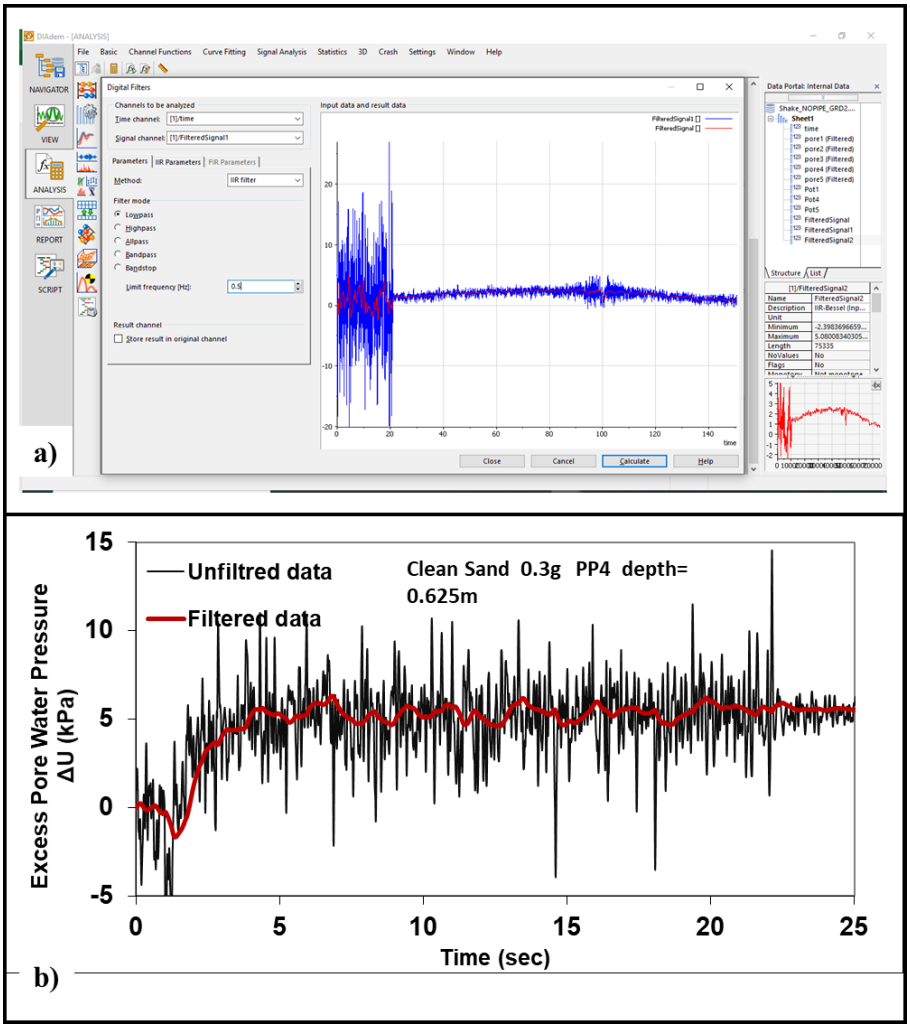

Figure 3.17. Examples of DIAdem filtering process

a) Screen view of the DIAdem, b) Example of raw and filtered data of EPWP.

3.5. Piezocone Penetration Test (CPTu) System

Piezocone Penetration Tests (CPTu) were performed for all shaking tests after saturating the soil deposit and before the shaking tests. The Cone Penetration Test (CPT) is a method used to determine the geotechnical engineering properties of soils and delineate soil stratigraphy. The Piezocone Penetration Test (CPTu) is a type of electrical CPT, which includes additional instrumentation to measure the pore water pressure during penetration at the level of the base of the cone.

The first electrical cone penetrometer was developed in 1948 by the municipal engineer Bakker in Holland, which was called as the ‘‘Rotterdam cone’’(Massarsch, 2014). Schmertmann (1974) added a feature in a probe to measure pore water pressures during cone penetrations and called this cone and probe as a piezometer probe. CPTu measure three major data continuously for all depth; the cone resistance (q_c), local shaft friction (f_s), and pore water pressure (u). In the late 1970’s, another CPT system was developed by Geotech Co. and has become popular for the last three decades. This CPTu system does not require a cable to transmit the measured data from probes, it uses a microphone and transmits the data acoustically. In this study, the wireless CPTu was used before all the shake table tests. The CPTu is a field test, and the cone must be penetrated in the field with a constant velocity. In the field, this work is usually done with a pushing mechanism on the truck. In this study, a special system consisting of a hydraulic pump and a platform was used to penetrate the CPTu cone into the soil model placed in the laminar box. The platform and hydraulic pump setup were developed by Ecemiş (2013). In this section, the CPTu system was described in detail.

The CPTu pieces of equipment can be divided into three parts; cone penetrometer, pushing equipment, and data acquisition system. Piezocone consists of a 60° cone with a 10 cm^2 base area (35.7 diameters) and a 150 cm^2 friction sleeve located above the cone. This model is the most widely used and accepted reference test equipment. In the piezocones, pore pressure is typically measured at three different locations, as shown in Figure 3.27. These pore pressure sensors are known as: on the cone (u_1), behind the cone (u_2), and behind the friction sleeve (u_3). For this study, the data acquisition system, piezocone, and other equipment for the CPTu test were manufactured by Geotech Co, Sweden.

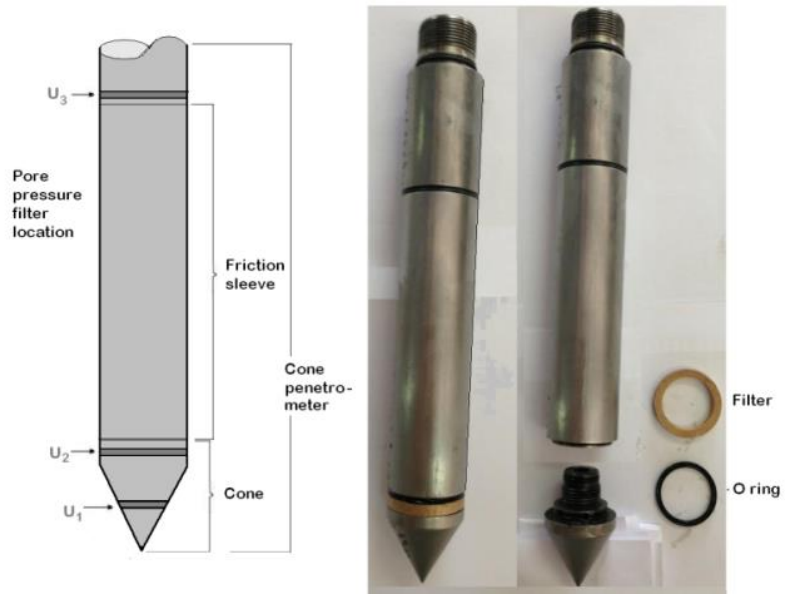

Figure 3.27. Schematic presentation and picture of the piezocone,
(a) shematic presentation, b) piezocone with its filter and O-ring elements

The wireless piezocone probe is shown in Figure 3.18. Components of the probe were numbered in the figure as follows; 1) Cone, 10 cm^2, 2) O-ring, 3) Filter Ring, 4) X-ring, 5) Support Ring, 6) O-ring, 7) O-ring, 8) O-ring, 9) Friction Sleeve, 10) Cone Body, 11) O-ring.

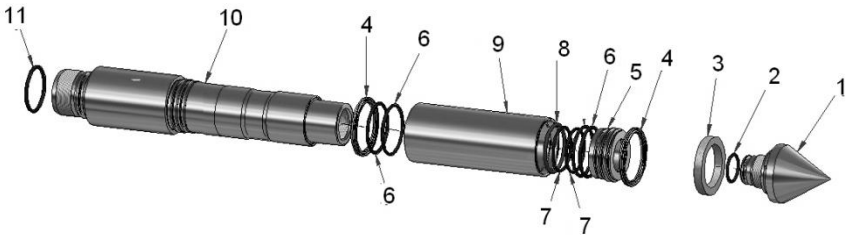

Figure 3.18. CPTu Probe with components
(Source: Geotech Nova CPT Acoustic Manual)

The data acquisition system is a part of the CPTu setup which is including a number of electrical components and software. The components of the system were listed and described as follows and also illustrated in Figure 3.19. Components of the CPTu data acquisition system were numbered in the figure as follows;

1) CPT probe,
2) Microphone,
3) Depth encoder,
4) Computer interface box,

5) Computer,

6) Nova,

7) Rod.

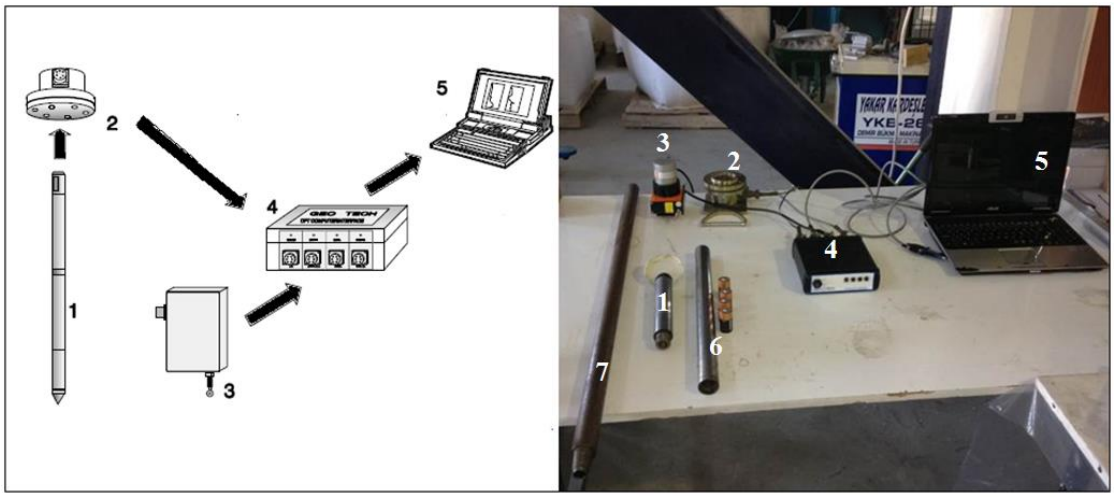

(a) (b)

Figure 3.19. a) Schematic illustration and b) picture of Geotech Nova CPT Acoustic Probe and Data Acquisition System

As mentioned before, the system did not require a cable to transmit measured data from the probe to the soil surface. This was done acoustically; the digitized coded data string was converted into a high-frequency acoustic signal by a piezoelectric element in the nova. The signal was then transmitted up through the steel of the rods to a microphone on the rig or penetrometer. No cable was used for transmitting the data from the probe to the recorder at the surface. From the microphone, the signals were transmitted to a computer interface box, which also received depth information from a depth encoder. The data was then sent to a computer. The data were presented simultaneously on the PC screen as engineering data and graphics (Figure 3.19).

The pore water pressure meter was normally a pressure transducer of steel type. It communicated with a porous filter on the surface of the cone penetrometer via a liquid chamber. The filter element and other parts of the pore pressure system were saturated with a liquid before use. This saturation should be maintained until the cone penetrometer reaches the groundwater surface or saturated soil. The filter should be saturated with de-aired glycerin, silicone oil, or similar which makes it easier to maintain saturation throughout the test. It was good practice to cover the filter element with a rubber membrane, which will burst when the penetrometer came into contact with the soil. The

cone penetrometer was designed in such a way that it was easy to replace the filter and that the liquid chamber was easy to saturate. In general, filter elements were saturated in the laboratory and kept saturated in airtight containers. One commonly used procedure to assemble and saturate the piezocone, when using glycerin or silicone oil, was to use a plastic funnel (Figure 3.20).

In this study, the filter rings were kept in glycerin in a container until they were used (Figure 3.20). To saturate the piezocone with a plastic funnel, the following procedure was done: First, the cone penetrometer was turned upside down, and the cone was removed. The funnel was mounted and slowly filled with glycerin or silicone oil. Using a plastic syringe and hypodermic needle, the cavities in the penetrometer were saturated. The filter was carefully transferred from its container to the funnel and all parts were assembled while submerged in the liquid. In this study, the excess pore water pressure data obtained from CPTu tests were not used.

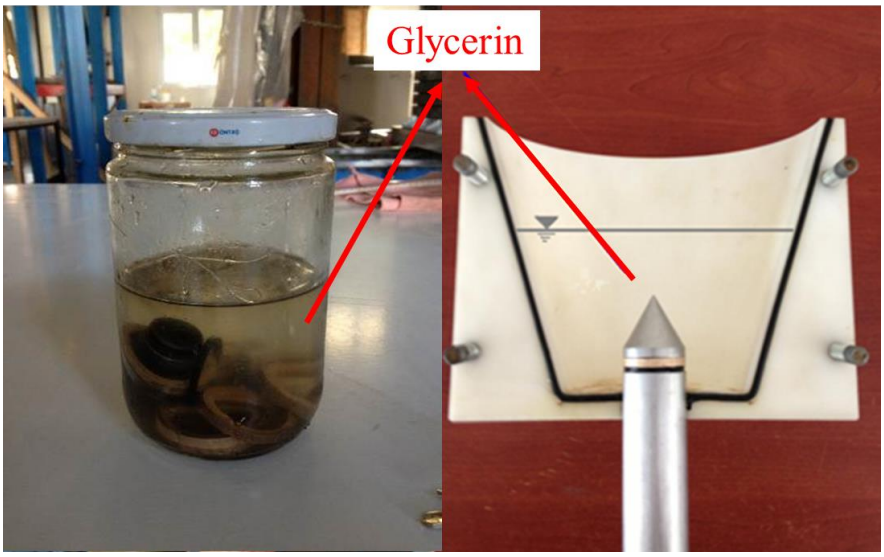

Figure 3.20. a) Filter rings in glycerin b) mounting the ring on a cone in a glycerin funnel

The nova is powered by four pieces of alkaline ‘C’ batteries. The batteries were installed in nova, and the probe and nova were mounted. The total height of the probe and the nova was 720mm, while their diameter was 34.8mm. The microphone should be mounted under the pushing system. The probe and the nova were placed under the microphone. This process is essential for achieving good sound transmission. The rod, which was added to the cone, was made from the best quality of steel available. The height

of this rod was 750mm. The total depth capacity of the CPTu system was 1470mm. A computer interface box and a depth encoder were the electronic components of the CPTu system. The computer interface box collected data from the depth encoder and the microphone, and transferred the data to the computer (Figure 3.19).

The hydraulic pump was carried by a platform made with a 1470mm x 750mm beam. Six plates were welded perpendicular to the beam. The capacity of the system was 5 tons. Four 281cm high U profiles were used as bearings. The bottom and top points of the U profiles were welded to 160mm x 160mm square plates which are connected to I-beams resting on the strong floor (Figure 3.21). Figure 3.21.a shows the schematic illustration and Figure 3.21.b shows the picture of CPTu system. Figure 3.22 shows the side view of the CPTu system illustrations. Figure 3.23.a shows the CPTu system consisting of the hydraulic pump and platform in detail while Figure 3.23.b-c show the CPTu test during the conducting of the penetration.

.

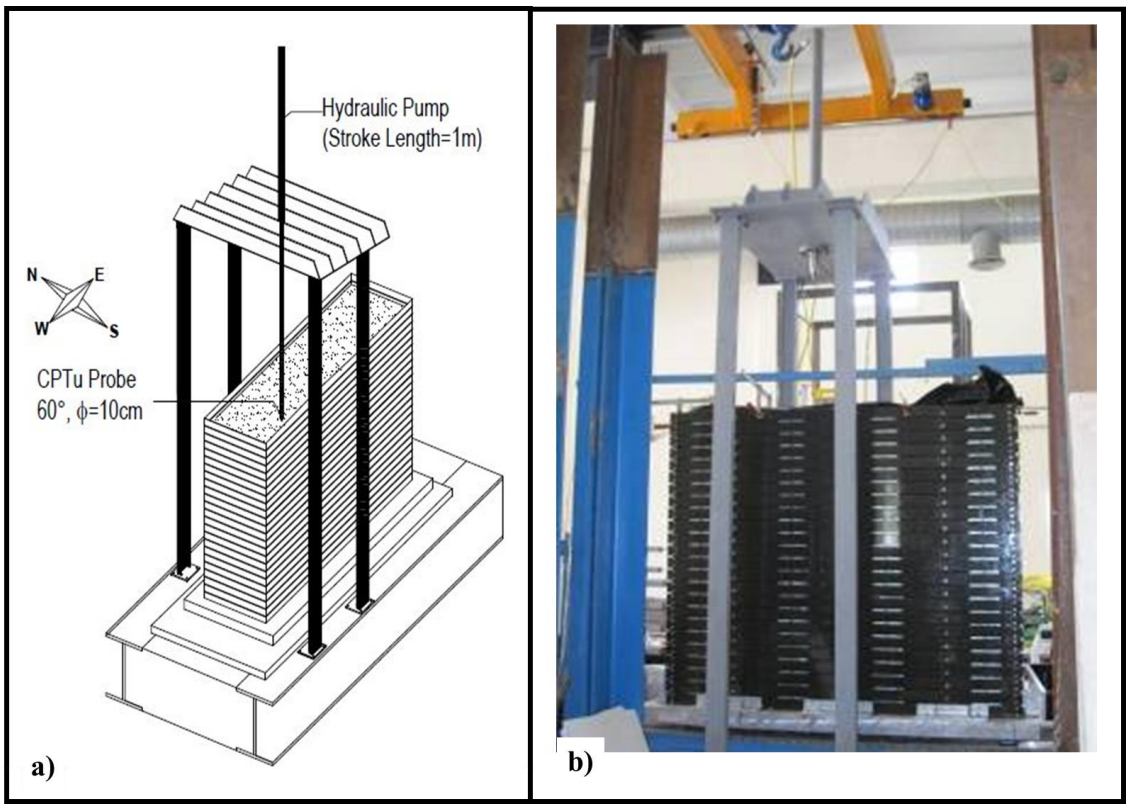

Figure 3.21. CPTu system a) schematic illustration b) picture

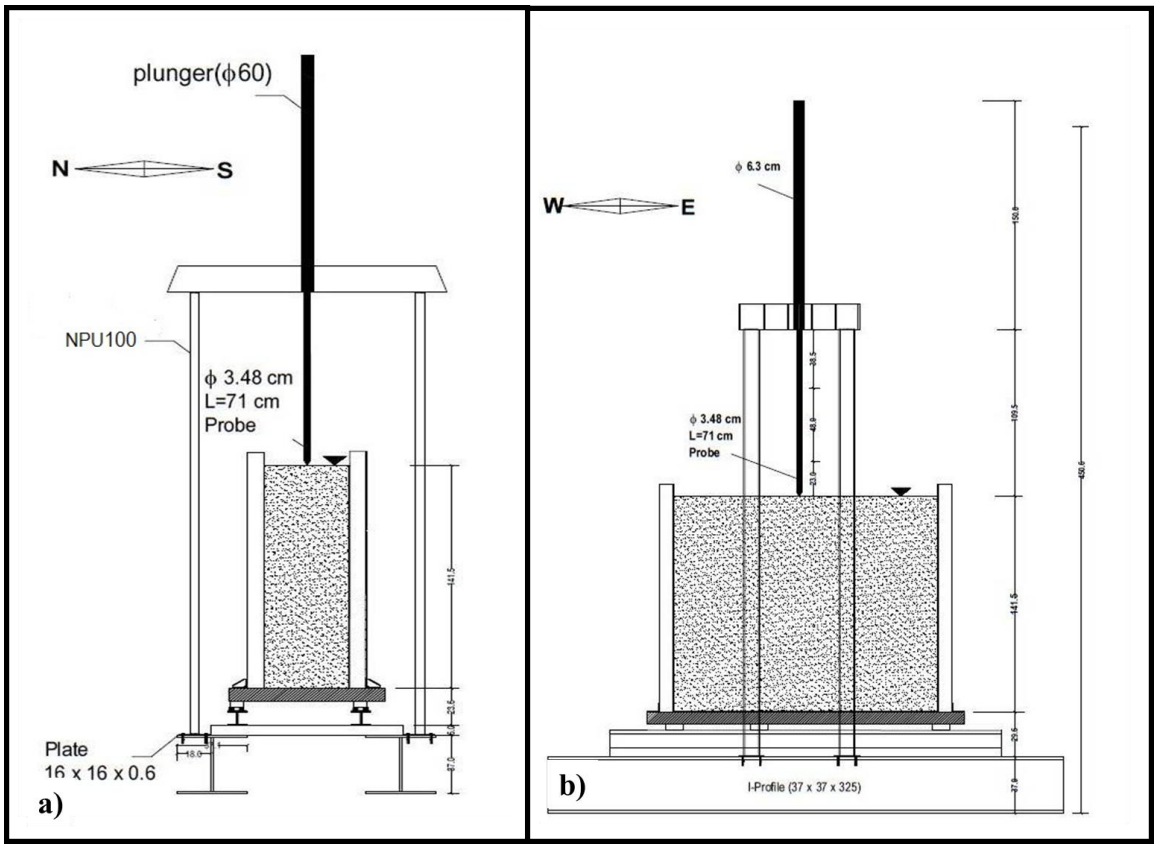

Figure 3.22. Schematic illustrations of CPTu System; side views

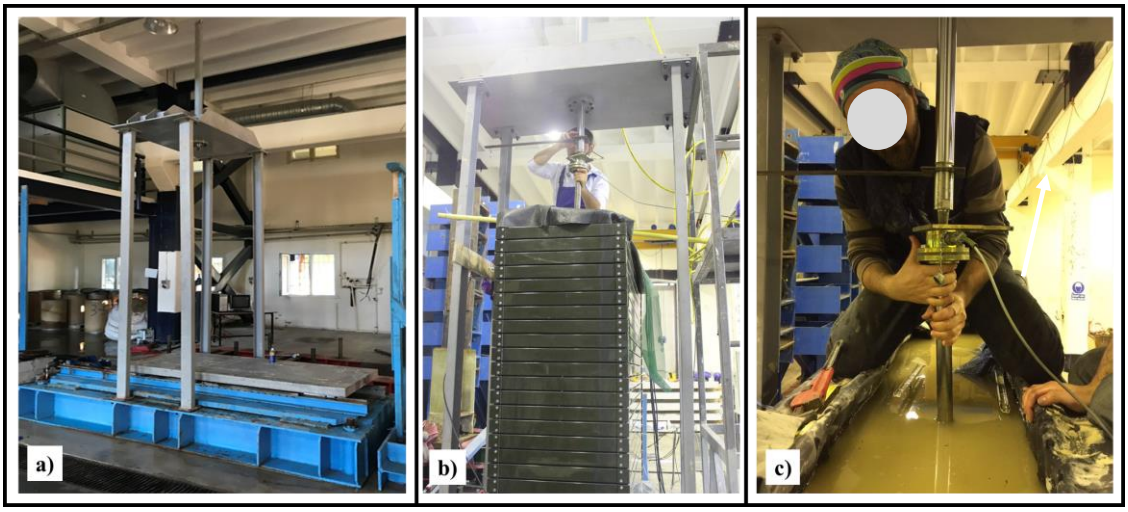

Figure 3.23. Pictures of CPTu System

a) the platform and hydraulic pump, b) and c) while performing the CPTu test

To sum up, the hydraulic pump mounted to the platform above the laminar box were used to penetrate the CPTu probe, and nova set through the soil with a constant penetrating velocity. Thanks to the wireless CPTu system, signals were transmitted from the probe to the microphone acoustically. These signals were transmitted to the computer

interface box and converted to the data there. CPTu tests allowed to record q_c, f_s and u_2 measured over the entire depth of the soil model before all shaking tests. The results helped to calculate the relative density of the soil model prepared in the laminar box and give a clear view to check the soil models density values through the entire depth and to discuss whether the soil model were prepared well or not. The CPTu tests results and calculations were discussed in detail in the results sections.

3.6. Shake Table Tests

For this chapter of the study, a total of ten shake tests were conducted under different backfill conditions to reach comparative results. CPTu tests were also performed to determine the relative density of the soil in the model before each shaking test started. In this section, the filling process of the GRS mixtures, determinations of unit weight of soil models by using buckets, CPTu tests, shaking tests, and the unfilling process were described for each trial. The experimental matrix of ten tests and their results are given below.

3.6.1. Seismic motion

First, the experimental matrix of the shaking test was explained to clarify the scope of the comparative study. All ten shaking tests were performed under the same seismic shaking conditions. The shaking acceleration was 0.36g, the duration was 20sec, and the frequency was 2Hz for all trials.

The seismic motion of the shake table was recorded by the linear potentiometer (LPMs), which was mounted on the laminar box horizontally and named “X-P5”. The displacement by time and acceleration by time plots derived from displacement-time values were showed in Figure 3.24.a and Figure 3.24.b, respectively. As seen in Figure 3.24, the shake table motion was sinusoidal, and the first and last 1 second were starting and ending part of the shaking, while the maximum acceleration was 0.35 g for 18 s duration.

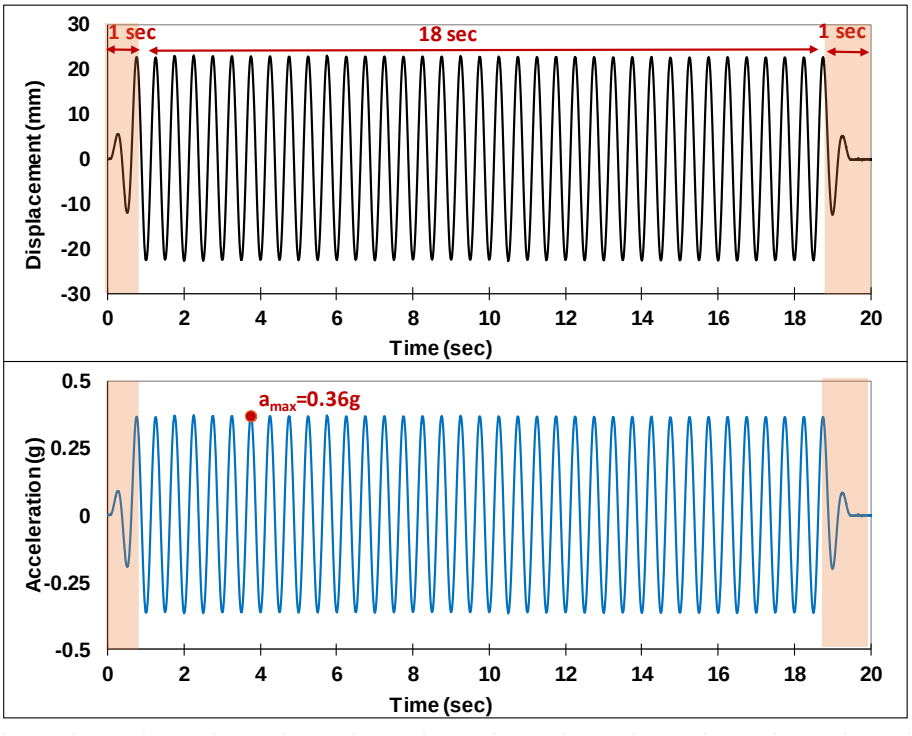

Figure 3.24. Shake table sinusoidal motion displacement and acceleration by time

The bottom layer of the laminar box was filled with compacted medium dense with 65cm thickness, and this layer was not changed during the ten tests. The upper layer of the laminar box was filled with backfill materials consisting of granulated rubber and sand mixture (GRS) with a thickness of 75cm. The Granulated Rubber (GR) size varied in three groups 2.5-5mm, 5-10mm, and 10-15mm, and used by each group three different mixtures were prepared with varying mixing ratios; Granulated Rubber/Sand; 10/90%, 20/80%, and 30/70% in volume. So total GRS mixture trials were nine. Another test was performed before the GRS mixtures tests with loose clean sand.

The experimental matrix of the laminar box shaking test is shown in Table 3.2. Note that in Table 3.2, the test name represents the filling deposits' conditions; "T1" represents the Tests with only Sand. For the other nine trials, the latter "T" is for "Test"; letters "GR" are for Granulated Rubber, S for small size of GR (2.5-5mm), M for middle size of GR (5-10mm), L is for large size of GR (10-15mm), and lastly, number of 1, 2 and 3 represents the ratio of GR in mixture for 10%, 20% and 30% respectively. In Table 3.2, "Acc" means maximum acceleration of shaking and it was derived from displacement data recorded by LPM. D_{10}, D_{50}, C_u, and C_c represent the effective particle size, mean particle size, uniformity coefficient, and the coefficient of gradation, respectively. γ_{sat} is saturated unit weight, and it was determined using small buckets. D_r represents the

relative density of samples, and it was derived from CPTu test data. Gradation curves of all GRS mixtures are shown in Figure 3.25. Pictures of small portions of GRS mixtures are shown in Figure 3.26.

Table 3.2. Experimental matrix of shake table tests

Test Name	GR Size	GR Ratio (by volume)	GR Ratio (by weight)	D_{10}	D_{50}	C_u	C_C	γ_{sat}	$D_{r(avg)}$
-	mm	%	%	mm	mm	-	-	kN/m^3	%
T-S	0	0	0	0.09	0.16	2.22	1.42	20.90	37
T-GR-S-1	2.5-5	10	6.76	0.11	0.2	2.05	1.31	19.27	26
T-GR-S-2		20	10.12	0.11	0.2	2.01	1.34	19.16	35
T-GR-S-3		30	14.35	0.12	0.2	1.91	1.28	18.65	39
T-GR-M-1	5-10	10	4.74	0.12	0.2	1.83	1.23	20.08	29
T-GR-M-2		20	9.08	0.11	0.2	2.10	1.18	19.47	42
T-GR-M-3		30	13.46	0.11	0.2	1.91	1.11	18.55	28
T-GR-L-1	10-15	10	6.43	0.11	0.2	1.91	1.28	20.08	10
T-GR-L-2		20	11.95	0.11	0.2	2.00	1.31	19.37	41
T-GR-L-3		30	13.77	0.11	0.2	2.00	1.02	17.94	20

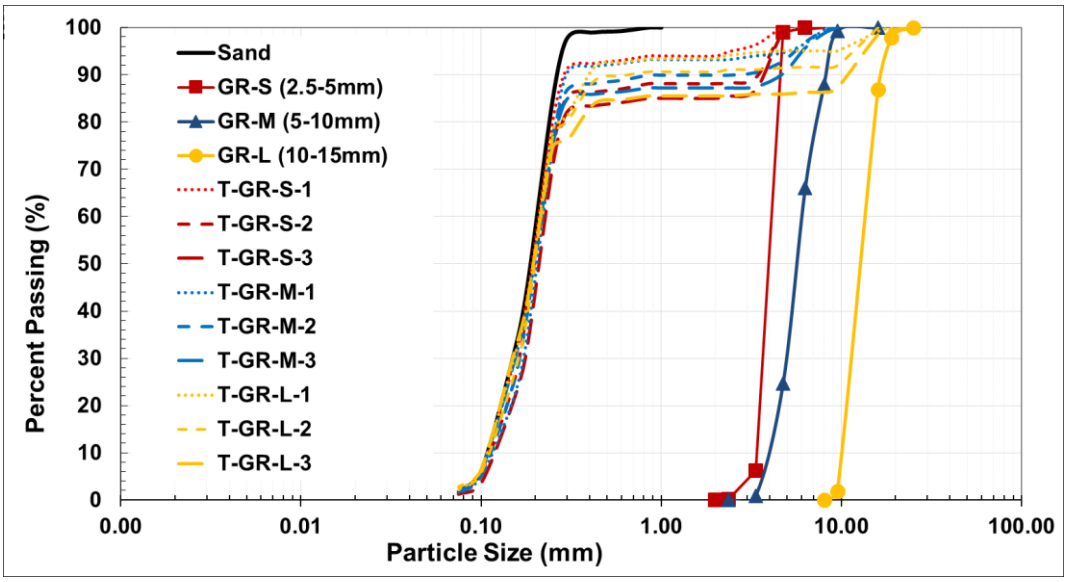

Figure 3.25. Gradation curves of GRs, Sand and GRS mixtures

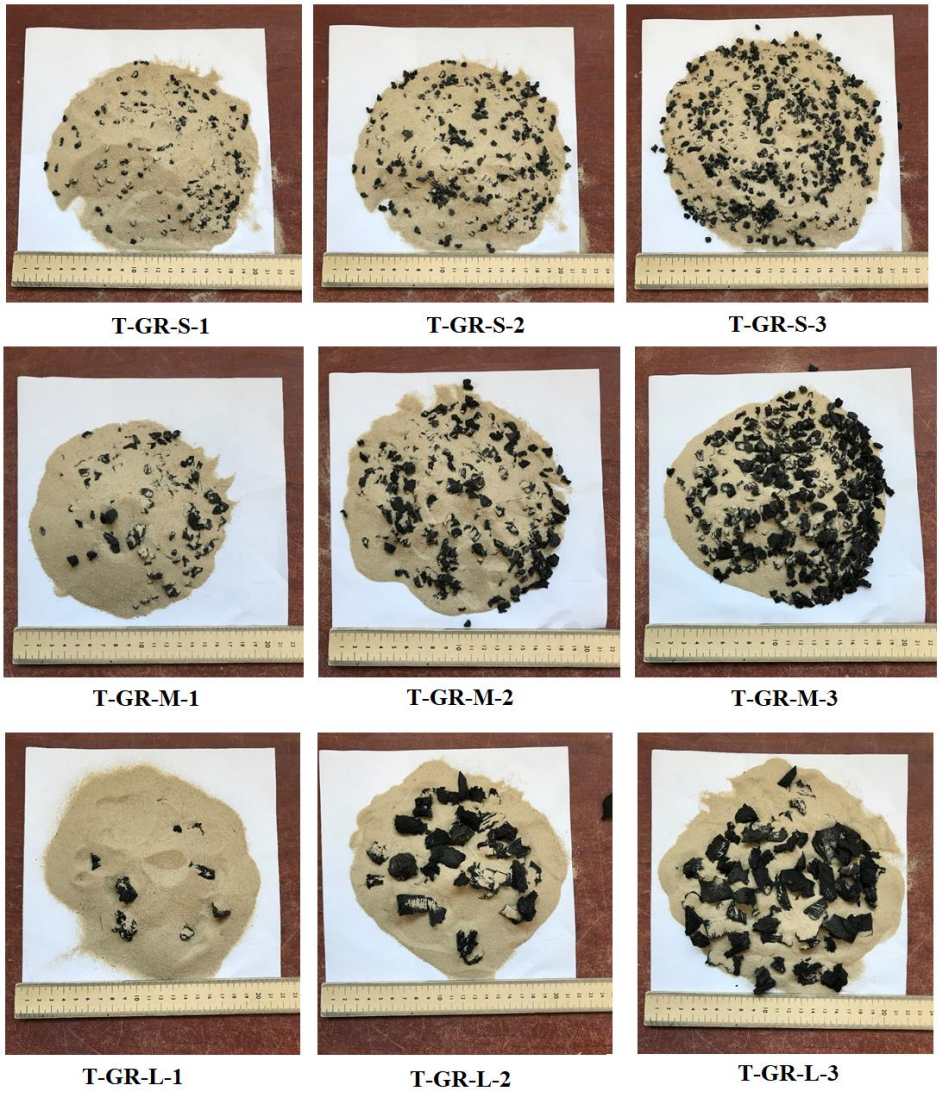

Figure 3.26. Pictures of small portions of GRS mixtures

3.6.2. Sample Preparation and Filling Process

As explained in detail in the previous section, the instruments placed on the nets were mounted vertically in the laminar box, and the EPWPT locations were rechecked. The laminar box was filled step by step with the sand. A fully saturated silica sand deposit was placed into the box by the hydraulic filling technique, allowing sand grains to sink slowly through the water and simulating the process of alluvial deposition of soils in rivers or coastal areas.

The hydraulic filling technique starts with mixing the sand with water in a preparation box and turning it into sand water slurry. This fluid slurry is filled into the laminar box with the help of a slurry pump. Then it is waited until the soil particles are

settle. When the soil particles are separated from the water and settling is completed, the remaining water is transferred back to the preparation box with another water pump placed in the laminar box. Water is mixed with sand for reuse. The slurry pumping process was repeated until the laminar box was filled. Thanks to the hydraulic filling technique, the sand was filled into the laminar box in a loose and saturated state. Figure 3.27.a shows the schematic illustration of hydraulic filling technique while Figure 3.27.c shows the picture pf hydraulic filling process. Water-soil sullry pump, hose and preparation box are shown in Figure 3.27.b.

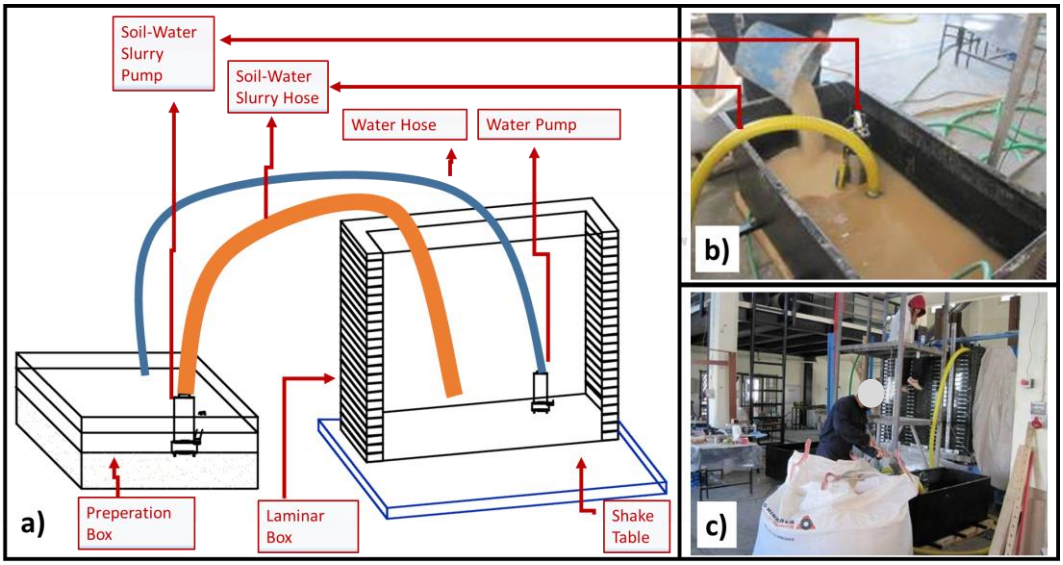

Figure 3.27. Hydraulic filling technique
schematic illustration, b) preparation box, sullry pump, c) filling process
(Modified from Kahraman,2013)

The dimensions of the preparation boxes were as follows; the length of the boxes was 1260mm, the width of the boxes was 650mm, and their height was 510mm. The volume of each box was 420lt. Figure 3.28 shows the preparation boxes.

After filling the sand into the laminar box up to 65cm height, the laminar box was shaken with various accelerations for several minutes to densify the soil. This dense sand layer was prepared to represent the non-liquefiable soil layer at the bottom of the laminar box. Two small buckets tied to rope were placed into the soil each step during the filling process, and water-saturated sand samples were taken from the buckets and weighted. Figure 3.29 shows the sample of saturated silica sand in the small bucket while weighting. The unit weight and relative density of the soil model were calculated thanks to these

samples. Preparation of the dense sand layer and sampling with buckets were schematically summarized in Figure 3.30. The calculated unit weights of the samples taken with the buckets were checked to be sure that the sand deposit was uniform and had the same density through the depth.

Figure 3.28. Soil preparation boxes

Figure 3.29. Weighting the sample in the small bucket

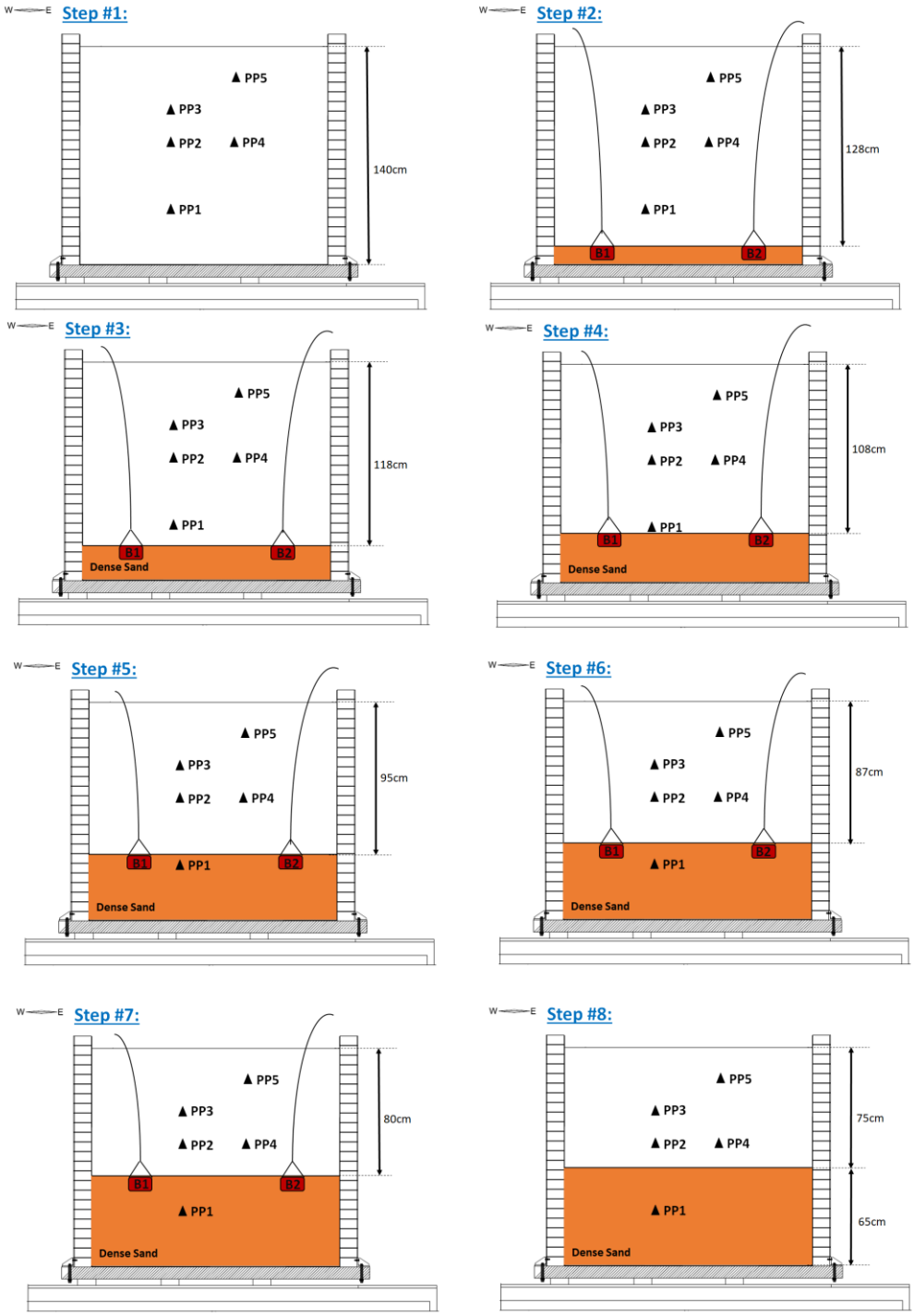

Figure 3.30. Filling the dense sand layer and sampling with buckets

Then, the upper 75 cm loose sand layer was started to be filled for the test “T1”. After the dense sand layer was prepared, the fully saturated silica sand deposit was placed into the box by the hydraulic filling technique for the upper layer. This loose sand layer was prepared to represent the liquefiable soil layer laying on non-liquefiable dense sand. Similarly, buckets were placed for different depths during filling and it was keeping the

collecting of the samples. Preparation of the loose sand layer and sampling with buckets were schematically summarized in Figure 3.31. Average unit weights of bucket samples were calculated and summarized in Table 3.2 as saturated unit weights of the layer.

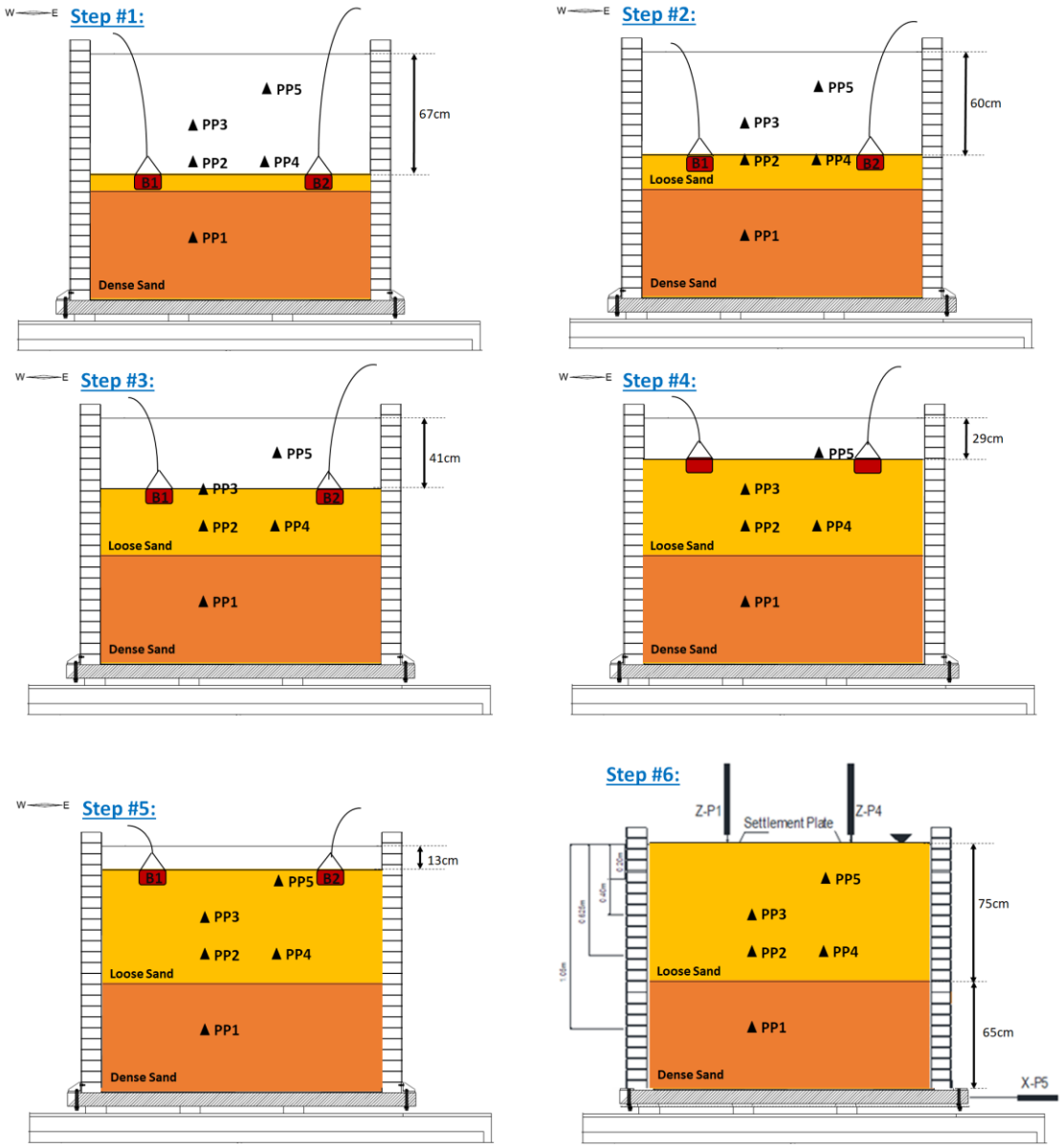

Figure 3.31. Filling the loose sand layer and sampling with buckets

For the other nine tests prepared with granulated rubber and sand ("T.GR.S.1 - "T.GR.L.3"), the upper part of the laminar box couldn't be filled by the hydraulic filling method because of the particle segregation problem. As mentioned before, granulated rubbers' specific gravity was about 1.1-1.3, while the specific gravity of silica sand was 2.6. In literature, it's reported that particle segregation occurs when mixtures are prepared

with two materials and the specific gravity of materials is significantly different (Mahboub and Massie, 1996). To prevent segregation, GR and sand were mixed in a graduated cylinder beaker with a volume of 10 liters (Figure 3.32.a) and placed in a larger bucket (Figure 3.32.b). These mixtures were slowly poured by hand into the laminar box from a height of 20 cm from the soil model surface. Then water is added to the laminar box up to the same level of the deposit for each step. No segregation was observed. The samples of the GRS mixtures, which became saturated at each step, were taken with cylindrical buckets, too. Preparation of the loose GRS layer and sampling with buckets were schematically summarized in Figure 3.33. Unit weights were summarized in Table 3.2. The graduated cylinder beaker, larger bucket, filled laminar box surface, and preparation box are shown in Figure 3.32.

Figure 3.32. Preparation of GRS mixture

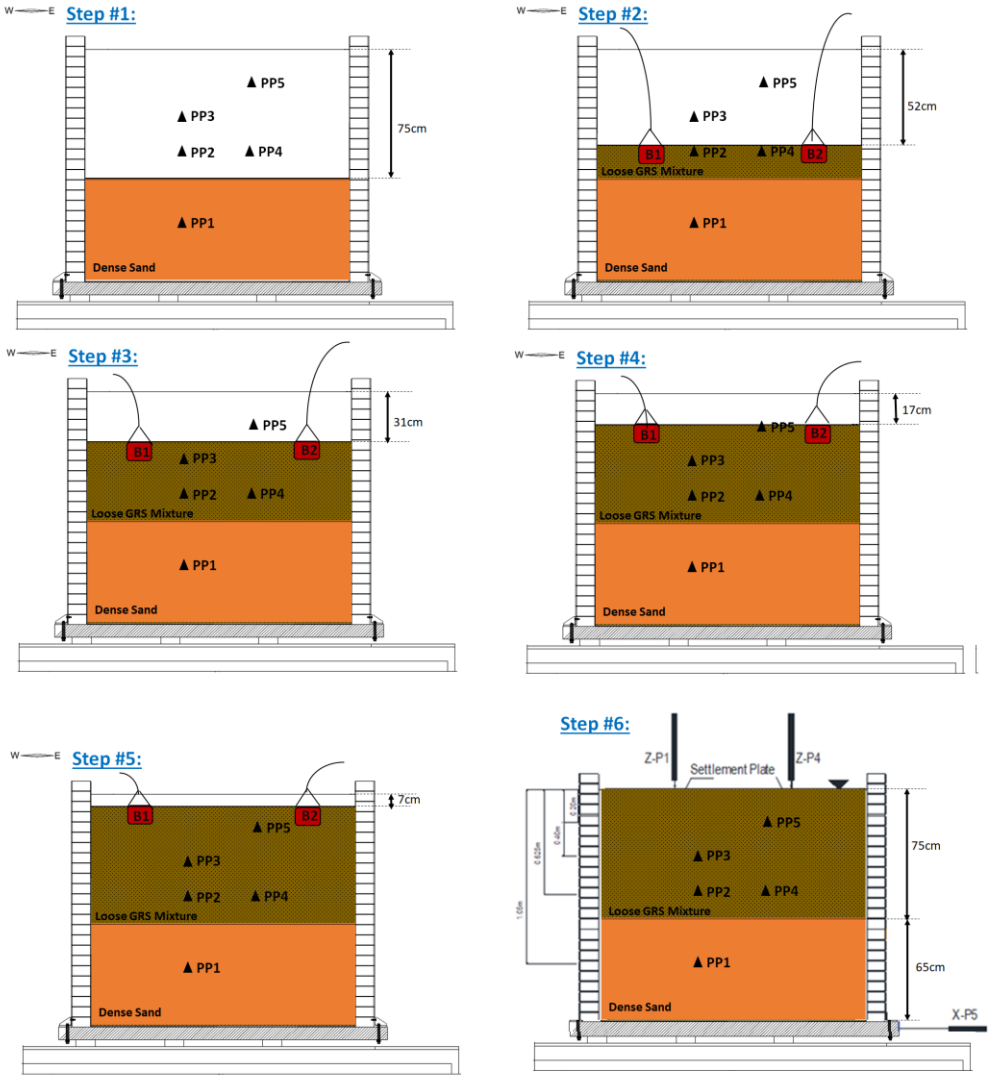

Figure 3.33. Filling the GRS mixture layer and sampling with buckets

3.6.3. Saturation of Soil Model

A series of calibration tests were conducted to ensure that the soil models became saturated with a cylindrical column with an inside diameter of 19cm and a height of 105cm. This cylindrical column was designed to perform water leaching tests, and it was described in Chapter 5 in detail. Nine different GRS mixtures at a prescribed ratio were prepared and filled for 75cm height laying on the 25cm dense sand layer into the cylindrical column. This cylindrical column and soil models were prepared to represent the soil models in the laminar box.

First, after filling the clean sand layer of 25 cm thickness at the bottom, it was compacted with the help of a hammer. Then water was added and waited for two days for

the sand to become saturated. This underlying layer represented the dense saturated sand layer in the laminar box. Then, GRS mixtures were placed on this layer with the same method as in the laminar box for 75cm thickness. Water was added to the loose dry backfill layer from the top of the column, and the water level was marked. As the water seeped downward, the surface's water level decreased. Meanwhile, the decrease in water level was measured in terms of velocity. While the mixture in the column was getting saturated and the water level dropped, water was slowly added after each measurement, and the level remained constant. The speed decreased as the saturation level of the deposit increased. These trials were conducted for each sample for at least 2 hours.

After a certain time, there was no change in the water level for all of the trials. Figure 3.34.a shows the soil model and cylindrical column. The slow process of saturation ensured that the deposit was not disturbed. Figure 3.34.b shows the water level at the top of the soil. Figure 3.35 shows the velocity of the water at the surface of the deposits for different GR diameters and ratios. A typical saturation process for each mixture took less than 1.5 hours. Therefore, for the full saturation process of the mixture deposits inside the laminar box, the sample was left quietly for at least 2 hours after the water was added slowly.

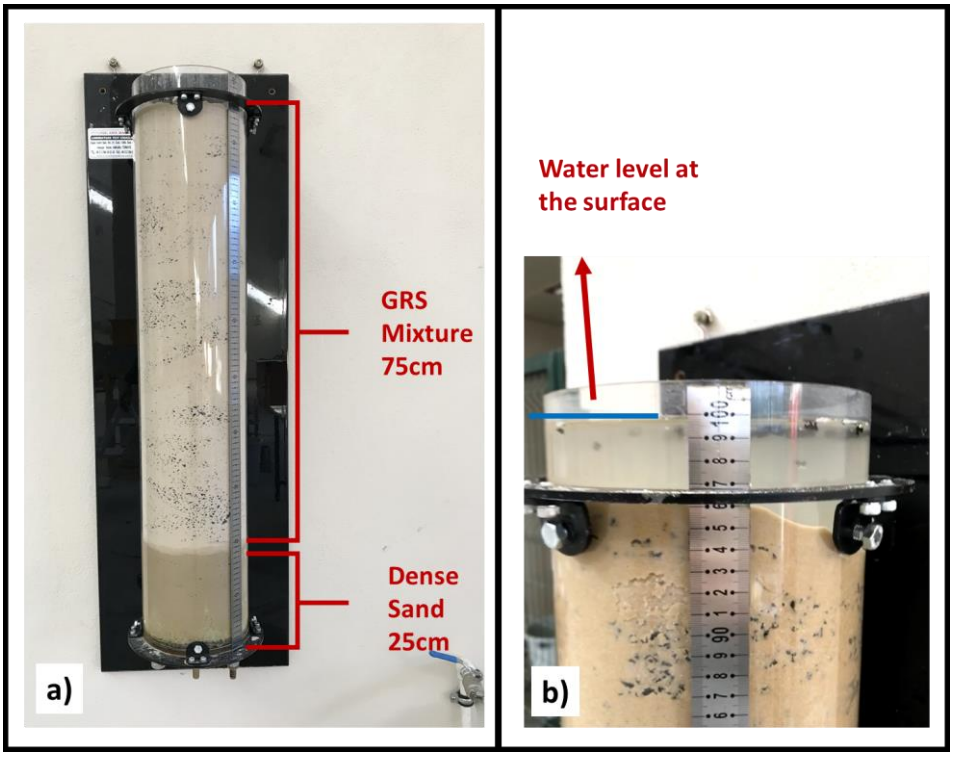

Figure 3.34. Cylindrical column to determine the duration of saturation

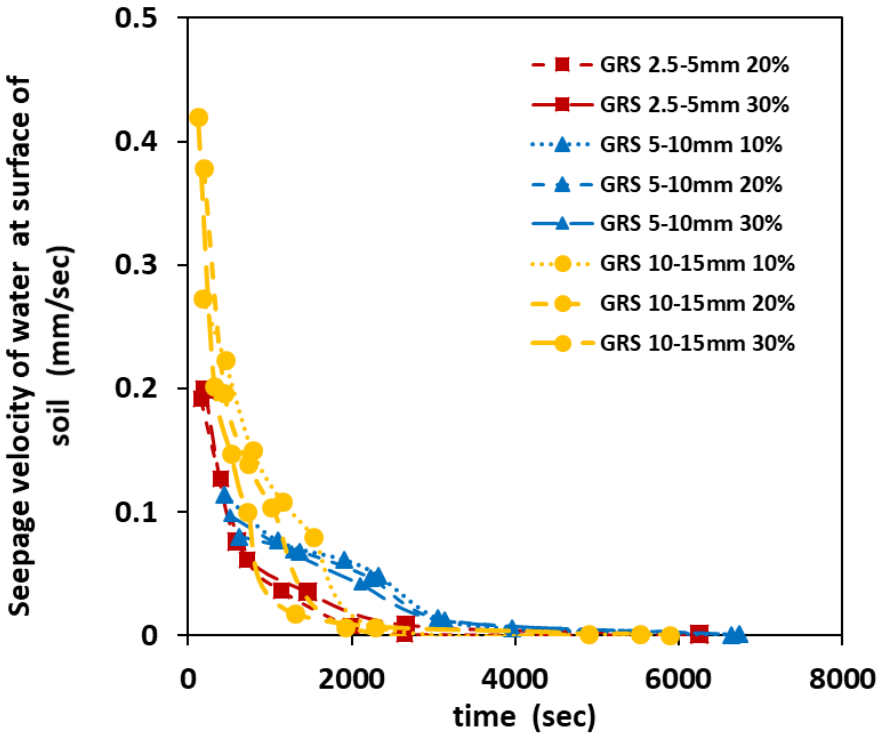

Figure 3.35. Duration for stabilization of water level above the soil surface

3.6.4. CPTu Tests

As mentioned before, CPTu is a field test, and adapting this test to a laboratory large-scale test such as the laminar box had some difficulties. One of the main concerns was the effects of the laminar box walls in terms of boundary conditions of CPTu. The boundaries of the laminar box should be far away enough from the CPTu probe to assume the boundary effects were negligible and represented the free field conditions. Phillips and Valsangkar (1987) determined a ratio between the dimeter of the box (R_{box}) and the diameter of the CPT probe (R_{CPT}) as $R_d=R_{box}/R_{CPT}$. They stated that the side-boundary effects are negligible, even when R_d is at least equal to 5. Renzi et al. (1994) determined that R_d should be equal to 11. CPTu tests were performed at a position where the R_{box} was 45cm, and the CPTu cone diameter was 3.57cm, so R_d=12.5 for the tests. This approves that the CPTu tests can represent the free field conditions without being influenced by side boundaries of laminar box. Figure 3.36 shows the position of the cone during the CPTu tests and the concentric circle of CPT in plan view.

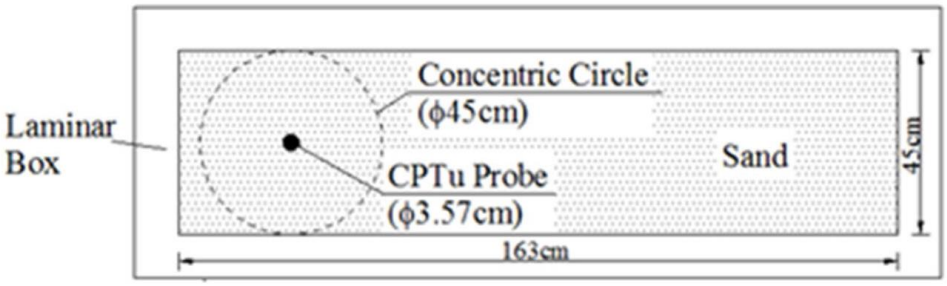

Figure 3.36. Position of CPTu test in laminar box.

CPTu tests were performed using a hydraulic pump as an actuator before each shaking. CPTu penetration velocity was 2cm/s and constant during penetration (ASTM D3441-16). A depth coder was mounted to the CPTu platform, and the tip of the depth coder wire was mounted to a rod that added to the tip of the CPTu pushing system and allowed the wire to move vertically. Before the penetration started, CPTu zero loading calibration was done. The tip of the CPTu cone was placed on the surface of the deposit, and the depth coder was calibrated as "0 cm" depth. Each test was performed until the cone reached the middle of the dense sand layer at the bottom of the laminar box. The q_c, $f_{s,}$ and u_2 values were recorded for 2 cm intervals through the depth.

The relative density (D_r) throughout the soil depth was determined from the measured CPT resistance using the equation proposed by Lunne et al. (1997). Lunne et al. (1997) proposed that;

$$D_r = -98 + 66 \log\left(\frac{q_c}{\sigma_{vo}'}\right) \ (\%) \qquad (3.1)$$

where; D_r is relative density, q_c is cone tip resistance (kPa), and σ_{vo}' is effective vertical stress (kPa) of soil at a cone depth.

The relative density reported in Table 3.2 for each test sample was obtained from the average amount of the initial relative density for the loose upper layer. Figure 3.37 shows the q_c and D_r values versus depth for all tests. In Figure 3.37.b, Dr values are negative which is physically unfeasible at the firsth 0-20cm depth of CPTu tests. The reason of this is the Equation 3.1 was proposed for field tests where the ground water level is at the surface of the soil or lower. In this studies, water level of the deposits in the laminar box is 1-2cm higher than the surface of the soil deposits. Thanks to these small diferenceses between level of water and soils, for the first 0-20cm depth, Dr values are neglectable.

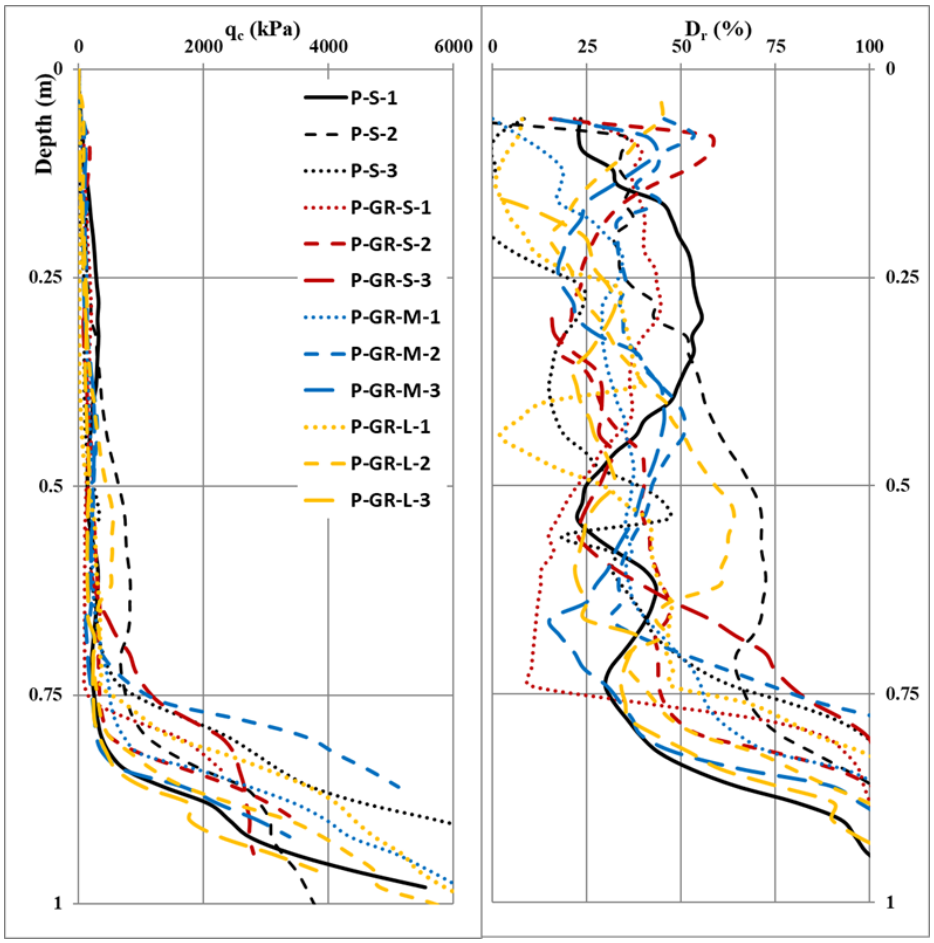

Figure 3.37. CPTu results of all tests,

(a) Variation of qc and (b) Dr values by depth

As seen in Figure 3.36, the first 75cm loose sand or GRS mixture layers tip resistance values were low, corresponding to the bottom layer. The qc values started to increase significantly when the CPTu cone started to penetrate through the dense sand layer for all tests. The results of CPTu tests prove that the dense sand layer and loose-fill layers existed as intended. The filling methods were successful for both dense sand and GRS mixture layers in terms of density and uniformity.

3.6.5. Unfilling Process

GRS layer was unfilled from the laminar box after performing each shaking. These saturated GRS deposits were dug by hand and poured into preparation boxes using big buckets. The water was drained with valves at the bottom of the preparation boxes. The deposits in the boxes were kept for at least one day for total drainage of the water. Then, these deposits were used to prepare another mixture by adding more GR, if the GR/Sand ratio and GR size were suitable for the subsequent trial. If it was not, the mixture

was poured into barrels, and empty preparation boxes were cleaned for the following trial. After the emptying of the upper layer of the laminar box, the instruments, the nets carrying the instruments and membrane were checked. The upper surface of the dense sand layer was cleaned and leveled for the next trial.

3.7. Results and Discussions

In this section, the result of ten tests which were conducted with a maximum acceleration of 0.35g and with clean sand and GRS mixture, were represented. These tests were listed in Table 3.4. In this section, excess pore water pressure (Δu) values during and after the shaking were observed in the sand and varying GRS mixture, effects of using the GR in sand as mixture backfill on liquefaction were discussed below. Also, the settlement of sand and GRS deposits were compared. Lastly, the effects of GR size and ratio on consolidation characteristics of backfills were obtained when the backfill was under the dynamic loading conditions. According to the findings, the discussions were defined in two sections; the effects of GR size and ratio on

a) excess pore water pressure and liquefaction,

b) settlement behavior of the backfill, and

c) consolidation characteristics of the backfill.

3.7.1. Effects of GR on Liquefaction Potential of GRS

Excess pore water pressure (Δu) values during and after the shaking were observed at five depths of deposits for all tests. Figure 3.38, Figure 3.39, and Figure 3.40 show the Δu changes during and after the shaking for tests performed with GR sizes of 2.5-5mm, 5-10mm, and 10-15mm, respectively. In this study, the pore pressure ratio (r_u), which is the ratio of excess pore water pressure (Δu) to the initial effective vertical stress (σ_{vo}'), was used to assess the full liquefaction. In general, liquefaction occurs when r_u reaches 1.0. So, the r_u values were also plotted in Figure 3.41, Figure 3.42, and Figure 3.43 for the test performed with GR size of 2.5-5mm, 5-10mm, and 10-15mm, respectively. Note that, for all six figures (Figure 3.38 - Figure 3.43); there are ten plots and plots in left column show the time depend values during shaking (for 0-20th sec), while plots in right column show the time depend values after shaking (for 20th -200th

sec). Also, in the figures each row belongs to the data obtained from a depth, the depth of the data from up to down are 0.20m, 0.40m,0.63, and 0.63m.

As seen in Figure 3.41-Figure 3.43, there were significant fluctuations for all data. Despite of fluctuations, it could be observed that, a short after the shaking started the Δu values in sand deposits increased, then kept its value until the shake stopped, after the shaking it started to dissipate. On the other hand, in GRS mixtures, Δu was generated immediately after the shaking started and reached the average values which were 1.5-2 times smaller than the values obtained from sand tests. From this perspective, it can be said that, using the GR in sand as a mixture material decreases the generated Δu.

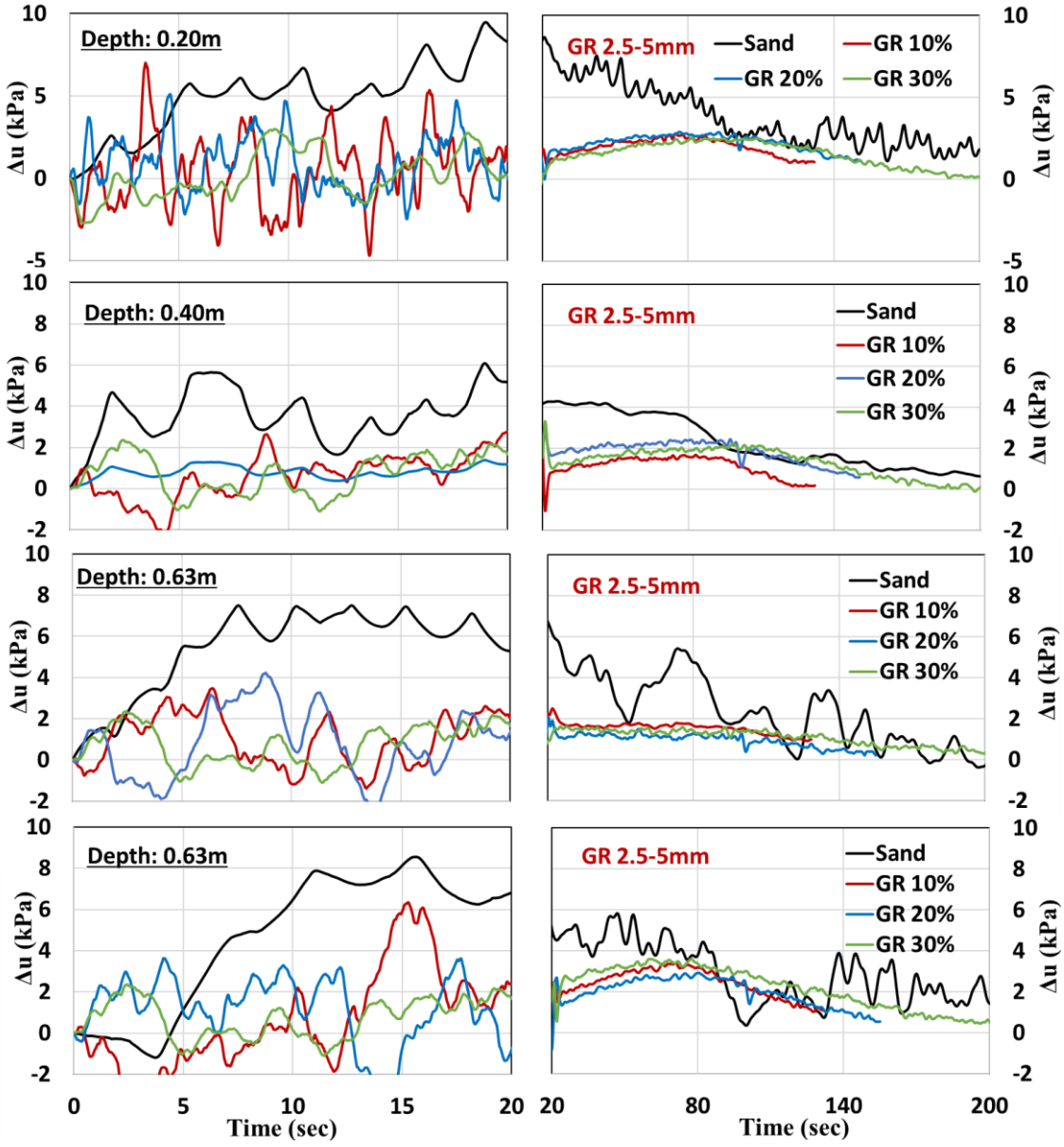

Figure 3.38. EPWP of the tests performed with 2.5-5mm GR

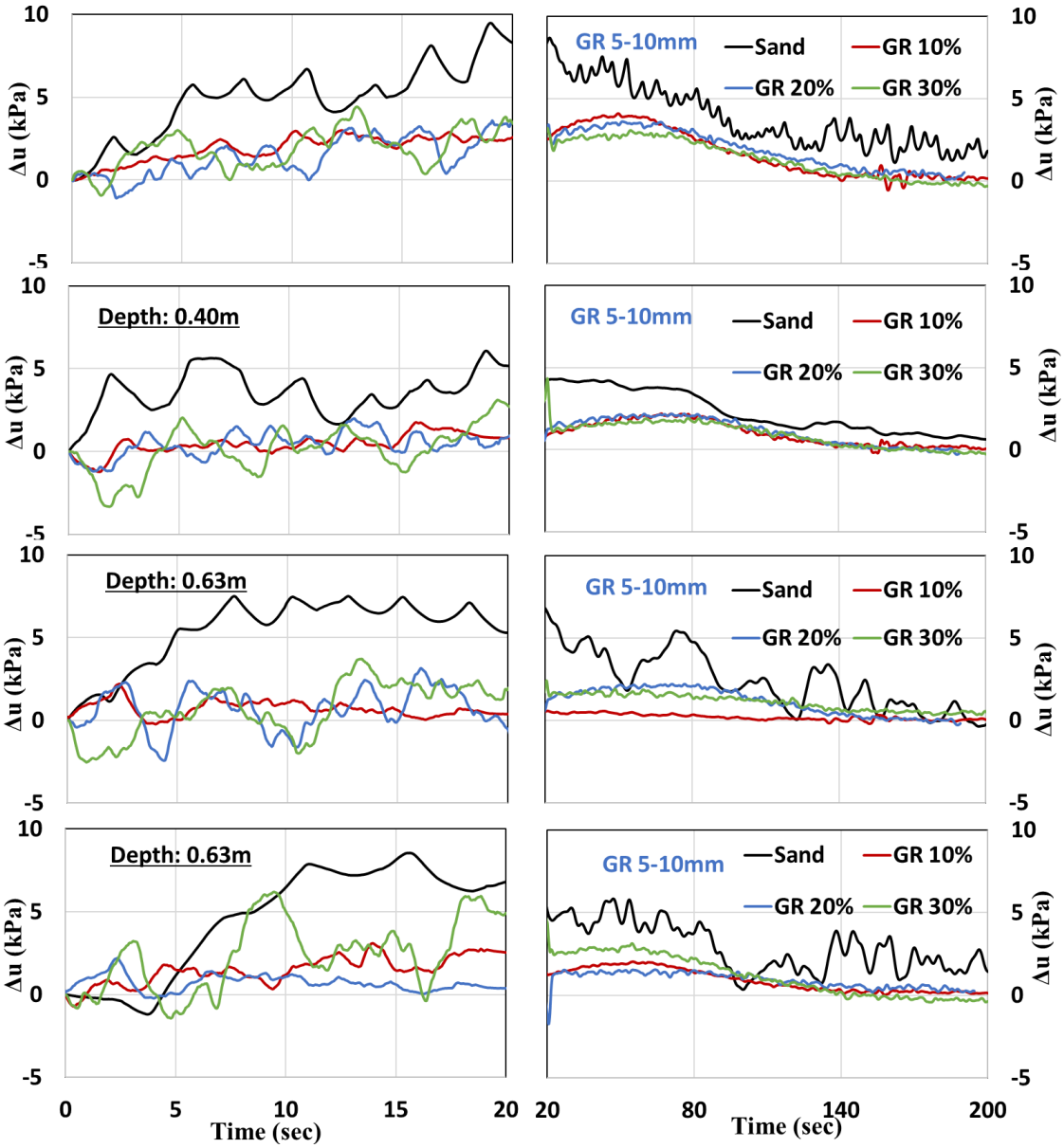

Figure 3.39. EPWP of the tests performed with 5-10mm GR

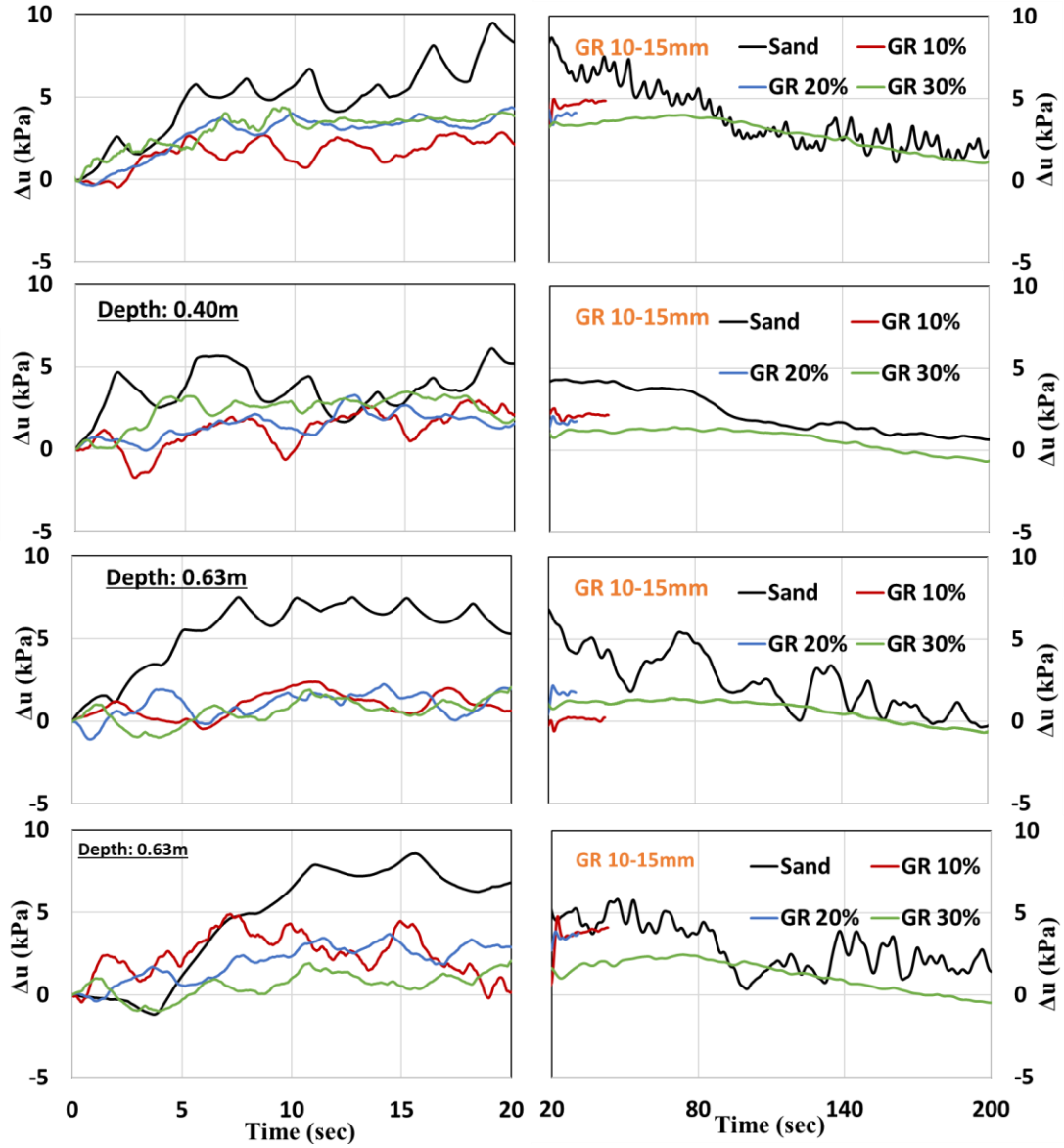

Figure 3.40. EPWP of the tests performed with 10-15mm GR

As seen in Figure 3.41-Figure 3.43, r_u values reached the limit of r_u=1, liquefaction occurred in all depths of sand deposit. The starting times of liquefaction were listed in Table 3.5. There were also liquefactions observed in the tests of GRS, but the r_u values reached 1 and decreased immediately, so it could be a data fluctuation caused by the dislocation of EPWPTs, but these values also were taken into consideration, and data were accepted as liquefaction occurred in these cases and listed in Table 3.5. as liquefied. As seen in figures of r_u by time, the r_u started to increase just after the starting of shaking, and it reached its limit value at a time between 1st -5th sec, then it continued to fluctuate until the shaking stopped (20 sec). Between these two times (from 1st-5th sec to 20 sec), the average Δu and r_u values were calculated and listed in Table 3.5. In the Table 3.5., γ_m

is the unit weight of the mixture, depth is the depth of EPWPTs, σ_{vo}' is the effective vertical stress of soil in this depth, Δu is excess pore water pressure generated during shaking, Δu_{avg} and $r_{u\text{-}avg}$ are average excess pore water pressure and average pore water ratio, $t_{0\text{-}liq}$ is the time of liquefaction has started, $t_{0\text{-}dis}$ is the time of dissipation has begun, and $t_{f\text{-}dis}$ is the time when dissipation has completed.

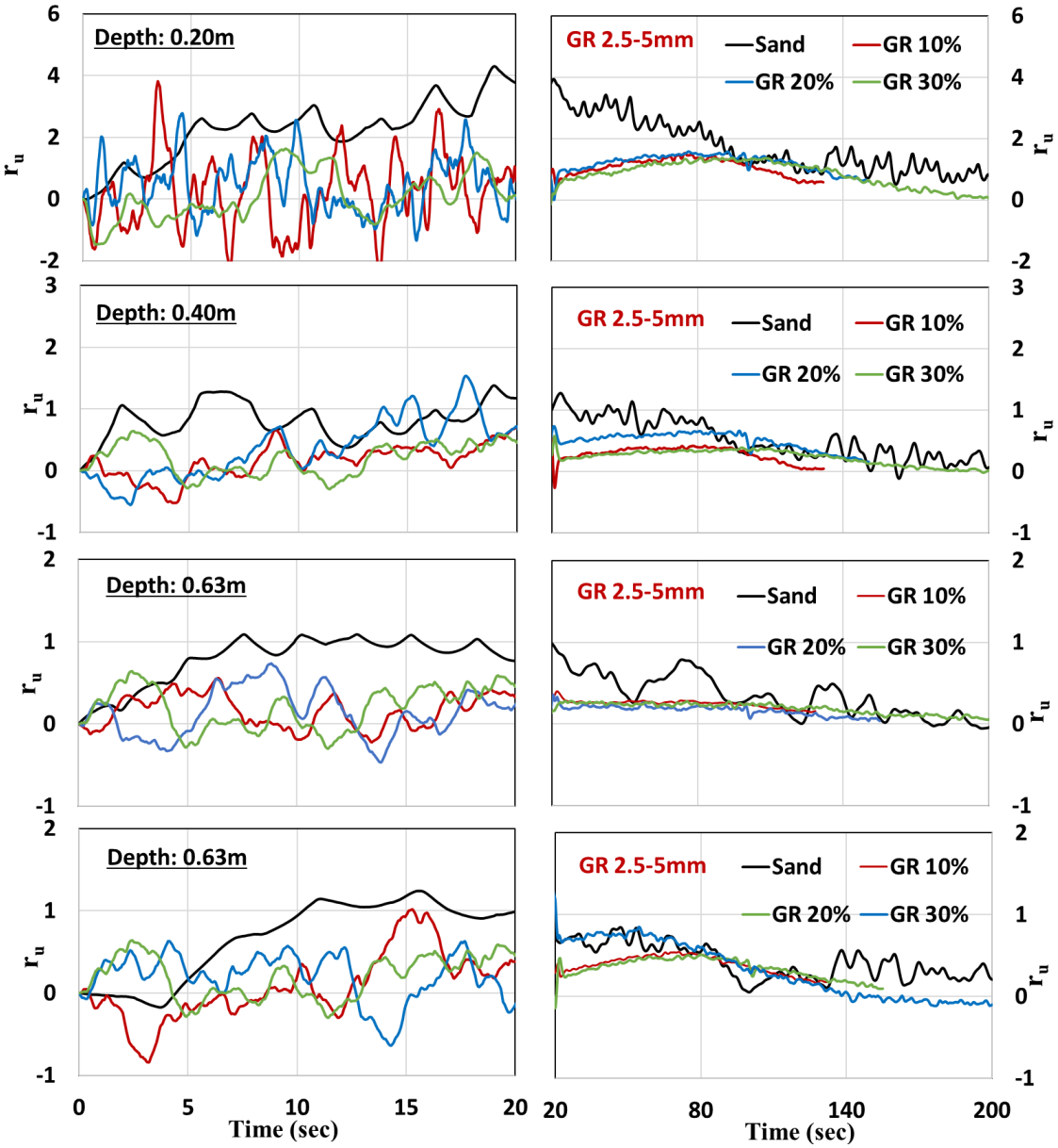

Figure 3.41. Pore water ratio of the tests performed with 2.5-5mm GR

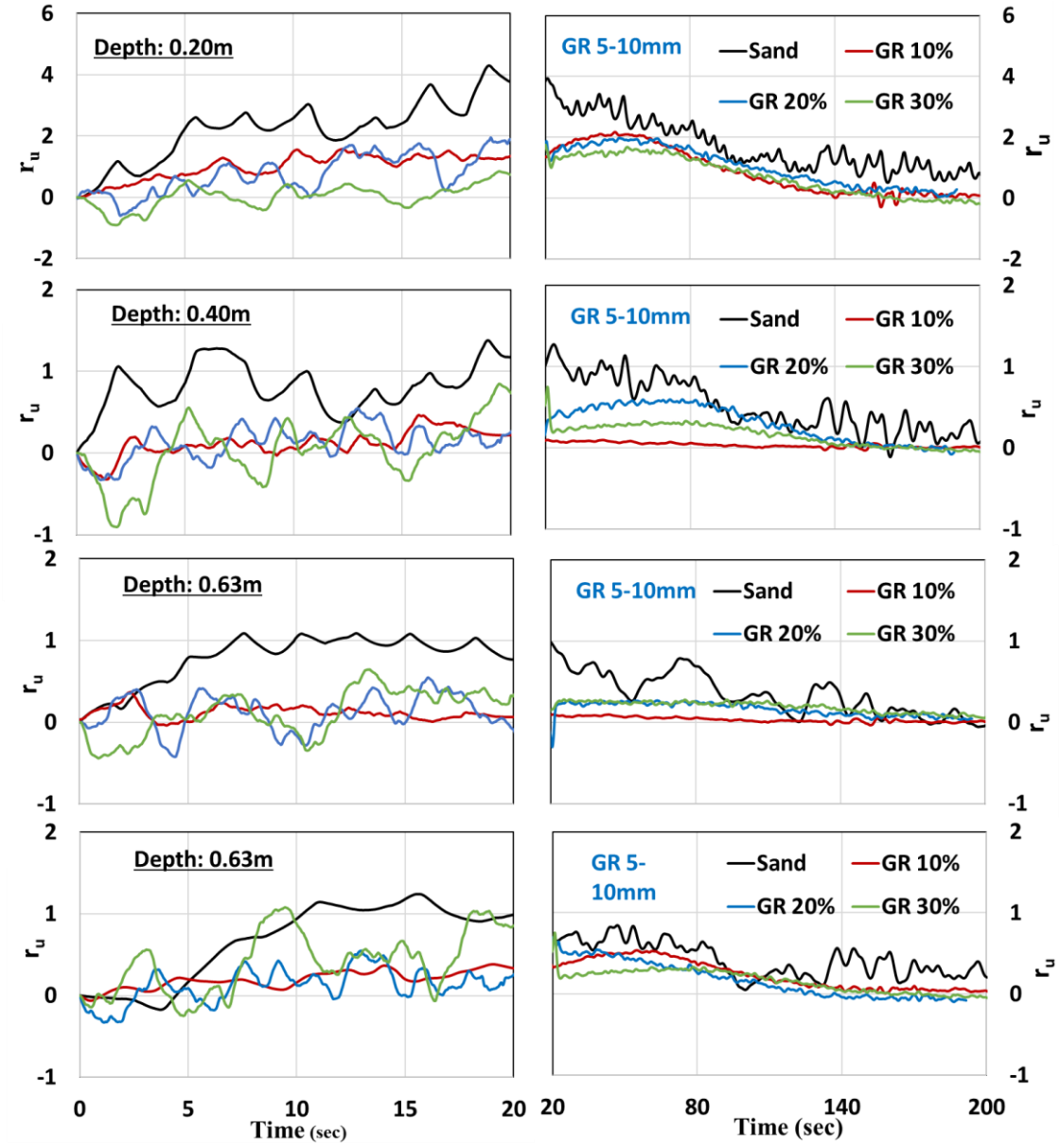

Figure 3.42. Pore water ratio of the tests performed with 5-10mm GR

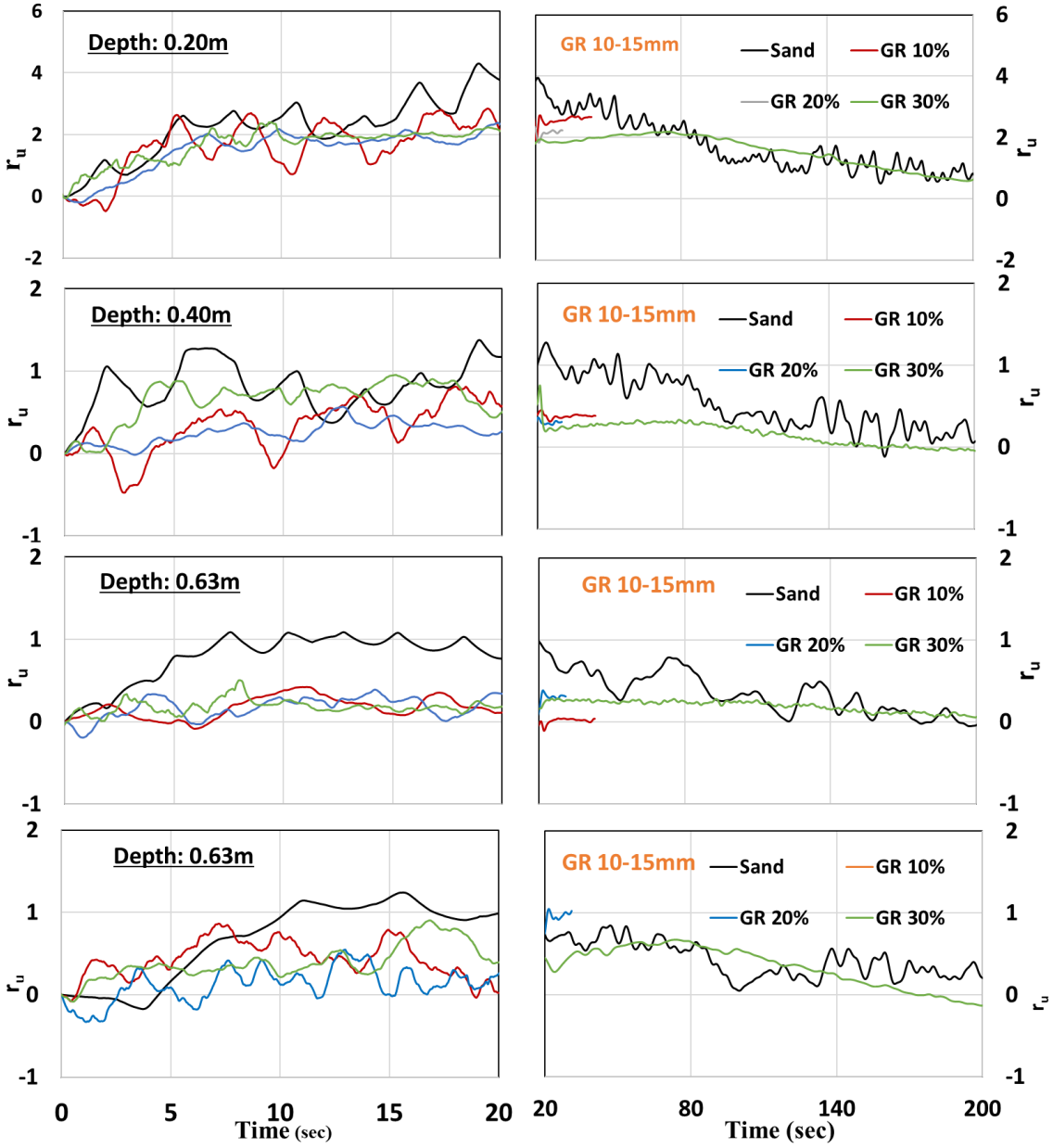

Figure 3.43. Pore water ratio of the tests performed with 10-15mm GR

Average r_u values during the shaking ($r_{u\text{-}avg}$) were plotted for two depths 0.40m and 0.63m, for each case in Figure 3.44. According to Figures 3.43 and Table 3.5, average ru values varied between 0.16-0.56. In other words, the GRS mixture decreased the excess pore water pressure 2-5 times than that generated in the sand. According to Figure 3.44 there was no a clear relation between the reduction of r_u and GR size or ratio.

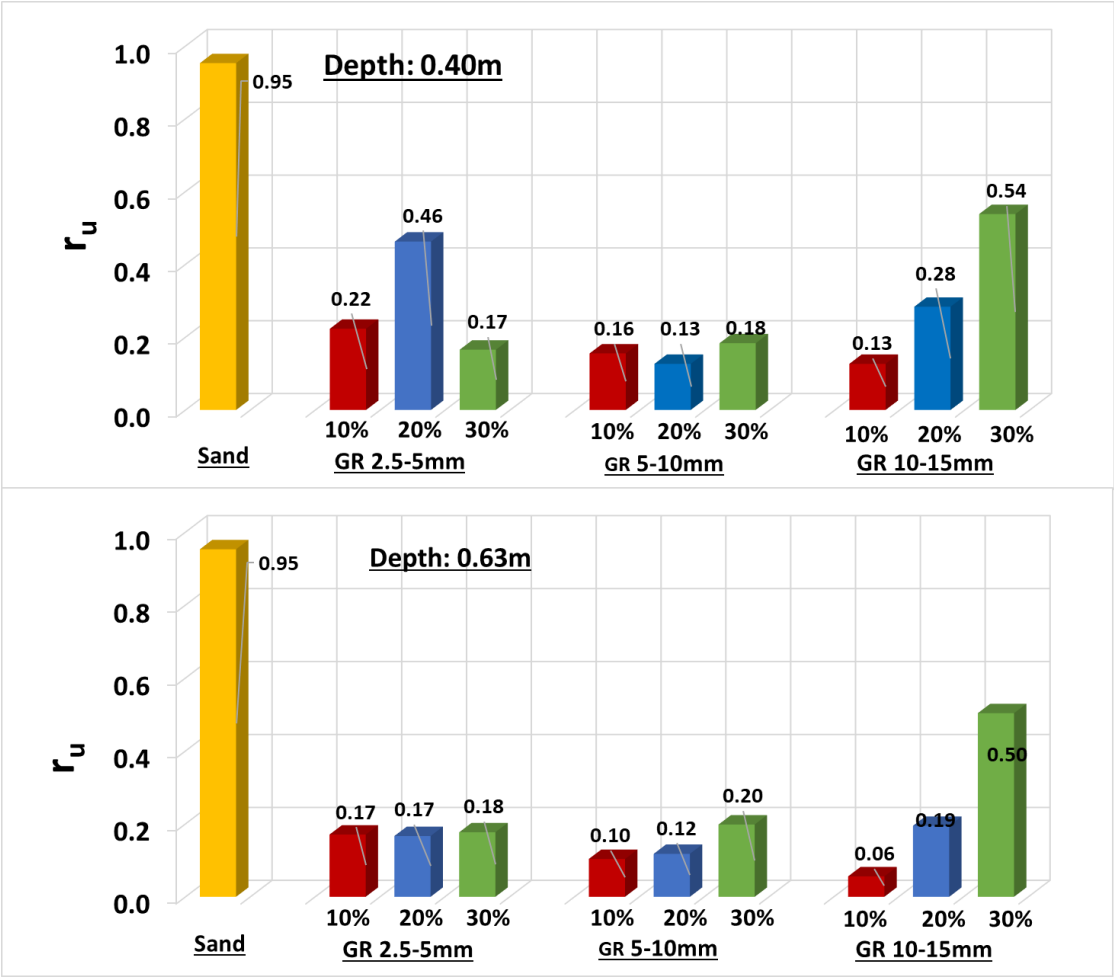

Figure 3.44. Average r_u values grouped by GR sizes

On the other hand, when the ratio of GR in the mixture was kept constant for each case and the sizes of GR and r_u values were compared, there were varying relation for each mixing ratio. When the GRS mixture was prepared with 10% of GR in volume, increasing the GR size from 2.5mm to 15mm caused a small decrease in r_u, quite the opposite, increasing GR size caused a clear increase of r_u for the mixtures prepared with 30% of GRs. On the other hand, for the 20% of GR in the mixture, using the 5-10mm of GR gave a much more reduction in r_u than bigger or smaller sizes (Figure 3.45).

Table 3.3. Summary of all test results

Test	GR size	GR ratio	γ_m	Depth	$\sigma_{vo'}$	Δu_{max}	Δu_{avg}	$r_{u\text{-}avg}$	$t_{0\text{-}liq}$	$t_{0\text{-}dis}$	$t_{f\text{-}dis}$	c_h	Settlement		
													During Shake	During Dissipation	Total
-	mm	%	kN/m^3	m	kPa	kPa	kPa	-	sec	sec	sec	cm^2/sec	mm	mm	mm
Sand	-	-	20.83	0.2	2.20	7.85	5.57	2.53	1.65	28	192	15.24	25.8	8.5	34.3
				0.4	4.41	5.64	4.20	0.95	1.77	29.00	185.50				
				0.63	6.89	7.25	6.19	0.95	7.13	20.5	180.5				
				0.63	6.89	7.97	6.36	0.92	10.08	16	185				
T.GR.S.1	2.5-5mm	10	19.78	0.2	2.00	2.81	0.62	0.31	L	75	122	18.82	25.0	0.2	25.2
				0.4	3.99	1.69	0.89	0.22	15.02	61	140				
				0.63	6.23	2.50	1.06	0.17	NL	26	210				
				0.63	6.23	3.41	1.17	0.19	NL	51	210				
T.GR.S.2	2.5-5mm	20	19.59	0.2	1.96	2.90	0.86	0.44	L	61	129	17.88	13.2	0.4	13.6
				0.4	3.91	2.51	1.81	0.46	14.14	21	125				
				0.63	6.11	2.05	1.02	0.17	NL	21	180				
				0.63	6.11	2.93	0.97	0.16	NL	64.0	180.0				
T.GR.S.3	2.5-5mm	30	18.9	0.2	1.82	2.55	3.38	0.35	L	81.5	182.0	17.52	24.1	0.4	24.5
				0.4	3.64	2.23	0.61	0.17	NL	99.0	198.0				
				0.63	5.08	1.62	1.00	0.18	NL	34.0	203.0				
				0.63	5.08	3.60	3.19	0.56	NL	60.5	210.5				
T.GR.M.1	5-10mm	10	19.31	0.2	1.90	4.12	2.16	1.14	6.02	49.0	216.0	24.29	48.2	3.6	51.8
				0.4	3.80	2.20	0.59	0.16	NL	67.5	210.0				
				0.63	5.94	0.57	0.62	0.10	NL	22.5	110.0				
				0.63	5.94	2.05	1.71	0.29	NL	54.0	158.0				
T.GR.M.2	5-10mm	20	18.9	0.2	1.82	3.62	1.69	0.92	7.42	51.0	186.5	18.26	21.4	5.9	27.3
				0.4	3.64	2.19	0.65	0.13	NL	77.0	178.0				
				0.63	5.74	1.54	0.68	0.12	NL	64.00	193.00				
				0.63	5.74	3.71	2.26	0.39	NL	23.00	192.00				
T.GR.M.3	5-10mm	30	18.94	0.2	1.84	3.59	2.12	1.16	NL	54	216	22.05	26.3	1.1	27.4
				0.4	3.62	1.91	0.46	0.18	NL	77	173				
				0.63	5.74	1.90	1.14	0.20	NL	43	179				
				0.63	5.74	3.13	2.65	0.46	8.23	53.5	153				
T.GR.L.1	10-15mm	10	18.07	0.2	1.81	4.85	1.90	1.05	L	36	350	9.38	29.1	0.2	29.30
				0.4	3.62	2.20	0.46	0.13	NL	33	350				
				0.63	5.66	4.13	0.32	0.06	NL	32	350				
				0.63	5.66	1.89	2.23	0.61	NL	39	350				
T.GR.L.2	10-15mm	20	18.87	0.2	1.81	4.16	1.94	1.07	L	22	340	8.94	16	0.2	16.20
				0.4	3.62	1.90	1.03	0.28	NL	22	340				
				0.63	5.66	2.11	0.40	0.07	NL	22	340				
				0.63	5.66	3.78	1.10	0.19	NL	22	340				
T.GR.L.3	10-15mm	30	17.8	0.2	1.60	3.97	2.56	1.60	L	77	300	11.86	31.4	3.7	35.1
				0.4	3.20	2.85	1.72	0.54	6.20	73	300				
				0.63	4.99	1.36	2.51	0.50	NL	106	300				
				0.63	4.99	3.45	0.68	0.14	6.23	81	300				

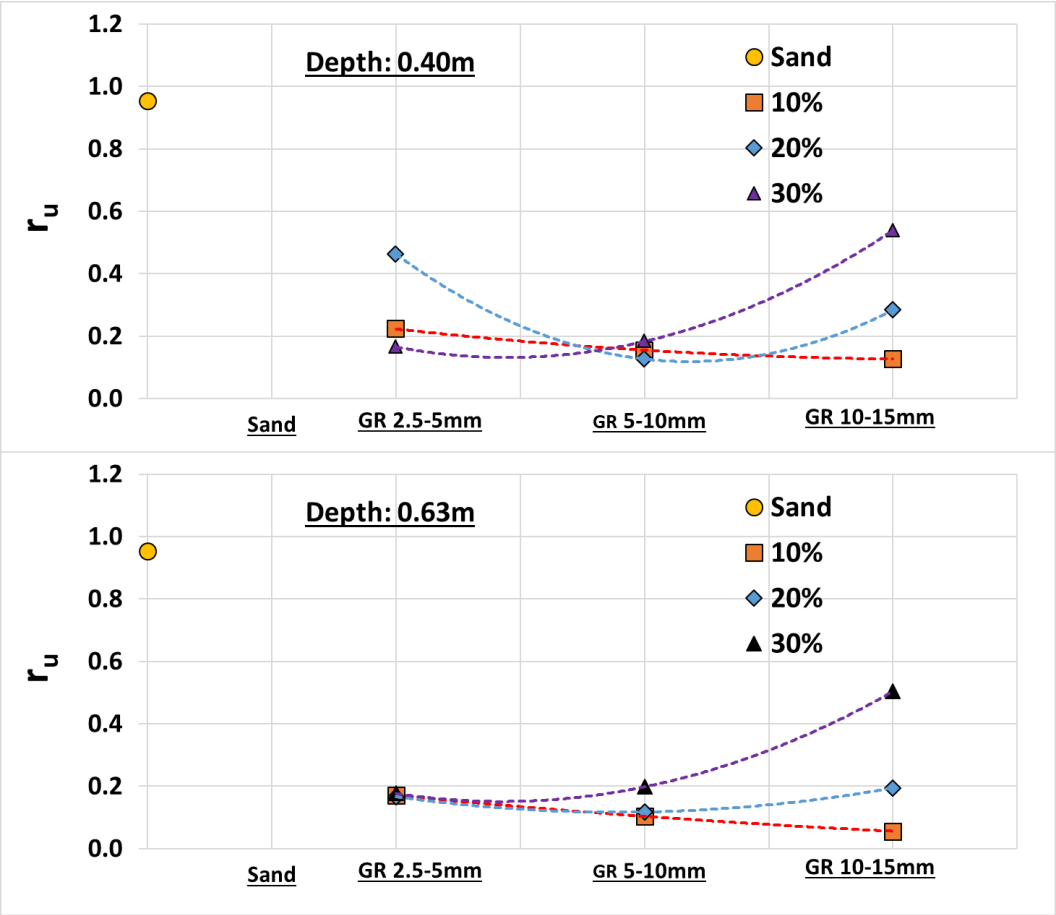

Figure 3.45. Average r_u values grouped by GR ratio in the mixture

The trends observed in Figure 3.45 can be explained with several reasons;

a) Firstly, the change in excess pore water pressure related to the drainage path of water (permeability) depends on the voids between the sand-sand, GR-GR, or GR-sand particles. When the GR was used with a small amount (10% in volume), the global void ratio and consolidation charaterstics of the deposits were not changed significantly with the increase of the GR size. So, the GR size did not cause a significant change in the reduction of pore water pressure.

b) When the GR ratio was 30% in the mixture, there was no difference between the generated Δu values for the size of 2.5-5mm and 5-10mm. However, using the GR with 10-15mm size caused more significant Δu values than others. The reason could be the shape of the GR with a 10-15mm diameter. Granulating the rubber into small pieces creates rubber particles with irregular shapes when the particle diameters are small (1-10mm). However, when the diameter of the particles are bigger (10-20mm), granulated rubbers usually have a flat surface on both side and semi-regular shape. Because of their shapes, the particles could be placed into a

mixture with a bigger contact surface and decrease the global void ratio of the mixture.

c) When the GR ratio was 20% in the mixture, the smallest and the largest GR provided an excellent increase in the permeability. And also the optimum mitigation of liquefaction was provided by GR with 5-10mm diameter.

3.7.2. Effects of GR on Settlements

The settlements of the deposits measured on the surface are plotted in Figure 3.46. As seen in Figure 3.47, the minimum settlement was observed with a 20% ratio for all GR sizes. The maximum settlement was observed in the test of GR size; 5-10mm, and ratio in the mixture; 10%. Also, it was the only case that the obtained settlement was larger than the clean sand deposits. First 2-5sec, there were upward and downward movements for all cases. Between the 2-20sec, the major settlements occurred for all cases. In some cases, the settlements continued after the shaking with a considerable amount (GR 5-10mm, 10% and GR10-15mm, 30%).

For other cases, there were too small settlements during the dissipation part. The settlements during the shaking and the dissipation stage were observed separately and listed in Table 3.5. Also, to compare the results of total settlements during the shaking stage and dissipation stage were plotted in Figure 3.47. All GRS mixture settled less than the sand deposit except in one case. For all GR size minimum settlement occurred at the cases with 20% mixing ratios. It was not observed a clear relation between the GR size or ratio and settlements. As seen in Figure 3.46, the smallest settlements during the shaking were observed from the tests with 20% GR ratios for all GR sizes. This can be explained by relative density and void ratio of mixtures are varying according to th GR-sand contacts. So, the smallest global void ratio of mixtures could be predicted when the mixing ratio is 20%. But, this disccustion would be not enough for the settlements. It's known that the settlements is not only related to the relative density of deposits and but also the consoliation charatersitics. To figure out the all reasons of the settlement behavior of GRS mixtures, the consolidation charactersitics sould be discussed.

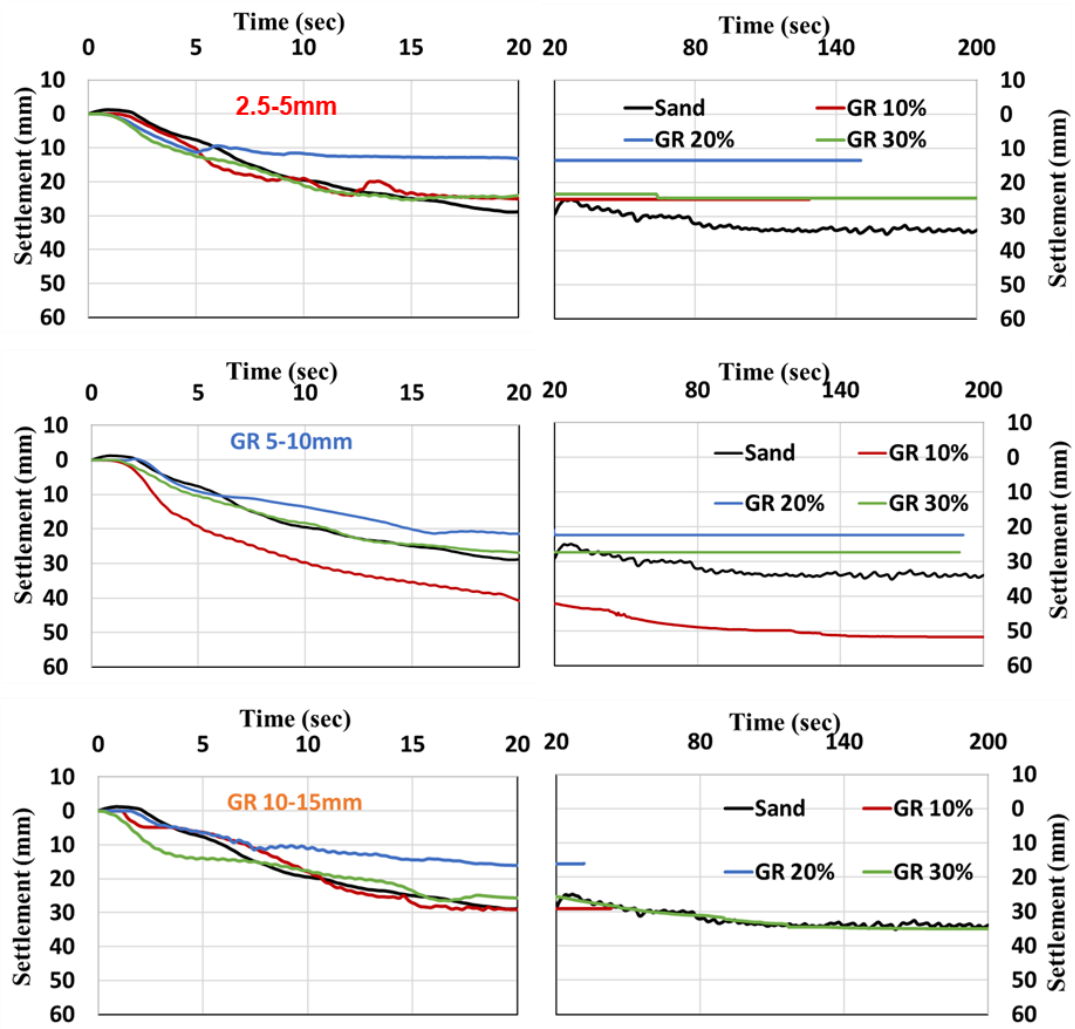

Figure 3.46. Surface settlements of the deposits by time during and after shakings for all tests.

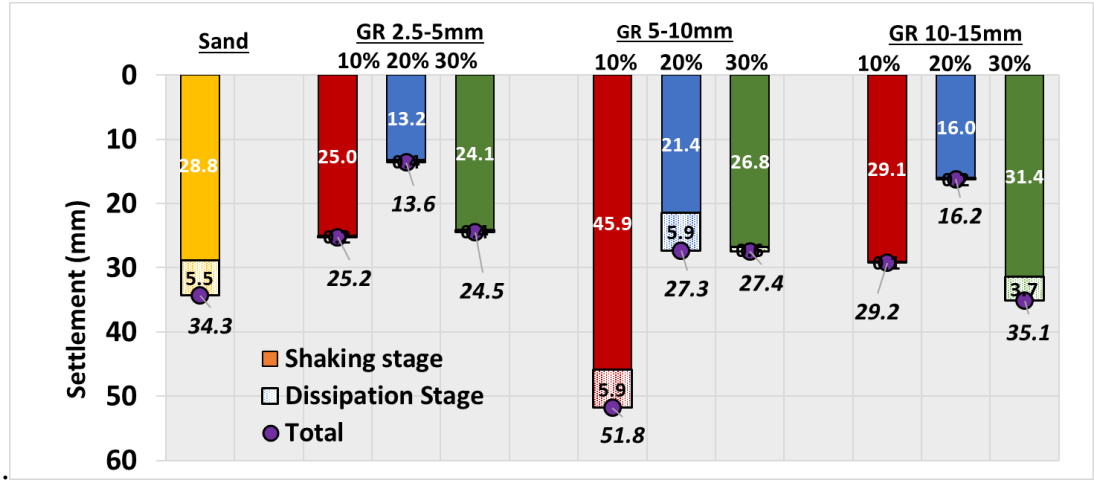

Figure 3.47. Settlements for all tests

3.7.3. Effects of GR on Consolidation Characteristics of GRS

There was no significant correlation between settlements and GR conditions. The consolidation characteristics of GRS, which were related to the compressibility and permeability of the mixture, were determined to compare GR effects on these phenomena in the dissipation part.

The coefficient of consolidation (c_v) is an engineering parameter to describe the rate at which saturated soil undergoes consolidation or compaction when pressure increases. It is measured in cm^2/sec or m^2/min. Terzaghi's 1-D consolidation theory gives the correlation as follows:

$$\frac{\partial U}{\partial t} = c_V \frac{\partial^2 U}{\partial z^2} \tag{3.2}$$

where; c_v is the coefficient of consolidation, U is pore water pressure, t is the time of consolidation, and z is the effective drainage path. Terzaghi (1922) considered that the following assumptions are valid for using Equation 3.1:

1) Soil is homogeneous and isotropic.
2) The soil is completely saturated.
3) The soil grains and water are incompressible.
4) Load is applied in the vertical direction only.
5) Drainage of pore water is one-dimensional, i.e., in the direction of the load.
6) Primary consolidation is totally governed by the expulsion of pore water, i.e., at the initial stage, pore water pressure (u_w) is 100%, and consolidation is 0%. At the final stage, pore water pressure (u_w) is 0%, and consolidation becomes 100%.
7) The soil mass remains saturated after primary consolidation.
8) The coefficient of permeability of the soil is constant.
9) The coefficient of compressibility (m_v) is constant for a given type of soil.
10) Darcy law is valid.

c_v indicates the speed with which consolidation takes place. The higher the value of the coefficient of consolidation, the faster the rate of consolidation will be, and less time will be required to complete the consolidation. Also, coefficient of consolidation (c_v) is determined as follows;

$$c_V = \frac{k}{m_V . \gamma_W} \tag{3.3}$$

where; k is the coefficient of permeability while m_v is the coefficient of compressibility of soil, γ_w is the unit weight of the water. As seen in Equation 4.2, c_v is related to permeability and compressibility of soil, where more permeable soil has higher c_v, and more compressible soil has lower c_v.

Applying Terzaghi's 1D consolidation theory on the Δu records in the dissipation part of all tests, c_v values of GRS mixtures were determined. In this study, changing the GR size and mixing ratio of GR in the sand mixture changed the consolidation characteristics of the GR-sand mixture. In Figure 3.48, the c_v values of each case were plotted. c_v values were also listed in Table 3.5., varying between 8.9 and 24.3 cm^2/sec. The c_v values were plotted in Figure 3.48. The c_v values of GRS mixtures were grouped according to GR sizes in Figure 3.48.a, while they were grouped according to the ratio of GR in the mixture in Figure 3.48.b.

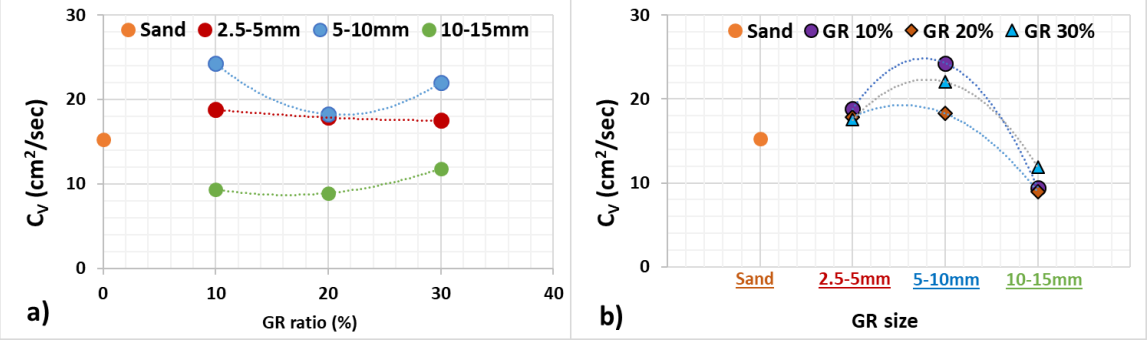

Figure 3.48. Coefficient of consolidation for all tests

As seen in Figure 3.48.a, for a constant GR size, increasing the GR ratio in the sand caused minor changes in c_v because increasing the GR amount in the mixture with 10% intervals made a small change in backfill characteristics in terms of permeability and compressibility. It was observed that the higher c_v values belonged to the mixture with 5-10mm GR while the lower c_v belonged to 10-15mm GR, which was also lower than the clean sands' c_v. As a result of these relations, the GRS mixture conditions were grouped according to their ratio in mixture (Figure 3.48.b). As seen in Figure 3.48.b, when GR size was increased from 2.5-5mm to 5-10mm, c_v values increased. In contrast, when the GR size was increased from 5-10mm to 10-15mm, c_v values decreased. Also, these relations were the same for all GR ratios in the mixture. As known, consolidation

characteristics depend on both the permeability and compressibility of soil. In this study, it was observed that increasing the percentage of GR in the mixture for a constant GR size affected both the permeability and compressibility. But for a constant ratio of GR in GRS mixture in volume, increasing the GR particles size influenced permeability and compressibility more strongly.

3.8. Concluding Remarks

In this chapter of the study, the liquefaction potential and settlements of saturated loose sand- granulated rubber mixture were compared with varying mixture conditions with 1-D shake table tests. The shaking tests were performed with sinusoidal motion and 0.35g maximum acceleration. The variants are granulated rubber diameters and the ratio of granulated rubber in the mixture in volume. Following observations are listed to summary the results of comperative study;

1. It is clear that, using the GR in sand as a mixture backfill decreases the generated excess pore water pressure, and decrease the potential of liquefaction.
2. For a small amout of GR in sand, (10%GR-90%Sand), increasing the diameter of GR caused a small decrease in the excess pore water pressure ratio.
3. For the case of granulated rubber ratio in mixture is 20%, smallest and biggest diameter of GR gave bigger excess pore water pressure ratio than 5-10mm GR.
4. Largest reduction of excess pore water pressure ratio is observed in the mixture for the 20% of GR ratio and 5-10mm of GR size.
5. The change in excess pore water pressure related to the drainage path of water (permeability) depends on the voids between the sand-sand, GR-GR, or GR-sand particles. When the GR was used with a small amount (10% in volume), the void ratios of the deposits were not changed significantly with the increase of the GR size. So, the GR size did not cause a significant change in the reduction of pore water pressure.
6. When the GR ratio was 30% in the mixture, there was no difference between the generated Δu values for the size of 2.5-5mm and 5-10mm. However, using the GR with 10-15mm size caused larger Δu values than others. The reason

could be the shape of the GR with a 10-15mm diameter. When the diameter of the particles are bigger (10-20mm), granulated rubbers usually have a flat surface on both side and semi-regular shape. Because of their shapes, the particles could be placed into a mixture with a bigger contact surface and decrease the void ratio of the mixture.

7. When the GR ratio was 20% in the mixture, the smallest and the largest GR provided an excellent increase in the permeability. The optimum mitigation of liquefaction was provided by GR with 5-10mm diameter.
8. For all GR size minimum settlement occurred at the cases with 20% mixing ratios.
9. For a constant GR size, increasing the GR ratio in the sand caused minor changes in c_v because increasing the GR amount in the mixture with 10% intervals made a small change in backfill characteristics in terms of permeability and compressibility.
10. Higher c_v values belonged to the mixture with 5-10mm GR while the lower c_v belonged to 10-15mm GR, which was also lower than the clean sands' c_v.
11. When GR size was increased from 2.5-5mm to 5-10mm, c_h values increased. In contrast, when the GR size was increased from 5-10mm to 10-15mm, c_v values decreased.
12. The most significant liquefaction mitigation was observed for 5-10mm GR diameter and 20% GR ratio in mixture, in terms of permability and compresibilty.
13. The increasing the percentage of GR in the mixture for a constant GR size affected both the permeability and compressibility. But for a constant ratio of GR in GRS mixture in volume, increasing the GR particles size influenced permeability and compressibility more strongly.

CHAPTER 4

USAGE OF TIRE GRANULATED RUBBER AND SAND MIXTURE AROUND THE BURIED PIPES: SHAKE TABLE TESTS

4.1. Introduction

One of the main purposes of the presented study is to investigate the effects of the GRS mixture on liquefaction potential and pipe displacements once the GRS are used as a filling material around pipelines. For this purpose, two different pipe models were placed into the laminar box, and several shake table tests were conducted under different filling material conditions. Laminar box, shaking table, CPTu system, filling and unfilling methods of deposits, GR sizes, and GRS mixture ratios are same as the tests represented in Chapter 3. By adding two identical pipe models and several instruments to the setup represented in Chapter 3, a total of 12 shake tests were conducted.

In this chapter, shaking tests and their results are given. The results showed pipe uplift movement due to the liquefaction and excess pore water pressure. The effects of GRS mixture ratio and GR size on pipe uplift movement and liquefaction remediation were discussed.

The materials and instruments, which were different from the tests described in Chapter 3, were explained in detail. The materials, which were the same in this chapter and Chapter 3, were referred briefly. Then, the experimental matrix and scope of the tests trials were described in detail. Results of the shaking test were discussed at the end of this section. For varying parameters, a novel critical design criteria was proposed to prevent the pipe from uplifting movements during seismic loading. Finally, the concluding remarks were summarized.

4.2. Materials

As it is stated above, twelve shake table tests were carried out in this chapter. Only clean sand was used in the first three experiments, and GRS mixture was used in the other

nine experiments. The GR and sand materials were the same as the materials described in Chapter 3. Section 3.3 can be seen for more detail. In this section, the pipe models and instruments which added to setups were described.

4.2.1. Shake Table and Laminar Box

The shake table and laminar box system consisting of a one-dimensional shake table, laminar box, membrane, and actuator were same as explained in Chapter 3. There was no additional component for the experiments of this chapter except pipe models and a number of additional instrumentations.

4.2.2. Pipe Models

There was two identical pipe model with different placing configurations. One of them was named as “free pipe” while the other one was named as “fixed pipe”. The pipe models were made of Polyvinyl Chloride (PVC), with a 385mm length, 50mm external diameter, and 1.8mm thick. The unit weight, ultimate tensile strength, bending strength, elasticity modulus, and Poisson’s ratio of the pipe material was 13.83 kN/m^3, 52 MPa, 88 MPa, 3,316 MPa, and 0.40, respectively. These pipes were placed into the laminar box and buried into sand and GRS mixture to represent the real-life conditions of small diameter gas pipelines buried below the groundwater level and at a shallow depth. PVC pipes are closed on both sides using caps so that they were empty. Photographs of the pipe model and caps can be seen in Figure 4.1.

Figure 4.1. PVC pipe model and its cap used in the physical model

4.3.2.1. Free Pipe

The free pipe had a configuration that allowed the pipe to make vertical displacements during and after the shaking. Rails were welded to steel rods, and the steel rods were mounted to free pipe with clamps. The steel rods were 76cm in length and kept the rails above the soil surface horizontally. These rails became the guide path channel for two LPMs which were placed on the deposit and measured the vertical displacements of the free pipe. LPMs and the purpose of the rails were explained in detail in the instrumentation section. Figure 4.2 shows a free pipe configuration consisting of the pipe model, clamps, and rails welded to steel bars. The total weight of the free pipe was 2.4kg with its rods, rails, and instruments.

This configuration which allowed to move of pipe vertically, represents the real-life pipelines buried into the liquefiable soil with a shallow depth under the ground water level, The pipe was used for all of the shaking trials.

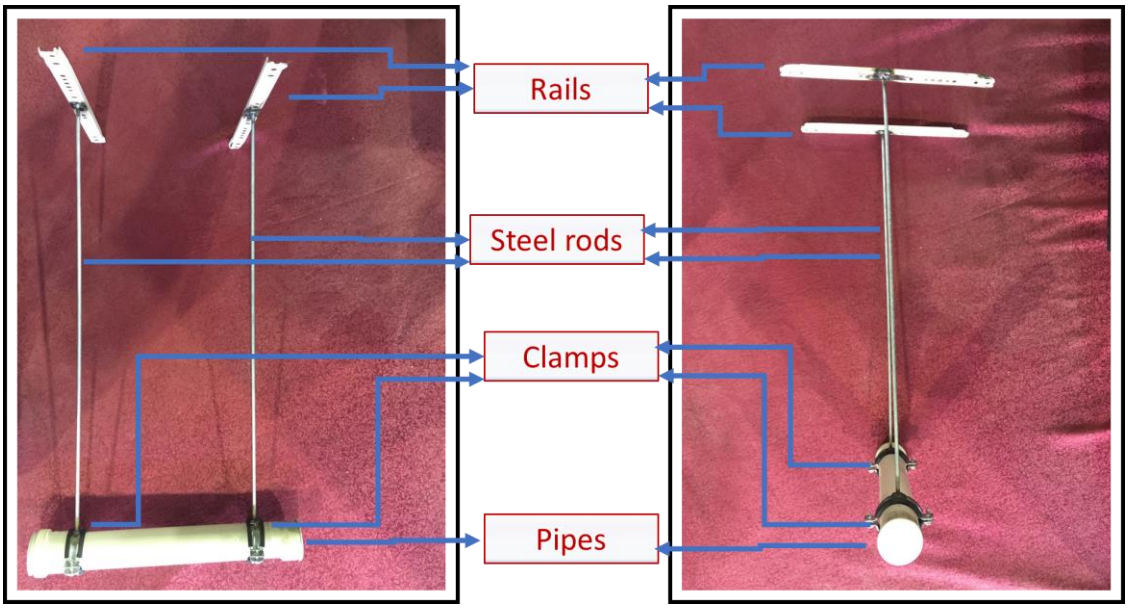

Figure 4.2. Free pipe configuration

4.2.2.1. Fixed pipe

Another pipe was prepared with exactly the same material and dimensions as the free pipe and called as the fixed pipe. The fixed pipe was attached with clamps to a fixed wooden frame placed above the laminar box setup with long steel rods. Uplift force data

were recorded from the Miniature Pressure Transducers attached to the lower outer surface of the fixed pipe. This was the only function of the fixed pipe. For nine shaking tests fixed pipe were used. Figure 4.3 shows the fixed pipe with its steel bars, and Figure 4.3 shows the fixed pipe as placed in a laminar box.

At the beginning of the study, what was expected from the free pipe was to observe the vertical displacement (LPMs) with the effect of excessive pore water pressure and to measure the uplift force from the bottom of the pipe with Miniature Flat Pressure Transducers mounted to the pipe. However, after performing the first three experiments with clean sand, it was seen that the free pipe, which was allowed to move vertically, started to uplift as soon as it was forced by upward pressure. So, it was impossible to determine the change of uplift force on the pipe over time.

It was decided to use a fixed pipe model to measure the uplift force acting on the pipe, while the free pipe was moving upward. For this reason, another pipe was prepared with exactly the same material and dimensions as the free pipe and buried at the same depth. The fixed pipe was clamped to a fixed wooden frame placed above the laminar box setup with long steel rods. Uplift force data were recorded from the Miniature Flat Pressure Transducers (EP) attached to the bottom outer surface of the fixed pipe. This was the only function of the fixed pipe. For nine shaking tests performed with GRS mixtures, fixed pipes were used.

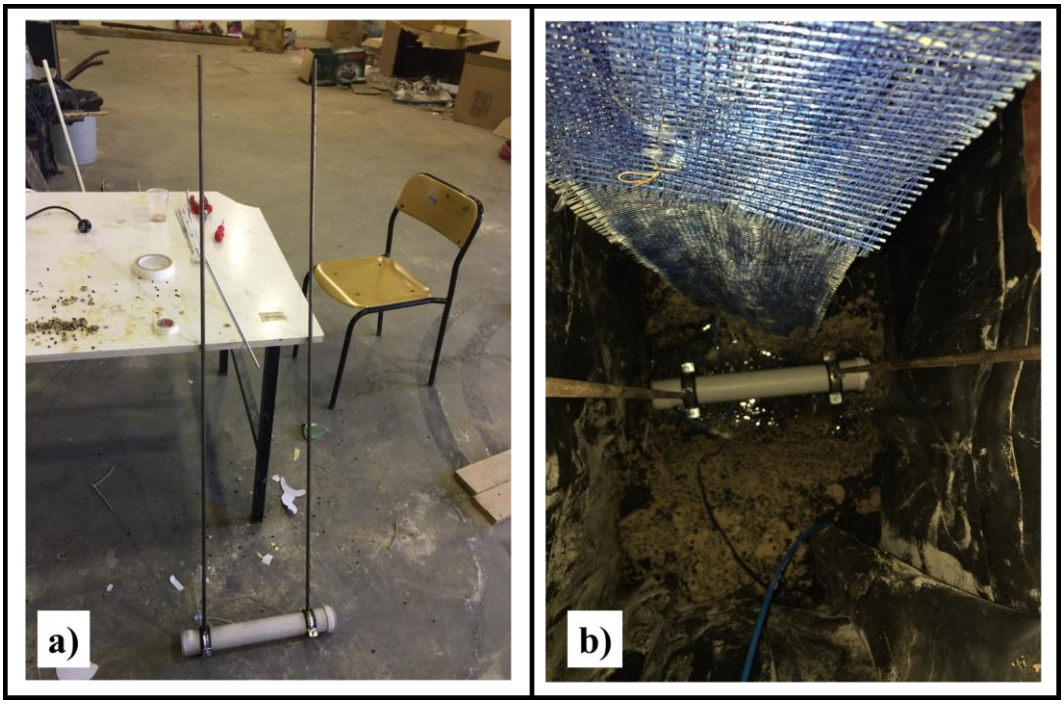

Figure 4.3. Fixed pipe a) itself b) placed into laminar box

4.3. Instrumentation

Shake table tests that were conducted for this part of the experimental work, required high-density sensors consisting of five excess pore water pressure transducers (EPWPT), five linear potentiometers (LPM), three Miniature Flat Pressure Transducers (MPT), and two submersible accelerometers (SA). All five EPWPTs and three of the LPMs were the same instruments that had been used in the experiments of Chapter 3. Two more LPMs were added to measure the upward movement of the free pipe. Three miniature pressure transducers (EP) and two submersible accelerometers (SA) were the instruments that were added for this chapter newly and were described in detail in this section.

4.3.1. Potentiometers

As known, three identical linear potentiometers (LPM) were used with a 300mm displacement capacity in the experimental work of Chapter 3. Two more identical LPMs were added to the system, and a total of five LPMs were used for this Chapter. As mentioned before, X-P5 were used to measure the horizontal displacement of the shake table tests during the shakings. At the same time, the other two potentiometers named Z-P1 and Z-P4 were placed vertically by fixing to wooden plate above the laminar box. The tips of these LPMs were mounted to the settlement plate to measure soil settlement during and after shakings (see section 3.5.1).

Newly, Z-P2 and Z-P3 were again placed vertically by fixing to a wooden plate above the laminar box, but the tips of these LPMs were placed on rails connected to free pipe which were existing on the soil surface. The LPMs were expected to measure vertical displacements precisely, so the LPM body should be fixed vertically and horizontally while LPMs' tips should be free vertically. But the pipe and soil model moved horizontally with varying displacements during the shaking. While measuring the vertical displacements of the free pipe, LPMs should not be affected by the horizontal displacements. Thus, it would be correct to neither constrain the LPM tips directly to the pipe nor leave them as free ends. For this reason, it was necessary to design a pin that is constrained in the vertical direction and free to move in the horizontal direction of the shake table.

This design was accomplished as follows: Small discs were attached to the LPM tips and placed inside the rails of the pipe. It was impossible for the discs to come out the rails, but they could move in rails freely in one horizontal direction. While the system was moving horizontally in one direction, LPMs bodies were not moving horizontally, thanks to the discs that were free to slide in one direction inside the rails. On the other hand, the vertical movements of the rails, as in other words, movements of the free pipe, were precisely measured. Figure 4.4. a shows the disc mounted to the tip of the LPM, Figure 4.4.b shows the LPM disc tip placed on rails, while Figure 46.c shows the LPM, rails, rod, and free pipe model together.

Figure 4.4.d and e show the Z-P2 and Z-P3 placed on the free pipe rails, which moved upward after a shake test. Z-P2 measured the moving side of the free pipe while Z-P3 measured the other part. Z-P1, Z-P4, Z-P3, and Z-P4 were shown in Figure 4.5 from different points of view.

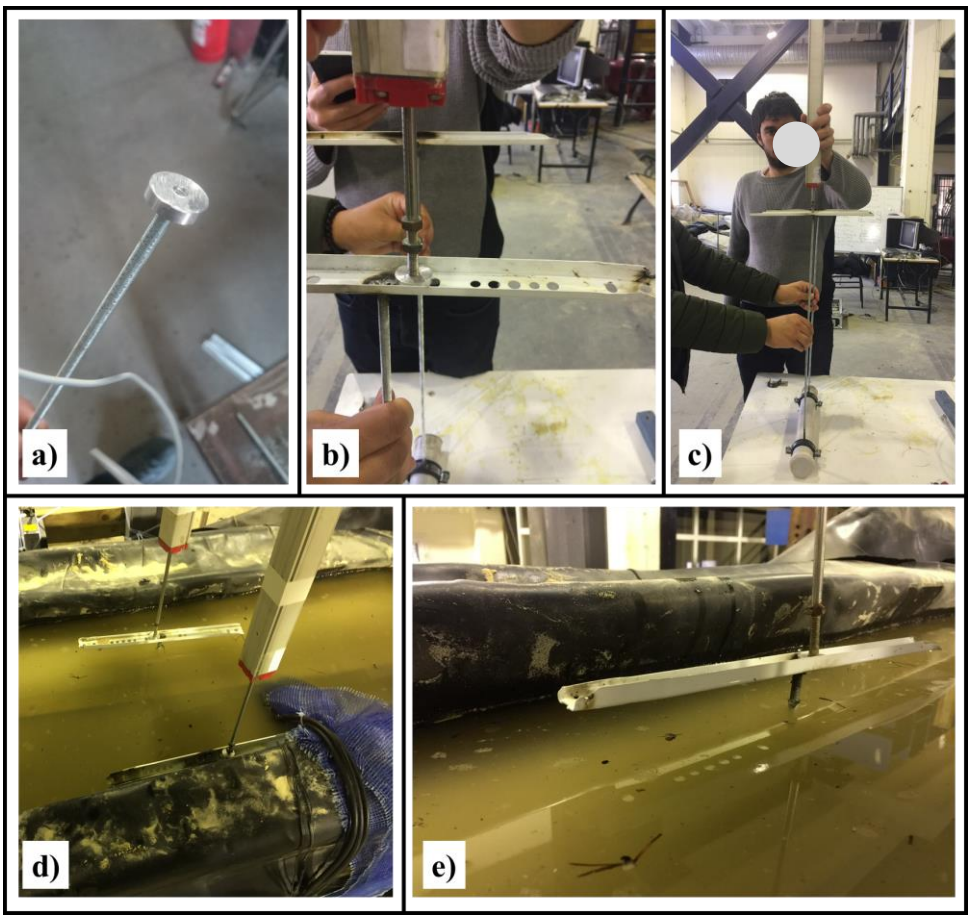

Figure 4.4. Free pipe and LPMs joints consisting of rails and discs
.a) the disc mounted on the tip of LPM, b) and c) the disc moving in rail, d) and e) Using the LPMs, discs and the rails during the tests.

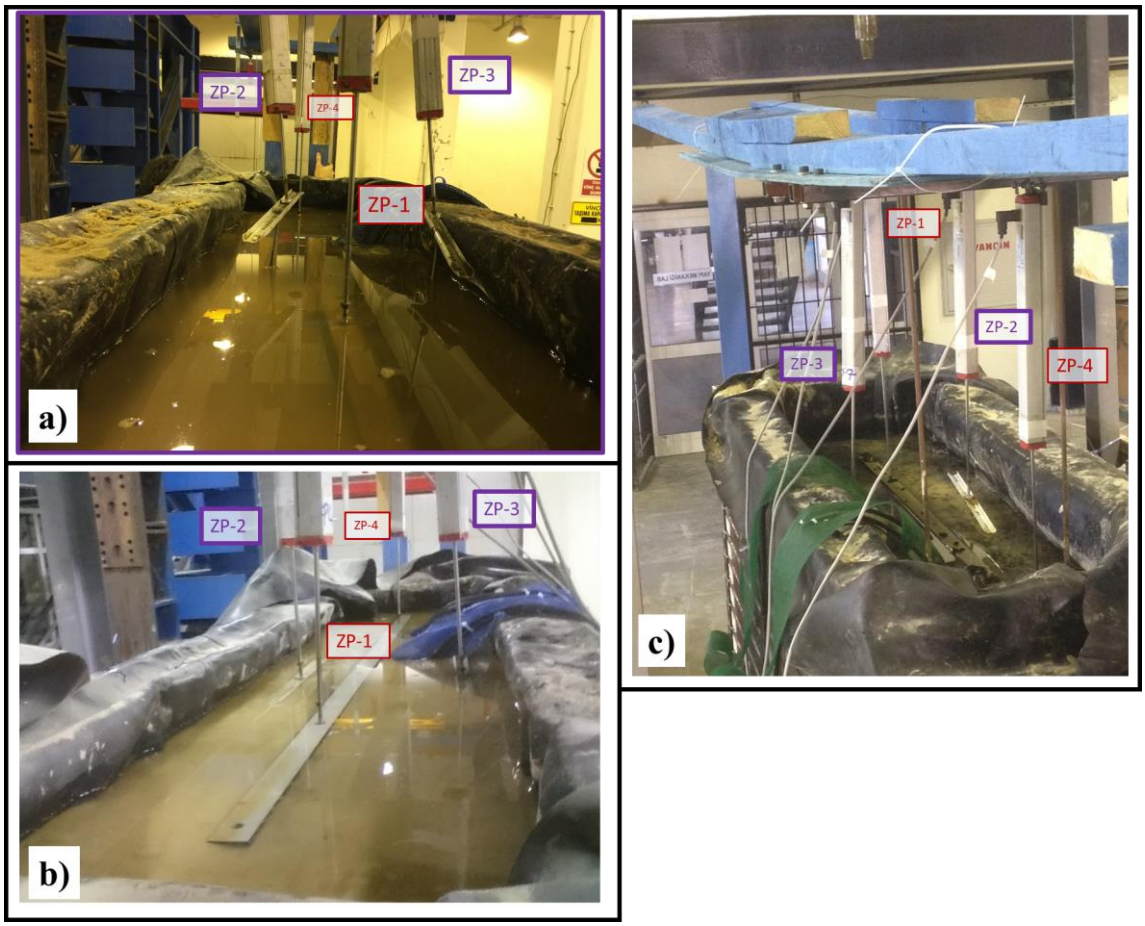

Figure 4.5. LPMs on the laminar box a-c) with different points of view

4.3.2. Pore Water Pressure Traducers

There was no additional instrumentation of EPWPT. Same nets and EPWTPs were used as mentioned in section 3.5.2. Remember, the names of the EPWPTs were PP1, PP2, PP3, PP4, and PP5; their depths from the surface of the filling soil were 1.05m, 0.63m, 0.40cm, 0.63m, and 0.20cm, respectively.

4.3.3. Miniature Flat Pressure Transducers

The Miniature Flat Pressure Transducers (EP) were PDA-200KPB, and the capacity was 200kPa. They were bought from Tokyo Sokki Kenkyujo Co. Ltd. MPT had 7.6mm diameter and 2mm thickness, and the shape of the EP was like a disc. The EP was a surface mount pressure sensor with a stainless-steel diaphragm. This was a miniature pressure transducer most suited to short-term measurement in model experiments. It had

simple waterproof construction, which allowed to use of underwater measurement in the short term. EP was easy to install on flat surfaces using elastomer or epoxy.

In this work, three identical EPs were used, which were named EP1, EP2, and EP3. In the first three tests, the EPs were pasted at the outside bottom face of the free pipe to measure the total pressure acting on the pipe during and after shaking. But the uplift movement of the free pipe made it difficult to precisely measure the differences in normal stress on the pipe, as mentioned above. Thus, during the shaking trials of the last nine tests, EPs were pasted at the bottom of the free and fixed pipes. Two EPs became out of order due to their cables breaking in different experiments. Only one EP remained until the experiments ended. Figure 4.6 a,b, and c shows the EPs pasted on the surface of the pipes from a different point of view, while a close-up view of the EP is shown in Figure 4.6. d.

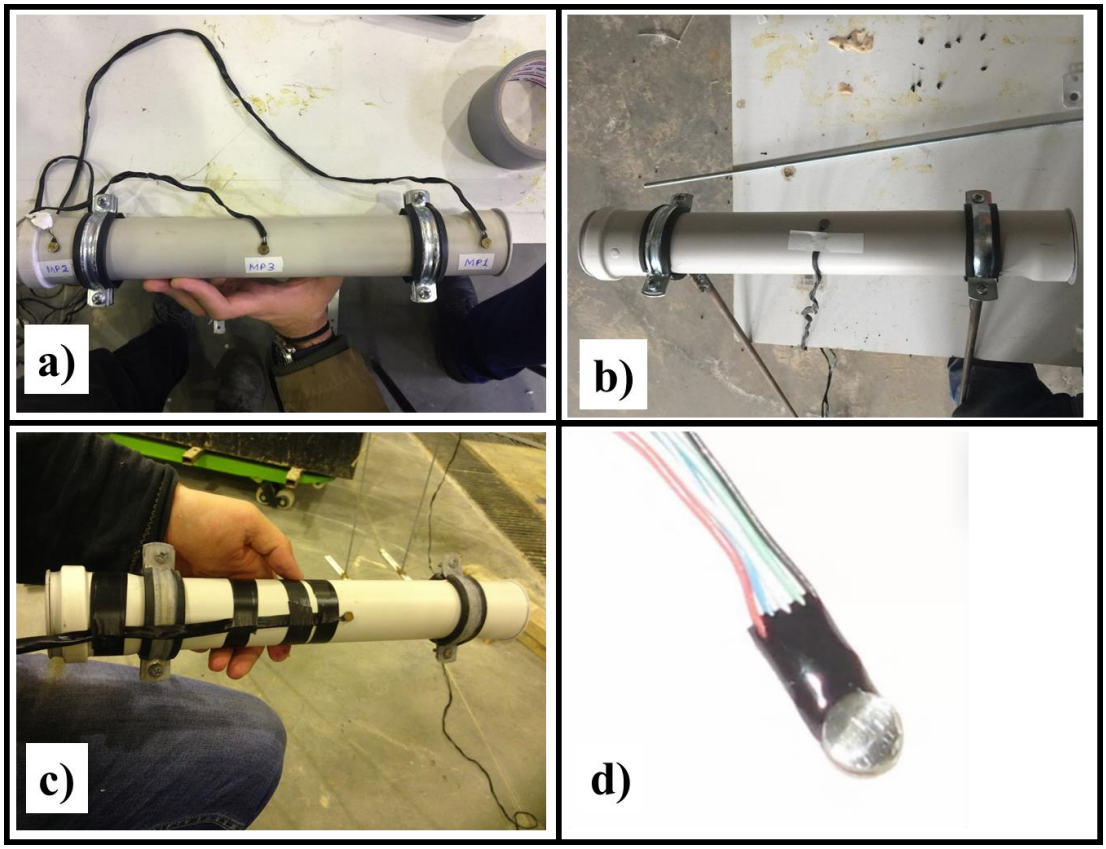

Figure 4.6. EPs pasted on pipes;
.a) EP1, EP2 and EP3 pasted on fee pipe, b) EP1 pasted on fixed pipe, c)EP2 pasted on free pipe d) Miniature Flat Pressure Transducers (EP), itself.

4.3.4. Submersible Accelerometers

The Submersible Accelerometers (SA) were ARH-A10 with a capacity of 10m/s^{2,} and they could measure the acceleration data in one direction. They were bought from Tokyo Sokki Kenkyujo Co. Ltd. SA had 16x16mm width and 28mm length, and the shape of the SA was like a rectangular prism. The weight of SA was 18gr. The SAs had a waterproof structure and could be installed in water or ground. It had resistant to 500kPa water pressure. Two identical submersible accelerometers (SA) were used. The SAs were mounted to nets at 62.5cm from the surface of soil deposits which is the same as the pipes' depth.

What was expected from SAs was to accurately record the acceleration of the soil deposit in the direction of shaking at the depth of the buried pipe. Figure 4.7.a shows the Submersible Accelerometers, and Figure 4.7.b shows the SA mounted on nets. But during all trials, the recorded acceleration data were wrong as aresult of SA chancing their direction during the shaking caused by generated water pressure or settlements of the soil particles for all trials.

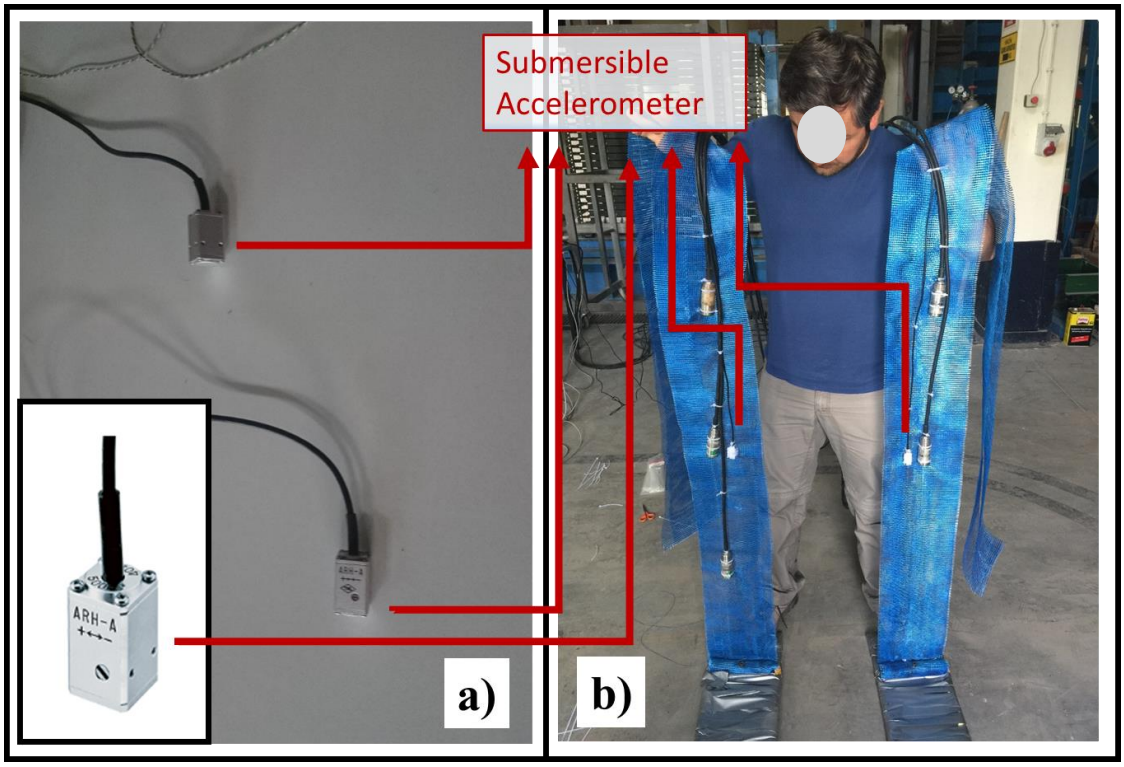

Figure 4.7. a) Submersible Accelerometers (SAs), b) SAs mounted on nets

4.3.5. Data Acquisition System and Software

The data acquisition box (DAQ) which was identified in Section 3.5.3. was used, and there were no additional operations for data acquisition. Please see Section 3.5.3 for details.

4.4. Piezocone Penetration Test (CPTu) System

CPTu has performed again for all shaking trials after the filling and becoming saturated the soil deposits and before performing the shaking tests. There was no difference from the CPTu system mentioned in Section 3.5. As known, the result of the CPTu test helped to calculate the relative density of the soil model prepared in the laminar box and give a clear view to check the soil models density values through the entire depth and discuss whether the soil models were prepared well or not. The CPTu tests results and calculations were discussed in the following sections in detail.

4.5. Tests Process

For this study chapter, twelve shake tests were conducted under the different placing conditions of pipe models and filling material to reach comparative results. CPTu tests were also performed before the shake table tests to determine the relative density of the soil in the model before each shaking test started. In this section, the filling process of the GRS mixtures, determinations of unit weight of soil models by using buckets, CPTu tests, the pipe models, and placing conditions of the pipe models, shaking tests, and the unfilling process are described for each trial. The experimental matrix of twelve tests and their results are given.

4.5.1. Shake Table Tests

First, the experimental matrix of the shaking test was explained to clarify the scope of the comparative study. A total of twelve tests were performed. The first three tests (P1-P3) were performed with clean sand deposits and by placing only the free pipe model, while the accelerations of the seismic shaking varied. The maximum shaking

accelerations of the tests P1, P2, and P3 were 0.2g, 0.35g, and 0.46g, respectively. For the last nine tests (P.GR.S.1 to P.GR.L.3), the maximum acceleration of shaking tests was 0.35g. These nine tests were performed with both free pipe and fixed piped. The filling material of these nine tests were GRS mixtures with varying GR size and GR/Sand mixing ratio in volume. The duration of shaking was 20sec, and the frequency was 2Hz for all trials.

The bottom layer of the laminar box was filled with compacted medium dense with 65cm thickness, and this layer was not changed during all tests. The upper layer of the laminar box was filled with loose sand for a test of P1-P3 with a thickness of 75cm. The granulated rubber and sand mixture (GRS) was filled for the other nine tests. The Granulated Rubber (GR) size varied in three groups 2.5-5mm, 5-10mm, and 10-15mm, and used by each group, three different mixtures were prepared with varying mixing ratios; Granulated Rubber/Sand; 10/90%, 20/80%, and 30/70% in volume similar to Chapter 3.

The experimental matrix of the laminar box shaking test with the pipe model is shown in Table 4.1. Note that in Table 4.1, the test name represents the mixture conditions; "P1-P3" represents the tests performed with the pipe model, and only sand was used as soil deposit. For the other nine trials, the letter "P" is for "Pipe"; the letters "GR" are for Granulated Rubber, S for the small size of GR (2.5-5mm), M for the middle size of GR (5-10mm), L is for large size of GR (10-15mm), and lastly, the numbers of 1, 2 and 3 are for the ratio of GR in the mixture for 10%, 20%, and 30%, respectively. In Table 4.1, "Acc" means maximum acceleration of shaking, and it was derived from displacement data recorded by LPM. D_{10}, D_{50}, C_u, and C_c represent the effective particle size, mean particle size, uniformity coefficient, and the coefficient of gradation, respectively. γ_{sat} is saturated unit weight, and it was determined using small buckets. D_r represents the relative density of samples, and it was derived from CPTu test data. Gradation curves of all GRS mixtures are already shown in Figure 3.25. Pictures of small portions of GRs mixtures were also shown in Figure 3.26.

The acceleration data was derived from displacement data recorded by LPM named "X-P5" during the shaking trials. Displacement and acceleration by time values were plotted in Figure 4.8. Figure 4.8.a shows the displacement and acceleration data for test P1, while Figure 4.8.c shows the data for test P3. Also, Figure 4.8.b shows the data of tests P2 and all tests performed with GRS mixtures (P.GR.S.1 - P.GR.L.3). As seen in

Figure 4.8, the first and last 1 second were starting and ending parts of the shaking, while the duration of sinusoidal shaking motion with its maximum acceleration was 18 sec.

The aim of performing the P1, P2, and P3 tests was to investigate the effect of the maximum acceleration on clean sand backfill and pipe response. For this purpose, the tests were performed under the same backfill conditions and with varying maximum acceleration.

The main purposes of the other nine tests were to investigate the effects of varying GR size and GRS mixing ratio on excess pore water pressure, liquefaction, and pipe response.

Table 4.1. Experimental matrix of shake table tests with pipe models

Test Name	GR Size	GR Ratio (by volume)	GR Ratio (by weight)	Acc	D_{10}	D_{50}	C_u	C_C	γ_{sat}	$D_{r(avg)}$	Pipe
-	mm	%	%	g	mm	mm	-	-	kN/m^3	%	-
P-S-1	-	-	-	0.2	0.09	0.16	2.22	1.42	20.90	33	Free
P-S-1	-	-	-	0.35	0.09	0.16	2.22	1.42	20.50	49	Free
P-S-3	-	-	-	0.46	0.09	0.16	2.22	1.42	20.90	24	Free
P-GR-S-1		10	6.76	0.35	0.11	0.2	2.05	1.31	19.27	26	Free/Fixed
P-GR-S-2	2.5-5	20	10.12	0.35	0.11	0.2	2.01	1.34	19.16	35	Free/Fixed
P-GR-S-3		30	14.35	0.35	0.12	0.2	1.91	1.28	18.65	39	Free/Fixed
P-GR-M-1		10	4.74	0.35	0.12	0.2	1.83	1.23	20.08	29	Free/Fixed
P-GR-M-2	5-10	20	9.08	0.35	0.11	0.2	2.10	1.18	19.47	42	Free/Fixed
P-GR-M-3		30	13.46	0.35	0.11	0.2	1.91	1.11	18.55	28	Free/Fixed
P-GR-L-1		10	6.43	0.35	0.11	0.2	1.91	1.28	20.08	10	Free/Fixed
P-GR-L-2	10-15	20	11.95	0.35	0.11	0.2	2.00	1.31	19.37	41	Free/Fixed
P-GR-L-3		30	13.77	0.35	0.11	0.2	2.00	1.02	17.94	20	Free/Fixed

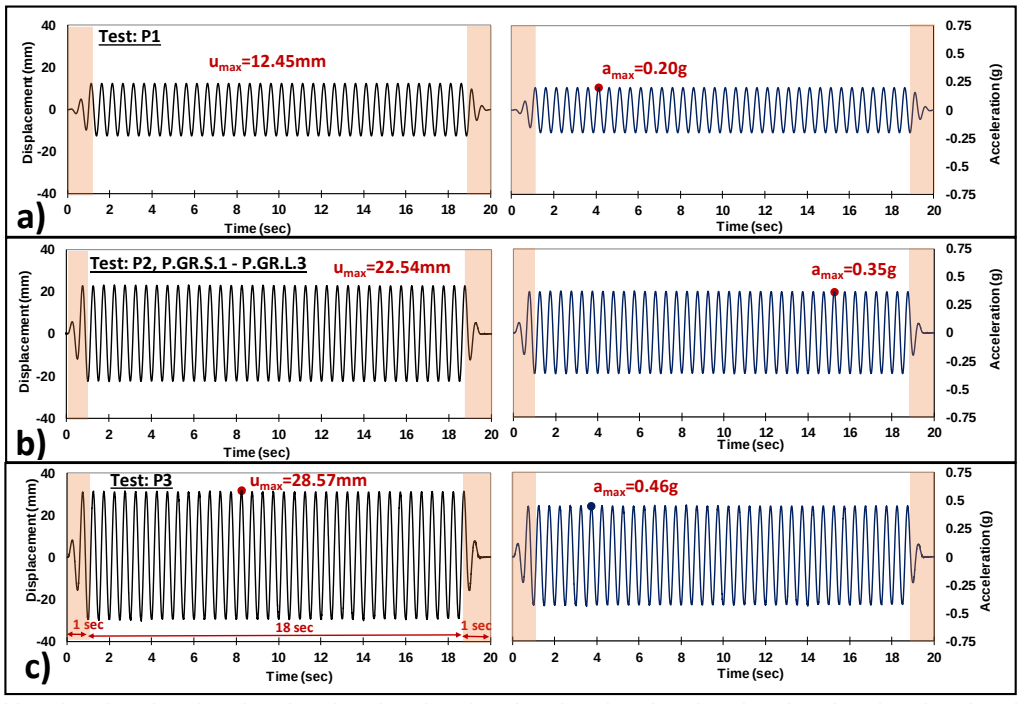

Figure 4.8. The acceleration and displacement by time graphics for all tests.

The only free pipe was placed into the laminar box for the tests P1, P2, and P3. In these tests, three EPs were pasted at the outer bottom face of the free pipe to measure the uplift pressure developed on the pipe during and after shaking. One of the SAs (SA1) was mounted to the side of the pipe, while the other one was mounted on nets. The purpose of using the SA1 was to record the acceleration of the pipe in the shaking direction and SA2 was used to record the acceleration of the backfill material at the same depth as the pipe.

The vertical movement of the pipe was recorded from two points of the pipe by Z-P2 and Z-P3. Two other potentiometers (Z-P1 and Z-P4) were positioned on the ground surface to monitor surface displacement of deposits during and after shaking. Five EPWPTs were placed at different depths of deposits and were used to record excess pore water pressure changes during and after the shakings.

Two EPWPTs; PP2 and PP4, were placed at the same depth as the pipes. The free pipe was placed 40cm away from the point where CPTu was performed and 25cm and 65cm away from Z-P1 and Z-P4, receptively. The data recorded came from five EPWPTs, two SAs, five LPMs, and three EPs (15 instruments in total) using the data acquisition system.

Two different text files that recorded 500 data per second and 2 data per second were obtained as output for each shaking trial thanks to code modeled using LabVIEW software. High-frequency data (500 data per second) was used to accurately examine rapid pore water pressure or settlement changes while shaking (first 20 seconds). Low-frequency data (2 data per second) was used to examine the dissipation of excess pore water pressure and settlements for a long time after the shaking (5-6 minutes). The configuration of the pipe within the test apparatus and the schematic sketch of instrumentation on the pipe, shake table, and sand deposit for the tests P1, P2, and P3 are shown in Figure 4.9.

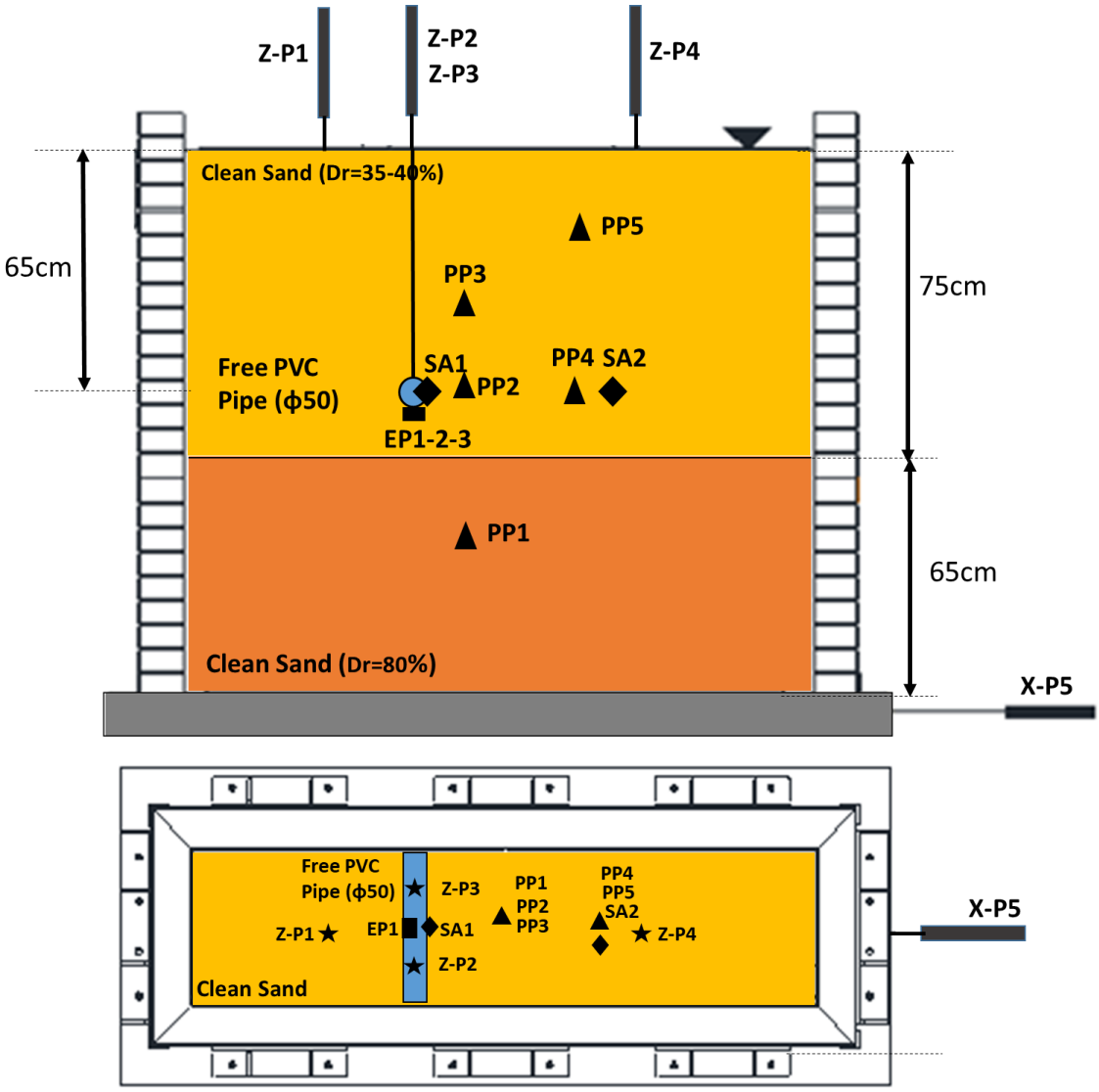

Figure 4.9. Configuration of model pipes within the test apparatus and the schematic sketch of instrumentation for tests P1-P3. (a) side view (b) plan view

Free and fixed pipes were buried into the GRS mixture for the nine tests (P.GR.S.1 to P.GR.L.3). In the first three tests, the EPs were pasted at the outside bottom face of the free pipe to measure the pressure. But the uplift movement of the free pipe made it difficult to precisely measure the differences in normal stress on the pipe, as mentioned before. So during the shaking trials of the last nine tests (P.GR.S.1 to P.GR.L.3), two of the EPs, (EP1, EP2), were pasted at the outside bottom face of the fixed pipe, because EP3 become out of order during the preparation of setup.

As known, the purpose of using the SA1 was to record the acceleration of the pipe in the shaking direction but mounting the SA1 on the surface of the PVC pipe was too difficult and SA was rotating during the shakings which caused to get wrong data. So the

place of SA1 was changed and it is mounted on one of the nets to record the acceleration of the backfill material at the same depth as the pipes similar to SA2. But also, recording the acceleration data from both SAs was unsuccessful because of the rotation of instruments. Hence, the place of free pipe and fixed pipe, the EPWPTs, and LPMs were not changed. GRS mixtures were filled into the laminar box with given configurations for each trial. The configuration of the pipes within the test apparatus and the schematic sketch of instrumentation on the pipe, shake table, and sand deposit for the tests P1, P2, and P3 are shown in Figure 4.10.

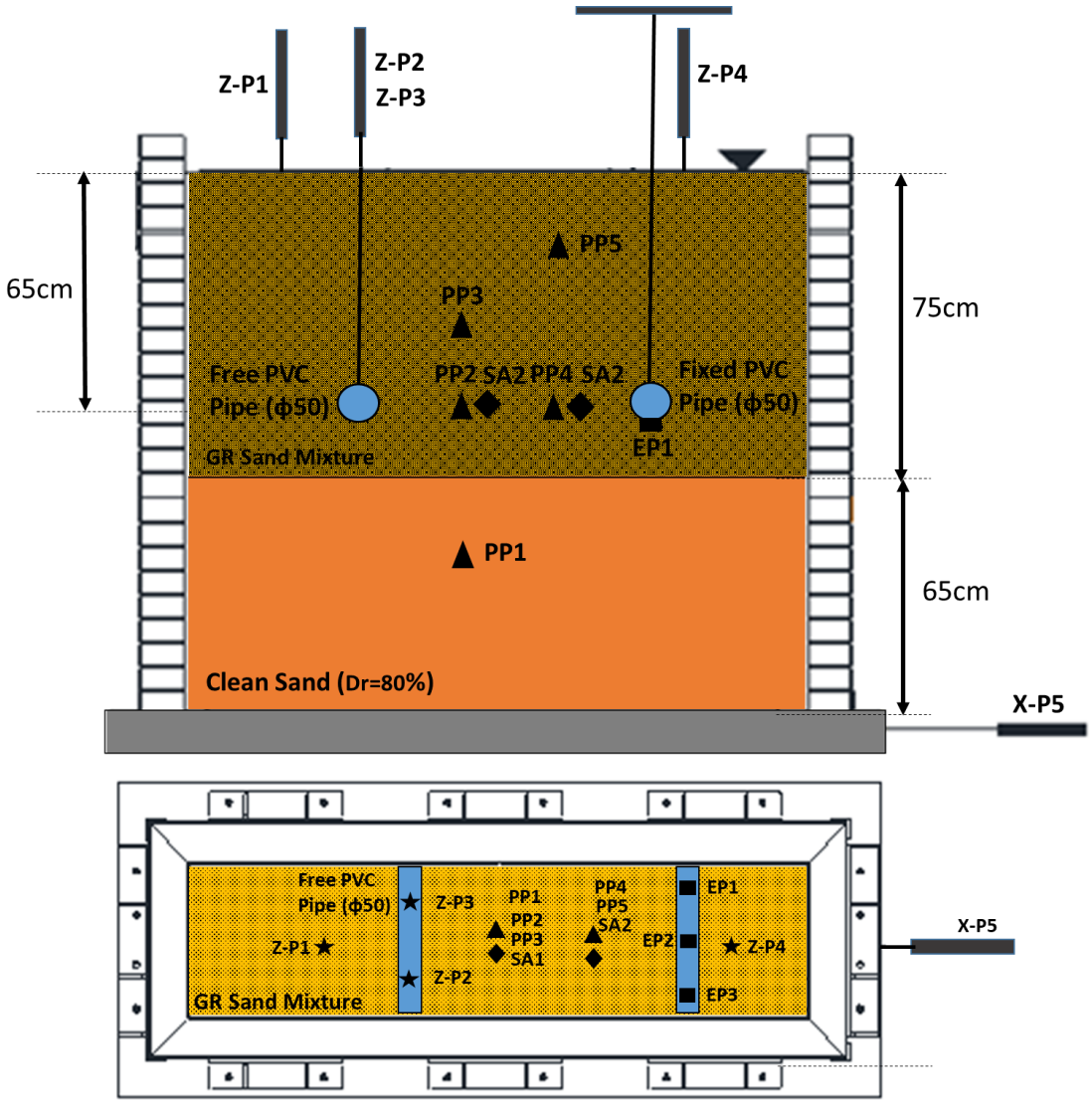

Figure 4.10. Configuration of model pipes within the test apparatus and the schematic sketch of instrumentation for tests P2 and P4-P12. (a) side view (b) plan view

4.5.2. Sample Preparation and Filling Process

As explained in detail in the previous section, the instruments were mounted vertically using nets in the laminar box, and the EPWPTs' locations were checked again. The laminar box was filled step by step with the sand. The soil deposits were prepared similar to Chapter 3. First layer was dense clean sand layer and it was filled at the beginning of the first test and used for all 12 tests without unfilling. The upper layer was filled and unfilled for each trial, the changes in filling materials were described in Section 3.6.2. Preparing process of the bottom layer with 65cm thickness and representing the non-liquefiable soil was same as the described in Section 3.7.2. Fully saturated silica sand deposit was placed into the box by the hydraulic filling technique, allowing sand grains to sink slowly through the water. The laminar box was shaken with various accelerations for several minutes to densify the soil. This time, the buckets were not used for bottom layer. Preparation of the dense sand layer and sampling with buckets were already summarized schematically in Figure 3.30 in Chapter 3.

Then, the upper loose sand layer was started to be filled for the tests named "P1-P3". The fully saturated silica sand deposit was placed into the box by the hydraulic filling technique for this layer again. This loose sand layer was prepared to represent the liquefiable soil layer laying on non-liquefiable soil. Similarly, buckets were placed for each step and different depths and collecting of the samples were continued. Preparation of the loose sand layer and sampling with buckets were schematically summarized in Figure 3.31, so it was not repeated in this section. Calculated unit weights of the samples were summarized in Table 4.1

As known for the nine tests prepared with granulated rubber and sand ("P.GR.S.1" - "P.GR.L.3"), the upper part of the laminar box couldn't be filled by hydraulic filling method because of the particle segregation problem, thus the sand and GRS mixtures were poured by hand (see Section 3.7.2). Preparation of the loose GRS layer and sampling with buckets were already summarized schematically in Figure 3.33. Unit weights of GRS mixtures were summarized in Table 4.1. After the filling process, the deposits were left for at least 2h to allow they become fully saturated.

4.5.3. CPTu Test

CPTu tests were performed after soil mixture deposits were filled into the laminar box and water-saturated before each shaking trial. CPTu tests were performed same as described in Section 3.7.3. The q_c, f_s, and u_2 values were recorded for 2cm interval through the all depth of loose backfill layer and a half part of the dense sand layer.

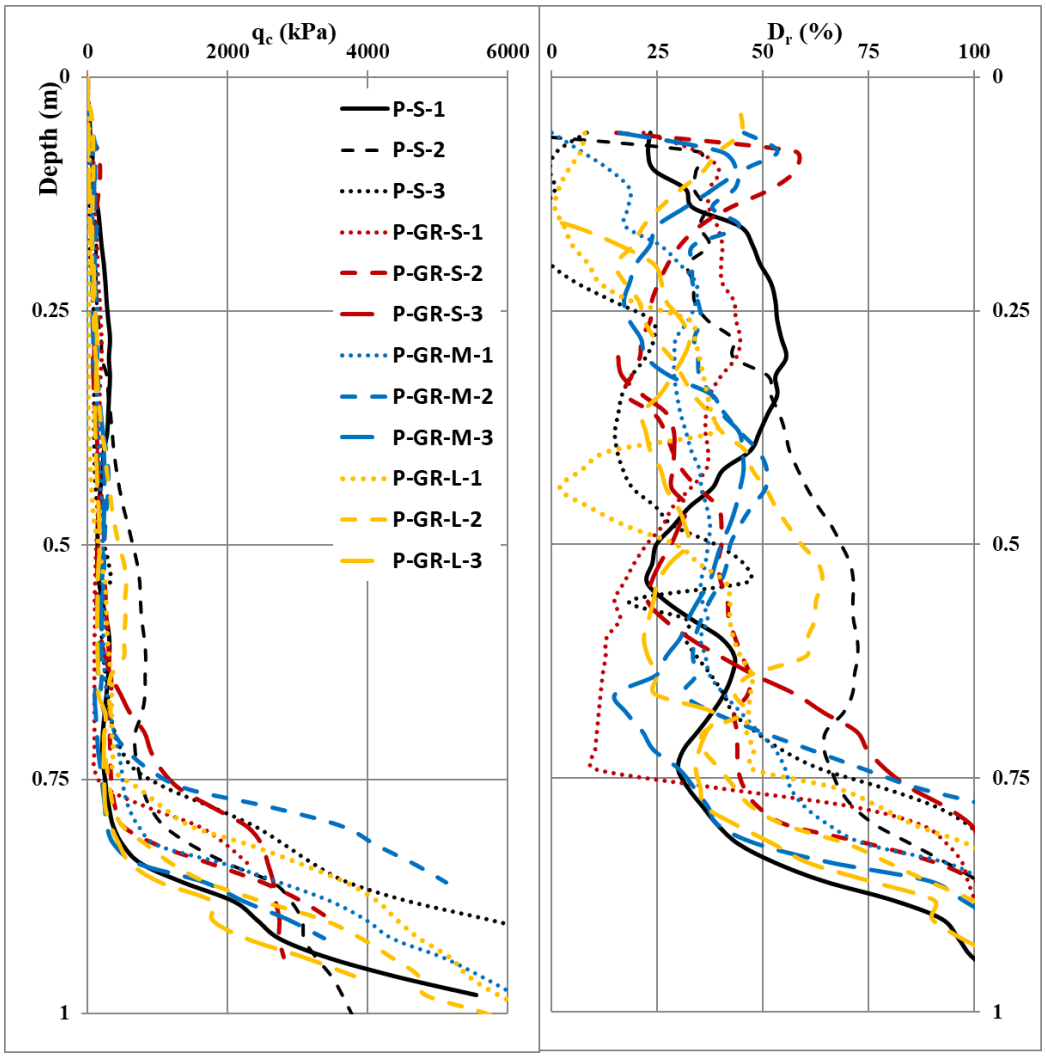

Figure 4.11. CPTu results; q_c and D_r values

Figure 4.11 shows the tip resistance qc and Dr values versus depth for all tests. As seen in Figure 4.11.a, the first 75cm loose sand or GRS mixture layers tip resistance values were lower when the CPTu cone started to penetrate through the dense sand layer, the qc values started to increase significantly for all tests. Relative density values are calculated using Equation 3.1. and plotted in Figure 4.11.b for through depth. In Figure

4.11.b, Dr values are negative which is physically unfeasible at the firsth 0-20cm depth of CPTu tests. The reason of this is the Equation 3.1 was proposed for field tests where the ground water level is at the surface of the soil or lower. In this studies, water level of the deposits in the laminar box is 1-2cm higher than the surface of the soil deposits. Thanks to these small diferenceses between level of water and soils, for the first 0-20cm depth, Dr values are neglectable. As seen in Figure 4.11, Dr values of the upper layer are lower, while the bottom dense sand Dr values are higher. Also, average Dr values of GRS layer or loose sand layer are listed in Table 4.1 for each trial. These results prove that the dense sand layer and the loose backfill layers exist as intended and filling of deposits were succeed again.

4.5.4. Unfilling Process

After performing of each shaking, GRS layer was unfilled form the laminar box. These saturated GRS deposits were taken and poured into preparation boxes using by big buckets. The water was drained with valves at the bottom of the preparation boxes. The deposits in the boxes were kept for at least one day for drainage of the water. Then, these deposits were used to prepare another mixture if the GR/S ratio and GR size were suitable to following trial. If it was not, the mixture was poured into barrels and empty preparation boxes were cleaned for next trial. After the unfilling of the upper layer of the laminar box, the instruments, the nets carrying the instruments and membrane were checked. The upper surface of the dense sand layer was cleaned and leveled for next trial.

4.6. Results and Discussions for Sand

In this section, the result of three tests which were conducted with clean sand were represented. These tests were P1, P2, and P3. In these tests, the free pipe was placed into the sand to represent a field condition with a buried pipeline in loose sand deposits under the groundwater level. The shaking tests P1, P2, and P3 were performed with varying maximum acceleration of 0.2g, 0.35g, and 0.46g, respectively. The results were discussed to observe the effects of the maximum acceleration on liquefaction sand and pipe response. According to the findings, maximum acceleration of 0.20g and 0.35g were comparable, while 0.46g caused a fluctuation of the pore water pressure results. Firstly,

the effects of maximum acceleration on liquefaction were discussed, then its impact on settlement and the pipe response were observed.

4.6.1. Effect of maximum acceleration on backfill and liquefaction

The changes in the excess pore water pressure ratio at 0.20 m, 0.40m, 0.625m, and 1.05m in depth during and after shaking tests P1, P2, and P3 are given in Figure 4.12. As seen in Figure 4.12, Excess Pore Water Pressure (Δu) results show fluctuation at each depth for the P3 performed with a_{max}=0.46 g. Therefore, the following tests with GRS were performed with a maximum ground acceleration of a_{max}=0.35g. As mentioned before in this study, the pore pressure ratio (r_u), which is the ratio of excess pore water pressure (Δu) to the initial effective vertical stress (σ_{vo}'), was used to assess the full liquefaction. In general, liquefaction occurs when r_u reaches 1.0. The r_u values are plotted in Figure 4.13. As seen in Figure 4.13, r_u values reach 1.0 during the shaking. However, for tests P1 and P2 at a depth of 0.20, 0.40m, and 0.63m, the r_u values were more or less than 1.0. Because, the EPWPTs were dislocated during and after the shaking. The water level was changed and the settlement was observed at the surface of the soil and these changes affected the vertical effective stress (σ_v') during the shaking. For example, the σ_{vo}' values at a depth of 0.63 m were 6.9, 6.9, and 5.7 kPa for tests P1, P2, and P3, respectively (Ecemis 2013, Ecemiş et al, 2021). The peak r_u values at 0.63m depth reached 0.9 (Δu = 6.12 kPa) and 1.0 (Δu = 7.3 kPa) for tests P1 and P2, respectively. As clearly shown in the pore pressure dissipation results of tests P1 and P2, the generated excess pore pressure essentially dissipated after shaking (Figure 4.13). Figure 4.12 shows the generated excess pore water pressure (Δu), while Figure 4.13 shows the r_u values of for tests P1-P3.

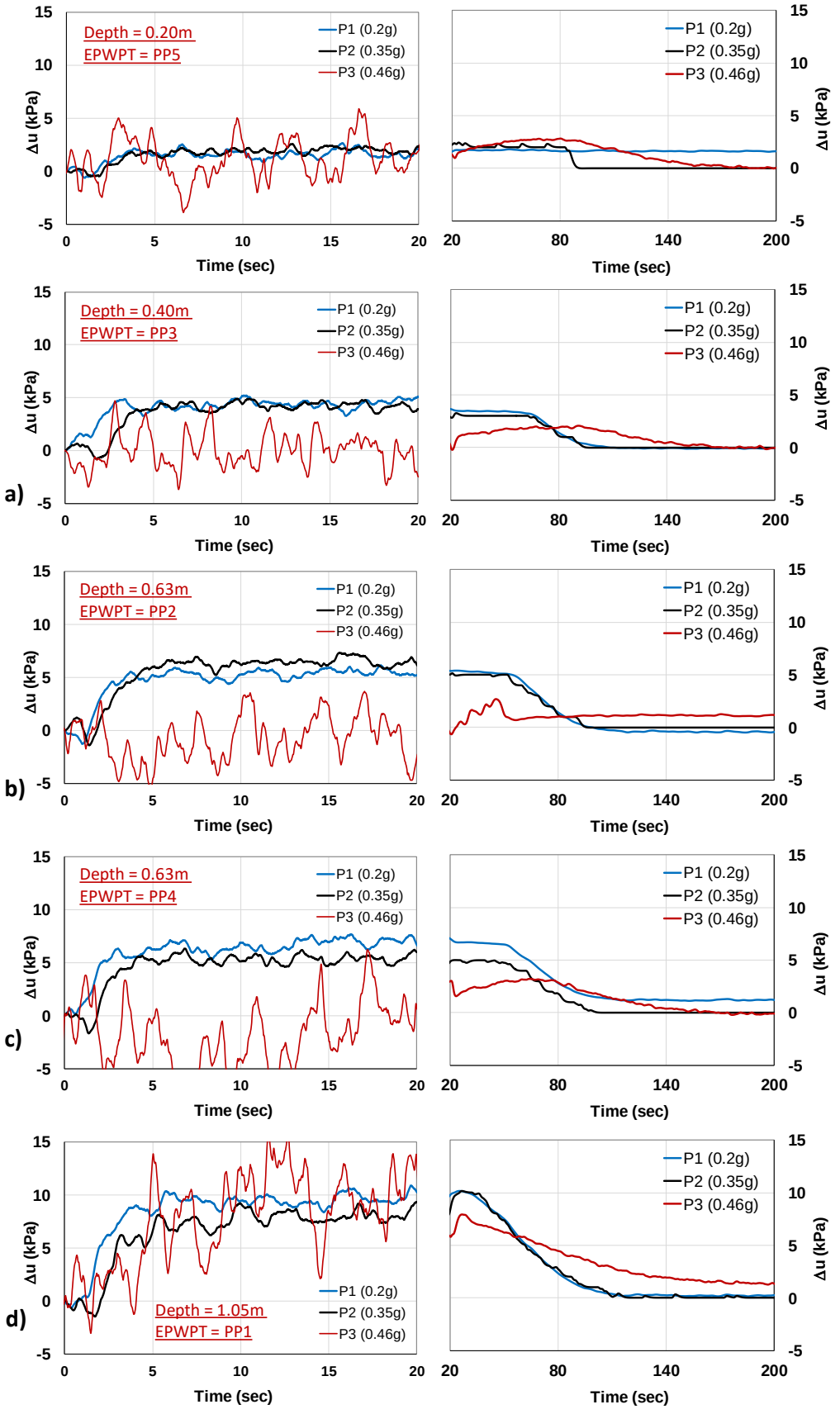

Figure 4.12. EPWP changes during (left column) and after (right column) shaking for each depth (a-d) for the tests P1, P2, and P3

For 0.20m depth, r_u returned to zero for Test P2, but there was no dissipation for Test P1. The reason was that there was a dislocation of the instruments (Figure 4.13.a).

For 0.40m depth, the liquefaction occurred for tests P1 and P2, and both of them dissipated at about the same time in post shaking stage. On the other hand, the duration for the dissipation of pore water pressure took about 1 minute more for Test P3. The σ_{vo}' values at a depth of 0.4 m were obtained 3.7 kPa for tests P1, P2, and P3. As shown in Fig. 9b, the peak r_u values at a depth of 0.4 m reached 1.4 (Δu = 5.21 kPa) and 1.3 (Δu = 4.9 kPa) for tests T1 and T2, respectively (Figure 4.13.b)

If two of the EPWPTs (PP2 and PP4) were at 0.63 depth were compared, it can be seen that there were dislocation issues. For EPWPT named PP2 (Figure 4.13.c), the r_u value returns to zero for both tests P1 and P2. On the other hand, for PP4 (Figure 4.13.d), the r_u value returned to zero for test P1, but it couldn't reach 0, and it became constant at 0.2 value for Test P2. Hence, subtracting the 0.2 value from the test P2 line in the PP2 graph (Figure 4.13.d), all the r_u values almost reached the limit, and liquefaction occurred (Figure 4.13.c-d).

At depth of 1.05m where the in the middle of the dense sand layer, for all three tests, liquefaction was not observed during the shaking (Figure 4.13.e). Remember that this dense sand layer had not been unfilled after the shakings and was used for all tests, so it became denser and denser after each test.

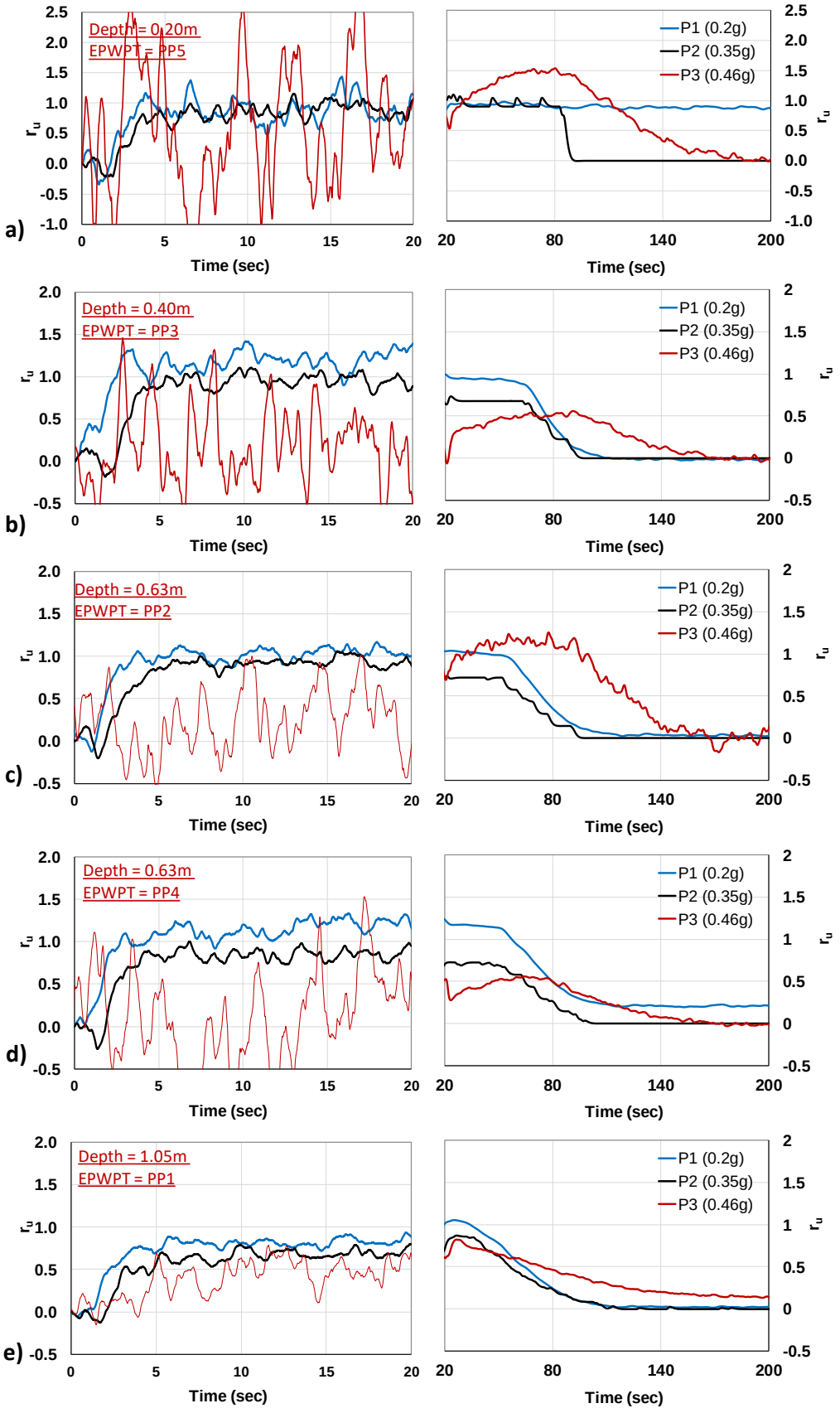

Figure 4.13. Pore water ratio during (left column) and after (right column) shaking for each depth (a-e) in the tests P1, P2, and P3.

4.6.2. Effect of maximum acceleration on liquefaction potential and settlement of backfill

The settlement that occurred at the soil's surface was observed with two LPM. One of the LPMs, Z-P2, didn't work regularly and broke out from the settlement plate. The results obtained from Z-P4 are plotted in Figure 4.14. As seen in Figure 4.14, settlement that occurred during the shaking was 20.1mm, and total settlement long after the dissipation stage was 27.3mm for test P1. Similarly, settlement during the shaking was 20.1mm, and total settlement after the dissipation stage was 31.4mm for test P2. The surface settlement values were close to each other for the test performed with a maximum acceleration of 0.2g and 0.35g. On the other hand, the settlement during the shaking was 54.9mm, while after the dissipation stage, it was 55.2mm, which was higher than the first two tests. These differences in settlement behavior of the tests partly explain the discrepancy of r_u values in Section 4.7.1.

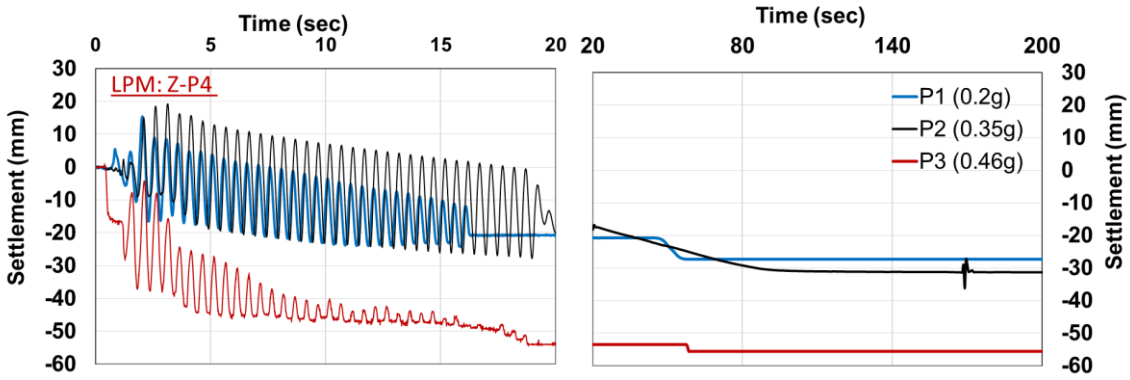

Figure 4.14. Settlement of soil for tests P1, P2, and P3.

4.6.3. Effect of maximum acceleration on pipe response

To compare the pipe response to uplift force during and after liquefaction, the pressure on the pipe was recorded by Miniature Flat Pressure Transducers (EPs) pasted on the bottom surface of the pipe. But as soon as the liquefaction occurred, the free pipe started to move upward, and the pore water pressure forcing the pipe was read as smaller than zero, which was not logical. Hence, the obtained pressure values applied on the pipe were not useful for the tests P1, P2, and P3. On the other hand, the pipe's upward movement was recorded by Z-P2 and Z-P3 precisely. Figure 4.15 shows the upward trend of the free pipe during and after shaking. Remember that Z-P2 was mounted to the free

pipe closer to the free end while Z-P3 was mounted closer to the other free end of the pipe (Figure 4.9). Differences between the pipe movement by Z-P2 and Z-P3 mean there was a lateral upward movement. Solid lines represent the movement data obtained from Z-P2, while dot lines represent the data from Z-P3 in Figure 4.15. So, the upward movements of both ends of pipe were about to equal for P1 and P2, but the movement of pipe was lateral and the differences between the two ends of the pipe at least 15mm after the shaking (Figure 4.15).

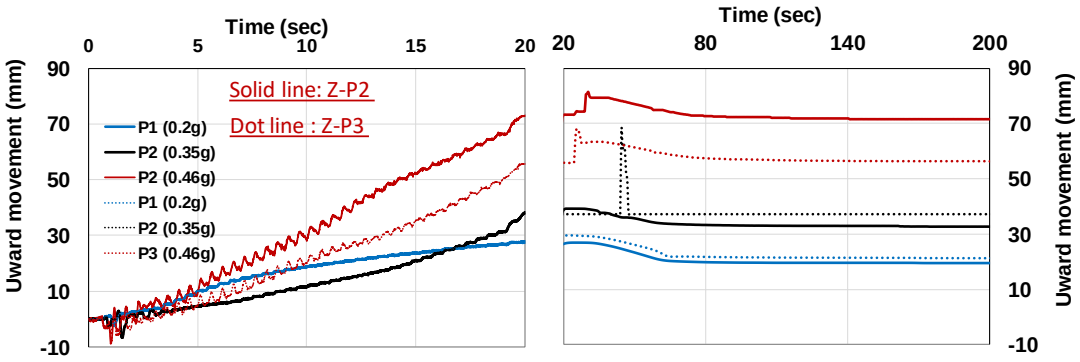

Figure 4.15. Upward movement of free pipe during and after seismic loading for tests P1, P2, and P3.

For the first 2-3 seconds of shaking, the pipe settled 2-5mm for all tests. This happened due to the settlement of the soil, then the pipe started to move upward due to the generated pore water pressure, and it had continued to move upward (15-70mm) until the shaking stopped. Then it settled a little bit and stopped (2-15mm). This also was caused by soil settlement during dissipation of pore water pressure for all three tests. Some local picks can be seen on the upward movement data in Figure 4.15. These were handmade disturbances of technicians who tried to fix or mount the instruments.

4.6.4. Effect of pipe on liquefaction resistance and settlement of backfill

A shaking test was conducted with clean sand and a maximum acceleration of 0.35g in Chapter 3, named “T1”. Also, there was a test conducted with clean sand and the same maximum acceleration (0.35g) in this chapter named “P2”. There was no pipe in T1 and there was a pipe model in P2, so comparing by these two test results, the effect of the

pipe presence on liquefaction of sand was observed in this section. The r_u values of T1 and P2 are plotted in Figure 4.16.

In the soil deposit with and without the pipe, r_u values reached 1.0 for the depths of 0.4 m and 0.65 m, representing the full liquefaction. It was seen in Figure 4.16 that Δu of the deposit was generated slower and dissipated more quickly when there was a pipe model in the backfill. At the beginning of the shaking, r_u reached 1 in 2.1 seconds in T1 while r_u reached 1.0 in 4.1 seconds in P2 for 0.40m depth. Similarly, the liquefaction starting times were 5.0 and 7.5 seconds for the tests T1 and P2, receptively for 0.63m depth. Also, the dissipation of excess pore water pressure took 140-150 seconds when there was no pipe in deposit, while it took 100 seconds to dissipate for the test performed with the pipe model. This faster dissipation of water was caused by pipe and its uplift movement. The moving upward of the pipe model allowed the water to flow around itself and caused quicker drainage.

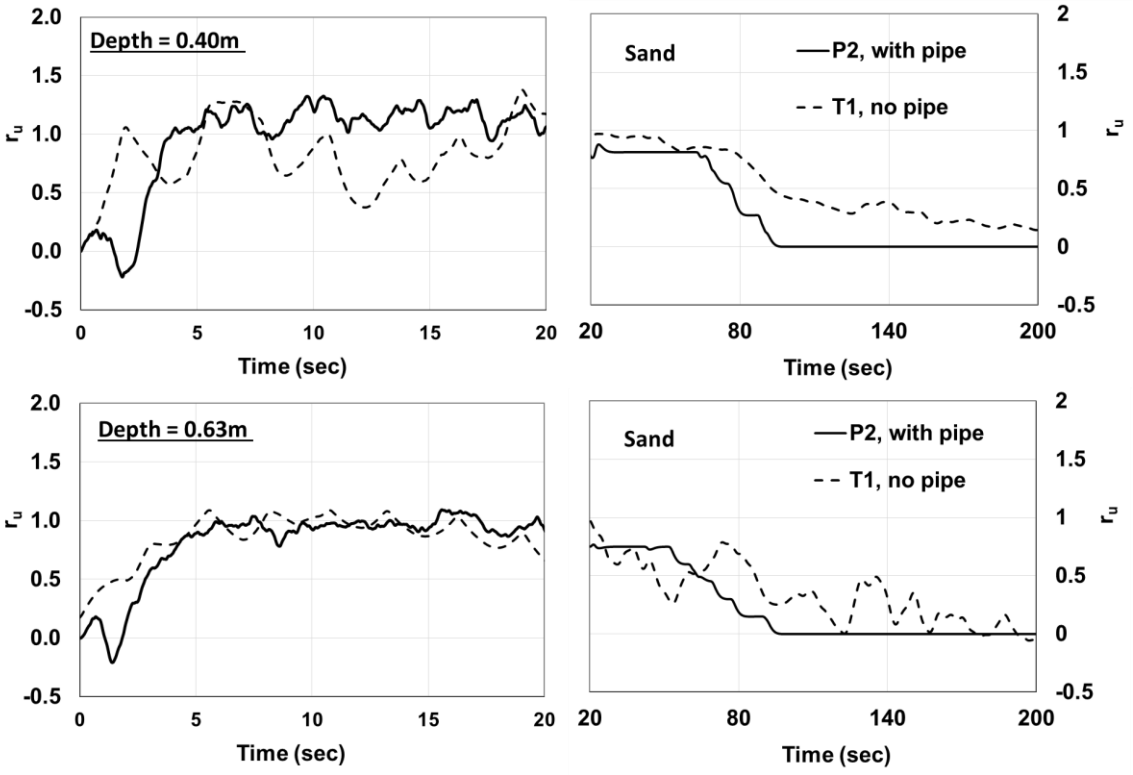

Figure 4.16. Effects of pipe on liquefaction and dissipation

To compare the settlements of the surface of sand deposits between these two tests are plotted in Figure 4.17. As seen in the figure, the settlement of the sand deposits in the test performed with the pipe model was less than in the test performed without the pipe.

Because of the lower duration of the full liquefaction stage, the settlement in P2 was lower than T1 during the shaking. On the other hand, the settlement of the test P2 was bigger and faster than the settlement in T1 for post shaking stage, in other words, the dissipation stage. This also could be explained as pipe increased the permeability of sand in the laminar box and changed the consolidation characteristics of the system with a small amount.

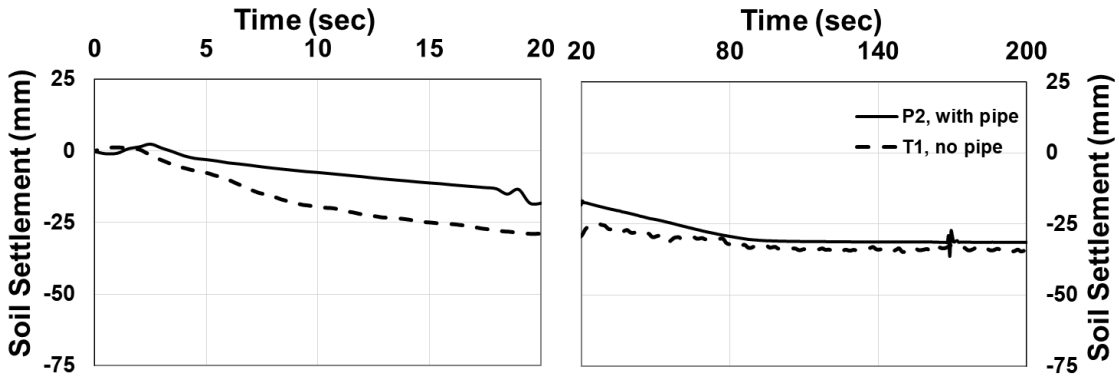

Figure 4.17. Effects of pipe model on soil settlement

4.7. Results and Discussion for GR size and ratio

In this section, the result of ten tests which were conducted with a maximum acceleration of 0.35g and with clean sand and GRS mixture, were represented. These test were P2, P.GR.S.1, P.GR.S.2, P.GR.S.3, P.GR.M.1, P.GR.M.2, P.GR.M.3, P.GR.L.2, and P.GR.L.3 (see Table 11). In these tests, free pipe and fixed were placed into sand and GRS mixture. The results were discussed to observe the effects of the GR size and ratio on liquefaction, backfill settlement, and pipe response. According to the findings, the discussions were defined in three sections; the effects of GR size and ratio on

a) excess pore water pressure and pressure changes on pipe,
b) settlement of backfill and uplift movement of pipe, and
c) pipe behavior due to the consolidation characteristics of mixtures.

4.7.1. Effects of GR on Excess Pore Water Pressure and Liquefaction

Change in pore water pressure (Δu) results obtained from EPWPTs for four different depths were plotted for all ten tests in Figure 4.18, Figure 4.19, and Figure 4.20.

Figure 4.18, Figure 4.19, and Figure 4.20 show Δu values by time for sand and GRS mixtures for GRS mixture prepared with GR sizes of 2.5-5mm, 5-10mm, and 10-15mm, respectively. Each of these figures has five parts named a-d, which show the Δu values for the depths of 0.20m, 0.40m, and two of 0.63m, respectively. Also, for all graphics left column shows the Δu changes during the shaking (0-20sec) while the right column shows Δu changes during the post-shaking / dissipation stage (20-200sec). As seen in the figures, some fluctuations make it difficult to get results for the 0.20m depths for the tests performed with all GR sizes. (Figure 4.18.a and Figure 4.19.a). In addition, for all tests performed with 10-15mm GR, there were also fluctuations for all depths (Figure 4.20). Despite the fluctuations in the data, there was a significant reduction in Δu values in GRS compared to sand deposits.

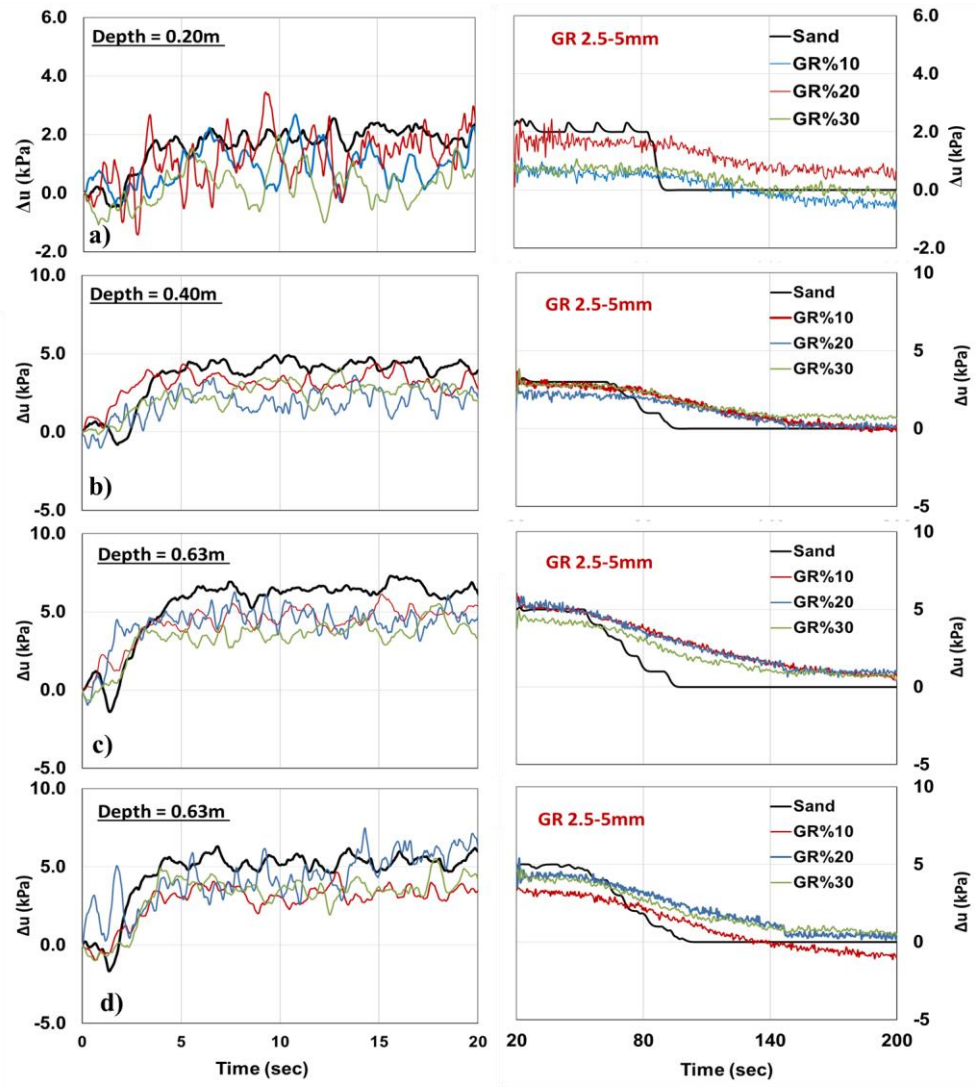

Figure 4.18. Pore water changes for several depths (a-d) in the tests performed with 2.5-5mm GR.

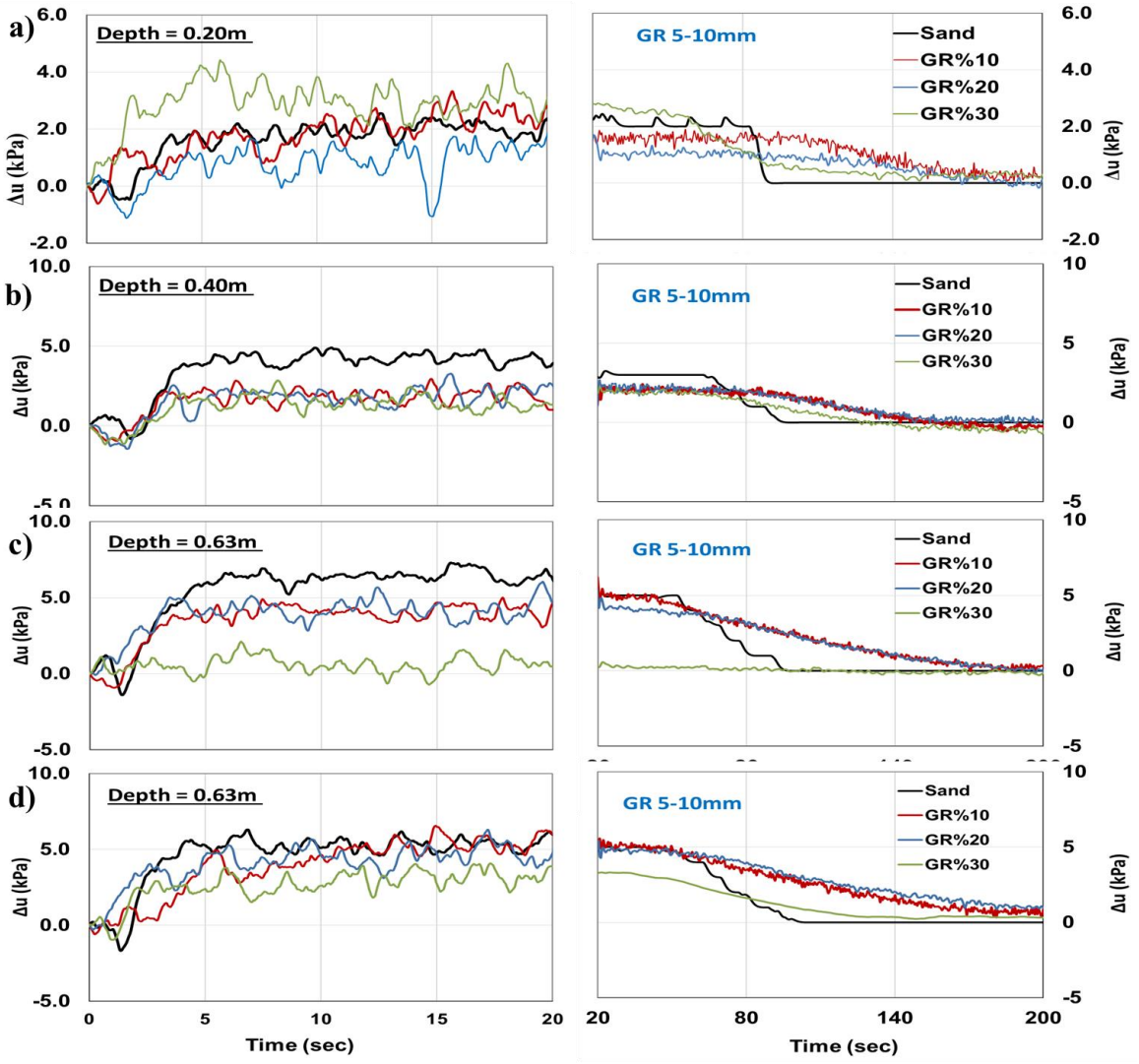

Figure 4.19. Pore water changes for several depths (a-d) in the tests performed with 5-10mm GR

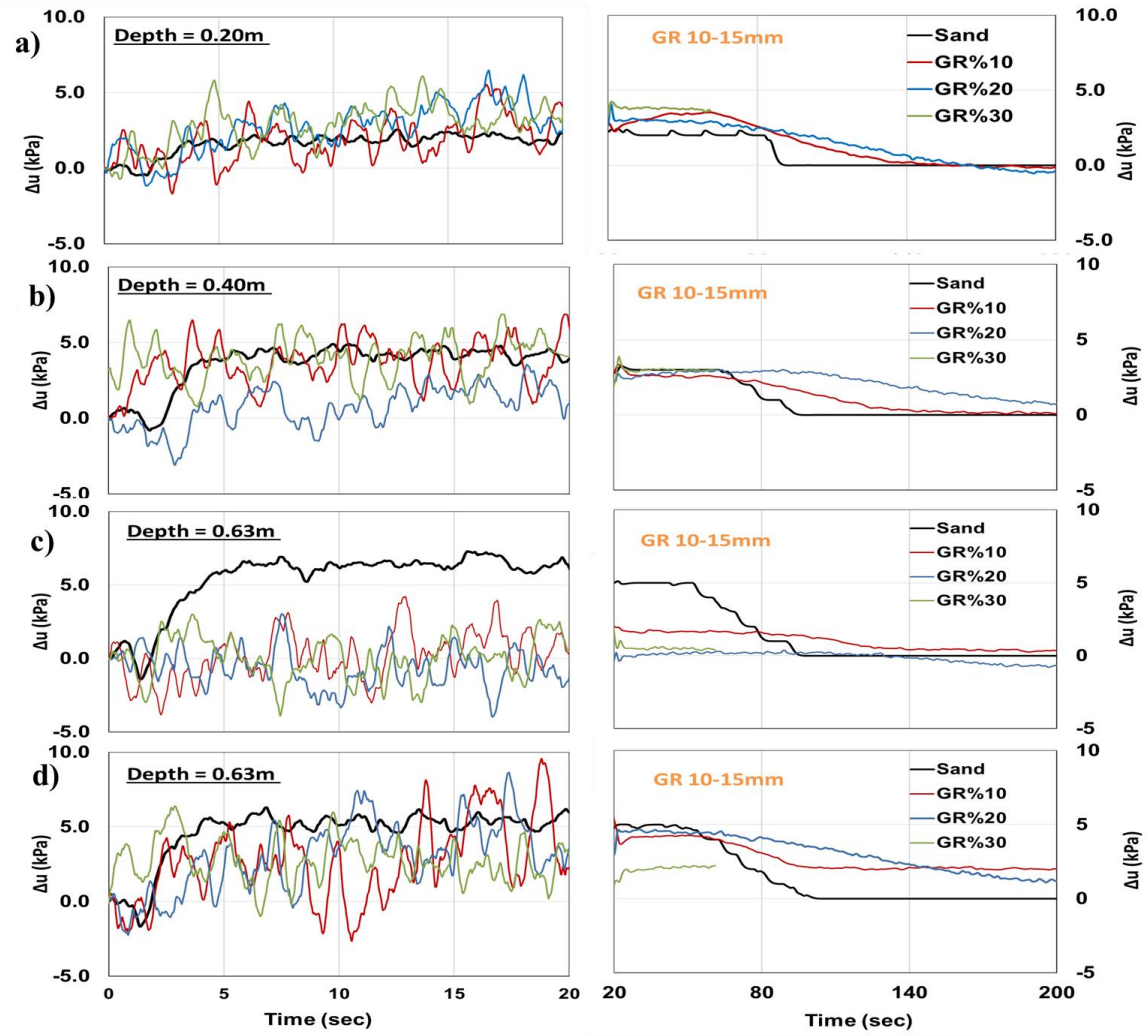

Figure 4.20. Pore water changes for several depths (a-d) in the tests performed with 10-15mm GR

Pore water pressure ratio, $r_u=\Delta u/\sigma_{v0}$' of soil were calculated for all data. The presence of GR in the sand caused smaller initial effective stress. Figure 4.21, Figure 4.22, and Figure 4.23 show the r_u values by time for all tests. The r_u reached 1, and liquefaction started at 4.1 sec at a depth of 0.40m and 7.5sec for the depth of 0.63m and constantly continued during the shaking in the test of clean sand.

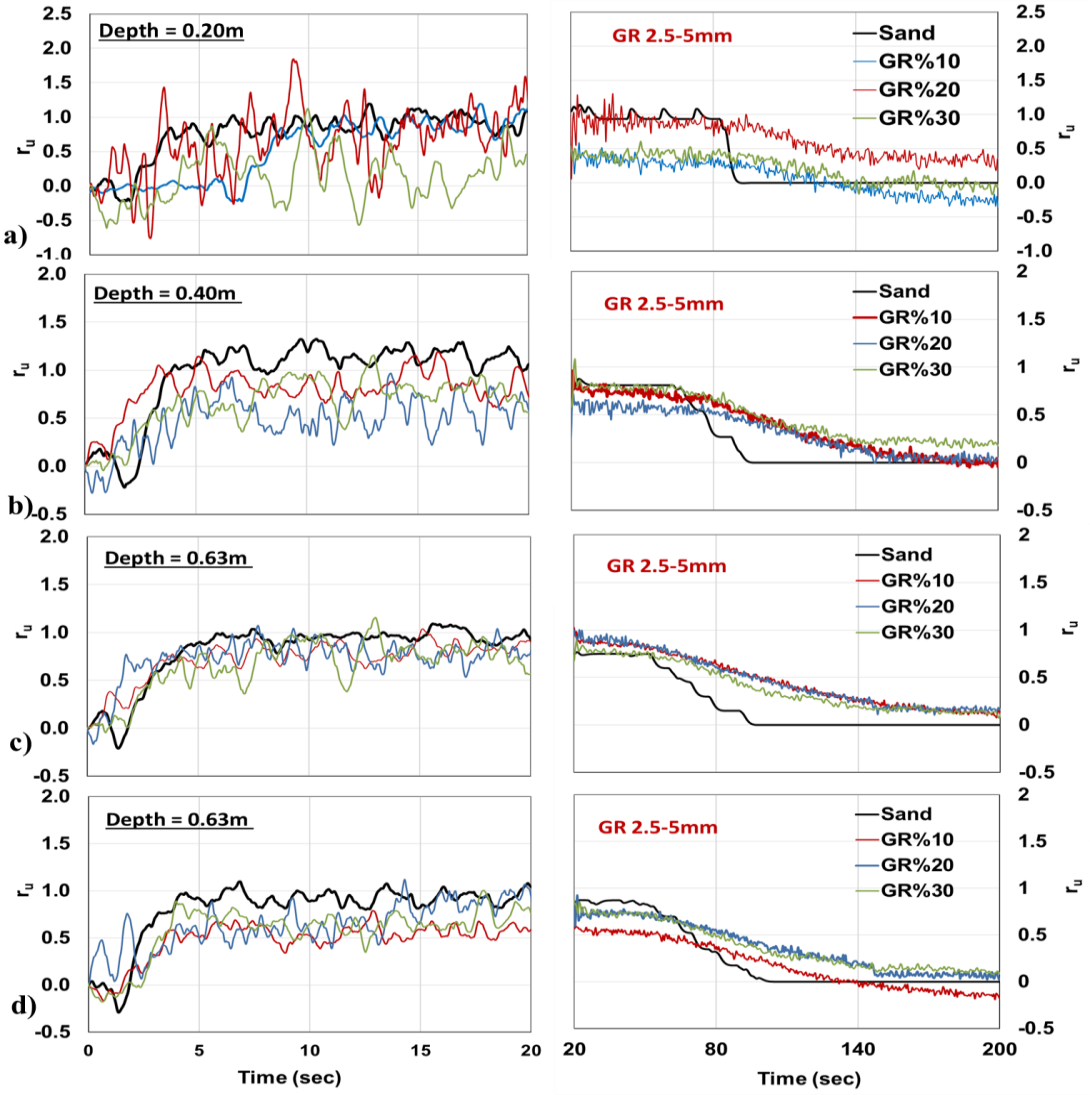

Figure 4.21. Pore water ratio changes for several depths (a-d) in the tests performed with 2.5-5mm GR

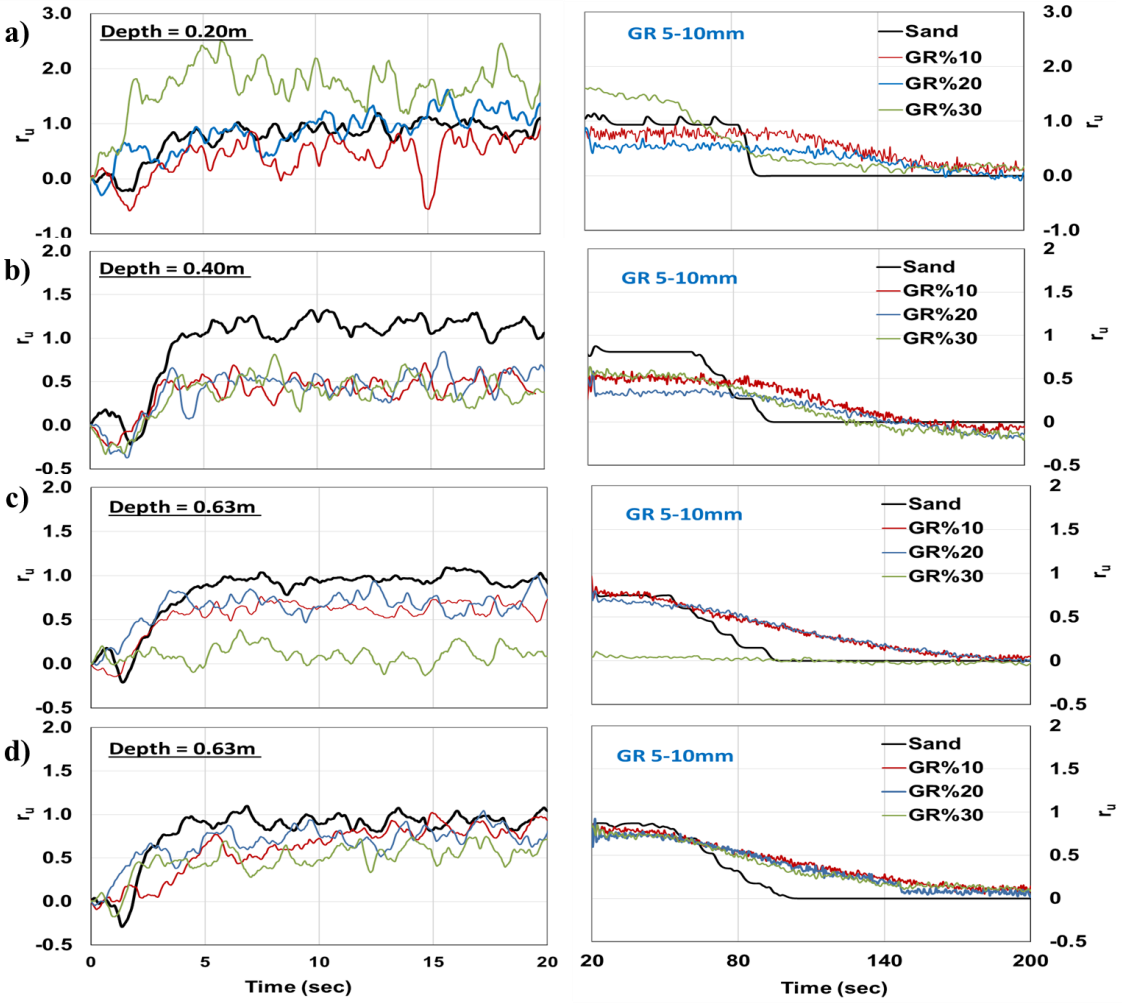

Figure 4.22. Pore water ratio changes for several depths (a-d) in the tests performed with 5-10mm GR

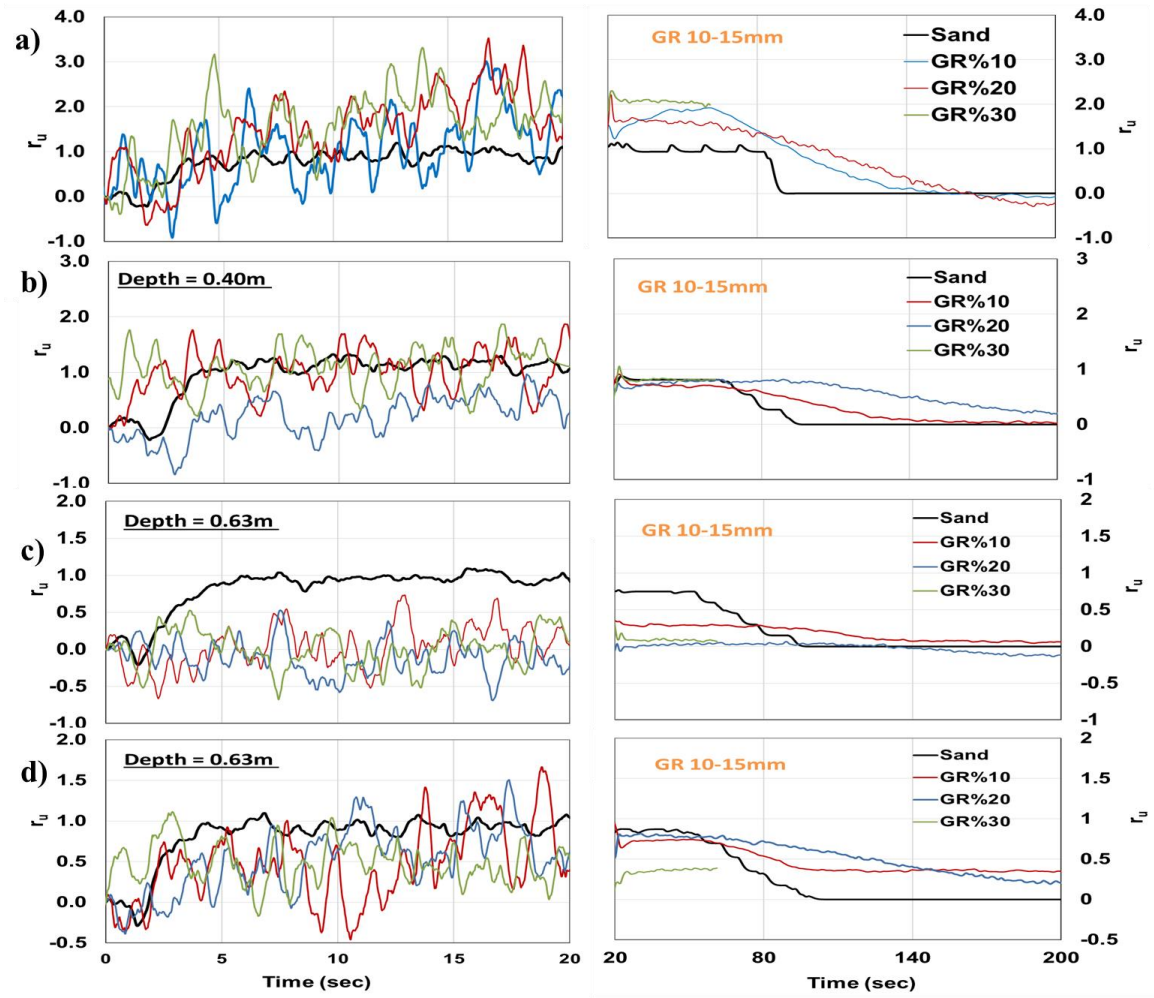

Figure 4.23. Pore water ratio changes for several depths (a-d) in the tests performed with 10-15mm GR

For the other nine tests consisting of varying GR size and ratio in the sand, r_u values were varying. It can be said that there was no liquefaction in all case case of the GRS mixture according to the average r_u values. The average r_u values were calculated time period where started at the time significant increase of r_u value stopped, and it reached its nearly constant values and where stopped at the time where the dissipation started.

For the depth of 0.63m which is the same as pipe depth; for the GR size of 2.5-5mm and GR ratio of 10,20 and 30 percent, the average r_u values were 0.8, 0.82, and 0.65, receptively. For the 5-10mm GR and the ratio of 10, 20, and 30 percent, $r_{u\text{-}avg}$ values were 0.63, 0.75, and 0.57, receptively. There were significant fluctuations in the cases of 10-15mm GR and the r_u values were not determined. The possible reason of these fluctuations of pore water pressure values could be the size of GR particles and their

deformable structures. The main reason for these significant fluctuations of pore water pressure, GR particles were deformed instead of transferring the pressure, so excess pore water pressure was not obtained. The pore water pressure obtained from the test with clean sand was clearer than others because the contact between the sand particles was more stable. In contrast, there was no observed significant deformation of GR particles after the shakings.

The results figured out that granulated rubbers with varying sizes and varying mixing ratios in the sand were all successful in mitigating the liquefaction at a depth of the pipe and above the pipe. The comparable results of tests; the vertical effective normal stress (σ_{v0}'), average pore water pressure ($\Delta_{u\text{-}avg}$), and average pore water ratio ($r_{u\text{-}avg}$), for all tests were listed in Table 4.2.

As seen in Table 4.2., there was no significant correlation between GR size or ratio and excess pore water ratio. However, it was clear that using GR mixing with sand as a backfill material around the pipe reduced the pore water ratio and did not allow the liquefaction to occur.

Table 4.2. Shake tests result

Test	GR size	GR ratio	γ_m	Pipe	Depth	$\sigma_{vo'}$	Δu_{avg}	$r_{u\text{-}avg}$	Uplift of pipe				Settlement of backfill			
									Stage 1	Stage 2	Stage 3	Total	Stage 1	Stage 2	Stage 3	Total
-	mm	%	kN/m^3	-	m	kPa	kPa	-	mm	mm	mm	mm	mm	mm	mm	mm
P2-Sand	-	-	20.5	Free pipe	0.625	6.68	6.48	0.97	-1.62	39.2	-3.9	33.7	0.97	-19.2	-12.8	-31.0
P.GR.S.1	2.5-5mm	10	19.27	Free/ Fixed pipe	0.625	5.91	4.73	0.80	-12.7	16.7	-4.4	-0.3	0.0	-24.4	-6.3	-30.7
P.GR.S.2	2.5-5mm	20	19.16	Free/ Fixed pipe	0.625	5.84	4.80	0.82	-2.11	41.3	-3.3	35.8	1.95	-8.3	0.0	-6.4
P.GR.S.3	2.5-5mm	30	18.65	Free/ Fixed pipe	0.625	5.53	3.71	0.67	-0.87	14.22	-2.5	10.8	0.02	-31.0	0.0	-31.0
P.GR.M.1	5-10mm	10	20.08	Free/ Fixed pipe	0.625	6.42	4.05	0.63	-3.25	61.0	-3.8	53.9	3.6	-18.4	-3.2	-18.0
P.GR.M.2	5-10mm	20	19.37	Free/ Fixed pipe	0.625	5.98	4.53	0.76	-8.11	20.3	-1.6	10.6	0.0	-11.6	-0.7	-12.2
P.GR.M.3	5-10mm	30	18.55	Free/ Fixed pipe	0.625	5.46	3.11	0.57	-4.0295	79.1	-4.4	70.7	0.0	-46.4	-11.3	-57.7
P.GR.L.1	10-15mm	10	20.08	Free/ Fixed pipe	0.625	6.42	-	-	-13.5	41.1	-4.4	23.2	2.8	-67.2	-1.6	-66.0
P.GR.L.2	10-15mm	20	19.37	Free/ Fixed pipe	0.625	5.98	-	-	-4.821	28.87	-3.9	20.2	0.5	-20.8	-1.2	-21.5
P.GR.L.3	10-15mm	30	17.94	Free/ Fixed pipe	0.625	5.08	-	-	-4.856	29.5	-4.5	20.1	-0.9	-25.2	0.0	-26.1

4.7.2. Effects of GR on Settlement of Mixture and Pipe Response

Settlement of filling was obtained by two LPMs on the surface of the deposits while the uplift movement of free pipe was obtained by another two LPMs. As mentioned before, there was a free pipe which is a free end, while the fixed pipe was mounted and it was not allowed to move. There was a flat mini pressure cell mounted bottom outer surface of the fixed pipe, which recorded the upward pressure acting on the pipe due to the pore water.

The settlement of backfill, the pipe uplift movement of free pipe, the upward pressure acting on the fixed pipe, and excess pore water pressure generated at a depth of pipe were plotted in Figure 4.24.a, .b, .c, and .d, respectively, for the test performed with 2.5-5mm GR. Similarly, Figure 4.25 and Figure 4.26 represent the test results for 5-10mm and 10-15mm of GR. Because of the fluctuation mentioned before, the upward pressure on pipe and pore water pressure was not plotted in Figure 4.26.

Remember that one of the LPMs (Z-P2) was mounted to the left free end of the free pipe while the other one was mounted to the right free end of the pipe. The uplift movement of pipe was shown with two lines, the letters L and R represents the free ends of the pipe, and the differences between these two lines shows the lateral uplift movement of the pipe. Also, the uplift movement of pipe at the center of the pipe model was obtained by calculating the average of these two pipe displacements and listed in Table 4.2.

.

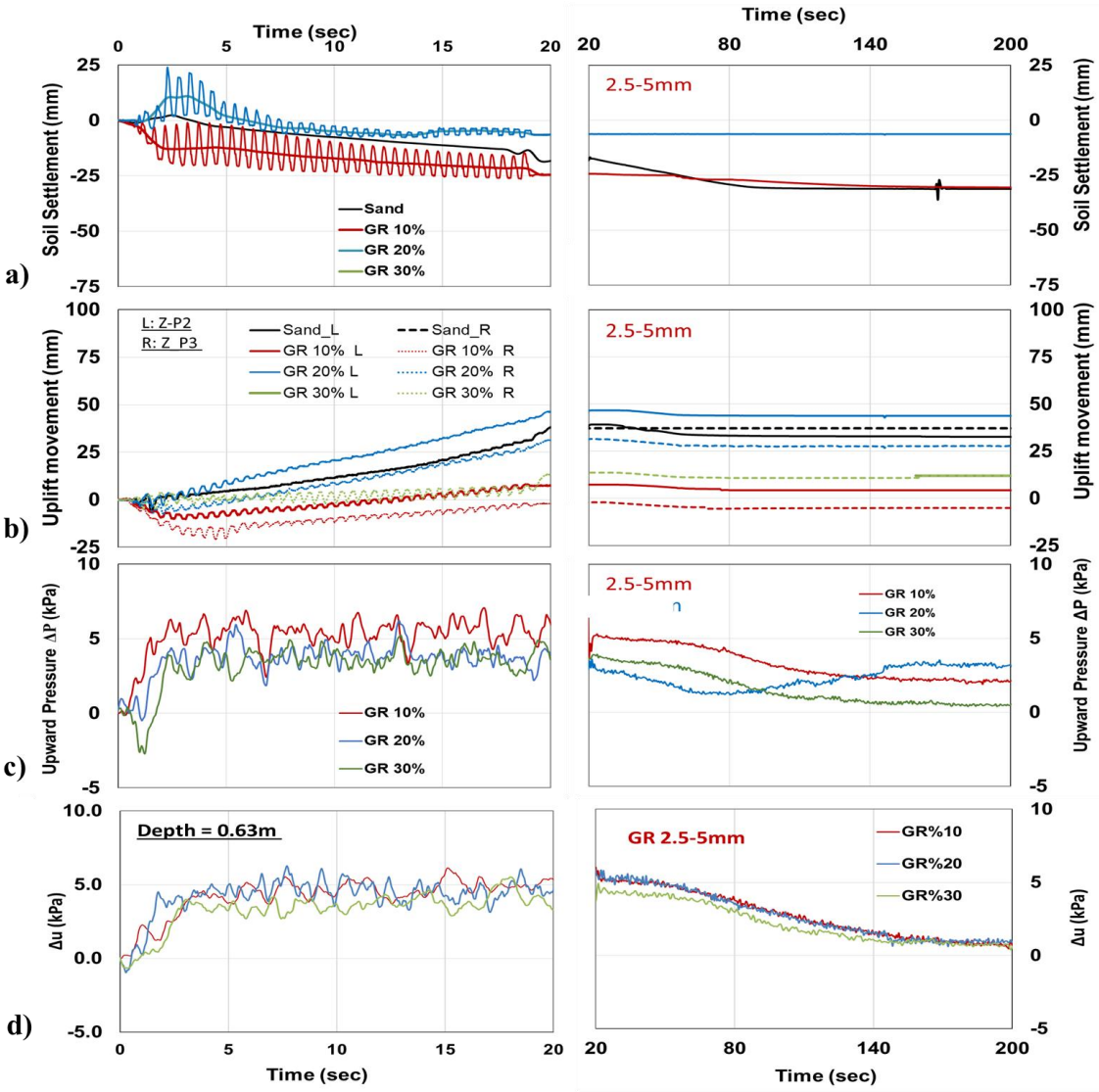

Figure 4.24. a) Surface settlement, b) uplift movement of pipe, c) uplift pressure on pipe, and d) excess pore water pressure for the tests with 2.5-5mm GR

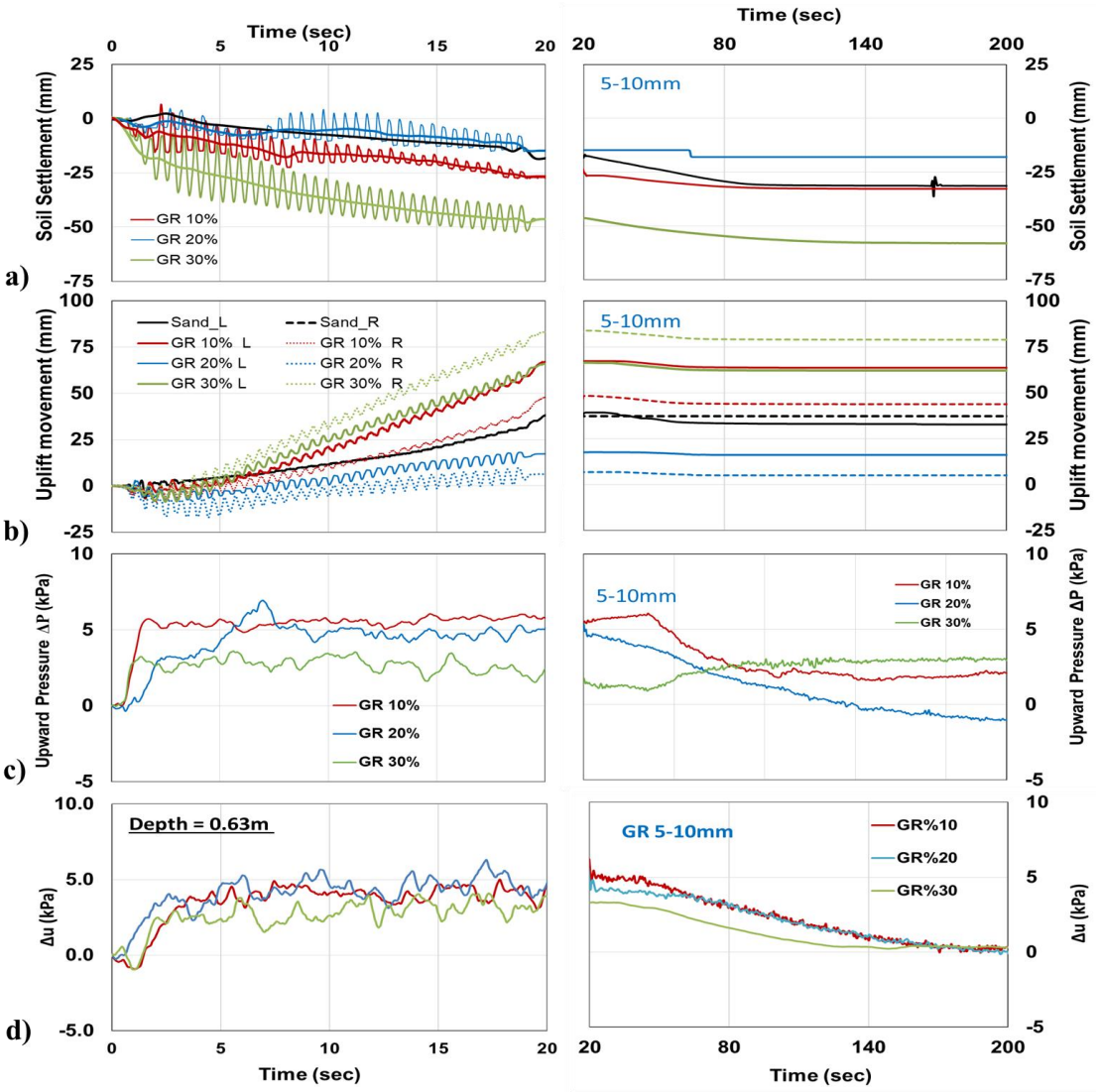

Figure 4.25. a) Surface settlement, b) uplift movement of pipe, c) uplift pressure on pipe, and d) excess pore water pressure for the tests with 5-10mm GR

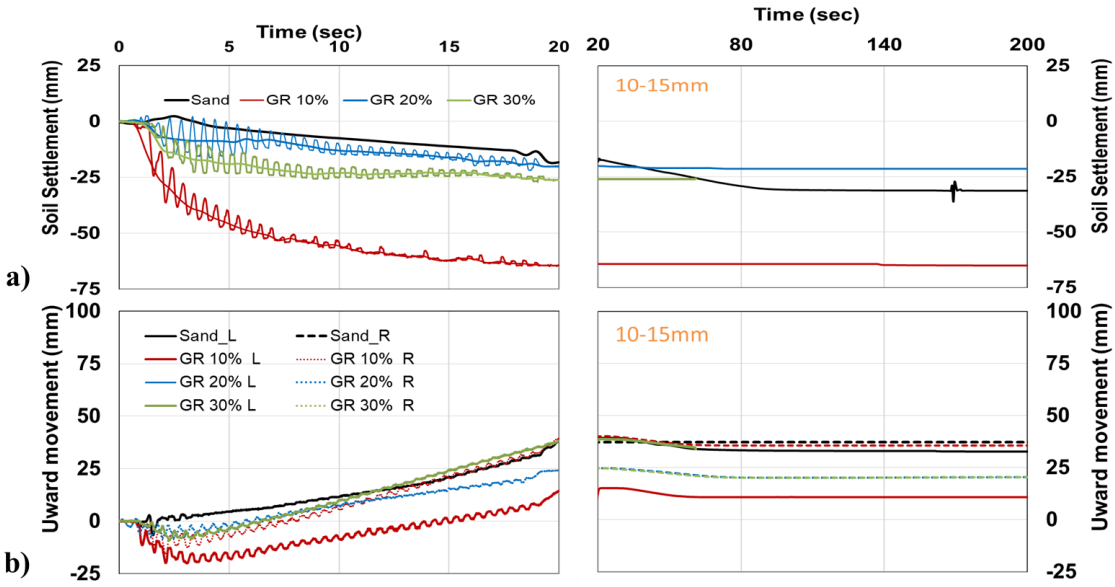

Figure 4.26. a) Surface settlement, and b) uplift movement of pipe for the tests with 10-15mm GR

The pore water pressure records at a depth of the pipe and the records of the pressures acting on the pipe showed similar values and trends for the tests of 2.5-5mm and 5-10mm GR where the upward pressures on the pipe were varying between 2-5kPa. These results proved that upward pressure acting on the pipe was generated by pore water pressure during the seismic loading. Total stress change on the pipe is caused by pore water pressure, the pipe's uplift movement, and the deposits' settlement.

As seen in the figures, the pipe lifted during the shaking and settled with a small amount after shaking in sand deposits. On the other hand, LPMs records obtained that there were small settlements of the pipe at the beginning of the shaking (0-3sec). There were varying uplift movements of the pipe during the remaining duration of shaking (3-20sec) for the tests of GRS mixtures. According to these observations, the response of the pipe and backfill were divided into three stages to discuss. Stage 1 represents the first 3 seconds of the shaking where the settlement of the pipe was varying between 0 to 10mm, backfill settlement was varying between 0-35mm, and upward pressure acting on the pipe was increasing rapidly but was not able to lift the pipe yet. There were small settlements of the pipe which were caused by settlements of the backfill in Stage 1.

Stage 2 was the remaining duration of the shaking, which was 17sec. (3-20sec). In Stage 2, excess pore water pressure reached its maximum value, the pipe's uplift movement occurred, and a significant part of the backfill settlement occurred. In each

shaking test, the uplift movement of the pipe was between 14 and 79 mm, while the settlements on the surface of the backfills varied between 1 and 67 mm.

At the end of the shaking, pore water pressure dissipated for each trial. The dissipation was caused by the drainage of water from the deposits and pipe uplift movement. The dissipation stage was named Stage 3 which started at 20-23th seconds of the test and continued up to 390th sec in some cases. The backfill deposits settled about 0-11mm, and thanks to the backfill settlements the pipe also settled by about 1-4.5mm, during the Stage 3.

In summary, the pipe settlements during the Stage 1 and Stage 3 were caused by settlements of backfills. In contrast, there was an uplift movement of pipe despite the backfill settlements during Stage 2. The soil settlements and pipe displacements in Stage 1, at the end of the Stage 2 and Stage 3 were plotted in **Error! Reference source not found.**. Also, total displacements of the pipe and surface of the deposits by the time are plotted in Figure 4.28.

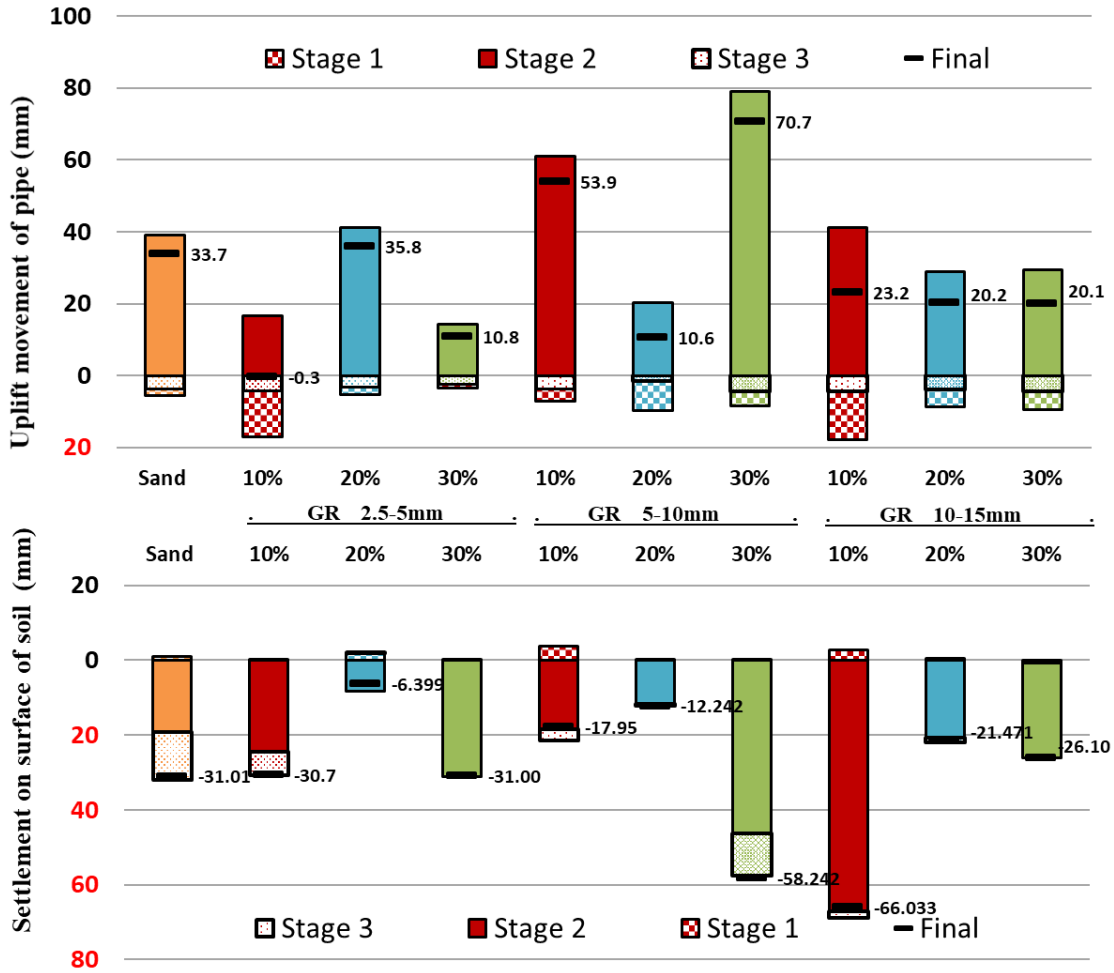

Figure 4.27. Displacements of pipe and surface of backfill at the end of the each stage

As seen in Figure 4.27, despite of not obtaining a clear relation between the varying GRS mixture and uplift movement of pipe or settlement of the backfill, it can be said that, the test performed with 5-10mm GR and 20% ratio conditions gave the lowest displacements for pipe and surface of backfill in each stage. According to the displacement results of pipe and backfill surface, it can be said that the displacements in Stage1 and Stage3 are lower than displacement in Stage2 (Figure 4.28).

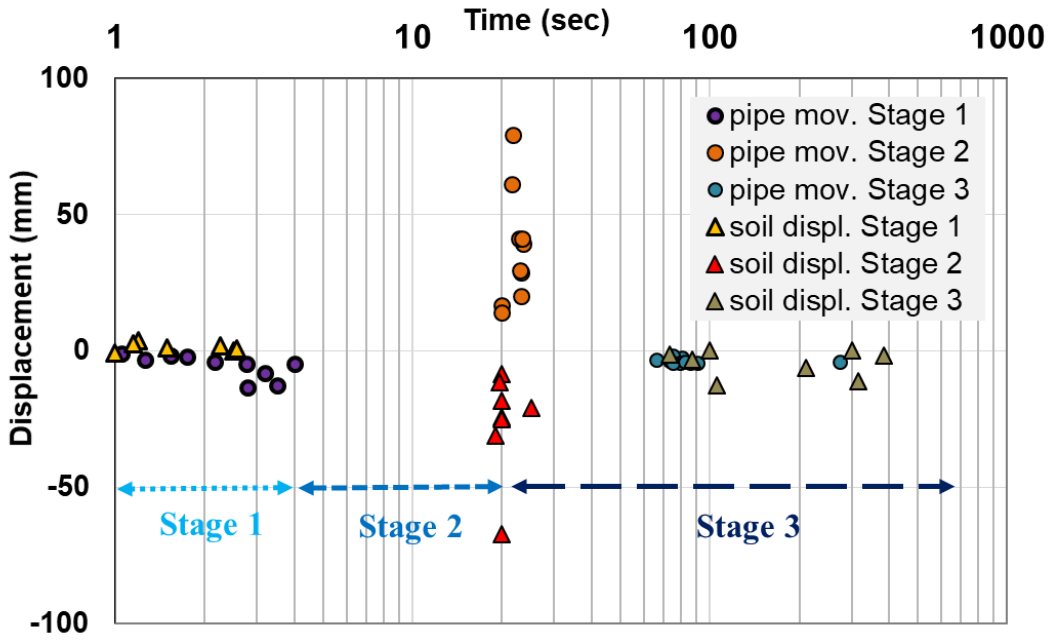

Figure 4.28. Displacements of the pipe and surface of the backfill by the time

4.7.3. Effects of GR on Consolidation Characteristics and Pipe Uplift Behavior

There was no significant correlation between pipe movement and upward pressure on pipe during the shaking. On the other hand, the consolidation characteristics of GRS which were related to the compressibility and permeability of the mixture were determined to compare GR effects on these phenomena in the dissipation part.

Applying the Terzaghi's 1D consolidation theory (Equation 3.1) on the Δu records in the dissipation part of all tests, c_v values of GRS mixtures were determined. In this study, changing the GR size and mixing ratio of GR in sand mixture was change the consolidation characteristics of GR-sand mixture. In Figure X, the c_v values of each case were plotted. They unit of c_v were varying between 8 and 20 cm^2/sec.

A non-dimensional parameter (α) was developed as follows:

$$\alpha = \frac{H\,D/t}{c_V} \tag{4.1}$$

Where; D was pipe diameter, H was the depth of buried pipe, consolidation coefficient (c_v) of the mixture, and the starting time of the uplift movement of pipe (t). In this study, c_v the only parameter which represented the varying conditions in terms of compressibility and permeability in the cases of different GR size and ratios. The starting time of pipe uplift movement (t) was directly related to the seismic loading conditions. In this study diameter of buried pipe (D=5cm), the depth of the buried pipe (H=0.63m) and the seismic loading of shaking tests (a_{max}=0.35g) was constant. Varying parameter in α was only c_v. The relation between the upward pressure applied on pipe (ΔP) and α was plotted for all cases (Figure 4.29). ΔP was the pressure measured in Stage 1, which was the result of Δu generated in Stage 1, and reason of the uplift movement of pipe.

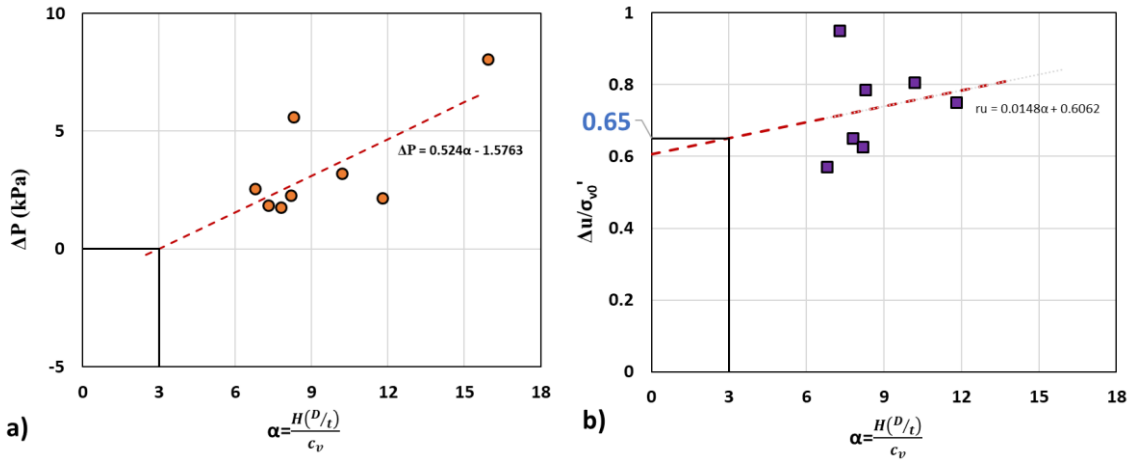

Figure 4.29. Correlations between α, uplift pressure and pore water pressure

As seen in Figure 4.29, while α was increasing, the pressure acting the fixed pipe increased. A linear fitting line was plotted in X, which represents the relations between ΔP and α. Using by this fitting line, the α value at equilibrium condition was determined. For α = 3.0, the ΔP was zero, and that means, there is no movement of the pipe (equilibrium condition). When α> 3.0, there was a positive pressure acting on the pipe. As a result, the pipe can be prevented against to uplifting for α < 3.0 conditions which related to different depths, pipe diameters, coefficients of consolidation (which represents the GR ratio and size), and uplift starting. As known the liquefaction only occurred in

clean sand deposit, instead there was no liquefaction in GRS mixture, the pipe movements were observed. Also, the variation of the pore pressure ratio with α was plotted in X. As seen in Figure 4.29, when α increased, the pore pressure ratio increased. The best fit line given in Figure 4.29, represented the relation between pore pressure ratio and with α. As known pore water pressure ratio, is a ratio of Δu to σ_{v0}' initial effective stress (σ_{v0}') is equal to H.γ'_m where H is the depth and γ'_m is the effective unit weight of the soil. Varying GR size and ratio changes not only the the γ'_m and Δu but also c_v value for each case. So, the e equilibrium condition of the pore pressure ratio can be determined as follows where α = 3.0:

$$\Delta u = 0.65\, \gamma'_m H \quad \text{for} \quad r_u = 0.65 \text{ and } \alpha = 3 \tag{4.2}$$

Saeedzadeh and Hataf (2011) suggested that dilatancy angle and density ratio of natural soil, diameter and burial depth of the pipe, underground water table, and thickness of the saturated soil layer effects the uplift of the pipe. According to Saeedzadeh and Hataf (2011), the excess pore water pressure causes an increase in the uplift force acting on the pipe and also causes decreases in effective normal stress of soil, so the Δu effect is doubled on uplifting of pipe. The forces resisting the uplift forces are the pipe's deathweight and the soil's effective weight above the pipe. The forces acting on the pipe are illustrated during shaking in Figure 4.30 which was modified from Figure 2.13.

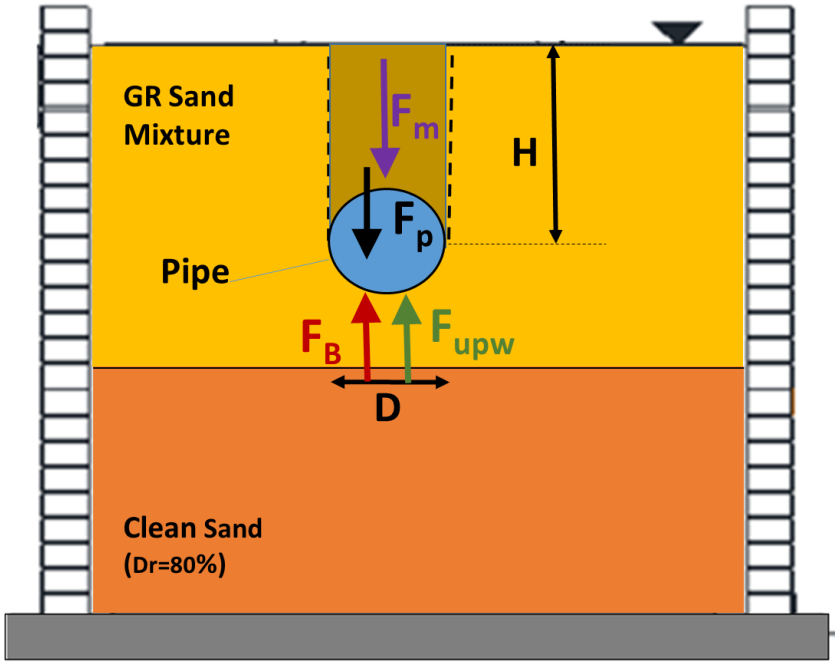

Figure 4.30. The forces acting on the pipe during shaking

The downward force induced by the weight of the SGR mixture above the pipe before shaking is calculated as follows (Chian and Madabhushi 2012):

$$F_m = \left[H.D - \left(\frac{\pi D^2}{8} \right) \right] \gamma'_m \tag{4.3}$$

where D is the pipe diameter, H is the depth of buried pipe, and γ'_m is the effective unit weight of the mixture. At the end of Stage, I, the downward force induced by the weight of the SGR mixture above the pipe is calculated as:

$$F_m = \left[H.D - \left(\frac{\pi D^2}{8} \right) \right] \gamma'_m - \Delta u.D \tag{4.4}$$

The downward force induced by the deadweight of the pipe is calculated as follows;

$$F_p = \pi \left(bD - b^2 \right) \gamma_p \tag{4.5}$$

where b is the thickness of the pipe and γ_p is the unit weight of the pipe material.

The Archimedes principle governs the buoyant force of the structure. This buoyancy force (F_B) is determined by using the Archimedes principle for the buoyant force of the structure:

$$F_B = \left(\frac{\pi D^2}{4} \right) \gamma_w \tag{4.6}$$

Upward force acting on the pipe (F_{upw}) can be expressed as follows:

$$F_{upw} = \Delta u.D \tag{4.7}$$

As seen in X, the equation of all forces acting on the pipe at equilibrium conditions is as follows:

$$F_{upw} = F_m + F_p - F_B \tag{4.8}$$

Substructing the Equations 4.4, 4.5, 4.6, and 4.7 into Equation 4.8;

$$\Delta u.D = \left[\left(H.D - \frac{\pi D^2}{8} \right) \gamma'_m - \Delta u.D \right] + \left[\pi (bD - b^2) \gamma_p \right] + \left[\left(\frac{\pi D^2}{4} \right) \gamma_w \right] \tag{4.9}$$

$$2.\Delta u.D = \left[\left(H.D - \frac{\pi D^2}{8}\right)\gamma'_m\right] + \left[\pi(bD - b^2)\gamma_p\right] - \left[\left(\frac{\pi D^2}{4}\right)\gamma_w\right] \quad (4.10)$$

In this study, the excess pore water pressure limit just before the uplift movement of the pipe started was determined in Equation 4.2. Subtrutcing the Equation 4.2 into 4.10; the following equation was suggested;

$$1.3\gamma'_m HD \leq \left[\left(H.D - \frac{\pi D^2}{8}\right)\gamma'_m\right] + \left[\pi(bD - b^2)\gamma_p\right] - \left[\left(\frac{\pi D^2}{4}\right)\gamma_w\right] \quad (4.11)$$

In this study, a limit value of pore water pressure was determined before the uplift movement of pipe just started. Equation 4.11 was proposed to design a critical condition for predetermined pipe material and diameter, burial depth of the pipe, backfill conditions for a known seismic loading to prevent the uplifting of the pipe. It was proven that the floating movement of pipe related to not only pipe and backfill material but also the diameter and the depth of the pipe.

4.8. Concluding Remarks

In this chapter of the study, the liquefaction potential and settlements of saturated loose sand- granulated rubber mixture were compared with varying mixture conditions with 1-D shake table tests similar to Chapter 3. In addition to all these, the pipe models were buried into backfill material in the test setup and the effects of the GR on pipe upward displacements during the earthquake shaking are obsereved.

Following observations are listed to summary the results of comperative study;

1. When a pipe buried into loose sand deposits, it decreases the time needed for full dissipation. This faster dissipation of water pressure is caused by pipe and its uplift movement. The moving upward of the pipe model allows the water to flow around itself and caused quicker drainage.
2. Because of the lower duration of the full liquefaction stage of sand, the surface settlement of sand in test with pipe was slower than the test without pipe during the shaking.

3. On the other hand, the settlement of the sand with buried pipe was bigger and faster than the settlement of test without pipe for post shaking stage, in other words, the dissipation stage. Because, the pipe increased the permeability of sand and changed the consolidation characteristics of the system with a small amount.
4. Granulated rubbers with varying sizes and varying mixing ratios in the sand are all successful in mitigating the liquefaction at a depth of the pipe and above the pipe.
5. The upward pressure acting on the pipe is generated by pore water pressure during the seismic loading. Total stress change on the pipe is caused by pore water pressure, the pipe's uplift movement, and the deposits' settlement.
6. The stresses acting on the pipe and displacements of the pipe were compared in three different stage of the shaking.
    a. Stage1 is the short time period at the beginning of shaking (0-3rd sec) where the shake was started, excess pore water pressure was increasing, backfill settlement occurred for a small amount, but upward movement of pipe did not started yet. In Stage1, the excess pore water pressure increases but not reach the pressure to move the pipe upward, also there are small settlements or uplifts of pipe due to the settlements of soil.
    b. Stage2 is the remaining time period of shaking (3rd -20th sec), where the excess pore water pressure reached its maximum value, the pipe moves upward and soil settlement occurs. In Stage2, the most significant uplift movement of pipe and settlement of soil are observed.
    c. Stage3 is the time period after shaking (20th-390th sec) . In Stage3, the dissipation of pore water pressure is obsereved. In this stage settelement of soil and also settlement of pipe are observed.
7. The GR in sand not only decreases the excess pore water pressure in mixture but also decreases the amplitutes of the dynamic waves. The GR is a efficient material to isolate the pipe from dynamic waves.
8. A non-dimensional parameter (α) is developed which is combination of pipe diameter (D), burial depth of pipe (H), consolidation coefficient (c_v), and initiation time of uplift to represent the varying GR and sand mixture

situations. In this study, c_v is only varying parameter. The pipe is in equilibrium condition (Equation 4.11) and there is no net uplift force increasement below the pipe if α=3. Equation 4.11;

$$1.3\gamma'_m HD \le \left[\left(H.D - \frac{\pi D^2}{8}\right)\gamma'_m\right] + \left[\pi(bD - b^2)\gamma_p\right] - \left[\left(\frac{\pi D^2}{4}\right)\gamma_w\right]$$

9. The study shows that the density and consolidation charaterisitics; compresibilty and permeability of backfill around the pipe are most efficient parameters to prevent the pipelines from uplift forces due to the excess pore water pressure and to isolate the pipeline from earthquake waves.

CHAPTER 5

EFFECTS OF RECYCLED TIRE GRANULATED RUBBER ON GROUNDWATER: LEACHING TESTS

5.1. Introduction

Usage of scrap tires was become not only common in geotechnical engineering but also environmental engineering applications. Several studies were conducted to understand the benefits of GR as a backfill material in terms of mechanical and physical properties. The usage of GR become more popular in geotechnical applications where the GR was embedded into soil or placed somewhere in contact with the natural soil as backfill material. So, new environmental concerns occurred like as wheter the usage of GR are toxic on not to environment, ground waters or life of creatures. So, the environmental effects of leaching components of GR have become an issue that needs to be investigated.

A literature study about this chapter was given in Section 2.6 in detail. Several researchers have focused on the leaching characteristics of GR in terms of contamination of inorganics and organics into groundwater. As seen in studies in the last three decades, scrap tire leaching has become a very common research topic. Differences in the results of leaching procedures performed in the laboratory led to extensive laboratory experiments prepared for more realistic scenarios. In order to define the leaching characteristics as a need for developed and widespread geotechnical applications, studies were carried out to evaluate the field and laboratory results together. Most studies used batch tests and column leaching tests to figure out the metals, anions, and cations concentrations leaching from GRs.

On the other hand, few studies have attempted to obtain more realistic results by mixing GR with soil type. These studies generally used ash or clay as soil to mix with GRs (Lee, 2011; Liu et al., 2020). There is no significant study examining the leaching effect of GR on water when they are mixed with sand and used as a backfill material mixture. This study determines the impact of the GR particles on water quality and figures

out the leaching characteristics of GR under varying GR size and sand-GR mixture conditions.

For this purpose, firstly, we performed batch tests (BTs) on scrap granulated GR with varying sizes under the varying pH conditions (4.6, 6, 8.3) to figure out the leaching inorganics from GR and sand particles and to determine the effect of the pH and GR size on the leaching of inorganics. Then, we used column leaching tests (CLTs) to evaluate the leaching characteristics of GR and silica sand mixtures (GR ratios were 10%: 20%, and 30% by volume) under the rainwater conditions.

We aimed to determine the leaching behavior of these materials as construction fill materials around buried structures proposed by previous chapters. We determined the selected metals, anions, and cations concentrations over time. We compared them with drinking water standards (DWS) of the US Environmental Protection Agency (US EPA) and the World Health Organization (WHO). We also compared the effects of GR sizes and GR ratios in GRS mixtures on both the total leaching inorganic amount and the leaching rate by time.

In this chapter, the conducted leaching experiments, which were Batch tests and Column Leaching Tests, were explained. Leaching characteristics of GR were obtained, and the leachate of inorganics was discussed in terms of metal, anion, and cations. Finally, the concluding remarks were summarized.

5.2. Material

5.2.1. Silica Sand

Silica sand used in BTs and CLTs was exactly the same sand explained in Section 3.3.1. For more detail, see Section 3.2.1. Energy-dispersive X-ray fluorescence (XRF) analysis provides an analytical method for determining the chemical composition of many types of materials (solid, liquid, and powdered samples). XRF analysis was performed to determine the chemical composition of silica sand and summarized in Table 3.2. As a reminder, according to the results of XRF, Silicon (Si) was the most abundant component in the sand with 85.8% by weight, and the second most abundant was Aluminum (Al) with 9.1% by weight, followed by K_2O, Fe_2O_3, CaO, P_2O_5, MgO, Ba, and Na_2O.

5.2.2. Tire Granulated Rubber

The scrap tire granulated rubber (GR) was same as GR used for laminar box tests and explained in detail in Section 3.2.2. Same groups were used with equivalent diameters; 3–5 mm, 5–10 mm, and 10–15 mm. Also, the GR composition determined by XRF is summarized in Table 3.. The three most abundant components in the GR are Zinc (27.4%); Sodium (25.9%), and Calcium (22%), respectively.

5.2.3. Leaching solutions

Leaching from GR and silica sand was investigated under three different conditions: in solutions at pH 4.1, 6.8, and 8.3 for batch tests. For the leaching solutions, the pH of distilled pure water (PW) was adjusted using high purity NaOH or HCl without using any buffer. Rainwater was used for nine different CLTs, while DDW was used for one of CLTs as a leaching solution. Rainwater (RW) was collected naturally from the laboratory building roof using big gallons with pH varying between 8.1-8.4.

5.3. Tests Process

The first part of the experimental work, the GR with three varying sizes and silica sand, was conducted with batch tests for three different pH conditions for 30 days. In the second part, different GRS mixture were prepared with varying GR size and GR ratios. Using these mixtures and only sand, ten leachate column tests were performed for 15 days under rainwater conditions. For both experimental works, several leachate water samples were collected and analyzed to determine the contamination of inorganics in leachate water.

5.3.1. Analysis of Inorganics Concentrations in Leachate Samples

The inorganic constituents and their concentrations in pure water (PW) and rainwater (RW) were determined by two analyses; (1) the Inductively Coupled Plasma Mass Spectrometry (ICP-MS) and (2) ion chromatography (IC) tests. These analyses were

performed by the Environmental Development, Application, and Research Center at the Izmir Institute of Technology (IZTECH). ICP-MS is an elemental analysis technology capable of detecting most of the periodic table of elements at the milligram to nanogram levels per liter. The ICP-MS tests were performed to determine the concentration of Zn, Cu, Mn, Fe, Al, and Pb. IC tests were performed to determine the concentration of $^{+2}$Ca, $^{-2}$SO4, $^{+}$Na, $^{-}$Cl, $^{+2}$Mg, and $^{+}$K.

5.3.2. Batch Tests

Toxicity Characteristic Leaching Procedure (TCLP) (USEPA, 1990) has been widely used to generate leachate concentrations for all types of solids for several metals and organic chemicals. The batch experiments in this study were based on the USEPA's TCLP test method. In this study, the same solid to liquid ratio was used as in the TCLP test with the difference in leaching solution and contact times to simulate the behavior of scrap tires under different pHs.

The GR particles were soaked in each leaching solution at a constant solid to solution ratio of 1:20 by mass at room temperature (22 ± 2 ^{o}C) and mixed steadily on a rotary tumbler. For each size, the GR number was adjusted to 20 grams. These chips were placed in 1liter wide-mouth amber bottle with Teflon lined cap and filled with 1L of the leaching solution. During each soaking cycle of one week, the pH of the leaching solution was recorded daily and adjusted to its initial value by using high purity NaOH or HCl. Following periodic removal of 30 mL of samples, the same volume of fresh leaching solution was added back to the reactors. Sampling days were set to 5, 7, and 30.

Twelve different batch tests were performed on three different sizes of GR (3-5 mm, 5-10 mm, and 10-15 mm) and silica sand under three different pH conditions (4.1, 6.8, and 8.3). The experimental matrix of BTs is shown in Table 5.1. Table 5.2. and Figure 5.1 show the time-dependent inorganic elements concentration of BTs under the different pH conditions. Due to Pb, Cu, K, and Mg concentrations being too low according to other elements and standards' limits, they are not shown in Figure 5.1.

Table 5.1 Experimental matrix of batch tests

Sample	Sand	GR 3-5 mm	GR 5-10 mm	GR 10-15 mm
	8.3	8.3	8.3	8.3
pH	6.8	6.8	6.8	6.8
	4.1	4.1	4.1	4.1

Table 5.2. Result of batch tests

Sample	pH	Day	Al	Mn	Fe	Cu	Zn	Pb	^{+}Na	^{+}K	^{+2}Mg	^{+2}Ca	^{-}Cl	$^{-2}SO4$
	-	-	µg/L	µg/L	µg/L	µg/L	µg/L	µg/L	mg/L	mg/L	mg/L	mg/L	mg/L	mg/L
Pure Water	-	-	0.58	0.49	0.63	0.35	9.02	0.31	0.09	0.16	<0,06*	<0,13**	0.25	0.10
GR 2.5-5mm	8.30	1	2.66	18.17	26.18	2.25	685.0	0.39	1.08	2.00	0.07	1.67	1.82	1.84
		5	2.10	33.20	31.74	3.40	1472.7	0.31	1.11	2.16	0.09	3.26	1.89	2.00
		7	14.48	49.95	35.74	5.14	2777.8	0.34	1.15	2.30	0.12	4.70	1.93	2.50
		30												
	6.80	1	1.02	6.05	3.41	1.50	665.2	0.28	0.87	0.64	0.06	1.05	0.35	1.20
		5	0.74	11.36	1.77	1.29	1289.0	0.16	0.75	0.87	0.08	1.83	0.34	1.41
		7	0.62	13.55	1.71	1.52	1571.7	0.24	1.09	6.55	0.12	2.80	5.88	1.64
		30	5.89	96.96	437.29	2.54	5389.3	0.70	1.19	1.68	0.31	6.39	0.35	8.49
	4.10	1	2.54	8.63	7.26	6.99	838.9	0.15	0.49	0.48	0.07	1.75	0.31	4.08
		5	1.42	14.59	2.91	3.07	1279.2	0.17	0.59	0.70	0.11	3.34	0.36	4.42
		7	1.48	15.80	2.66	3.93	1533.9	0.16	0.64	1.22	0.13	3.99	0.80	4.52
		30	5.77	95.00	239.67	5.17	7430.8	0.61	1.03	1.40	0.46	7.84	0.42	8.18
GR 5-10mm	8.30	1	1.63	11.36	28.93	2.29	399.6	0.36	1.79	4.87	0.11	1.87	5.59	1.48
		5	2.25	19.81	27.20	5.27	1033.2	0.31	1.85	5.07	0.13	2.56	5.70	2.16
		7	1.90	33.57	27.85	22.38	2032.7	0.33	1.90	5.19	0.17	4.12	5.76	2.52
		30	1.73	39.81	31.85	13.51	2385.9	0.22	1.92	10.70	0.18	4.77	10.94	2.63
	6.80	1	0.87	7.33	1.44	2.64	237.6	0.15	0.63	0.45	0.08	1.87	0.36	2.97
		5	0.79	16.95	3.12	4.52	723.5	0.16	0.74	0.66	0.12	3.30	0.44	3.67
		7	1.64	22.96	4.06	6.78	1077.0	0.18	0.90	5.62	0.14	4.18	4.98	3.81
		30	5.57	211.50	556.84	8.32	6134.1	0.47	1.20	1.16	0.61	10.92	0.51	10.11
	4.10	1	1.18	9.44	3.22	2.86	408.5	0.16	0.56	0.39	0.08	1.98	0.43	4.02
		5	1.95	18.19	12.41	1.97	704.8	0.21	0.67	0.58	0.12	4.17	0.49	4.44
		7	1.88	23.65	12.09	2.74	997.2	0.23	0.72	0.92	0.14	5.18	0.79	4.61
		30	1.81	149.38	39.93	1.72	5024.6	0.20	1.14	1.05	0.61	10.22	0.54	9.26
GR 10-15mm	8.30	1	1.46	8.81	37.53	1.84	430.6	0.28	1.30	4.54	0.06	1.05	4.29	1.22
		5	1.25	15.98	28.20	3.59	1073.0	0.17	1.35	4.64	0.07	1.96	4.32	1.91
		7	1.55	29.90	52.49	15.69	2173.4	0.30	1.36	4.82	0.11	3.96	4.40	2.67
		30	2.06	31.29	41.02	14.69	2153.4	0.34	1.39	4.88	0.13	4.50	4.44	3.10
	6.80	1	0.56	7.29	1.57	3.84	295.7	0.23	0.44	0.46	0.06	1.14	0.11	1.56
		5	0.45	11.57	2.22	2.38	644.9	0.17	0.55	0.63	0.09	2.22	0.13	2.02
		7	0.91	13.66	1.52	3.66	977.4	0.16	0.68	3.78	0.11	2.96	3.12	2.20
		30	2.39	72.71	35.30	39.01	4962.4	0.19	1.05	1.08	0.37	6.64	0.19	6.23
	4.10	1	1.20	8.01	2.82	9.33	283.8	0.18	0.46	0.47	0.08	2.28	0.19	4.64
		5	1.78	13.34	1.96	5.01	487.8	0.19	0.56	0.65	0.13	4.36	0.23	5.17
		7	2.44	16.23	1.52	4.76	683.9	0.19	0.62	0.82	0.15	5.35	0.35	5.42
		30	3.71	101.02	39.19	56.94	5207.0	0.25	1.07	1.11	0.53	9.36	0.28	9.97
Silica Sand	8.30	1	37.93	2.59	66.61	22.63	33.64	2.50	5.01	5.43	0.29	6.32	9.62	3.60
		5	22.76	13.42	45.65	16.71	11.46	0.77	5.19	6.05	0.31	7.65	9.36	4.15
		7	21.65	3.06	38.17	18.43	25.93	0.17	5.25	6.25	0.48	12.47	9.41	4.26
		30	27.74	6.61	41.70	23.02	37.51	0.19	6.22	7.47	0.58	14.75	11.14	5.10
	6.80	1	182.30	8.22	76.31	5.56	3.91	0.87	2.91	1.10	0.51	5.54	1.99	1.55
		5	138.86	2.68	56.32	5.76	3.44	0.39	3.45	1.41	0.60	6.45	2.31	1.92
		7	150.42	5.26	55.64	6.34	9.04	0.55	3.61	5.37	0.68	7.30	5.97	1.91
		30	85.35	0.93	91.50	0.00	4.82	0.67	3.37	1.18	0.88	9.61	0.88	1.37
	4.10	1	106.38	12.02	38.12	12.49	9.23	1.26	3.38	1.19	0.62	7.05	2.61	4.93
		5	126.35	6.88	55.21	10.68	8.23	2.00	3.53	1.39	0.75	7.96	2.56	4.94
		7	186.02	6.49	76.54	11.18	14.65	2.18	3.66	2.74	0.85	8.93	3.81	4.92
		30	67.17	0.43	41.93	0.00	3.12	0.09	3.10	1.18	1.06	11.59	0.71	4.21

Note: Zn, Fe, Mn, and Al concentrations units are µg/L while Na, Ca, Cl, and SO_4 concentrations unit are mg/L

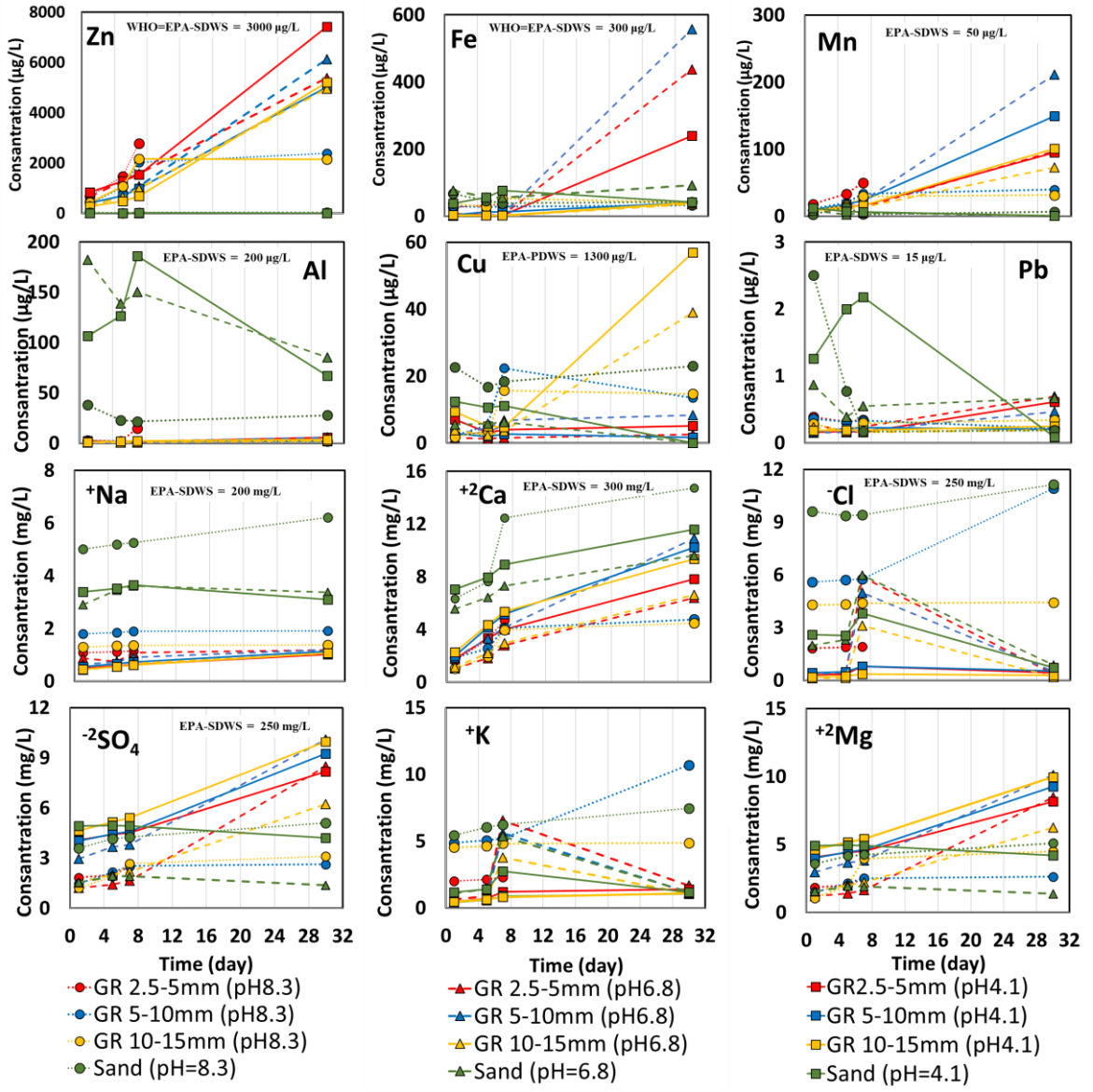

Figure 5.1. Time-dependent inorganic elements concentration of BTs under the different pH conditions

As seen in Figure 5.1; the main source of Zn leachate was GR, while Fe, Al, and Na concentrations leaching from the sand were much more than GR. Concentrations of other elements from sand and GRs showed similar values. Contamination of Zn, Fe and Mn reached above the international usable water standards after a week, while contaminations of other selected inorganics were below the standards during the batch tests. Further discussions about pH and selected inorganics concentration are made in the next section, supported by some analytical methods.

5.3.3. Column Leaching Tests

CLTs were conducted to assess leaching behavior under conditions resembling those that exist in the field. Figure 5.2 illustrates the setup for the CLTs. The column leach test setup, pictures of sand-GR mixtures, and mixture preparation mold are shown in Figure 5.2a-c, respectively. As shown in the figure, the cylindrical Plexiglas column had a 19 cm inner diameter and 100 cm inner height. GR with varying sizes (3-5mm, 5-10mm, 10-15mm) were mixed with silica sand for three different ratios (10%GR - 90% Sand; 20%GR -80%Sand; and 30%GR -70% Sand in volume). DDW was used for one of the CLTs, and RW was used for other CLTs as leachate solutions.

Ten different CLT experiments were performed, and the experimental matrix is shownin Table 5.2. Note that in Table 5.3, the test name represents the mixture conditions; the letter of "C" represents the tests of Column Leachate Test, while "PW" represents the pore water and "RW" represents the rainwater as the leaching solution of tests. The letters "GR" are for Granulated Rubber, S for the small size of GR (2.5-5mm), M for the middle size of GR (5-10mm), L is for the large size of GR (10-15mm), and lastly, the number of 1, 2 and 3 are for the ratio of GR in the mixture for 10%, 20%, and 30% respectively.

Table 5.3. Experimental matrix of Column Leaching Tests

Test Name	TDA Size (mm)	TDA/Sand Ratio in Volume	Permeability ($x10^{-2}$cm/s)	Leachate Solution
PW-3-5mm- 1/9	3-5	1/9		Ultra Pure Water
RW-3-5mm-1/9	3-5	1/9	1.932	Rain Water
RW-3-5mm-2/8		2/8	2.060	
RW-3-5mm-3/7		3/7	2.133	
RW-5-10mm-1/9	5-10	1/9	1.700	
RW-5-10mm-2/8		2/8	1.933	
RW-5-10mm-3/7		3/7	1.984	
RW-10-15mm-1/9	10-15	1/9	2.372	
RW-10-15mm-2/8		2/8	2.479	
RW-10-15mm-3/7		3/7	3.052	

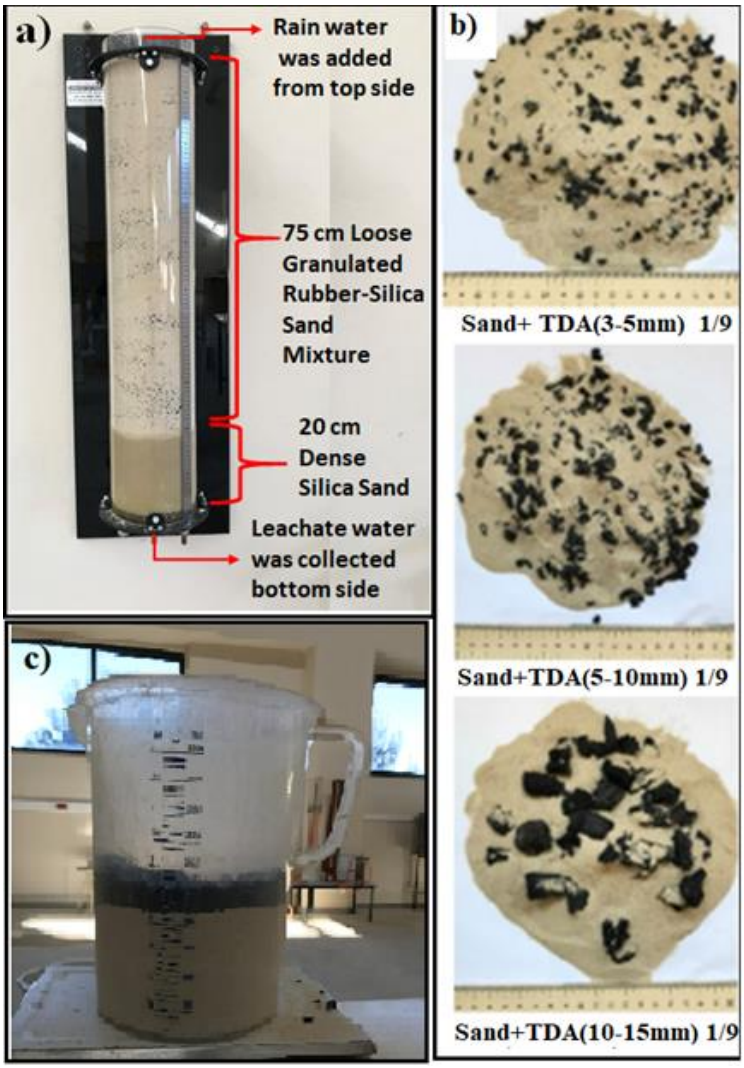

Figure 5.2. Column Leachate Test Setup and GRS mixtures

Clean silica sand was filled at the bottom side of the column with 20 cm height and compacted by a hammer to make the soil dense until a relative density (D_r) of 70% was reached. Relative density was measured by placing a small sample can in the column. The can be taken after sand compaction and weighted (for more detail, see; Karaman 2022). Then, the GRS mixture was prepared in a graduated cylinder beaker and poured loosely with a constant speed from 20 cm height into the Plexiglas column (Figure 4. c) to prepare a homogenous GR-S mixture layer that had a height of the 75 cm. The leaching test setup created in this study represents a realistic model of GR-S filled around the buried infrastructures (Ecemis et al., 2022). In the current study, the groundwater table is assumed below the GR-S layer, while solution water represents a surface water leachate through the bottom.

Solution water was poured from the top of the column, and the water was kept added until dense sand, and GRS layers became saturated (about 30 min). Before pouring the solution water into the column, a water sample was collected and named an “RW” sample. Leached water samples were collected from the bottom of the column using a valve for the first hour, the third hour, the sixth hour, the twelfth hour, and once for each day from 1st to 15th day (total of 20 samples for 15 days). After each 500 ml leachate sample was collected, solution water was added from the top of the column. All CLT experiments were carried out under room conditions, and pH and temperature values were not interfered with during the experiment. The leachate sample's temperature, electrical conductivity, and pH values were measured immediately after each sample was taken and noted. Figure 5.3 shows the values of the temperature, electrical conductivity, and pH for all CLTs during the tests. The CLTs' temperatures vary between 17-23 ^{0}C, and there is no significant temperature change in any of the CLTs (Figure 5.3.c).

Electrical conductivity (EC) is a measure of the saltiness of the water and is measured on a scale from 0 to 50.000 in micro siemens per centimeter (µS/cm). The EC of water is its ability to conduct an electric current. Salts or other chemicals that dissolve in water can break down into positively and negatively charged ions. These free ions in the water conduct electricity, so the water's electrical conductivity depends on the concentration of ions. Salinity and total dissolved solids (TDS) are used to calculate the EC of water, which helps to indicate the water’s purity. Freshwater is usually between 0 and 1.500 µS/cm, and typical seawater has a conductivity value of about 50.000 µS/cm. When EC reaches high levels in freshwater, it can cause problems for aquatic ecosystems and human uses. US EPA (1990) reported that water with EC between 0 and 800 µS/cm was classified as good drinking water for humans, while humans can consume approximately 800–2500 µS/cm for tap water. Figure 5. b illustrates the electric conductivity (EC) change during all CLTs. The biggest EC value has been seen in the tests performed with PureWater; reached 2100µS/cm and its decreasing to a constant value takes too much time (>15 days) than others. There is no significant relationship between GR size or GRS ratio in the mixtures with EC. According to some observed changes in EC values, it can be said that; the leaching of inorganics started leaching faster for bigger sizes of GR but it took longer time to decrease the leaching concentration to a constant rate for bigger size GR.

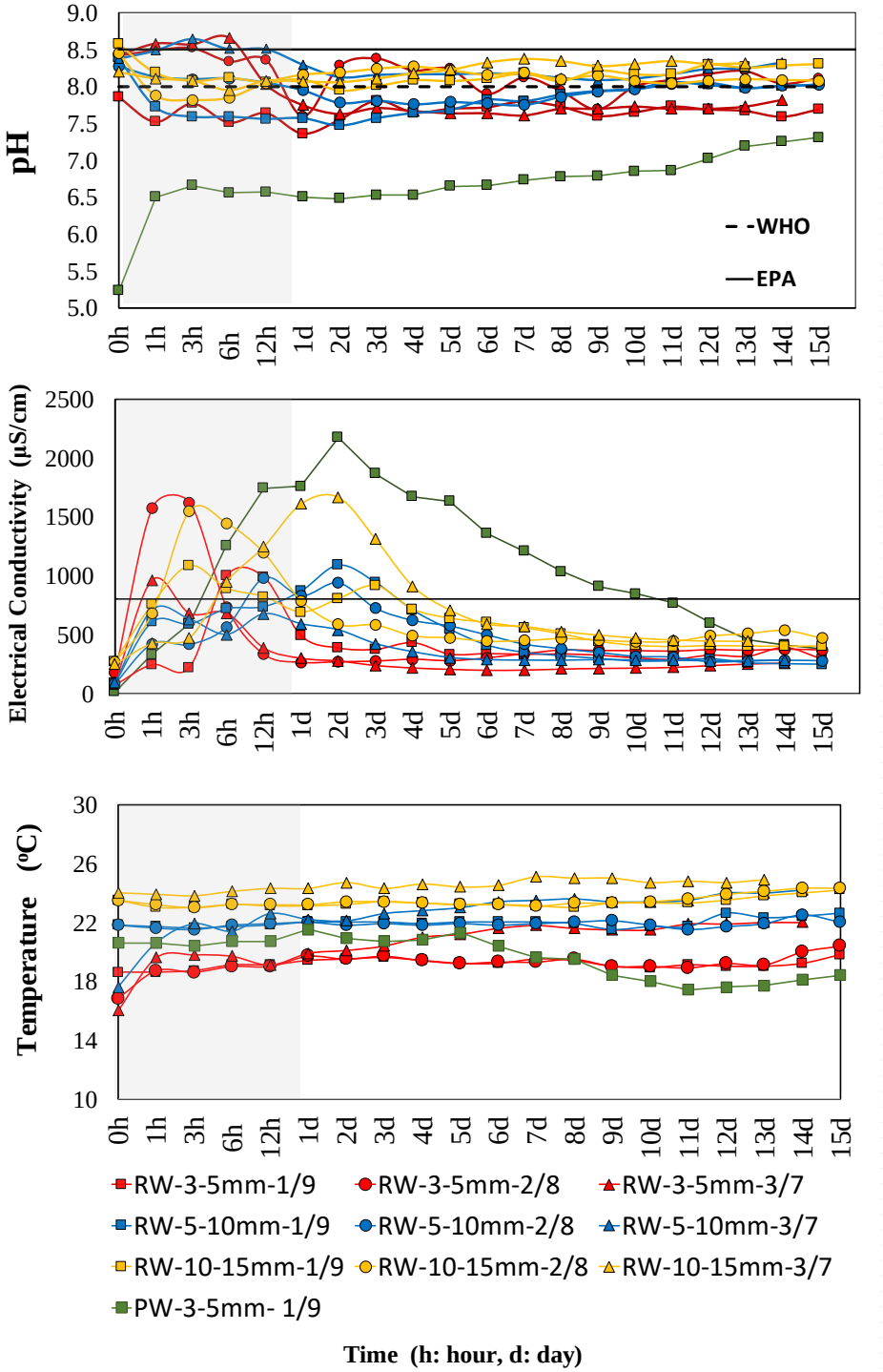

Figure 5.3. Time-depend values of the pH, electrical conductivity, and temperature for all CLTs

The change of EC by time showed that small sizes of GR interacted easier and faster with leaching solution than larger sizes of GR. Granulated rubbers are impermeable materials, so the leaching of inorganic from GRs is directly related to the rubber's surface

area in contact with the leaching solution. If the size of GR is smaller, the surface of GR is bigger for a constant volume (Selbes, 2015; Maeda, 2017). On the other hand, the EC of the 10–15 mm GR-sand mixture leachate sample at the end of the 15th day was 400 μS/cm, while others were about 240–290 mS/cm. This difference can be due to the steel and fiberglass belts in GR particles. Although all GR used in this study were free of steel and fiber belts, they might not be scraped out completely from GR with 10–15 mm. Scraping the fiberglass and steel belts from rubbers is easier and more effective for smaller diameters of GR than scraping from the larger size. Alternatively, the fact that steel and fiber belts are easy to separate from small size GR could not prevent metal powders from holding onto GR surfaces.

Figure 5.4 shows the concentration of metals in all leachate samples during the tests, while Figure 5.5 shows the concentrations of anions and cations in leachate samples. Note that; the horizontal axis is not in scale; a grey area represents the first day, while each point represents a day. The units of concentration of elements in Figure 5.4 are microgram/Liter, while the unit of concentration of elements in Figure 5.5 is milligram/Liter.

All test results were discussed with global water quality standards limits. pH values of leachates performed with RW solutions are higher than the limit reported by the WHO. In contrast, pH values approach the limits of U.S Environmental Protection Agency Primary / Secondary Drinking Water Standards (EPA-PWDS or EPA-SWDS) but mostly do not exceed them.

In all CLTs, Mn concentration was well above the limits (80-300 times) on the first day and showed a significant decrease until the 6th day. However, local increases and irregularities are seen afterward. Also, Fe concentration increased 10-20 times above the limits in almost all CLT tests. While the concentration was expected to decrease over time, local increases and peak values did not allow for observation of a significant trend. Although Zn, Cu, Pb, and Al approached the limits slightly in a few CLTs, they were generally below the limits (Figure 5.4). Although it is difficult to say that there is a significant trend, each metal concentration in leaching water increases at the beginning of the experiments (on the first day) and completes its dramatic decrease within the first 7–8 days.

Although no significant amount of Mn and Fe was detected in XRF analysis of rubber, contaminations of them were found higher than others, as seen in the literature (Selbes et al.,2015, Meida,2017). It can be observed that an insignificant portion of Mn

and Fe contamination came from the GR, while the major source was steel and fiberglass particles that have been pulverized during the removal process of steel belts and came by adhering to the surface of GR. The ideal sample for XRF analysis should have a perfectly flat surface. In this study, we performed XRF analyses on GR samples that had a flat surface and were cleaned from the pulverized steel and fiberglass particles. But leaching column tests were performed on irregular-shaped and unwashed GR particles. For this reason, it should be taken into account that there are several pulverized metals carried by GR particles, although it is not seen in the XRF analysis.

Ca^{2+}, SO_4^{2-}, Na^{+}, Cl^{-}, Mg^{2+}, and K+ contaminations for 20 samples plotted for 15 days in Figure 5.5. Na concentration slightly exceeded the limit in three experiments (PW 2,5-5mm-1/9, RW5-10mm 2/8, and RW10-15mm 3/7), while Cl^{-} exceeded the limits in more than half of the CLTs. The Ca concentration approached but not exceeded the limits in experiments performed with only 5-10mm GR, and it was very low in other CLT conditions. SO_4^{2-}, Mg^{2+} and K^{+} concentrations were well below the limits. Again, there is no significant trend, but it can be seen that each ionic element concentration in leaching water increases at the beginning of the experiments and completes its dramatic decrease within the first 7–8 days.

Although GR was free of fiber belts and steel wires, we know some metals and other elements come in a powder form adhering to the GR surface. Also, for 10–15 mm GR, steel wires and fiber belts may not have been removed. Because of these reasons, it was necessary to add the steel wire group while grouping the elements. So, to discuss the leaching concentration values, it is necessary to determine the major source of leachate elements. Here, the term major source indicates which of these is the source of most of the leachate elements; rubber, steel belts, or silica sand.

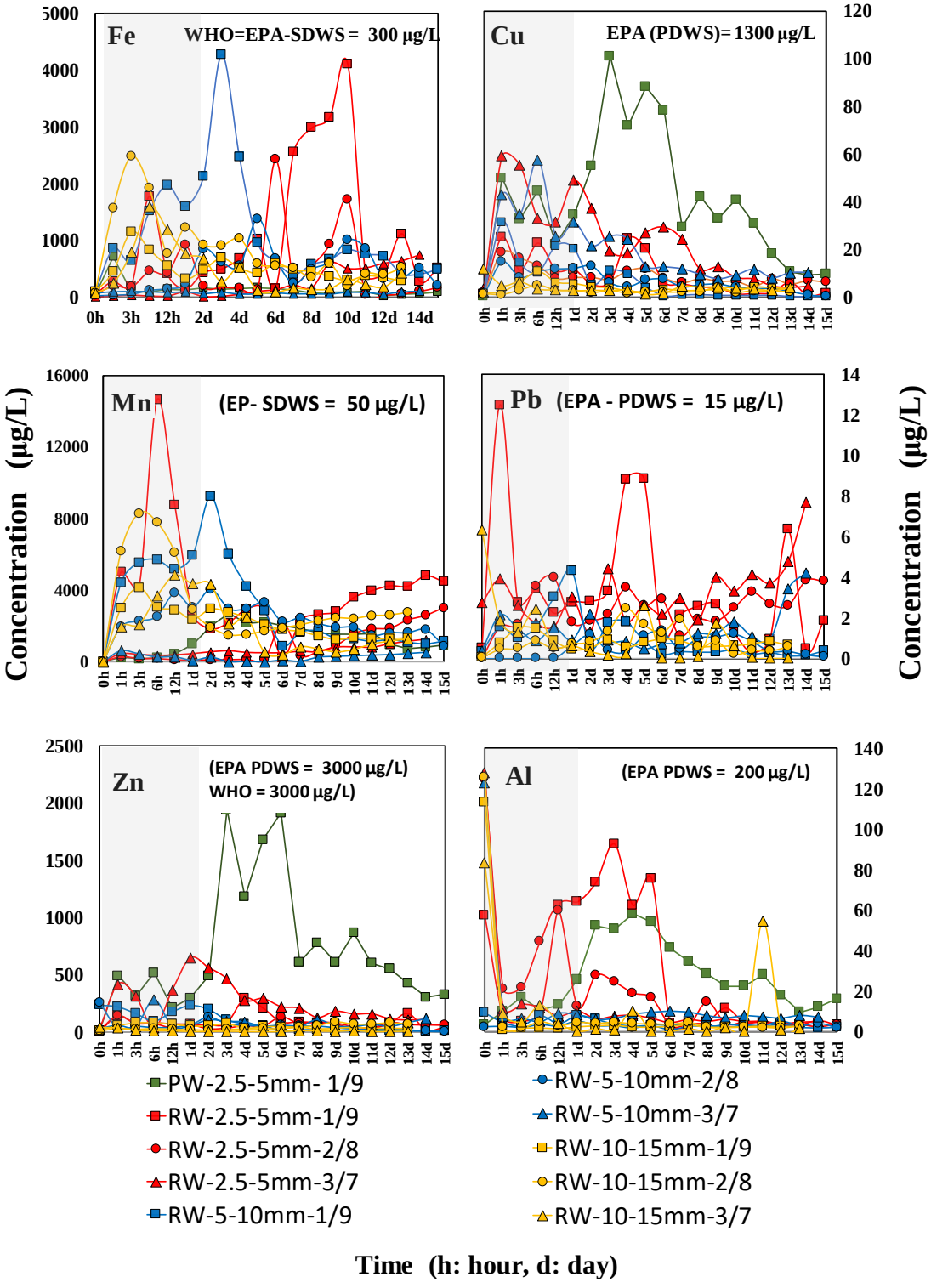

Figure 5.4.Time depend-concentration of metals in leachate samples taken from CLTs

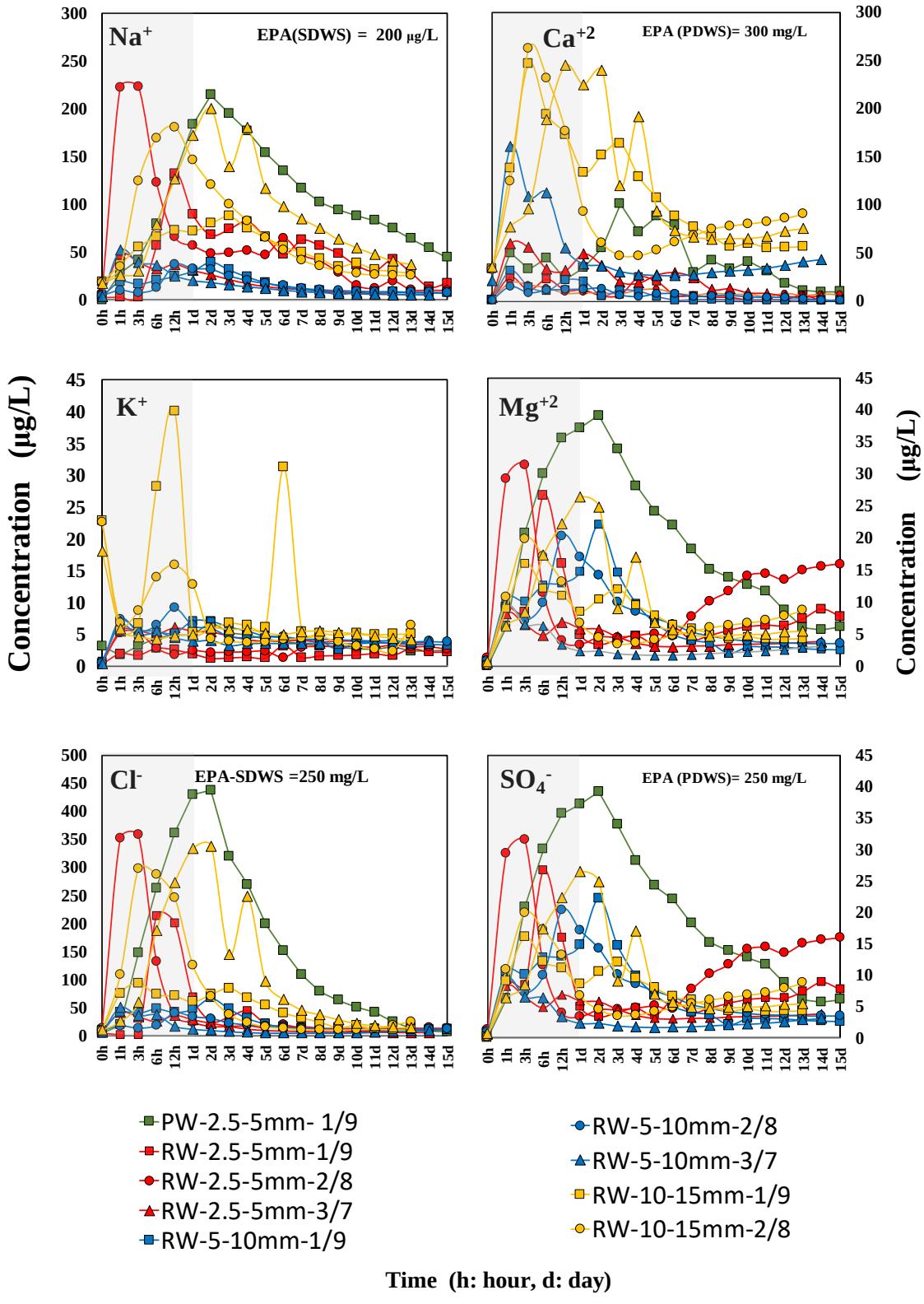

Figure 5.5. Time depend-concentration of anions and cations in leachate samples taken from CLTs

5.4. Discussions

Batch tests result were discussed to obtain the effects of pH on leachate of metals and anion/cations for varying GRS conditions. On the other hand, CLTs were performed to represent field conditions in the GRS mixture used as backfill and rainwater seepage through the backfill. The aim of the CLTs were to obtain the effects of GR ratio and GR size in a mixture on leachate of selected inorganics. So, firstly the leaching response of GRS mixture under the varying pH was discussed, then the effects of GR on leaching characteristics were determined under the same rainwater and similar environmental pH conditions.

5.4.1. pH

As seen in Figure 5.3. a, during all CLTs, the pH value was under the limit value of 8.5, classified as a limit of drinkable water by National Secondary Drinking Water Regulations by the Environmental Protection Agency of the US (EPA-SDWRs). At the end of the 15 days, the pH values varied between 7.5 and 8.2. Figure 5. shows that the CLTs were started under basic conditions except for the first test (C.PW.S.1). The pH value was 5.2 at the beginning of the CLT test C.PW.S.1. GRS layer drove the pH value to the basic stage, and pH reached 7.2 on the 15th day. For all other CLTs, the pH of RW was about 8.3 at the beginning, and the GRS layer caused a slight decrease in the pH value in leachate water. The decreasing pH value is bigger when the GR size is small in the CLT setup with rainwater solutions.

If the two tests which have the same GRS mixture but have different water solutions (C.PW.S.1 AND C.RW.S.1)) are compared, it can be said that; GRS drives the pH of the leachate environment to 7.5-8.0, regardless of whether the initial conditions are acidic or basic. While 10–15 mm size GR did not significantly affect pH value, 3–5 mm and 5-10mm size GR- tried to drive pH to the neutral condition. This is a trend known from the previous studies (Humphrey and Sweet, 2006; Maeda et al., 2017; O'Shaughnessy and Garga, 2000). Also, the similarity between pH conditions in this study and recent field studies (Aydilek et al., 2006; Maeda et al., 2017) suggested that leaching tests successfully represented the natural pH conditions in the geotechnical applications under rainwater.

As seen in Figure 5.1 showing the results of batch tests, Contamination of Zn reached the 3mg/L limit of EPA-SWDS for all GR for pHs of 4.3 and 6.8, while it was below the limit for pH of 8.3. While decreasing the GR diameter increased the Zn contamination by a small amount, changing the pH of the solution from the basic stage to the acidic stage significantly affected and increased the contamination of Zn. On the other hand, there was no clear relation between pH and change in contamination of Fe and Mn for all GRs diameters. In contrast, the incensement in contamination of Fe and Mn for 5-10mm GR was bigger than other GR diameters for a constant pH in all acidic, basic or neutral cases. Also increasing the pH value was caused to decrease in contamination of Al, while caused to increase in contamination of Na^{+} and Ca^{2+} for clean sand during the BTs.

In this study, to compare the leaching behavior of elements in Batch Tests under different pH conditions; leaching intensity (I_L) was used as proposed by Wang et al. (1999);

$$I_L = \frac{a_x V 10^3}{A_x M t} \qquad (5.5.1)$$

where I_L is the leaching intensity (h^{-1}), ax is the concentration of element x in leachate (µg/ml), V is the total volume of leached solution (mL), A_x is the concentration of element x in the original sample (µg/g), M is the total weight of the sample (g), and t is the leaching time. The larger the leaching rate means stronger the leaching intensity (Wang et al., 1999; Lee, 2011).

Wang et al (1999) suggested that the leaching charactersitics of elements under different pH conditions can be divided into four classes depending on the I_L value. That is, strong for I_L >5, medium for l<I_L<5, weak for o.5<I_L<1, and very weak for I_L< 0.5. It has been calculated for all inorganic elements for 30 days. The leaching intensity values of inorganic elements under the three different pHs (4.1, 6.8, and 8.3) for all GR sizes are shown in Figure 5.6. As seen in Figure 5.6, IL is strongest for Fe, and the second strongest one is SO_4^{2-}, followed by Zn, and Mn. Leaching intensity of Al, Cu, Pb and $^{-}$Cl can be classified as medium while Mg^{2+} and Na^{+} have weak leaching intensity. Ca^{2+} has a very weak leaching intensity according to the batch tests. One of the most apparent results from BTs was that; there was an increase in leaching concentrations when the pH changed to acidic conditions for metals except Pb. On the other hand, there was no clear relation

between the pH of the environment and the leaching of selected anions and cations from GRS.

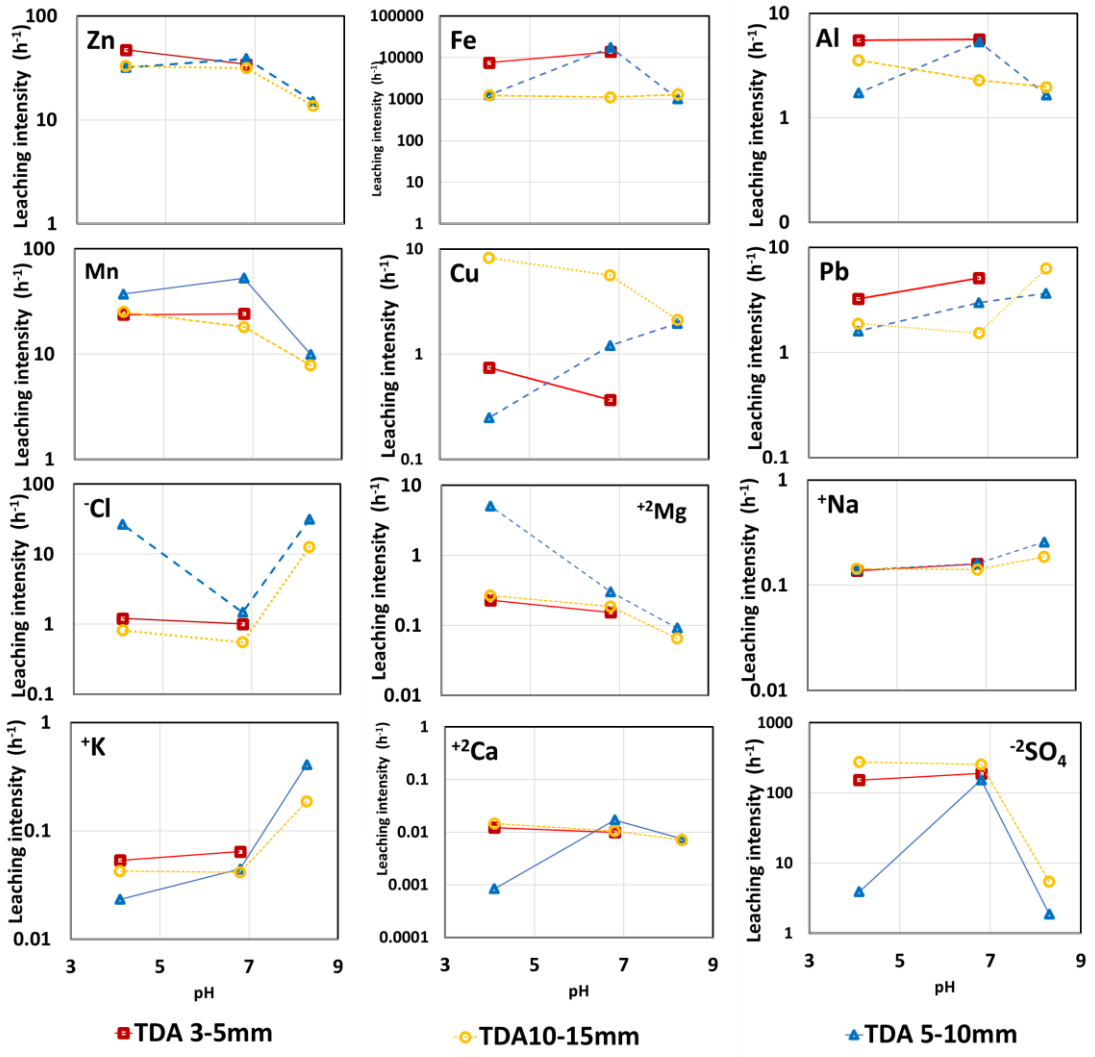

Figure 5.6. The leaching intensity values of selected inorganic elements under the three different pHs (4.1, 6.8, and 8.3) conditions for all GR sizes.

In Chapter 3 and Chapter 4, GRS mixtures represented the backfill, a saturated shallow filling layer lying on the sand layer. CLTs were performed to simulate the same layering conditions, and the leaching solution was rainwater which was basic (pH=8.0-8.3) in the study to represent the natural field conditions. According to the results of the batch tests, it was figured out that metals leach much more when pH increases to the acidic stage. So, CLTs were not performed under the most critical pH conditions, and the leaching inorganics from GRS mixtures under acidic rain conditions can be a concern to investigate for future studies.

5.4.2. Leaching of Inorganics

5.4.2.1. Metals

According to both BTs and CLTs experimental studies, most leachate metals were Fe, Zn, and Mn. When we see the BTs results (Figure 5.1) and CLTs results (Figure 5.4) over time, it can be seen that the concentration of these metals increased by time in BTs while they increased in the first 1h-1day period then started to decrease or to give a trendless value. The reasons are that BTs was a test in which the solution was prepared at the beginning of the test, and the GRs were soaked into it. Hence, BTs, each obtained value of any element's concentration can be considered. On the other hand, in CLTs, the water was allowed to seep through the GRS mixture, and each concentration of any element value was the concentration of that time.

To obtain the leaching amount of selected inorganics from CLTs, data analyses were observed based on the cumulative mass of each parameter obtained at the end of the 15 days leaching period. This cumulative mass at the end of 15 days was used as 100% of leaching (M_{Max}) for the data set, and for each day, the ratio of cumulative metals mass leached to total leached amount mass was calculated (M/M_{Max}) (Selbes, 2015). The cumulative results of metals leached from CLTs are provided in Figure 5.7. As seen in Figure 5.7, the leaching amount of metals is greater in pure water conditions than in rainwater conditions (compare PW2.5-5mm-1/9 and RW2.5-5mm-1/9). 5-10mm and 10-15mm GR sizes give a close leaching amount for Mn, Fe, and Zn under the same GRS mixture conditions if the GR ratio is bigger than 20%. On the other hand, while the mixing ratio (10-30%) has a significant role in increasing leaching metal mass for 3-5mm and 5-10mm GR, the differences between leaching mass for all mixing ratios of GRS are not too dramatic for 10-15mm GR.

Figure 5.8 shows each cumulative mass loss rate of metals by time. For Fe; the mass-loss rate (MLR) on the first day is nearly equal to 40-50% for the biggest GR size, while MLR is between 10-30% for middle size GR and between 5-15% for the smallest GR. In other words, MLR is the fastest for the biggest GR size, while it has the slowest MLR with the smallest GR in CLTs. There is a significant relationship between GR size and MLR, but it is difficult to say that the mixing ratio of GRS and MLR has a clear relationship.

It can be observed that only the mixing ratio of GR in the sand as filling material has a significant role in the mass-loss rate of Fe if the GR size is too small (2,5-5mm). Selbes et al. (2015) suggested that the average mass loss rate of Fe and Mn for all tests (varying pH and GR sizes) in 30 days shows a nearly linear trend. However, this study shows that, under the same pH condition (8.3), the ratio of GRS and GR sizes causes a change in the leaching rate of Fe and Mn. The trends vary in an extensive range, similar to the trends proposed by Maeda et al. (2017) with the 70 weeks field study result. For Mn, Cu, Pb, and Zn; the fastest mass loss rate was 5-10mm, while it was slowest for 2.5–5 mm GR.

For Zn; all the CLTs show closer trends, which are similar to the trend proposed by Selbes (2015), except for only two CLTs; RW3-5mm1/9 is the fastest, and RW10-15mm2/8 is the slowest. Also, the MLR of Zn trend for the RW2.5-5mm-1/9 is close to the results of Maeda et al.(2017).

MLR of Cu for all tests has closer trends which show nearly linear relations by time. For Pb and Al, the fastest MLR was in the CLT with 5-10 mm GR, while the slowest was in 10–15 mm GR. Selbes et al. (2015) used average values of tests and plotted the trend of the leaching rates by times, while Maeda et al. (2017) plotted the trends for different leaching solution conditions (varying pH). This study suggests that GR size and pH conditions have a significant role in the leaching of metals but not enough to explain the leaching characteristics over time. The leaching of metals is not only related to the size of GR and pH but also GR mixing ratio if the GR is used with sand as a mixture for backfilling.

The filing conditions and mixing ratio can change both the leaching amount and leaching rate under the condition of mixing the GR with sand or other soils. When the silica sand particles are mixed with GR particles, they create different leaching surfaces for different GR sizes and GRS ratios.

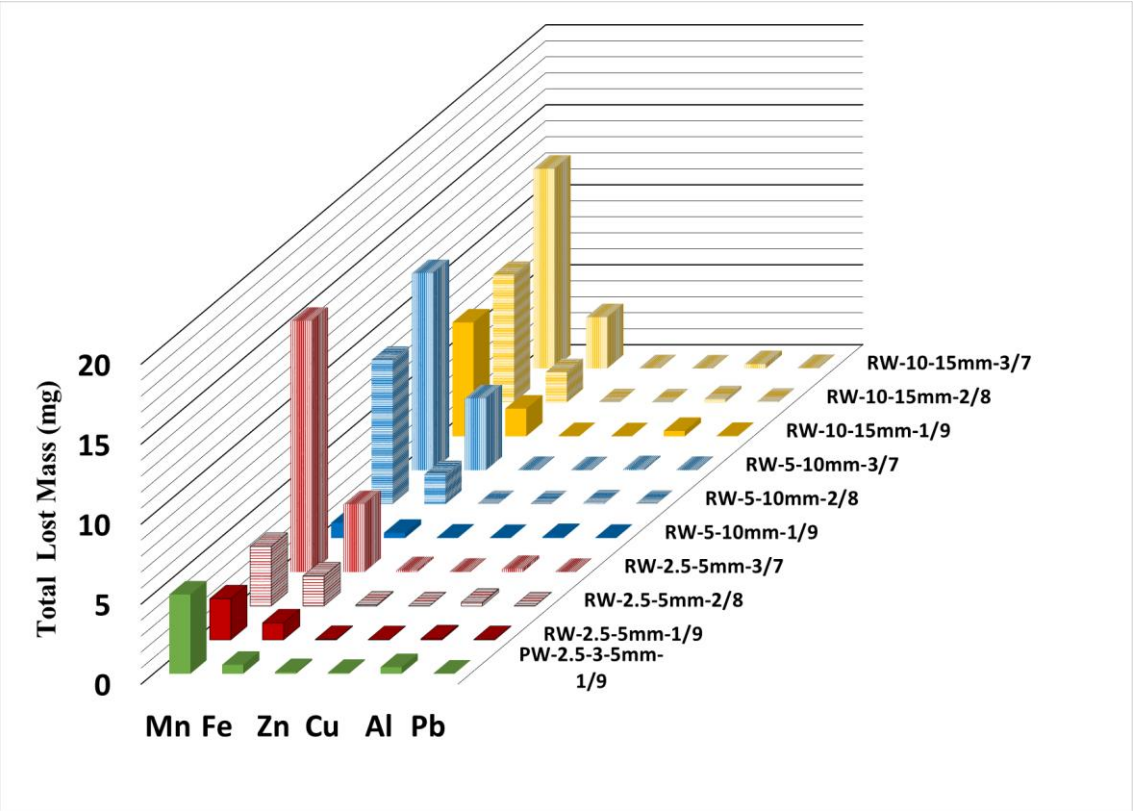

Figure 5.7. The cumulative amount of metals mass for different CLT conditions.

When the total amount of leaching metals and time-dependent leaching rates of metals are discussed together, the following results are obtained, as shown in Figure 5.7 and Figure 5.8. The smallest GR size carries a more pulverized form of metals on its surface, and the total leachate metal increases when the GR size decreases if the GR size is smaller than 10mm. GR size that is bigger than 10mm can cause a decrease in leachate metal mass. Alternatively, leaching mass-loss rates of metals are related to GR size or surface. We can explain this situation: rainwater must contact the rubber surface to leachate the metals into the groundwater.

For the smallest GR size (2.5-5mm), the GRS mixture settled together with fewer voids, and the silica sand particles covered the GR surface better, and this caused reducing the contacted surface area of GR with rainwater. The surface of the largest GR size (10–15 mm) was covered by sand because it has a more rectangular shape than the other two GR size particles, and again, the contact surface area of GR with rainwater was reduced. Here, the medium-size GR (5–10 mm) between the sand particles performed the fastest leaching into groundwater. As a result, the leaching of metals when GR is mixed with soils depends not only on the size of GR but also on the filling conditions, such as the soil type in the mixture, the ratio of GR in the mixture, and the shape of the GR.

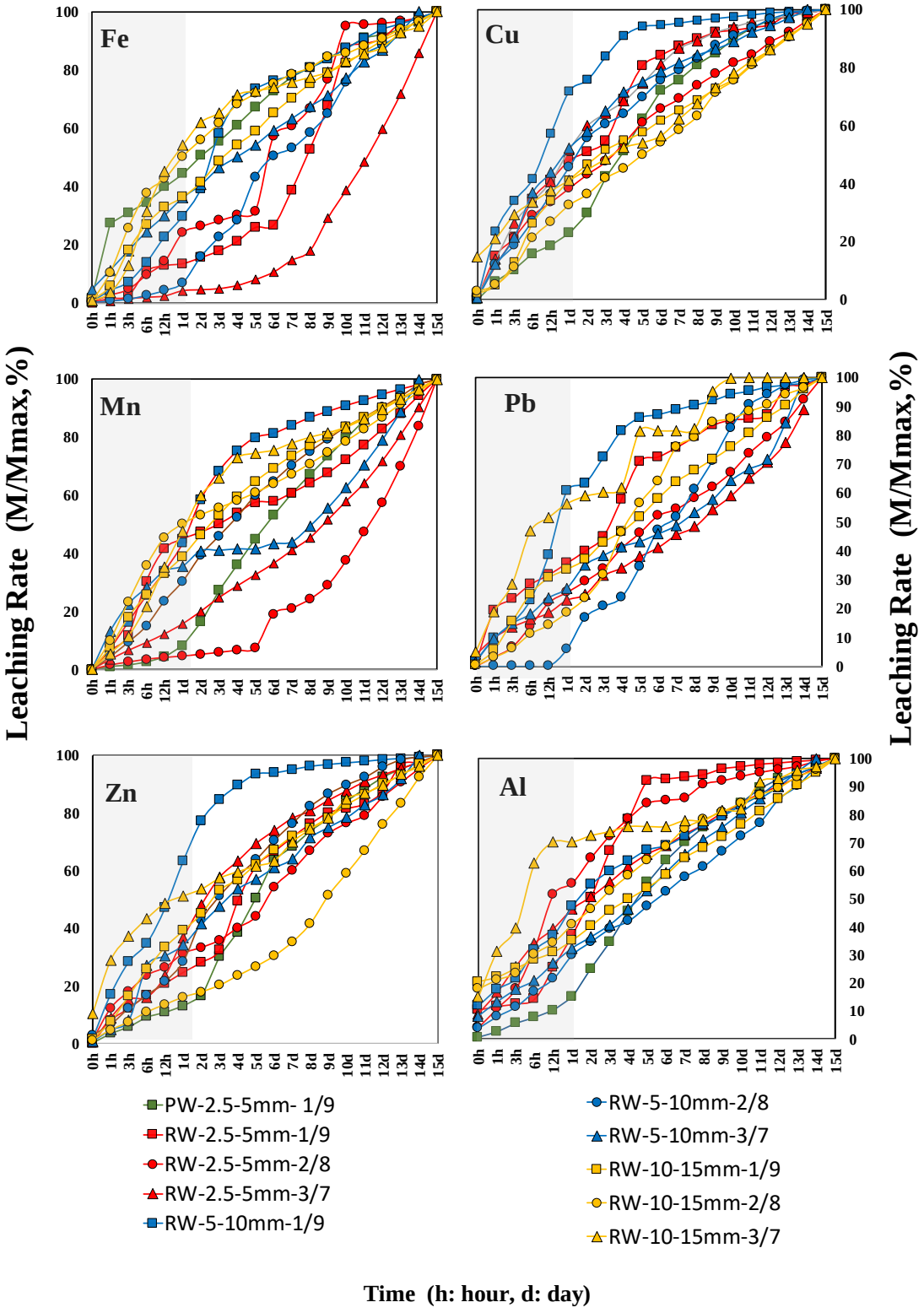

Figure 5.8. The cumulative mass loss rate of metal elements by time.

5.4.2.2. Anions and Cations

According to the CLTs, which were reasonable, realistic set up to represent the field conditions, leaching of SO_4^{2-} was pretty lower than the international usable water standard, but it had the strongest IL values according to BTs. In contrast, Cl^- and Na^+ reached their limit value determined by EPA in one day, then started to decrease in CLTs. On the other hand, its IL values were medium and weak, respectively, according to the BTs.

According to the CLTs, Ca^{2+} is the most leaching cation by mass, while the second is SO_4^{2-} and the third is Cl^- (Figure 5.9). Ca^{2+} and SO_4^{2-} are the elements that came from rubber, while the Cl^-, which is the third most leaching element, came from silica sand. Mg^{2+} and K^+ have too small mass compared to others, and the MLR for all ten CLTs are close to each other (Figure 5.9 and Figure 5.10). For the ratio of GR is 10% in the mixture, it is clear that; increasing GR sizes increases the total leachate mass of Ca^{2+} and SO_4^{2-}. If the ratio of GR is between 20-30%, 5-10mm GR gives less leachate mass for Ca^{2+} and SO_4^{2-}. For Cl^- there is no significant relation between GR sizes and the leachate mass (Figure 5.8).

Figure 5.9 shows the cumulative mass loss rate of selected anions and cations in percentage by time. As shown in the figure, for Ca^{2+} , SO_4^{2-} and Mg^{2+}, whose major source is rubber, the total mass loss trend from fastest to slowest is; 5–10mm < 10–15mm < 2.5–5mm of GR for the first day, while the same trend is 2.5–5mm < 10-15mm < 5-10mm for from the 1st day to 15th day period. The total mass loss rate of Na^+ is 2.5–5mm <10–15mm < 5–10mm GR during the whole test. The total mass loss rate of ^-Cl, whose major source is silica sand, is the fastest in all tests performed with 2.5–5 mm GR, while the trends of rates were slower for the other seven tests during the whole tests. The reason is that Chlorine (Cl^-) that comes from silica sand captures calcium (Ca^+) and sodium (Na^+) elements coming from rubber and allows them to leach rapidly within the first day for all three tests. This interaction also explains the leaching test's time-dependent electrical conductivity (EC) behavior (see Figure 5.3.a).

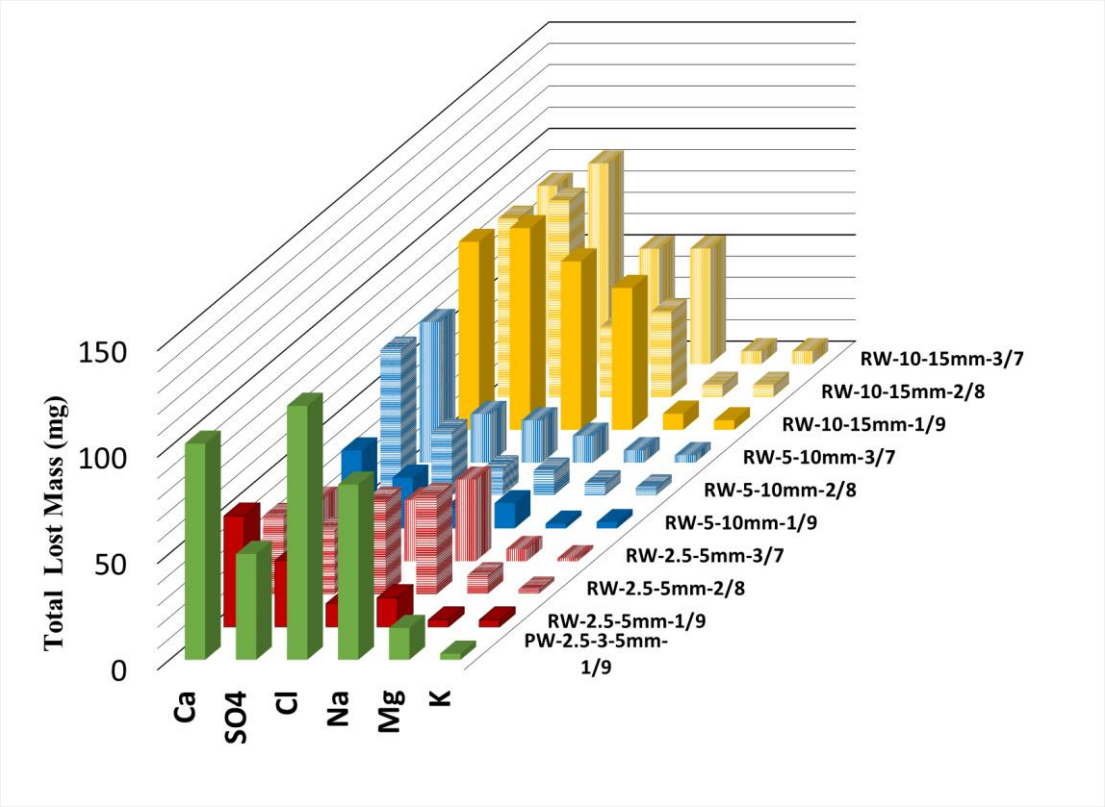

Figure 5.9. The cumulative amount of anions and cations for different CLT conditions.

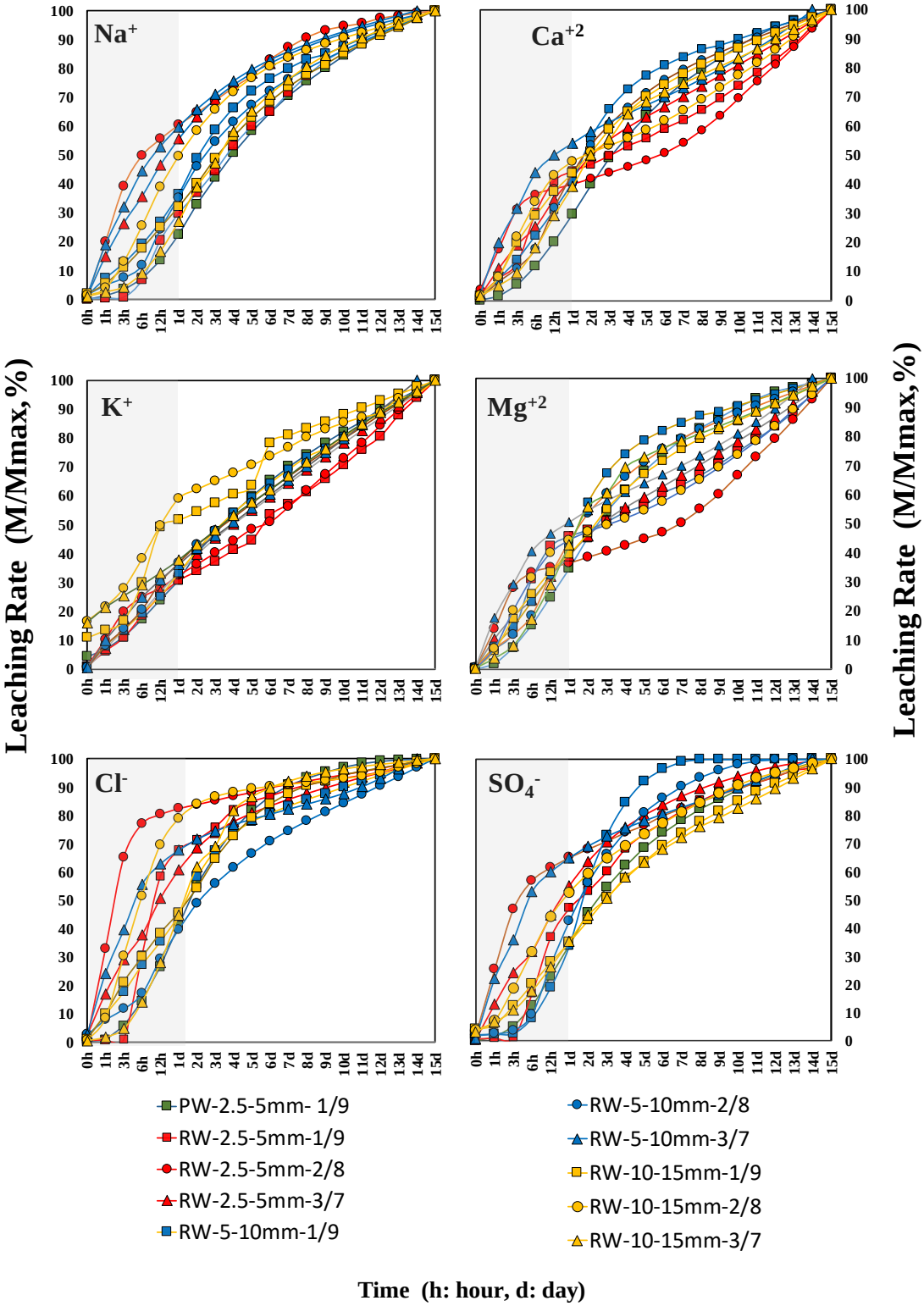

Figure 5.10. The cumulative mass loss rate of anions and cations by time (microgram/gram).

5.5. Concluding Remarks

In this study, three sizes of GR were mixed with sand in the same volumetric ratio of 10%,20%, and 30%, and a filling material model was created. A series of batch tests and column-leaching tests were performed, and distilled water and natural rainwater were used as surface water. The following results were obtained from this comparative study;

1) When the pH of the environment increases, the concentrations of most leachate metals decrease from GRS mixture, whose main sources are GR particles. On the other hand, most leachate anions and cations are not directly related to pH. They were mainly related to the NaCl and NaOH in sands.
2) When granulated scrap tire rubber is mixed with sand and used as filling material around infrastructures, it leachates the groundwater in a hazardous way in terms of Zinc, Manganese, Iron, and Chloride. It is not hazardous for groundwater in terms of other metals, anions, or cations.
3) While there is an inversely proportional relationship between the scrap tire GR size and the total leaching mass of metal elements, no significant relationship was determined by the total leaching mass of anion and cations.
4) Despite the inverse proportionality between the total mass of leachate metal elements and the size of the GR; the rate of total mass loss leaching to the groundwater -defined in terms of the rate of the cumulative leachate mass loss to the total leachate mass-, is the fastest for the 5–10 mm sized granulated rubber. In contrast, it is slower for 3–5 mm and 10–15 mm granulated rubber.
5) The leaching rate of metals into groundwater is not only dependent on the size of GR but also on the filling conditions, the shape of the GR, and the removal progress of its steel and fiber belts.
6) About 40% of the total leachate mass of inorganic was leached out of the system on the first day. So, it's beneficial to soak the scrap tire GR particles in water for at least one day or to rewash them carefully before being used as filling material in geotechnical applications.
7) Laboratory experiments in which many environmental conditions such as pH are controlled give valuable information about the scrap tire GR behavior. Considering these studies, laboratory experiments demonstrating the field

conditions are an essential bridge between material behavior information and field tests or applications to determine the environmental effects of GRs.

CHAPTER 6

SUMMARY AND CONCLUSIONS

6.1. Summary

The thesis addresses a series of experimental studies shake table tests to determine the effects of the granulated rubber in granulated rubber sand mixture on liquefaction potential and pipeline behavior when granulated rubber sand mixture are used as filling material around pipelines Another concern of the thesis is the leaching effects of granulated rubber in mixture on groundwater quality when the surface water leachate through the mixture when the diameter of GR or mixing ratio of GR are varying. The concluding remarks are listed at the end of the each chapter. These observations are sum up in this section.

6.2. Conclusions

According to the results obtained throughout the study, the following conclusions can be drawn:

Chapter 3 showed that; granulated rubber are usefull materials to remedation of liquefaction when they are used as a mixture with sand. If the granulated rubber diameter and the ratio of granulated rubber in mixture varys, the increase in excess pore water pressure changes. Granulated rubbers decrease the excess pore water pressure and not allow the liquefaction to occur. The decreasing of pore water pressure is related to not only the quicker drainage of the water, but also the lower dynamic waves of earthquake. Granulated rubber increased the permeability of the mixture and also change the compresibility of the mixture. According to the reduction in pore water pressure ratio and coeficent of consolidation of mixtures, if granulated rubbers with 5-10mm diameter is mixed with sand with ratio of 2/8, most efficient remedation is observed.

Chapter 4 showed that, adding the granulated rubber into sand and used them as a filling material around buried pipeline is succesful method to prevent the pipe from upward displacement. As shown in Chapter 3 and Chapter 4, granulated rubber diameter and ratio of granulated rubber in mixture directly effects the consolidation coeficent of

mixture. The pipeline uplift movements are related to stresses acting on it. An equibilirium condition is observed which the total net stress acting on the pipe are equal to zero. This equibilirium condition is determined as a situation when a non-dimensional parameter (α) is equal to 3. This non-dimensional parameter is a combination of the pipe diameter, the burial depth of pipe, the time of initiation of upward movement and consolidation coefficient of backfill. Using by the proposed non-dimensional parameter and the equibilrium state it can be design a critical condition for predetermined pipe material and diameter, burial depth of the pipe, backfill conditions for a known seismic loading to prevent the uplifting of the pipe.

In Chapter 5, it was seen that leaching of metals, anions and cations from granulated rubbers are not a threat for groundwater quality. The total leachate amount increase when the granulated rubber ratio in mixture increases. Also for a constant ratio, there is no clear relation between the granulated rubber and the total amount of leachate metals. About 40% of the total leachate mass of inorganic was leached out of the system on the first day under the rainwater leaching conditions. So, it's beneficial to soak the scrap tire granulated particles in water for at least one day or to rewash them carefully before being used as filling material in geotechnical applications. The leaching rate of metals into groundwater is not only dependent on the size of GR but also on the filling conditions, the shape of the GR, and the removal progress of its steel and fiber belts.

REFERENCES

Abdullah, W., Ashkanani, A., Eid, W., Al-Fares, R., & AlKhamis, M. (2022). Evaluation of Sand–tire Crumb Mixtures as Lightweight Fill Materials. *Geomechanics and Geoengineering*, 1-14.

Alzabeebee, S. (2022). Tire Derived Aggregate as a Sustainable Technique to Mitigate Transient Seismic Effect on Buried Concrete Pipes. *In Sustainable Cities and Resilience* (pp. 317-328). Springer, Singapore.

Anastasiadis, A., Senetakis, K., Pitilakis, K., Gargala, C., Karakasi, I. (2012) Dynamic behavior of sand/rubber mixtures, Part I: Effect of rubber content and duration of confinement on small-strain shear modulus and damping ratio. *J ASTM Int 9(2).*

ASTM D6913/D6913m-17 (2009). Standard Test Methods for Particle-Size Distribution (Gradation) of Soils Using Sieve Analysis.

ASTM D6270-20, (2020). Standard Practice for Use of Scrap Tires in Civil Engineering Applications.

ASTM D4253-00 (2000). Standard Test Methods for Maximum Index Density and Unit Weight of Soils Using a Vibratory Table.

ASTM D854-14 (2014). Standard Test Methods for Specific Gravity of Soil Solids by Water Pycnometer.

ASTM D5681-22 (2022). Standard Terminology for Waste and Waste Management.

ASTM D3441-16. (2016). Standard test method for mechanical cone penetration testing of soils. Annual Book of ASTM Standards, West Conshohocken, PA.

Attom, M.F. (2006). "The use of shredded waste tires to improve the geotechnical engineering properties of sand," Envion. Geol., 49:497–503. https://doi.org/10.1007/s00254-005-0003-5.

Aydilek, A.H., Madden, E.T., Demirkan, M.M. (2006) Field evaluation of leachate collection system constructed with scrap tires. *Journal of Geotechnical and Geoenvironmental Engineering 132(8): 990-1000.* https://doi.org/10.1061/(ASCE)1090-0241(2006)132:8(990)

Bahadori, H., Manafi, S., (2014). Effect of tyre chips on dynamic properties of saturated sands. *Int J Phys Model Geotech*. https://doi.org/10.1680/ijpmg.13.00014.

Bahadori, H., Farzalizadeh, R., (2018). Dynamic properties of saturated sands mixed with tyre powders and tyre shreds. *International Journal of Civil Engineering*, 16(4), 395-408.

Bosscher, Peter J., Tuncer B. Edil, and Neil N. Eldin. (1992). Construction and performance of a shredded waste tire test embankment. *Transportation Research Record* 1345.

Busic, R.; Milicevic, I.; Sipos, T.K., Strukar, K. (2018). Recycled Rubber as an Aggregate Replacement in Self-Compacting Concrete—Literature Overview. Materials, 11, 1729.

Castiglia M, Santucci de Magistris F, Koseki J (2019) Uplift of buried pipelines in liquefiable soils using shaking table apparatus. *In 7th International Conference on Earthquake Geotechnical Engineering*, ICEGE 2019, 1638–1646. ISBN 978–0–367–14328–2

Castiglia M., Santucci de Magistris F., Morgante S., Koseki J. (2020) Geogrids as a Remedial measure for seismic-liquefaction induced uplift of onshore buried gas pipelines. *National conference of the researchers of geotechnical engineering*, CNRIG 2019: Geotechnical Research for Land Protection and Development, 649–657. DOI: https://doi.org/10.1007/978-3-030-21359-6_69

Chian, S. and Tokimatsu, K. (2011). Floatation of underground structures during the Mw 9.0 Tōhoku Earthquake of 11th March 2011. *in Proceedings of the 15th World Conference on Earthquake Engineering*, Lisbon, Paper ID, vol. 3705.

Chian S. and Tokimatsu, K. (2012). Floatation of underground structures during the Mw 9.0 Tōhoku Earthquake of March 11 2011. in Proceedings of the 15th World Conference on Earthquake Engineering, Lisbon, Paper ID, vol. 3705.

Chian, S.C., Madabhushi, S.P.G. (2012). Effect of buried depth and diameter on uplift of underground structures in liquefied soils. *Soil Dynamics and Earthquake Engineering*, 41, 181–190. http://dx.doi.org/10.1016/j.soildyn.2012.05.020.

Chian, S.C., Tokimatsu, K. and Madabhushi, S.P.G. (2014). Soil liquefaction–induced uplift of underground structures: physical and numerical modeling. *Journal of Geotechnical and Geoenvironmental Engineering*, vol. 140 ,no. 10, p. 04014057.

Christ, M., Park. J.B., (2010). Laboratory determination of frozen rubber-sand mixtures. Cold *Regions Science and Technology*, 60 (2) (2010), pp. 169-175.

Cox, B.R., and Griffits, S.C. (2010). Practical Recommendations for Evaluation and Mitigation of Soil Liquefaction in Arkansas. *American Society of Civil Engineers*. *Seismic Evaluation and Retrofit of Existing Buildings (ASCE/SEI 41-13).*

Cubrinovski, M., Hughes, M., Bradley, B., McCahon, I., McDonald, Y., Simpson, H., ... & O'Rourke, T. (2011). Liquefaction impacts on pipe networks. Recovery Project, (6), 149.

Cubrinovski, M., Henderson, D., & Bradley, B. (2012). Liquefaction impacts in residential areas in the 2010-2011 Christchurch earthquakes.

Dadkhah, H., Kalatehjari, R., Hajihassani, M., Kharghani, M., & Asteris, P.G. (2021). Sand–Tire Shred Mixture Performance in Controlling Surface Explosion Hazards That Affect Underground Structures. Applied Sciences, 11(24), 11741.

Downs, L.A., Humphrey, D.N., Katz, L.E., Rock, C.A. (1996) Water quality effects of using tire shreds below the groundwater table. Technical Report 94-I, Department of Civil Environmental Engineering, University of Maine, Orono.

Ecemis, N. (2013). "Simulation of seismic liquefaction: 1-g model testing system and shaking table tests," European Journal of Environmental and Civil Engineering, Vol. 17, No. 10, 899–919. http://dx.doi.org/10.1080/19648189.2013.833140.

Ecemis, N., Valizadeh, H., Karaman, M. (2021). "Sand-Granulated-Rubber Mixture to Prevent Liquefaction-Induced Uplift of Buried Pipes: A Shaking-Table Study," Bulletin of Earthquake Engineering, Volume 19, pages 2817–2838. https://doi.org/10.1007/s10518-021-01091-3.

Edil T.B., Bossher, P.J. (1992). Development of Engineering Criteria for Shredded Waste Tires in Highway Applications, Research Report GT-92-9, University of Wisconsin, Madison, Wisconsin.

Edil T.B., Bossher, P.J. (1994). Engineering Properties of Tire Chips and Soil Mixtures. *Geotechnical Testing Journal* 17, no. 4 (1994): 453-464. https://doi.org/10.1520/GTJ10306J

Edil, T.B., Park, J.K., Kim, J.Y. (2004). Effectiveness of scrap tire chips as sorptive drainage material. *Journal of Environmental Engineering*, ASCE, 130(7): 824-831. https://doi.org/10.1061/(ASCE)0733-9372(2004)130:7(824)

Edil T.B. (2008). A review of environmental impacts and environmental applications of shredded scrap tires. *In Proceedings of the International Workshop on Scrap Tire Derived Geomaterials, Yokosuka, Japan, 23–24 March 2007*. Edited by H. Hazarika and K. Yasuhara. Taylor and Francis, London. pp. 3–18.

Edinçliler A., Baykal G., and Saygılı A. (2010). Influence of different processing techniques on the mechanical properties of used tires in embankment construction. *Waste Management*, 30(6): 1073–1080.

Edinçliler A., and Yıldız O., (2021). Effects of processing type on shear modulus and dampingratio of waste tire-sand mixtures. *Geosynthetics International.* https://doi.org/10.1680/jgein.21.00008a

ETRMA. (2019). End of Life Tires Management - Europe 2018 Status Data. *European Tyre Rubber Manufacturers' Association.*

Fakharian, K., and Ahmad, A. (2021) Effect of anisotropic consolidation and rubber content on dynamic parameters of granulated rubber-sand mixtures. Soil Dynamics and Earthquake Engineering. Volume 141, February 2021. https://doi.org/10.1016/j.soildyn.2020.106531.

Feng, Z.Y., and Sutter, K.G. (2000). Dynamic Properties of Granulated Rubber/Sand Mixtures. . *J ASTM Int Volume 23, Issue 3.*

Finney, B., Chandler, Z. H., Bruce, J. L., Apple, B. (2013) Properties of tire-derived aggregate. *California Dept. of Resources Recycling and Recovery, Sacramento, CA.*

Ghazavi, M., and Sakhi, M.A., (2005). Influence of Optimized Tire Shreds on Shear Strength Parameters of Sand. *International Journal of Geomechanics/Volume 5 Issue* 1 https://doi.org/10.1061/(ASCE)1532-3641(2005)5:1(58).

Gotteland, P., Lambert, S., Balachowski, L. (2005). Strength characteristics of tire chips-sand mixture, Stud Geotech Mech 27(1):55–66.

Hazarika H, Hyodo, M., Yasuhara K. (2010). Investigation of tire chips-sand mixtures as preventive measure against liquefaction. *In Ground Improvement and Geosynthetics (Puppala AJ, Huang J, Han J and Hoyos LR (eds)).* American Society of Civil Engineers, Reston, VA, USA, ASCE Geotechnical Special Publication 207, 338–345. DOI: https://doi.org/10.1061/41108(381)44.

Hazarika, H., Pasha, S. M. K., Ishibashi, I., Yoshimoto, N., Kinoshita, T., Endo, S., ... & Hitosugi, T. (2020). Tire-chip reinforced foundation as liquefaction countermeasure for residential buildings. *Soils and Foundations*, 60(2), 315-326.

Hazen, A., (1920). Hydraulic-Fill Dams., Transactions of the ASCE, pp. 1713-174, 1920.

Hennebert, P., Lambert, S., Fouillen, F., Charrasse, B. (2014) Assessing the environmental impact of shredded tires as embankment fill material. *Canadian. Geotechnical Journal.,* 51(5), 469–478. https://doi.org/10.1139/cgj-2013-0194

Hyodo M, Yamada S, Orense RP, Okamoto M, Hazarika H (2008) Undrained cyclic shear properties of tire chip-sand mixtures. *In: Proceedings of the international workshop on scrap tire derived geomaterials opportunities and challenges.* London: Taylor and Francis; 187–196. ISBN 978–0–415–46070–5.

Humphrey, D.N., Katz, L.E. (2000). Water-quality effects of tire shreds placed above the water table: a five-year field study. Transportation Research Record 1714, 18-24. https://doi.org/10.3141/1714-03

Humphrey, D.N., Katz, L.E. (2001). Field study of the water quality effects of tire shreds placed below the water table. Proceedings of the International Conference on Beneficial Use of Recycled Materials in Transportation Applications, Arlington, VA, 699-708.

Humphrey D.N., Sweet M. (2006). Literature review of the water quality effects of tire-derived aggregate and rubber modified asphalt pavement., Technical Report for U.S. Environmental Protection Agency Resource Conservation Challenge, Univ. of Maine, Orono, ME.

Idriss, I. M., and Boulanger, R. W. (2008). Soil liquefaction during earthquakes. *Monograph MNO-12,* Earthquake Engineering Research Institute, Oakland, CA, 261 pp.

Ishihara, K., (1985). Stability of Natural Deposits During Earthquakes., 11th International Conference on Soil Mechanics and Foundation Engineering, San Francisco, Vol. 1, p321-376, 1985.

Izadifar, M., Mousavi, H., Zadehmohamad, M., & Hosseini, S.M.M.M. (2021). Evaluating the isolation effect of the soil-rubber mixture (SRM) around buried pipes during ground vibrations. In 7th International Conference on Civil Engineering, Architecture and Urban Planning, At Tehran. https://doi.org/10.6084/m9.figshare(Vol.14998317).

IZTECH Environmental Development, Application and Research Center. https://cevrearge.iyte.edu.tr/en.

Jeon, S. S., and O'Rourke, T. D. (2005). Northridge earthquake effects on pipelines and residential buildings. *Bulletin of the Seismological Society of America,* 95(1), 294-318.

Kahraman, İ. (2013). Seismic liquefaction: 1-G model testing system and shake table tests. Master Thesis. Izmir Institute of Technology (Turkey).

Kaneda, K., Hazarika, H., and Yamazaki, H. (2007). The Numerical Simulation of Earth Pressure Reduction Using Tire Chips in Backfill. *Proceedings of the International Workshop on Scrap Tire Derived Geomaterials–Opportunities*

and Challenges, Yokosuka, Japan, H. Hazarika and K. Yasuhara, Eds., pp. 245–251.

Kaneko T, Rolando PO, Masayuki H, Norimasa Y (2013) Seismic response characteristics of saturated sand deposits mixed with tire chips. *J Geotech Geoenviron Eng*. 139(4):633–643. https://doi.org/10.1061/(ASCE)GT.1943-5606.0000752

Kang, G. C., Tobita, T., Iai, S., & Ge, L. (2013). Centrifuge modeling and mitigation of manhole uplift due to liquefaction. Journal of geotechnical and geoenvironmental engineering, 139(3), 458-469.

Kang, G. C., Tobita, T., & Iai, S. (2014). Seismic simulation of liquefaction-induced uplift behavior of a hollow cylinder structure buried in shallow ground. Soil Dynamics and Earthquake Engineering, 64, 85-94.

Kang, G. C., Chung, J. W., & Rogers, J. D. (2014). Re-calibrating the thresholds for the classification of liquefaction potential index based on the 2004 Niigata-ken Chuetsu earthquake. Engineering geology, 169, 30-40.

Kim H.K., Santamarina J.C. (2008) Sand–rubber mixtures (large rubber chips). Can Geotech J. 45(10):1457–1466. https://doi.org/10.1139/T08-070.

Lee C., Truong Q.H., Lee W., Lee J.S. (2010) Characteristics of rubber-sand particle mixtures according to size ratio. J Mater Civ Eng 22(4):323–331. https://doi.org/10.1061/(ASCE)MT.1943-5533.0000027

Lee, T. (2011). Leaching characteristics of bottom ash from coal fired electric generating plants, and waste tire; individually and mixtures when used as construction site fill materials. Waste Management, 31(2), 246-252.

Lerner, A., Naugle, A., LaForest, J., Loomis, W. (1993) A study of waste tire leachability in potential disposal and usage environments. Amended Volume 1: Final Report. Department of Environmental Engineering Sciences. The College of Engineering, University of Florida.

Li B, Huang M, Zeng X. (2016) Dynamic behavior and liquefaction analysis of recycled rubber sand mixtures. J Mater Civ Eng 2016;28:04016122.

Li W., Kwok C.Y., Sandeep C.S., and Senetakis K. (2019). Sand type effect on the behaviour of sand–granulated rubber mixtures: integrated study from micro- to macro-scales. *Powder Technology*, 342: 907–916.

Li, H., Zhu, H., Li, Y., Zhang, C., & Shi, B. (2022). Experimental study on uplift mechanism of pipeline buried in sand using high-resolution fiber optic strain sensing nerves. *Journal of Rock Mechanics and Geotechnical Engineering*.

Ling HI, Mohri Y, Kawabata T, Liu H, Burke C, Sun L (2003) Centrifugal modeling of seismic behavior of large-diameter pipe in liquefiable soil. *J Geotech Geoenviron Eng.* 29(12):1092–1111. https://doi.org/10.1061/(ASCE)1090-0241(2003)129:12(1092)

Liu, L., Cai, G., Liu, S. (2018). Compression properties and micro-mechanisms of rubber-sand particle mixtures considering grain breakage. Construct Build Mater 2018;187: 1061–72. https://doi.org/10.1016/j.conbuildmat.2018.08.051.

Liu, L., Cai, G., Zhang, J., Liu, X., Liu, K. (2020). Evaluation of engineering properties and environmental effect of recycled waste tire-sand/soil in geotechnical engineering: A compressive review. Renewable and Sustainable Energy Reviews, Volume 126, 109831. https://doi.org/10.1016/j.rser.2020.109831.

Maeda, R., Finney, B. (2017) Water Quality Assessment of Submerged Tire-Derived Aggregate Fills. *Journal of Environmental Engineering* 114(2). https://doi.org/10.1061/(ASCE)EE.1943-7870.0001322

Mahboub, K. C., & Massie, P. R. (1996). Use of scrap tire chips in asphaltic membrane. *Transportation research record*, 1530(1), 59-63.

Marto, A., Latifi, N., Moradi, N., Oghabi, M., and Zolfeghari S.Y. (2013) Shear properties of sand-tire chips mixtures. *Electronic Journal of Geotechnical Engineering*, 18B, pp. 325-334.

Massarsch, K.R., (2014). Cone Penetration Testing – A Historic Perspective. 3rd International Symposium on Cone Penetration Testing, Las Vegas, Nevada, USA.

Mitchell, J.K., and Soga, K. (2005) Fundamentals of Soil Behavior. 3rd Edition, John Wiley and Sons, Hoboken.

Mittal, R.K., Gill, G., (2016). Recent developments in utilizing waste tires to reduce seismic earth pressures and liquefaction potential. *Int. J. Adv. Struct. Geotech. Eng*., 5 (3) (2016), pp. 107-114.

Mohajerani, A., Kurmus, H., Conti, D., Cash, L., Semcesen, A., Abdurahman, M., & Rahman, M. T. (2022). Environmental impacts and leachate analysis of waste rubber incorporated in construction and road materials: A review. *Science of The Total Environment*, 155269.

Mohri Y., Kawabata T., Ling H.I. (1999) Experimental study on the effects of vertical shaking on the behavior of underground pipelines. *Proc 2nd Int Conf on Earthquake Geotechnical Engineering*, Lisbon, Portugal,489–494.

Mukherjee, K., and Mishra, A. K. (2021). Recycled waste tire fiber as a sustainable reinforcement in compacted sand–bentonite mixture for landfill application. Journal of Cleaner Production, 329, 129691.

Nair, G.S., Dash, S.R., and Mondal, G. (2018). Review of pipeline performance during earthquakes since 1906. *Journal of Performance of Constructed Facilities*, 32(6), 04018083.

Noorzad, R., Raveshi, M. (2017). Mechanical Behavior of waste tire crumbs-sand mixtures determined by triaxial tests. *Geotech Geol Eng* 35:1793–1802. https:// doi. org/ 10. 1007/ s10706- 017- 0209-9.

Orense, R. P., Pender, M. J., & Wotherspoon, L. M. (2012). Analysis of soil liquefaction during the recent Canterbury (New Zealand) earthquakes. *Geotechnical Engineering Journal of the SEAGS & AGSSEA*, 43(2), 8-17.

Orense, R.P. (2015) Recent trends in ground improvement methods as countermeasure against liquefaction. *6th International Conference on Earthquake Geotechnical Engineering*. Christchurch: New Zealand.

O'Shaughnessy, V., Garga, V.K. (2000) Tire-reinforced earthfill, part 1: Construction of a test fill, performance, and retaining wall design. Canadian Geotechnical Journal. 37(1): 75-96. https://doi.org/10.1139/t99-084.

Otsubo, M., Towhata, I., Hayashida, T., Shimura, M., Uchimura, T., Liu, B., ... & Rattez, H. (2016). Shaking table tests on mitigation of liquefaction vulnerability for existing embedded lifelines. *Soils and Foundations*, 56(3), 348-364.

Pitilakis, K., Trevlopoulos, K., Anastasiadis, A., and Senetakis, K. (2011). Seismic Response of Structures on Improved Soil. Proceedings of the 8th International Conference on Structural Dynamics (EURODYN2011), Leuven, Belgium.

Phillips R, Valsangkar A.J., (1987). An experimental investigation of factors affecting penetration resistance in granular soils in centrifuge modelling. *Technical Report No CUED/D-Soils TR210,* Cambridge University,UK.

Promputthangkoon, P., and Hyde, A.F.L., (2007). Compressibility and liquefaction potential of rubber composite soils. *In Proceedings of the international workshop on scrap tire derived geomaterials-opportunities and challenges* (pp. 161-170).

Rowe, R.K., Babcock, D. (2007) Modelling the clogging of coarse gravel and tire shreds in column tests. Can. Geotech. J., 44 (11) (2007), pp. 1273-1285.

Renzi R, Corte JF, Bagge G, Gui M, Laue J (1994) Cone penetration tests in the centrifuge: experience of five laboratories. *In Proceedings of international conference centrifuge* 94, Singapore, 77–82.

Rubber Manufacturers Association (1990), "RMA Leachate Study," Radian Corporation.

Saeedzadeh, R., Hataf, N. (2011) Uplift response of buried pipelines in saturated sand deposit under earthquake loading. *J Soil Dyn Earthquake Eng* 31:1378–1384. https://doi.org/10.1016/j.soildyn.2011.05.013

Schmertmann, J.H. (1974). Penetration pore pressure effects on quasi-static cone bearing, qc. Proc. of the European Symposium on Penetration Testing, ESOPT, Stockholm, 2.2, 345-51.

Selbes, M., Yilmaz, O., Khan, A. A., and Karanfil, T. (2015). Leaching of DOC, DN, and inorganic constituents from scrap tires. Chemosphere, 139, 617-623.

Senetakis, K., Anastasiadis, A., Pitilakis, K., Souli, A. (2012) Dynamic behavior of sand/rubber mixtures, Part II: Effect of rubber content on G/Go-γ-DT curves and volumetric threshold strain. *J ASTM Int 9(2*).

Tatlisoz, N., Craig H. B., and Edil. T., (1998). Effect of Fines on Mechanical Properties of Soil-Tire Chip Mixtures. ASTM Special Technical Publication 1275.93–108.

Tergazhi, K. (1922). Der grundbruch an stauwerken and seine verhiltung. Die Wasserkraft 17, 687445–449, 1922.

Thomas, B.S., and , Gupta, R.C. (2016). A comprehensive review on the applications of waste tire rubber. *Renewable and Sustainable Energy Reviews*. Volume 54, Pages 1323-1333.

Tobita, T., Iai, S., Kang, G. and Konishi, Y. (2009). Observed damage of wastewater pipelines and estimated manhole uplifts during the 2004 Niigataken Chuetsu, Japan, earthquake in *TCLEE 2009: Lifeline Earthquake Engineering in a Multihazard Environment*, pp. 1-12.

Tsang, H.H. (2008). Seismic isolation by rubber-soil mixtures for developing countries. *Earthquake Eng. Struct. Dyn.*, 37(2), 283-303.

Tsang, H.H. (2009). Geotechnical Seismic Isolation. *In: Earthquake Engineering: New Research, Takumi Miura and Yuuki Ikeda (Eds.)*, ISBN: 978-1-60456-736-6, Nova Science Publishers, Inc., New York, U.S., pp. 55-87.

Tsang, H.H., Lam, N., Yaghmaei-Sabegh, S., Sheikh, M.N., Xiong, W.,and Shang, S.P., (2009). Protecting low-to-medium-rise buildings by scrap tyre-soil mixtures 2009, 1-8. https://ro.uow.edu.au/engpapers/1400.

Tsuchida, H. (1970). Prediction and countermeasure against the liquefaction in sand deposits. *Seminar in the Port and Harbor Research Institute,* 3.1- 3.33.

Twin City Testing Corporation (TCTC) (1990) Environmental study of the use of shredded waste tires for roadway sub-grade support. Report to Waste Tire Management Unit, Site Response Section, Groundwater and Solid Waste Division, Twin City Testing Corporation Minnesota Pollution Control Agency, St. Paul, Minnesota.

Uchimura, M., Chi, N.A., Nirmalan, S. (2007) Shaking table test on the effect of tire chips and sand mixture in increasing liquefaction resistance and mitigation uplift of pipe. *International Workshop on Scrap Tire Derived Geomaterials*, Yokosuka, Japan.

Uchimura, T., Chi, N.A., Nirmalan, S., Sato, T., Meidani, M., Towhata, I. (2008) Shaking table tests on effect of tire chips and sand mixture in increasing liquefaction resistance and mitigating uplift of pipe. *In: Proceedings of the international workshop on scrap tire derived geomaterials—opportunities and challenges*. London: Taylor and Francis, 179–86.

Yamaguchi, A., Mori, T., Kazama, M., Yoshida, N. (2012). "Liquefaction in Tohoku district during the 2011 off the Pacific Coast of Tohoku Earthquake," Soils and Foundations, Volume 52, Issue 5, Pages 811-829. https://doi.org/10.1016/j.sandf.2012.11.005

Youd, T. L., and Perkins, D., M. (1978). Mapping Liquefaction Induced Ground Failure Potential. *Journal of the Geotechnical Engineering Division, ASCE,* Vol. 104 No. GT4 Proc. Paper 13659, pp 433-446, 1978.

USTMA. (2020). The 2019 Scrap Tire Management Report. *U.S. Tire Manufacturers Association, USA.* https://www.etrma.org/key-topics/circular-economy.

USEPA. (1992) Method 1311: Toxicity Characteristic Leaching Procedure (Report). Part of "Test Methods for Evaluating Solid Waste, Physical/Chemical Methods." U.S. Environmental Protection Agency, Document no. SW-846.

US EPA-SDWS., Secondary Drinking Water Standards: Guidance for Nuisance Chemicals, National Primary Drinking Water Regulations.

Wang, Y., Ren, D., & Zhao, F. (1999). Comparative leaching experiments for trace elements in raw coal, laboratory ash, fly ash and bottom ash. International Journal of Coal Geology, 40(2-3), 103-108.

Whitman, R.V., and Lambe, P.C. (1986). Effect of boundary conditions upon centrifuge experiments using ground motion simulation. *Geotechnical Testing Journal*, 9(2), 61-71.

Zhang, H.Z., Xu, G., Chen, X., Wang, R., and Shen, K. (2019). Effect of long-term laboratory aging on rheological properties and cracking resistance of polymer-modified asphalt binders at intermediate and low temperature range. *Construction and Building Materials*. Volume 226,767-777. https://doi.org/10.1016/j.conbuildmat.2019.07.206

Zornberg, J.G., Carbal, A.R., Viratjandr, C. (2004) Behavior of tire shred–sand mixtures. *Can. Geotech* J 41:227–241.

VITA

Mustafa Karaman

EDUCATION

M.Sc. in Civil Engineering **2014**
İzmir Institute of Technology, İzmir, Turkey
Thesis: Effects of consolidation characteristics on CPT cone resistance and liquefaction resistance in silty soils
Advisor: Assoc. Prof. Nurhan Ecemiş

B.Sc. in Civil Engineering **2010**
Ondokuz Mayıs University, Samsun, Turkey
Graduation Project: Investigation of mechanical properties of Samsun Clay.
Advisor: Assoc. Prof. Nurdan Yavuz Işık

ACADEMIC EMPLOYMENT

Research Fellow **07/2018-12/2018**
Department of Civil and Environmental Engineering
University of Surrey

Research Assistant **2012 - 2020**
Civil Engineering Department
Izmir Institute of Technology

PUBLICATIONS

ARTICLES

Karaman, M., Demirci H.E., Ecemiş N., Bhattacharya S. (2022). Usage of Tyre Derived Aggregates as backfill around buried pipelines crossing strike-slip faults; model tests. Bulletin of Earthquake Engineering. DOI: 10.1007/s10518-022-01383-2

Demirci H.E., **Karaman, M.,** Bhattacharya S. (2021). A survey of damage observed in Izmir due to 2020 Samos-Izmir earthquake. Natural Hazards. DOI: 10.1007/s11069-021-05085-x

Ecemiş N., Valizadeh H., **Karaman, M.** (2021). Sand-Granulated-Rubber Mixture to Prevent Liquefaction-Induced Uplift of Buried Pipes: A Shaking-Table Study. Bulletin of Earthquake Engineering. DOI: 10.1007/s10518-021-01091-3

Demirci H.E., **Karaman, M.,** Bhattacharya S. (2021). Behavior of buried continuous pipelines crossing strike-slip faults: Experimental and numerical study. Journal of Natural Gas Science and Engineering. DOI: 10.1016/j.jngse.2021.103980

Ecemiş N., Demirci H.E., **Karaman, M.,** (2015). Influence of consolidation properties on the cyclic re-liquefaction potential of sands. Bulletin of Earthquake Engineering. DOI: 10.1007/s10518-014-9677-y

Ecemiş N., **Karaman, M.,** (2014). Influence of Non/Low Plastic Fines On Cone Penetration and Liquefaction Resistance. Engineering Geology. DOI: 10.1016/j.enggeo.2014.08.012

CONFERENCE PAPERS

Demirci H.E., Bhattacharya S., Karaman, M., Nikitas G. (2020). Experimental Modelling Of Buried Continuous Pipelines Crossing Strike-Slip Faults. 17th World Conference on Earthquake Engineering, (17WCEE). Sendai, Japan.

Karaman M., Ecemiş N., (2017). Investigation of The Effect Of Sand-Tire Chips Mixture on Liquefaction Potential With Shake Table Tests. 7th Geotechnics Symposium, Istanbul, Turkey (in Turkish)

Karaman M., Ecemiş N., (2017). The Effect of Sand-Tire Chips Mixture on Liquefaction Potential and Deformations. 3rd International Soil-Structure Interaction Symposium. Izmir, Turkey

Ecemiş N., Demirci H.E., Karaman, M., (2015). Effects of relative density and coefficient of consolidation on re-liquefaction potential of sand. Second European Conference on Earthquake Engineering and Seismology. Istanbul.

Karaman, M., Ecemiş N. (2014). Silt Oranının ve Relatif Sıkılığın CPT Penetrasyon Direncine Etkisi. Zemin Mekaniği ve Temel Mühendisliği 15. Ulusal Kongresi – ZM15, Ankara, Turkey